Towards microbial electrochemical technologies for metal recovery

Juan Anaya Garzon

Communauté
UNIVERSITÉ Grenoble Alpes

THÈSE

Pour obtenir le grade de

DOCTEUR DE LA COMMUNAUTE UNIVERSITE GRENOBLE ALPES

Spécialité : **Mécanique des fluides, procédés, énergétique**

Arrêté ministériel : 25 mai 2016

Présentée par

« Juan ANAYA-GARZON »

Thèse dirigée par **Pierre-Xavier THIVEL** et codirigée par **Gérard MERLIN** et **Nadine COMMENGES-BERNOLE**

préparée au sein du **Laboratoire d'Electrochimie et de Physicochimie des Matériaux et des Interfaces - LEPMI** dans **l'École Doctorale IMEP2**

Towards microbial electrochemical technologies for metal recovery

Thèse soutenue publiquement le **« 29/03/2019 »**,
devant le jury composé de :

Mme Isabelle BILLARD
Directrice de recherche, CNRS, LEPMI, Grenoble, France. Présidente.
M. Alain BERGEL
Directeur de recherche, CNRS, LGC, Toulouse, France. Rapporteur.
M. Maxime PONTIE
Professeur, Université d'Angers, GEIHP, Angers, France. Rapporteur.
Mme Xochitl DOMINGUEZ-BENETTON
Directrice de recherche, VITO, Mol, Belgique. Examinatrice.
M. Timothy VOGEL
Professeur, Université of Lyon, AMPERE-ECL, Lyon, France. Examinateur
M. Pierre-Xavier THIVEL
Maître de conférences - HDR, UGA, LEPMI, Grenoble, France. Directeur
M. Gérard MERLIN
Professeur, Polytech-USMB, LEPMI, Chambéry, France. Co-directeur
Mme Nadine COMMENGES-BERNOLE
Maître de conférences, Grenoble INP, LEPMI, Grenoble, France. Co-encadrante.

Acknowledgment

Three years of PhD only represents a stone in the building of knowledge, but not even a single stone is built alone. This journey is just amazingly coming to an end thanks to so many people. Goals require skills, motivation and a bit of luck. I got all that from you.

I want to start with Yann Bultel, my teacher and master mentor who was at the right moment at the right place to propose this adventure to me in the first place. PX, my PhD supervisor, who bravely accepted to enter the Bioelectrochemistry world to guide me. Thank you for putting your trust in me and for being flexible with my caprices (*e.g.* exchanges, courses, trips). Gerard and Nadine, you patiently co-mentored me no matter my divergent thoughts. I learnt a lot from your critical spirit and thank you for keeping the calm in the tough moments.

To all the jury members I'm very grateful for their participation. To Alain Bergel and Maxime Pontie for accepting to review my work. To Xochitl Dominguez, you are a terrific scientist but specially such as creative person. Tim, your simplicity and goodwill encouraged me to overcome the initial adversities. Finally, to Isabelle who nicely supported my scientific career and gave me some pitiless chess lessons.

I would also like to express my gratitude to the LEPMI team. First, to all the colleagues I shared my office with. Florence Degret, the open minded and embodied feminist force. Lucien Duclos, the unpredictable. If your life has another 360° change, I hope you take Sophie with you this time. To Pierre Belleville, you saved my back and made fun of it countless times. I owe you a lot and hope one day I can return the favors. Matthieu Gras, worthy opponent at chess and pastis tasting. Eris, the sociable who is friend with everyone including the police. A big up to Jean-Pierre Magnin for the technical training and for the access to his laboratory, *aka* the Ali Baba's cave. Also, to Jonathan Deseure, for his constant encouragement and wide expertise (especially when it comes to explosion risks).

To Celine, for sharing with me the world of ionic liquids. To the technical and administrative service, for your time and patience. And of course, to all the previous and current colleagues for the parties, dinners, laser games, soccer games, barbecues, board games and dancing demonstrations. Good luck to those who bravely stay in the ring, specially to Francois, who must be dealing with his manuscript right now. Hold the last strike!

Many thanks to my second family, all the amazing flat-mates I've had during my thesis: Luis the most loyal buddy you can ever find; Axel the businessman that handles everyone's finances; the always smiley Angela and her good vibes; Solene the positive soul who sets the mood; Brecht the musician and etiquette specialist; Pacome the sportive man and Sophie the eco-friendliest. A special word to my more recent *collocs* Maurine the designer and Martin the genius, who have fed me with love and tasty food during this last tortuous writing period. Their artistic and scientific *touch* were very motivating! To the KIC Innoenergy program, including Isabel and Christine to give me the grant and the help; and to my comrades for the great experiences all around Europe (Barcelona was the best).

This journey had a special moment in Belgium and I will need to split it into two: Ghent and Boeretang.

Staring in Gent, I have to thank all the CMET laboratory and MeCat group. To Nico Boon and Korneel Rabaey for hosting in me in the first place. Antonin, you helped a lot here. To Jeet for carrying out this work together no matter the challenges. To Suanny, *la compañera*, who shared this adventure unconditionally since I arrived in the lab. You really are symbol of perseverance, discipline and friendship. To Cristina, for sharing your Raman expertise with us. To all the colleagues for the serious and not so serious discussions at *koepuur,* cinema nights and clean-ups on Fridays at 9am.

Boeretang, the place in the middle of nowhere that outsiders are so scare of, was actually full of amazing people. Thanks to Guillermo for guiding my research with your very practical vision, to Vincent for sharing this lab experience and to all the

colleagues I spent so many hours with either at nuclea, the lakes, the tennis courts, and all the events at the 203 dorms.

James Nicolas, my first nephew, is born the same day I'm submitting this manuscript! If you ever read this because of the love of science or just for curiosity, this day was very special for both of us. Last but not least, to God and my family, my electrochemical and non-electrochemical reference. Pa, Ma, Diana, gracias por estar ahí. My PhD life wouldn't have been the same without you and this work is as yours as mine.

Table of content

List of Figures

List of Tables

List of Abbreviations

BES: Bioelectrochemical system

NP: nanoparticles

REE: Rare earth element

TM: Transition metals

GDEx: Gas Diffusion Electro-crystallization

IL: Ionic liquid

WE: working electrode

RE: reference electrode

CE: counter electrode

SHE: Standard hydrogen electrode

ICP-OES: Inductively coupled plasma-optical emission spectroscopy

SEM: Scanning electron microscopy

EDS: Energy dispersive X-ray spectroscopy

XRD: X-ray diffraction

Introduction

To avoid a limit global earth warming to 1.5°C, sustainable processes and low-carbon emission technologies are targeted as priority. The European Commission has adopted an action plan towards a circular economy, where resources are sustainably used, and metals are a core of this strategy. The mining industry processes need to enhance metal provisioning while reducing their environmental impact. Several challenges can be highlighted from this:

- High metal recovery efficiency
- Minimize the environmental burdens and public health impact
- Maximize metal recycling rate

Metals are a limited resource and their abundance depends on their nature. Elements with lower atomic number are normally more present on the Earth's continental crust. Mineral ores generally containing a major metal (*e.g.* Cu, Ni, Pb, Zn, Cr) are carriers of other metals at minor concentration (*e.g.* Au, Co, Ag, Cd). Mining from natural resources, also called primary mining, focuses on the major metal production which is more economically profitable. Due to their low concentration, minor metals often require more natural resources (ore, energy and water) and a higher environmental impact. In some cases, minor metals are considered as impurities that drive up production costs of major metal mining[1]. Furthermore, end of life (EoL) products recycling, also called secondary mining, is becoming an important source of minor metals.

A major minor metal mining's bottleneck, from primary and secondary sources, is the embodied energy. It is the energy required to extract and treat a material from its raw form per unit mass of material produced. In natural sources, carrier elements will normally have up to an order of 10^2 MJ kg^{-1}, whereas minor metals may require embodied energies up to 10^5 MJ kg^{-1} .[2]

Renewable energies and new generation batteries are claimed to replace polluting fossil fuels responsible of climate change. However, these “green” technologies are paradoxically constrained to non-renewable energy demanding resources. For instance, electronic components used in these new devices utilize minor metals at low concentration. When these devices reach their life-time, metals recovery is often very low due to the complex and variated matrices (*e.g.* alloys, polymers, organic solvents, among others).

To face the emerging metal dependence challenges, numerous promising solutions are under investigation including: to extend the products life-time and reuse time, to replace harmful elements and to develop more efficient and sustainable technologies to recover metals from ores and EoL products. The latter solution will be considered in this work. Three sustainable metal recovery technologies based on microbial electrochemical systems are explored in this work. The guideline of this project will be the following: **Chapter I** will present a compilation of the state of the art; **Chapter II** will introduce a concept of biosynthesis of metallic nanoparticles as added-value products, which is based on metal-reducing bacteria stimulated by a polarized cathode; **Chapter III** will focus on metal precipitation from marine environments *via* interactions between an halophilic bioanode and a gas diffusion cathode; and **Chapter IV** will explore the feasibility and challenges of coupling Ionic Liquids for REE electrodeposition with a sacrificial oxidation catalyzed by a bioanode.

This work has been supported by the academic laboratory LEPMI from Grenoble Alpes University, France and collaborations with:
-EIT KIC InnoEnergy (Knowledge & Innovation Community), Europe
-CMET (Center for Microbial Ecology and Technology), Ghent University, Belgium
-VITO (Flemish Institute for Technological Research), Belgium.

CHAPTER I

State of the Art

The Hall of Bulls. One of the prehistoric paintings discovered in Lascaux cave, France. Picture taken by the Daily Herald.

I.1 Introduction to Metal Recovery

I.1.1 An overview of the metal relevance in society

Metals have been remarkably related to human evolution across the history. The Hall of Bulls, one of the first prehistoric paintings made by the human around 17000 years ago, was colored with pigments made of: manganese dioxide (black), iron oxides and hydroxides (black, red, yellow), silicates (yellow) and calcium carbonate (white). From the Iron Age, known for the ferrous based tools and weaponry, to the Bronze Age, where copper-arsenic alloys increased materials hardness and durability, metals have disrupted periods of human civilization. Thanks to the industrial revolution, many sectors including the energy field have considerably enlarged and diversified the metals panel of application over the last 300 years (**Figure I.1**). During the 18th century, the energy demand was supplied by mills made of stone, wood and iron. From the end of that century to the next one, the First Industrial Revolution represented by the steam engine enabled to elaborate more sophisticated machines with copper boilers, lead pipes, chromium-manganese materials (steel) and tungsten light bulbs. The internal combustion engine invention in the 20th century introduced the catalytical properties of platinum and molybdenum and improved the steel and alloys properties by combining more metals. Today, nuclear energy uses uranium as fuel; photovoltaic panels are based on silicon, cadmium, gallium, germanium and tellurium; and wind turbines use neodymium and dysprosium among other rare earth elements (REE)[3].

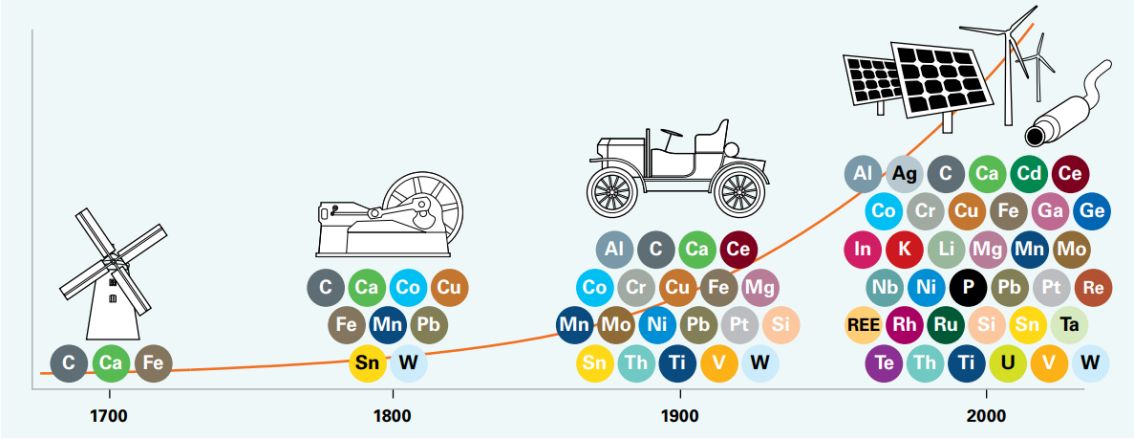

Figure I.1. Metals across energy-related technologies during the last 300 years[3].

The renewable energies emergence described as the "Third Industrial Revolution" by the economist Jeremy Rifkin, in addition to the human population growth, has a consequent metal dependence accompanied by a metal scarcity risk[4]. Metals are geologically limited and have been depleted from natural resources at such a high rate that estimations describe the supply of certain metals as potentially critical. Therefore, a better management of our resources including sustainable metal extraction must be upgraded. To do so, some challenges must be highlighted.

I.1.2 Challenges for a sustainable metal dependence

A sustainable metals dependence englobes scarcity, economic, geopolitics, technological and environmental challenges:

Scarcity

Metal concentration in natural minerals deposits, also called ore grade, is being depleted. Professor Mudd[5] from RMIT University in Australia reported in 2007 how ore grades are declining at a critical rate (**Figure I.2**). The general trend shows that ore grades have dropped more than 4 times over the last 100 years.

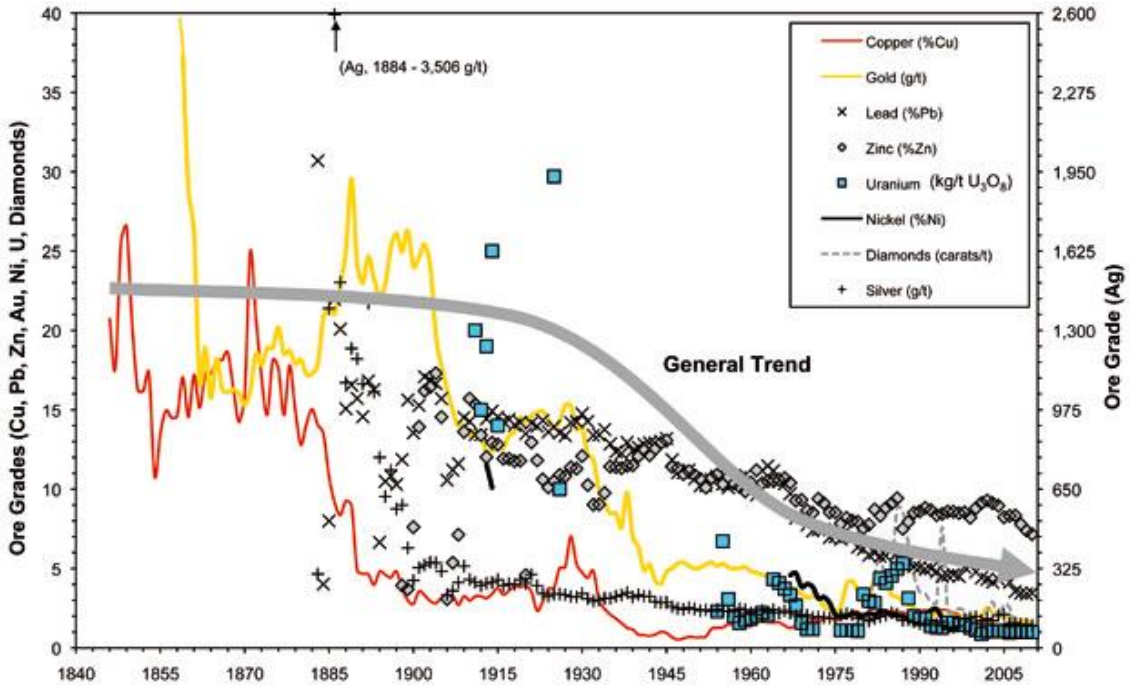

Figure I.2. Ore grades evolution within time. Taken from Mudd[5] and adapted by Öhrlund[6].

Despite the ore grade depletion, metals demand keeps growing. The hidden face of the energy transition is described by the French journalist Guillaume Pitron in his recent book "*La Guerre des métaux rares*"[7]. He emphasizes the alarming raw materials supply risk generated by the REE dependence, which will need to double the extraction rate every 15 years to support the emerging energetic model. An optimized model should consider lowering the amounts of metals employed on our devices. Substituting bulk metals by metallic nanoparticles is among the alternatives.

Economic

Metal price variations are not significantly correlated to the ore grades evolution since 1900[8]. Instead, a linear correlation is exhibited between the final metal price and the energy requirements to produce it (**Figure I.3**)[2].

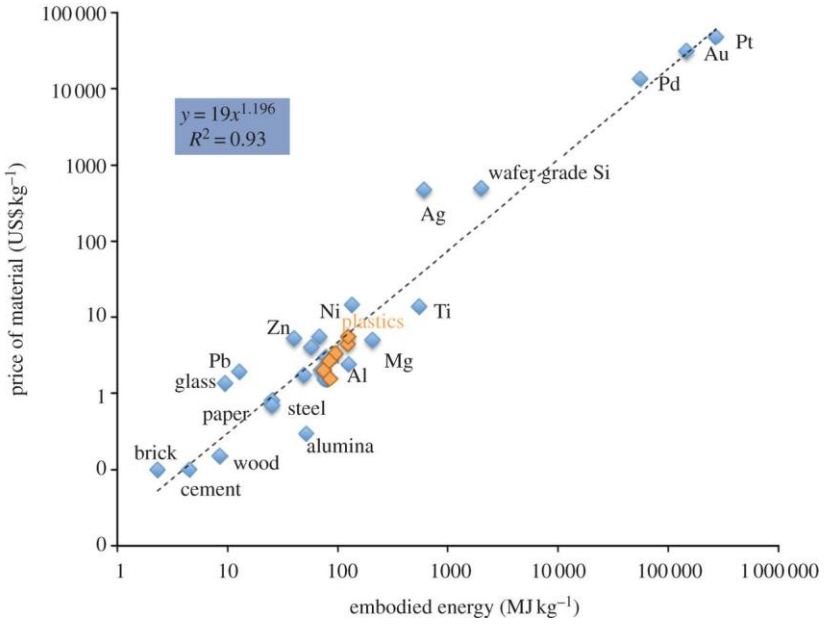

Figure I.3. Relationship between the embodied energy and its commodity price reported in 2009[2].

As consequence, metals such as gold (Au) are at least 10 times more expensive than silver (Ag), despite their similar abundance in the lithosphere. From an economic point of view, it is convenient to treat expensive with lower energy inputs. Nevertheless, international policies on metal prices that considers the conservation of geologically scarce minerals should be formulated.

Environmental

In 2015, Professor Graedel[9] and his team from Yale University, mapped the criticality of 62 metals based on their geological abundance, the current technologies performance to extract them and their economic importance. A major finding was that metals with low supply risk could still be unsustainable in terms of environmental implications and vulnerability to supply restrictions. Likewise, an extensive life cycle analysis published by Nuss and Eckleman[10] reveal environmental issues related to sustainable mining. They present metals criticality from a perspective of energy consumption, global warming potential, human and ecosystems implications. As a matter of example, gold is not scarce but it is one of the most impacting extraction processes in terms of CO_2 emissions (12.5 T CO_2-eq kg^{-1} Au), cumulative energy required (208 GJ kg^{-1} Au), freshwater eutrophication (230 kg P-eq kg^{-1} Au) and human toxicity (0.39 CTUh kg^{-1} Au)[10]. A sustainable metal use must reduce the high environmental burdens of mining from both primary and secondary sources.

Geopolitics

Metals natural sources are localized in different countries, leading to a geopolitics dependence and sometimes to monopolies. To look for a metal sourcing independency, the EU commission launched in 2008 the European Raw Materials Initiative to secure Europe's access to strategic raw materials from both primary and secondary resources[11]. This initiative has facilitated a partnership between some actors from the industrial sector and stakeholders to develop a more sustainable mining industry, increasing the process efficiency and reducing waste. Besides, sustainable development policies have been stablished to limit the energy and emissions required for mining. Finally, the project goes beyond sustainable metal supply by covering a social, economic and environmental scope. Indicators such as employment turnover, biodiversity conservation and integration into a circular economy are hence also considered.

I.1.3 Towards a circular economy

One of the principles of the sustainable metal supply relies on the circular economy. The concept is based on three rules: reuse, substitute and recycle. To

develop it, certain conditions need to be met: the process must be focused on developing high quality products to find its reintegration into the market; and the revenues must exceed recycling chain costs (*e.g.* collection, transportation, storage, treatment)[12]. The EU action plan "Closing the loop" aims to maintain the value of products, materials and resources in the economy for as long as possible, minimizing the waste at each step of the chain value (**Figure I.4**).

Figure I.4. Circular economy defined by KIC RawMaterials[13].

The development of proper metal waste recycling processes, also called secondary mining, is a key activity to reach this purpose. In 2018, the European Budget for research on strategic critical metals made the highest investment on secondary mining with 111 M €, which represents 29% of the total investment over the overall chain value[14]. LEPMI[1] and CMET[2] are committed with this goal and have participated in research projects to develop new metal recovery. KIC InnoEnergy and KIC RawMaterials programs also participate by framing research into the materialization of innovation projects with an entrepreneurial perspective.

[1] RECYPAC: Pt recovery from fuel cells, BATRe ARES: Battery Recycling: Achieving Rare Earth Separation.

[2] METGROW+: Metal Recovery from Low Grade Ores and Wastes Plus, GetAMET: Groundbreaking Extraction technology for critical Metals and Metalloids from industrial wastewater.

Secondary mining has a tremendous economic potential since geological resources are massively shifting towards anthropogenic "deposits"[15]. Metal concentration in electronic waste (e-waste) could be 60 times more concentrated than in mineral ores[15]. However, a major bottleneck of metal recycling is the complexity of "raw materials". Secondary resources are very diverse in terms of composition and concentration. Common policies across Europe have tried to classify E-waste into different categories to facilitate recycling standardization. A special treatment to metal resources such as landfills, hazardous, industrial and domestic waste streams also require well-defined policies. In all cases, to go towards a circular economy, the core of a sustainable metal exploitation is the metal recovery technology.

I.1.4 Metal recovery technologies

Metal mining is rarely a single step process. A common pretreatment consists in a mechanical process where most of the components mixed with metals are discarded. Subsequently, metals are concentrated by either hydrometallurgical or pyrometallurgical processes. Within the hydrometallurgical treatment, metals are firstly solubilized (*e.g.* acid leaching, bioleaching) and then selective extracted from the parental metal matrix. This extraction also called recovery is considered as one of the most energy and chemical intensive steps of metal mining[10]. Transition metals with high economic importance such as chromium may need up to 95% of the cumulative energy demand only for this step[10]. Several techniques have been therefore studied to tackle this problem (**Figure I.5**).

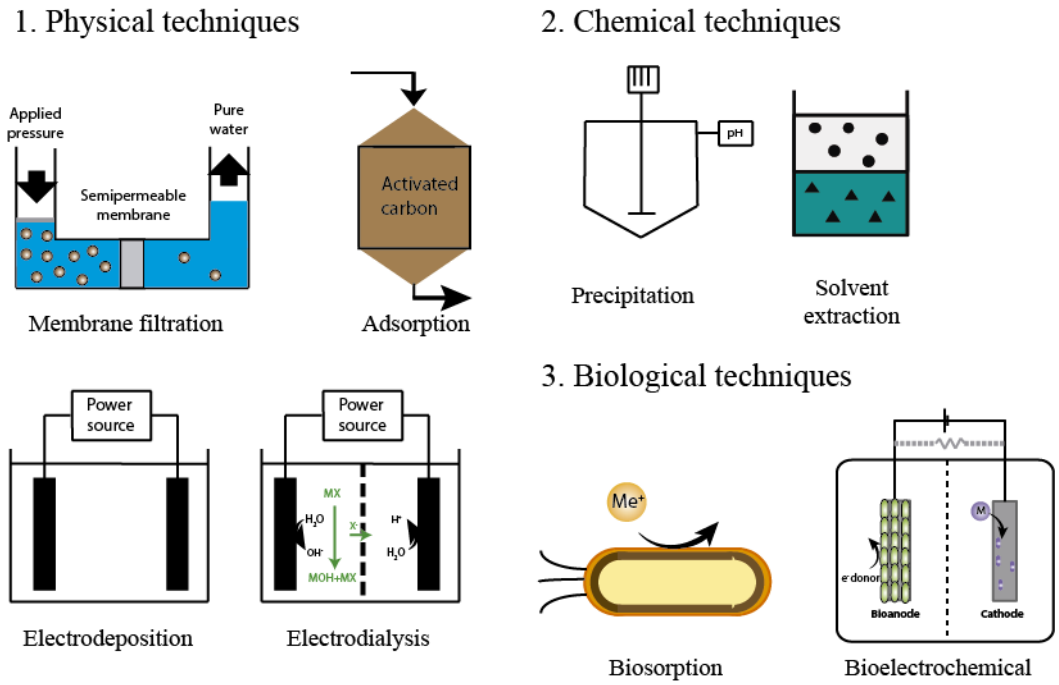

Figure I.5. Metal recovery processes.

Physical techniques such as membrane filtration pressure metal-containing solutions over a porous membrane to physically retain metals while water passes through. Membranes can play with the pore size and modify their structure with chemical sorbents (*e.g.* polyglutamic acid, poly-cysteine) to favorize a selective retention of certain metals. Depending on the nature of the membrane, metals can also be transferred from one solution to another through by applying an electric field (*e.g.* electrodialysis). Ion-exchange membranes facilitate the passage of salt ions from a diluted feed solution to a concentrated stream. Low molecular weight ions transfer is favorized over the higher and less mobile ions. Electrodeposition also applies an electric potential difference between two electrodes. In this case, metals migrate to the cathode and precipitate as layers on the electrode surface. Membrane technologies may have a low footprint but are constraint to high operational costs related to the energy consumption and membrane fouling[16].

Adsorbents can also physically retain metals and has been reported as very efficient in heavy metals removal from wastewater[17]. Adsorbents range from expensive activated carbon to low cost alternatives such as agricultural waste and fly ashes. A major bottleneck of adsorption is nevertheless their low selectivity.

Among the chemical techniques, precipitation is the most widely used because of its simplicity and low cost despite the large amounts of chemicals required. Hydroxide, sulphide and chelation precipitation are the most common methods[16]. Solvent extraction selective dissolve/dilute a metal-rich extractant in a volatile organic solvent (VOS). Some of the most common VOS are acetone, formaldehyde and benzene, dangerous chemicals to human health and to environment. Therefore, enormous improvements have recently shown the potential of less harmful acidic aqueous biphasic systems to replace them[18].

Finally, biologic-based techniques harness microorganisms, enzymes and living plants properties to retain metals. They are considered cost-effective and environmentally friendly techniques for heavy metals bioremediation/phytoremediation[19]. Here, we studied microbial-based techniques to explore possibilities of effective, low energy and chemical demanding metal recovery processes.

I.2 Bacterial potential in metal recovery

I.2.1 Bacterial historical background

Bacteria constitute a part of the prokaryote microorganisms. They obtain energy either from chemical compounds or light. This work focuses on those who harness electrons as energy source from oxidizing chemical compounds, also called chemotrophs. **Figure I.6** classifies them depending on their carbon source, energy source (e- donor) and respiration pathway (final electron acceptor). Bacteria growth and survival is constraint to the presence and type of e- donors and acceptors in their environment, where metals play an essential role.

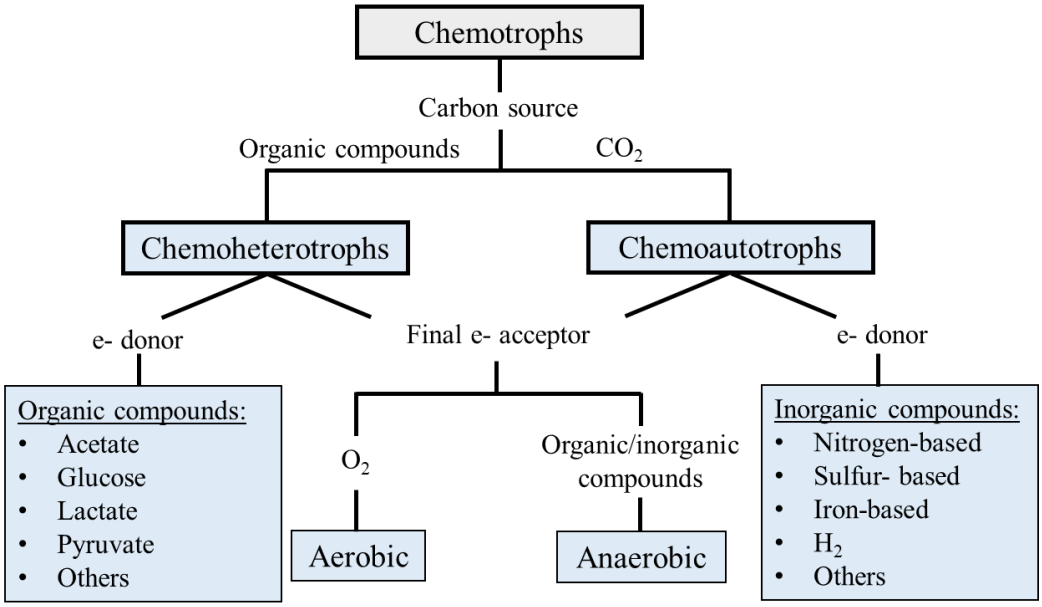

Figure I.6. Chemotrophs metabolism classification.

Microorganisms in general interact with a broad range of metals, metalloids and radionuclides. They are responsible of the formation of a variety of minerals, both inside and outside the cell[20]. Significant scientific advances about the bacterial contribution on these mineralization processes were described in the 1970s by Beveridge and Murray[21,22]. The microbiology presence in minerals and their ability to adapt to extreme conditions has also been reported[23]. These interactions affect the metal physiochemistry and have inspired the development of bio-technologies to either solubilize or immobilize metals (**Figure I.7**).

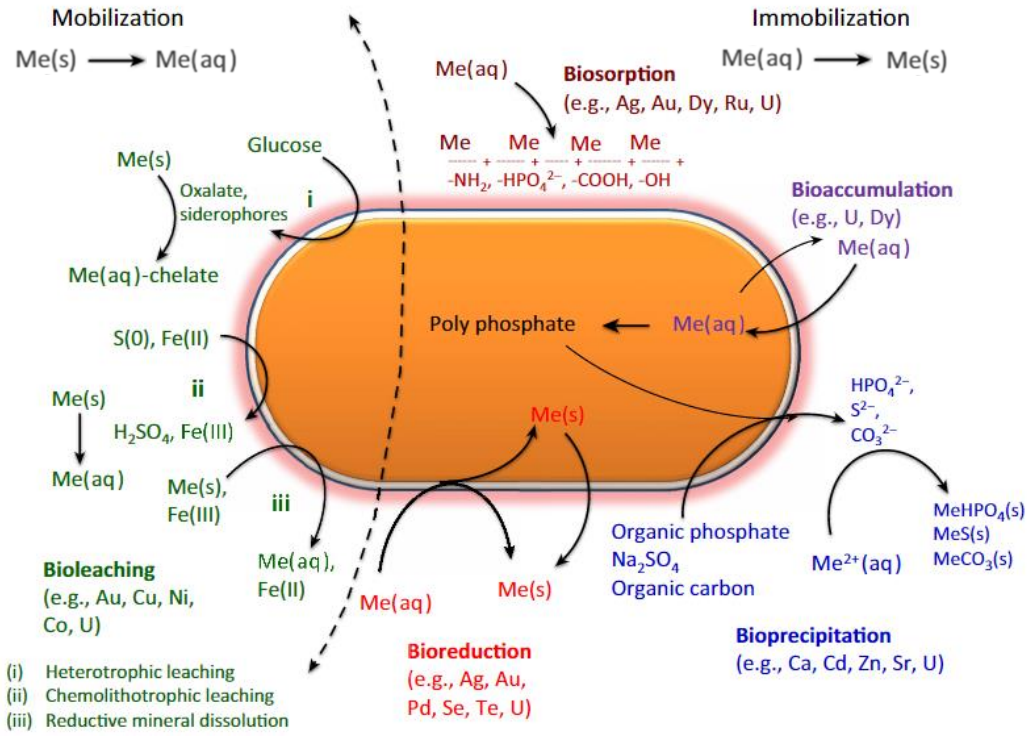

Figure I.7. Bacteria-metal interactions applied for metal recovery (adapted from Nancharaiah *et al.*[20]).

Bacterial metal mobilization, also called bioleaching, is mainly based on three principles: (i) the excretion of metal complexing agents such as siderophores, oxalate, malonate, citrate and succinate by heterotrophic bacteria[24,25]; (ii) the production of inorganic or organic acids by chemotroph species, also called acidolysis, which will chemically leach the solid metals[26]; and (iii) direct dissimilatory metal reduction, where microorganisms use inorganic (*e.g.* S_2 and H_2) or organic (glucose, lactate) compounds as electron donors and metals as electron acceptors, creating electrochemical gradients that provide energy for their metabolism[27,28].

Metal immobilization can be a passive and/or an active bacterial mechanism. Microbial cell walls, outer layers, and extracellular polymeric substances (EPS) can for instance sorb, bind or entrap many soluble and insoluble metal species as well as other elements (*e.g.* minerals, oxides, colloids) with sorption properties[29]. From the other hand, bacteria can also insolubilize metals by direct bio-reduction (dissimilatory metal reduction) or by indirect intermediates (bio-precipitation). Some bacteria have developed resistance mechanisms for toxic metals including

extracellular sequestration, transport followed by an accumulation inside the cells, and/or chelation processes[30]. These mechanisms of metal immobilization were widely used for *in situ* bioremediation in the 1980s[31,32]. More recently, microorganisms-metal interactions have extended to other applications such as metal recovery and nanoparticles synthesis[32,33].

I.2.2 Strategies for metal recovery

a. Metal nanoparticles synthesis

Bacteria has evidenced to ability to precipitate metals at a nanometric size and trap them extracellularly, intracellularly, or even on the cell wall[34]. Metallic nanoparticles (NPs) synthesis has attracted substantial attention as added-value products, especially because of their enhanced surface properties, since nanoparticles have a higher specific surface area compared to bulk metals. NPs characteristics (*e.g.* size, distribution, shape) and applications will certainly depend on the nature of the metal and the bacteria. **Table I.1** summarizes some of the most relevant recent studies on NP bio-synthesis. A single bacteria strain mediated the synthesis of different transition metals, precious metals and REE. Applications were very diversified based on the optical, magnetic and catalytic properties of the NPs.

Table I.1. Metal NPs biosynthesis mediated by bacteria.

Bacteria	Metal NP	Characteristics	Applications	Authors
Shewanella oneidensis MR-1	Au^0	2-50 nm spheres	Antibacterial	*Suresh et al. 2011*[35]
	Te^{4+} - Cr^{3+}	13 ± 3 nm	Bioremediation	*Kim et al. 2014*[36]
	CuS	5 nm	Photothermal therapy	*Zhou et al. 2016*[37]
	Pd^0	8 - 50 nm	Pollutants treatment	*Ng et al. 2013*[38]
Cupriavidus Metallidurans CH34	Au^0	20 - 60 nm, triangular	Optical biosensors	*Montero-Silva 2018*[39]
	Pt^0	1-2 nm	Catalyst	*Campbell et al. 2018*[40]
Medicago sativa	Nd^0	2 – 6 nm, hexagonal	Nuclear medicine	*Ascencio et al. 2006*[41]
	Sm^0	2 – 8 nm	Nuclear medicine	*Ascencio et al. 2005*[42]
Serratia Marcescens	Au^0	20 - 40 nm, prismatic	Nano-medicine	*Dozie-Nwachukwu et al. 2017*[43]
	CuO	10 - 30 nm	Catalyst	*Hasan et al. 2007*[44]
	Bi^0	< 150 nm	Nano-medicine	*Nazari et al. 2012*[45]
Pseudomonas putida	Se^0	70 - 360 nm	Nano-medicine	*Avendaño et al. 2016*[46]
	Ag^0	5 - 16 nm	Antibacterial	*Gopinath et al. 2017*[47]

Much attention has been given to the biosynthesis of zero-valent metal NP. Different pure strains have demonstrated the ability to reduce metal ions by several metabolic pathways. As described in **Section I.2.1**, bacteria can adsorb metal ions and transfer electrons from an electron donor (*e.g.* H_2, formate, lactate) to promote a metal reduction (**Figure I.8**). This bacterial property is known as electroactivity.

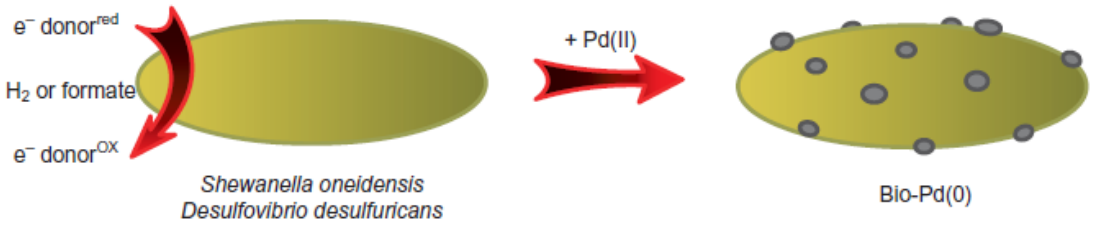

Figure I.8. Reduction of Pd^{2+} and PdNP biosynthesis assisted by an e^- donor [48].

b. Electro-activity

Electro-active bacteria are exoelectrogen microorganisms, which means they are capable of transferring electrons extracellularly *via* their cellular respiration. For instance, they generate energy by oxidizing nutrients into smaller molecules, protons and electrons. Electrons are carried through an electron transport chain (ETC) and are finally released to the environment where external electron acceptors such as sulfates, nitrates and metals (*e.g.* FeO_3, MnO_2) get reduced[49,50]. Protons are transferred across the internal membrane *via* a proton pump, creating a transmembrane pH gradient and electrical potential, responsible of driving the ATP synthesis. In 1910, the botanic professor Michael Potter demonstrated this electroactivity on *Escherichia coli* (*E. coli*)[51,52]. He placed them in platinum electrodes, fed them with glucose and observed a potential difference and a current generation. Basically, catabolic oxidation of glucose resulted in and electrochemical gradient where the platinum electrode replaced the natural final electron acceptors of the ETC.

The extracellular electron transfer (EET) vary depending on the species, but they are all catalyzed by a large variety of oxidoreductases enzymes[53]. However, when an electrode gets involved, three EET mechanisms between bacteria and the

surface have been described: direct electron transfer (DET), mediated electron transfer (MET) and indirect electron transfer (IET) (**Figure I.9**).

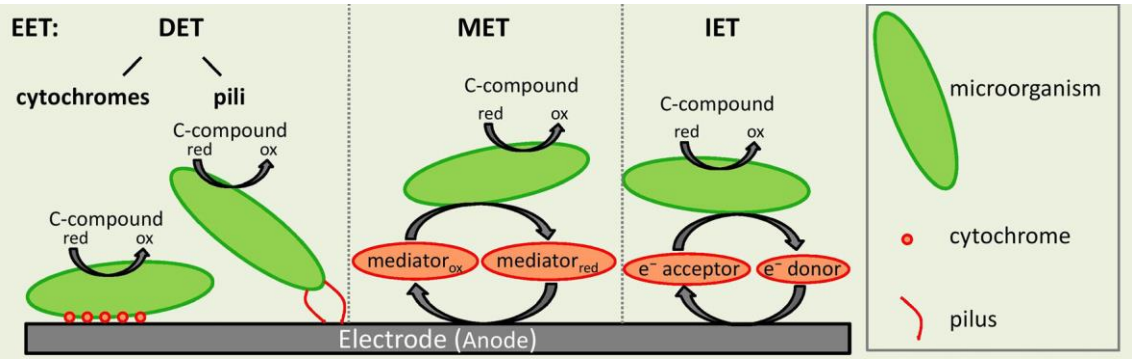

Figure I.9. Extracellular electron transfer paths between electroactive bacteria and electrodes [53].

DET is possible due to mobile proteins called c-type cytochromes, which transfer electrons across the cell barrier through a series of redox reactions until the solid surface. Besides, some bacteria produce cellular appendages, also called pili, improving the physical connection between the microorganisms and the solid surface[54]. MET involves shuttle molecules (mediators) that transfer electrons between the surface and the microorganisms even at larger distances[53]. Mediators such as flavins, phenazines, methyl viologen and humic acids can be secreted by the bacteria or simply added to the medium[50]. Finally, IET uses microbial electron carriers electrochemically synthesized such as hydrogen or formic acid. In contrast to the MET, the electron carriers undergo irreversible redox processes[53].

Besides the *E. Coli*, numerous bacteria strains have revealed exoelectrogenic activity but not consensus has been established about the ideal type[55,56]. Those who do not retain the crystal violet stain developed by Danish biologist Hans Gram, also called Gram-negative bacteria, are primarily used for electroactive bacteria applications[53]. For instance, *Geobacter sulfurreducens* has been extensively studied because of its respiratory versatility and abundance in the environment[53,57,58]. This gram-negative strain lives in anaerobic conditions and plays an important role in the global cycling of metals and carbon[59]. *Shewanella oneidensis* MR-1 (*S. oneidensis* MR1) is another largely studied electroactive strain[60,61]. It is a facultative anaerobic, non-fermentative bacterium outstanding for its ability to use a large variety of insoluble and soluble metals as

electron acceptors. Oxygen, nitrate, nitrite, sulfur, thiosulfate, fumarate, sulfite, DMSO, and trimethylamine-N-oxide are other common electron acceptors of this species[62]. Based on the microbial electroactivity characterization and potential applications, the concept of Bioelectrochemical system (BES), has emerged.

I.2.3 The Bioelectrochemical System

a. Generalities

BES enables microorganisms to convert chemical energy stored in biodegradable materials into electric current and chemicals[16]. These materials could be wastewater or biomass, turning it to a cheap renewable "fuel"[49]. BES is composed of at least two electrodes, an electrolyte and an external circuit (**Figure I.10**).

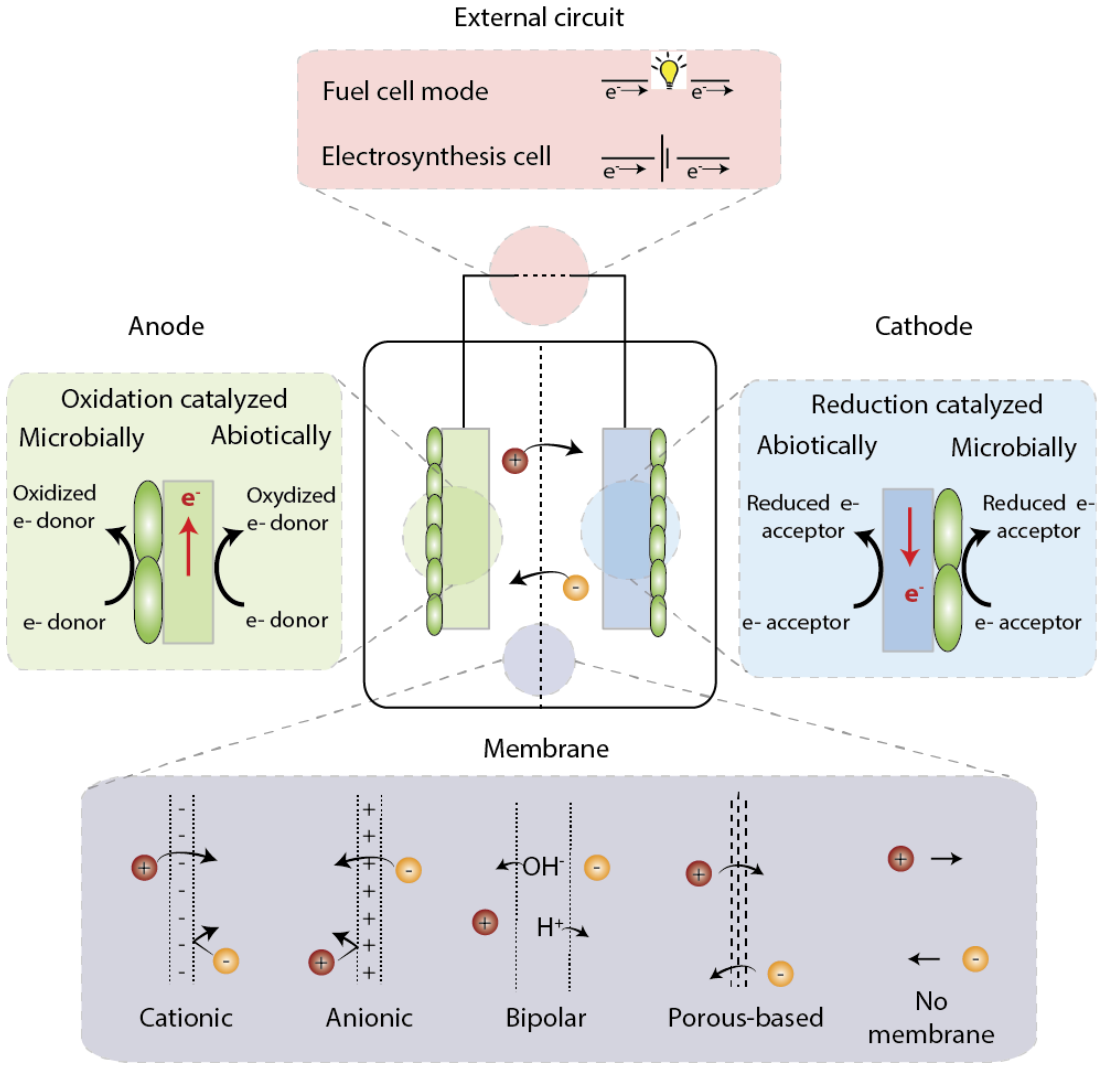

Figure I.10. Schema of microbial electrochemical systems (adapted from Belleville *et al.*[63]).

Soluble ions considered as electron donors are oxidized at the anode while simultaneously soluble ions as final electron acceptors are reduced at the cathode. Depending on whether the electrodes are connected to an external load or a power source, two types of systems can be distinguished: Microbial Fuel Cells (MFC) and Microbial Electrosynthesis Cells (MEC). Finally, electrodes may be separated by a membrane. In that case, cathode and anode chambers are called anolyte and catholyte respectively.

Electrodes

Electrodes potential is function of the redox couple of materials, concentration of the species and temperature and is described by the Nernst law:

$$E = E^0 + \frac{RT}{nF} ln \frac{a\ Ox}{a\ Red} \quad \textbf{(I-1)}$$

E = Potential of one electrode (V)
E^0 = Standard potential of one redox couple (V)
n = Number of exchanged electrons
R = Constant of the ideal gas law = 8.314 $Jmol^{-1}K^{-1}$
F = Faraday's constant = 96500 C
T = Temperature (K)
$a\ Ox$ and $a\ Red$ = Chemical activity of species

BES operating voltage (E_{cell}) is extracted as the electrodes potential difference (ΔE) subtracting all the irreversible losses:

$$E_{cell}=\Delta E-[(\eta_{act}+\eta_{conc})_{cathode}+(\eta_{act}+\eta_{conc})_{anode}]-IR_{ohm} \quad \textbf{(I-2)}$$

Where activation losses (η_{act} in V) are linked to the electro-catalytic properties of the electrode materials for a specific reaction; concentration losses (η_{conc} in V) involve the depletion of charge-carriers at the electrode surface compared to the bulk solution; and ohmic losses, product of the multiplication between the exchanged current (I in A) and the ohmic resistance (R_{ohm} in Ω), is related to cell design parameters such as electrolyte and membrane ionic resistance, distance between electrodes and electrodes electrical resistance.

Electrodes have the role of transferring electrons through an external circuit by catalyzing redox reactions. Therefore, they must be electrically conductive, stable and possess a high catalytical activity for the desired reactions. Bioelectrodes are referred to biofilms grown on an electrode surface with the purpose of catalyzing an electrochemical reaction to either generate electrical current or reduce the energy requirements. Suitable electrodes materials for biofilm growth must have high volumetric current density. This supposes to have a high specific surface area accessible for microbial development and high current production per area[64]. Macroscale porous electrodes are appropriate for bacterial colonization, even though parameters like the tortuosity, pore shape and size must be considered to avoid clogging. The current density production will depend on material properties like its biocompatibility, conductivity, roughness, micro-porosity, hydrophilicity and charge storage[64]. So far, carbon fiber based porous electrodes have shown the best performance in terms of current output[64]. Carbon foams[65], brushes[66], felts[67], graphene oxides[68] and activated carbon[69] have shown performances up to 390 A m^{-2}. Some of the non-porous materials reported are gold[70], copper silver and nickel[71].

Electrolyte

Electrolytes desired properties are mainly high ionic conductivity, good electrochemical stability and low electrical conductivity. Aqueous systems from synthetic solutions to wastewater are commonly used as electrolytes. As microorganisms generally grow at approximately neutral pH, room temperature and low salinity, high ohmic resistance (R_{ohm}) due to low ion-conductive electrolytes can be a major drawback for the BES performance[72,73]. Buffer solutions such as phosphates and carbonates are usually added to the system to assure a suitable pH and to decrease resistance losses. However, high buffer concentrations are inconsistent with real wastewater and are neither economically nor environmentally relevant[73]. Reducing the distance between electrodes is an effective and cheaper alternative to reduce losses related to the electrolyte.

Membrane

Membranes are used in dual-chambers systems to have a better control over the operating conditions on each chamber. They must have a high ionic conductivity

since as mentioned before, they add a supplementary resistance. Besides, they must satisfy the following requirements: acceptable cost, low electronic conductivity, high chemical and mechanical stability, bio-compatible, low (bio)fouling and undesired crossover[74,75].

Separators are mostly polymers or ceramics and range from porous-based to ion exchange membranes (IEM). A number of porous materials including cloth layers[76], microfiltration[77] and ultrafiltration[78] membranes have been reported as separators for BES. Very original low-cost materials have also came out such as newspapers and rolling paper[79]. Among the conventional IEM, a wider variety of materials has been explored. Cationic exchange membranes (CEM) are the most common types[3]. Polymer chains with negatively charged ions (*e.g.* $–SO_3^-$, $–COO^-$, PO_3^{2-}, and PO_3H^-) are commonly used to efficiently transport cations between the chambers[72]. Proton exchangers with supported ionic liquids membranes have also been investigated[80]. Anionic exchange membranes (AEM)[4] use positively charged cation groups (*e.g.* NH_4^+, NHR_2^+, NR_2H^+, NR_3^+, PR_3^+, and SR_2^+) attached to the polymer matrix to allow anions passage through the membrane[74]. Finally, bipolar membranes club together a CEM and an AEM to transport selectively protons and hydroxyl ions to a specific chamber. At the membrane junction, water splits into H^+ and OH^- due to the applied electric field. Subsequently, protons migrate through the CEM to the catholyte and hydroxides to the anolyte trough the AEM[81].

b. <u>BES configurations</u>

Microbial Fuel Cell (MFC)

MFC is characterized for having a spontaneous electron transfer from an anode to the cathode at a higher potential (**Figure I.11**). The system releases energy to a lower thermodynamically stable energy state at a constant pressure and temperature, which corresponds to a negative Gibbs free energy ($\Delta G<0$). Electrical energy is therefore generated as electrons are transferred through an external load.

[3] Nafion, Hyflon, Zifron, Ultrex, CMI-7000 are some of the most common commercial CEMs.

[4] QPEEK, QPEI, QPSU, RALEX are some of the most common commercial AEMs.

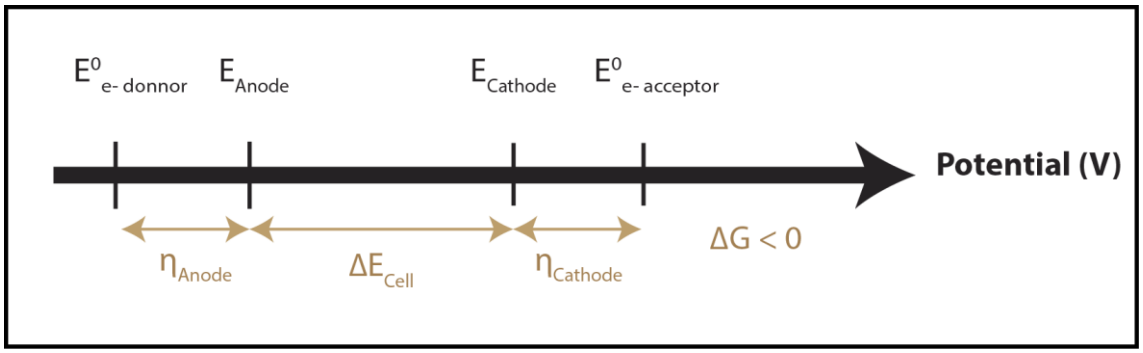

Figure I.11. Schema of redox potentials in a MFC.

A typical MFC has a biofilm on the anode surface to catalyze oxidation reaction and to favorize electron transfer to the system. Electrons are firstly transferred from an e- donor to bacteria thought their ETC *via* different redox reactions (*e.g.* $Ferredoxin_{ox/red}$, $NaD^+/NADH$, $FAD^+/FADH_2$)[82]. A fraction of these electrons is used to the cell synthesis and maintenance, while the remnant goes to generate electricity. Bacteria obtain this energy from either organic (heterotrophic) or inorganic (autotrophic) external substrates. When there is a mixed microbial community, electroactive bacteria compete with non-electroactive bacteria for the substrate consumption[64]. Nonetheless, the presence of a substrate in the electrolyte as an electron donor is mandatory. Some of the most common compounds are presented in **Table I.2**.

Subsequently, it is thermodynamically possible to transfer the electrons spontaneously to the cathode if the cathode potential and the final electron acceptor potential at the cathode are greater. Final electron acceptors are often O_2, nitrates, sulfates and some metals[64]. Metal recovery strategies *via* BES utilize often metals as final electron acceptors.

Table I.2. Electron donors used for bioanodes (taken from Xie *et al.* 2015[64]).

e- donor	Reaction	E° (V *vs.* SHE)*
Organic matter	$\frac{1}{e}C_aH_bO_cN_d + \frac{2a-c}{e}H_2O \leftrightarrows \frac{a}{e}CO_2 + \frac{d}{e}NH^{3+} + H^+ + 2e^-$ where e=4a+b-2c-3d	-0.42 to -0.20
H_2	$2H^+ + 2e^- \leftrightarrows H_2$	-0.41
HS^-	$SO_4^{2-} + 9H^+ + 8e^- \leftrightarrows HS^- + 4H_2O$	-0.22
S	$SO_4^{2-} + 8H^+ + 6e^- \leftrightarrows S + 4H_2O$	-0.20
AsO_3^{3-}	$AsO_4^{3-} + 4H^+ + 2e^- \leftrightarrows H_2AsO_3^{3-} + H_2O$	+0.15
Se	$SeO_4^{2-} + 8H^+ + 6e^- \leftrightarrows Se + 4H_2O$	+0.33
NH^{4+}	$NO_3^- + 10H^+ + 8e^- \leftrightarrows NH^{4+} + 3H_2O$	+0.36
Mn^{2+}	$MnO_2 + 4H^+ + 2e^- \leftrightarrows Mn^{2+} + 2H_2O$	+0.47
U^{4+}	$UO_2(CO_3)_3^{4-} + 3.52H^+ + 2e^- \leftrightarrows UO2 + 2.48HCO_3^- + 0.52H_2CO_3$	+0.59

*Values at 298 K and pH=7.

Microbial Electrosynthesis Cell (MEC)

MEC integrates an external power to assist the electrochemical reactions. Reactions are therefore not spontaneous (ΔG>0) and electrons are transferred from the anode to the cathode at a lower potential (**Figure I.12**). The main advantage is to target final electron acceptors with low E^0 (*e.g.* H^+/H_2, Co^{2+}/Co, Nd^{3+}/Nd). As in MFC mode, a substrate is needed to transfer electrons between the biofilm and the electrode. However, microbial electrodes aim to reduce the required energy instead of generating it.

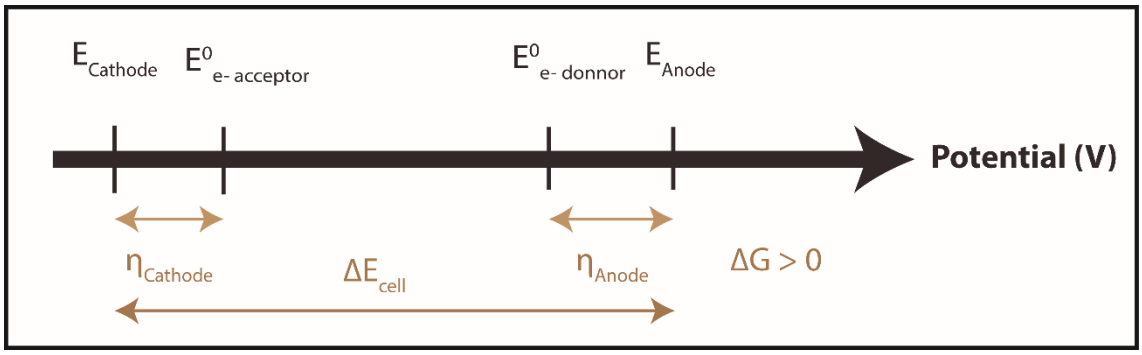

Figure I.12. Schema of redox potentials in a MEC.

Configurations may have bioanodes and/or biocathodes to catalyze desired electrochemical reactions. In the 2000s, the concept was used to polarize bioanodes and favorize water electrolysis in the (bio)cathode for H_2 production[83,84]. Later on, biocathodes have been demonstrated the elongation of short carbon chains (*e.g.* CO_2, acetate) to valuable organic compounds (*e.g.* succinate, butyrate)[85,86].

c. Microbial Electro-Metallurgy (MEM)

The versatility of BES for metal recovery has given rise to the microbial electro-metallurgy[32]. Metal ions are removed from aqueous solutions by two approaches: as final e- acceptors, where metal ions are electrochemically reduced; and by ion complexation with the final e- acceptor. In both cases, metal solubility is lowered and followed by a precipitation. A summary of most relevant studies is presented in **Table I.3**. Metal removal efficiency (η), a common indicator of the MEM performance, is defined by the equation **(I-3)**. C_0 and C_t are the initial and the final metal concentrations (mM), respectively.

Recovery efficiency (η) $$\eta = \frac{C_0 - C_t}{C_0} \times 100 \qquad \textbf{(I-3)}$$

Table I.3. Metals recovered by BES systems (inspired from Nancharaiah *et al.*[87]).

Metal ion	Metal content	pH	Bacteria	Electron donor	η (%)	Authors
Cr(VI)	39.2 mg L^{-1}	2-6	Cr adapted consortium[a]	NaOAc	99 in 7 h	*Huang et al. 2010*[88]
	100 mg L^{-1}	2	Anaerobic sludge[b]	NaOAc	100 in 48 h	*Gangadharan and Nambi 2015*[89]
	204 mg L^{-1}	2.5 *	Anaerobic sludge[b]	NaOAc	100 in 25 h	*Li et al. 2008*[90]
Co(III)	874 µM	4-6	Anaerobic[a]	NaOAc	92 in 6 h	*Jiang et al. 2014*[91]
	1 g L^{-1}	1-3	Mixed culture[b]	NaOAc	99 in 48 h	*Huang et al. 2013*[92]
Cu(II)	1 g L^{-1}	4.7	Anaerobic[b]	Glc	>96 in 264 h	*Tao et al. 2011a*[93]
	2 g L^{-1}	2	Anaerobic[b]	NaOAc	92 in 480 h	*Tao et al. 2011b*[94]
	1 g L^{-1}	3	Mixed culture[b]	NaOAc	100 in 6 d	*ter Heijne et al. 2010*[95]
Cd(II)	50 mg L^{-1}	6	Anaerobic sludge[b]	NaOAc	94 in 60 h	*Choi et al. 2014*[96]
Au(III)	200 mg L^{-1}	2	Anaerobic[b]	NaOAc	98 in 12 h	*Choi and Hu 2013*[97]
Hg(II)	100 mg L^{-1}	2	Anaerobic[b]	NaOAc	99 in 10 h	*Wang et al. 2011*[98]
Se(IV)	75 mg L^{-1}	7	Anaerobic[b]	NaOAc, Glc	99 in 48 h	*Catal et al. 2009*[99]
Ag(I)	50 mg L^{-1}	7	Anaerobic sludge[b]	NaOAc	100 in 8 h	*Choi and Cui 2012*[100]
	1 g L^{-1}	9.2	Anaerobic sludge[b]	NaOAc	100 in 21 h	*Wang et al. 2013*[101]
Ni(II)	50 mg L^{-1}	5	Mixed culture[a]	NaOAc	99 in 20 h	*Qin et al. 2012*[102]
V(V)	500 mg L^{-1}	2	Mixed culture[b]	Glc	25 in 72 h	*Zhang et al. 2009*[103]
Cr(VI), V(V)	250 mg L^{-1} 250 mg L^{-1}	2*	Anaerobic sludge[b]	Glc	75, 68 in 240 h	*Zhang et al. 2012*[104]
Cu(II), Pb(II), Cd(II), Zn(II)	0.8 g L^{-1}, 0.4 g L^{-1}, 0.8 g L^{-1}, 0.3 g L^{-1},	<0	Mixed culture[a,b]	NaOAc	100 in 300 h	*Modin et al. 2012*[105]
Cu(II), Fe(II), Ni(II)	5 mM, 9 mM, 5 mM	2.8 *	Anaerobic[a]	NaOAc	100 in 90 h	*Luo et al. 2014*[106]

*Waste stream, [a]MEC, [b]MFC.

Metal concentrations were always below 2 g L^{-1}. Even though, the total metal recovery took from 6 hours to several days. pH is often acid since metals are previously leached in acidic solutions. A mixed culture, usually anaerobic, is preferred; electron donors vary between different organic matter such as sodium acetate (NaOAc) and glucose (Glc).

Mixed cultures acclimatized with sodium acetate (NaOAc) as e^- donor are preferred for bioanodes. Despite the preference for synthetic one-metal solutions, some studies have focused on metal recovery from more complex matrixes such as fly ashes[105] and acid mining waste[106]. To our knowledge, BES configurations haven't focused on REE recovery so far.

η was close to 100% in most of the cases and faster by MEC compared to MFC. In a configuration bioanode-abiotic cathodes, precious metals such as gold and silver has shown the potential of metal removal and electrical energy production[97,107]. Chui *et al.* reported 100% removal efficiency from 200 mg L^{-1} Au^{3+} and a power density generation of up to 6.6 W m^{-2} with 2 g L^{-1} Au^{3+}. Biocathodes started to be implemented in MFC systems as well for Cr^{6+} reduction to $Cr(OH)_3$. Tandukar *et al.* reported a maximum rate of 0.46 mg Cr^{6+} g VSS^{-1} h^{-1}. The resulted current and power density was 123.4 mA m^{-2} and 55.5 mW m^{-2} (against the anode surface), respectively[108]. Finally, selectivity was addressed in some cases based on the redox potentials of metals[105] and the hydraulic retention time of the catholyte[106].

I.3 Specification of the study

Metals are crucial in the global economy as key raw materials for the energy transition and a variety of industrial applications. Sustainable processes to manage metals along their value chain in a suitable way is essential. In this project, we benefit from the versatility of BES to study metal recovery from natural and anthropogenic sources. The present work aims to explore the feasibility of three innovative technologies for metal recovery detailed in the following chapters:

- **Chapter II** focuses on metal-bacteria interactions for chromium and gold recovery. The concept of electrodes as electron donor for nanoparticles biosynthesis is introduced.
- **Chapter III** presents an innovative cathode to favorize the production of intermediate species (*e.g.* H_2O_2, OH^-) for metal precipitation from marine environments.
- Finally, **Chapter IV** explores ionic liquids as potential solvents for neodymium electrodeposition in a MEC system.

CHAPTER II

Metal-bacteria interactions for gold and chromium recovery

Anton van Leewenhoek, father of microbiology. Picture taken from Discover magazine.

II.1 Introduction

One of the biggest ironies of microbiology is the fact that microorganisms, the oldest self-replicating organisms on Earth, were among the last to be discovered. It is not until the late 17th century that the wholesaler Leewenhoek designed a single-lensed microscope and observed microbes including bacteria for the first time. Since then, the understanding of microbes and their interactions with the metals has been remarkably expanded, as already highlighted in **Chapter I**.

Inspired on these interactions, **Chapter II** explores the feasibility of a new bioelectrochemical process to recover and valorize metals from low metal-content streams. It utilizes bacteria in suspension, *idem* planktonic bacteria, as driving agents for transforming metal ions into nanoparticles. Gold and chromium are reviewed in this chapter; two strategic metals that exemplify different behaviors with bacteria. Two bacterial strains known for their versatile interactions with metals were studied: *Shewanella oneidensis* MR-1[60] (*S. Oneidensis* MR1) and *Cupriavidus metallidurans* CH34[109] (*C. metallidurans* CH34). First, parameters that influence the most the metal recovery efficiency and nanoparticle synthesis are explored in a screening design of experiments (DOE). Based on that, a microbial electrochemical technology is proposed to intensify the metal recovery rate and improve the efficiency whilst keeping the nanoparticle synthesis formation. Implications of microbial-metal interactions and some of the possible applications are discussed.

This chapter is the result of a collaboration between the CMET laboratory at Ghent University and LEPMI, co-elaborated with Suanny Mosquera's Master thesis, and financially supported by the French Ministry of Education, METGROW+ project and the KIC InnoEnergy PhD school.

II.1.1 General principle

Here, initially viable cells in suspension are employed to recover metals from a low metal content stream. Metal ions can be recovered as nanoparticles on the bacterial surface or inside the cells through a series of passive and active mechanisms[110]. This is a slow process that often requires the presence of a reducing agent, also called electron donor. Bioreactors with either *S. oneidensis* MR1 or *C. metallidurans* CH34 is firstly evaluated in a closed system with two known soluble electron donors: lactate or H_2 (**Figure II.1A**). Secondly, the introduction of a cathodic environment by the presence of a polarized cathode as an electron donor is explored (**Figure II.1B**). The cathode is intended to participate in the metal electrochemical reduction, whereas bacterial cells act as support for metal NP synthesis. This new approach differentiates from classic bioelectrochemical systems, where well-stablished electroactive biofilms are required as electron transfer shuttle for metal recovery. In this case, bacterial integrity is not intended to be conserved and neither its electroactivity. The cathode provides with electrons for metal reduction and bacterial cells are used as support for metal nanoparticles synthesis.

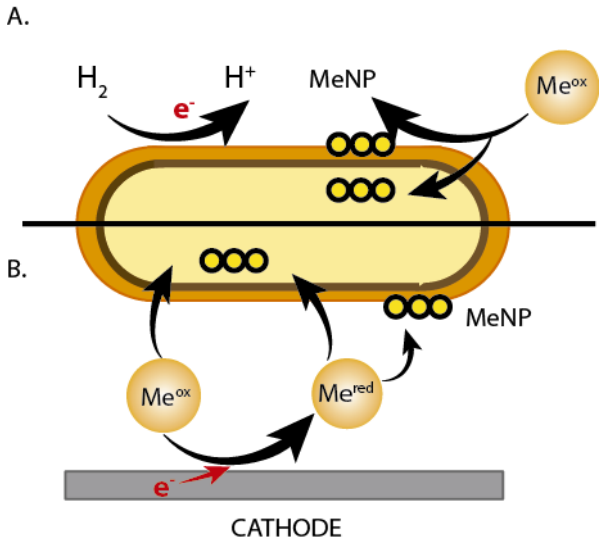

Figure II.1. Principle of metallic nanoparticles synthesis by coupling: (A) a cathodic environment and (B) bio-recovery mediated by electron donors (*e.g.* H_2, cathode).

II.1.2 Bacterial strains preparation

Frozen cells (in 20 % glycerol at −80 °C) of *Shewanella oneidensis* MR-1 (LMG 19005) and *Cupriavidus metallidurans* CH34 (SCK CEN Mol, Belgium) were revived under aerobic conditions on tryptic soy agar (Oxoid, England). Individual colonies were inoculated in tryptic soy broth (TSB, Carl Roth, Germany) continuously agitated under aerobic conditions at 28 °C. Following the procedure detailed elsewhere[111], cells were harvested at the stationary growth phase (typically 72-96-hours of incubation, optical density (OD_{610nm}) ≈ 1) by centrifugation (Sorval RC 6+, Thermo Scientific, USA), washed twice with sterile 0.9% w/v NaCl, and finally concentrated to reach a value of OD_{610}≈7 in a sterile 0.9% w/v NaCl aqueous solution (**Figure II.2**). Subsequently, these concentrated bacterial cells stock was made anoxic by degassing for 21 cycles of vacuum and filling with N_2 gas (Linde, Germany). Initially non-viable bacteria controls were set with cells autoclaved for 21 minutes at 121°C.

S. oneidensis MR1 *C. metallidurans* CH34

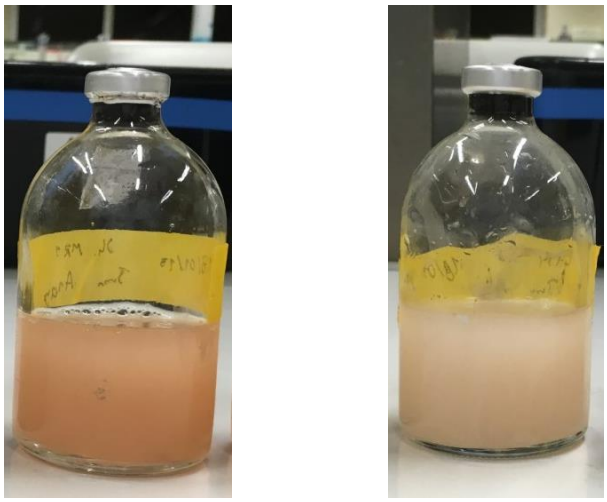

Figure II.2. Bacterial cells stock (OD_{610}≈7) of *S. Oneidensis* MR1 and *C. metallidurans* CH34.

To determine the mass of cells to inoculate the system (M_C in g), a relationship between the cell volume and concentration previously reported[112,113], was used with the following equation:

Mass of cells applied (in g) : $$M_c = C_b \times V_c \times M_b \quad \textbf{(II-1)}$$

Where M_c considers the initial bacterial cell concentration (C_b) in cells mL^{-1}, V_c as the volume of cells in mL injected into the reactors (typically 5 or 10 mL), and the bacterial cell mass (M_b) in g cell^{-1}. M_b is calculated from Equation **II-2**, where V_b is the cell volume in μm^3 (given by Equation **II-3**), 435 is a constant that represents the conversion factor between weight and volume, and 0.86 is a scaling factor[113]. The average volume of bacterial cells (**Table II.1**) was calculated from measurements of 25 bacterial cells from TEM analysis. It considered the allometric measurements of the width (w) and the length (l), of bacterial cells unexposed to metal ions.

Bacterial cell mass (in g): $$M_b = 435 V_b^{0.86} \quad \textbf{(II-2)}$$

Bacterial volume (in L): $$V_b = \left[\left(w^2 \times \frac{\pi}{4}\right)(l - w) + \left(\pi \times \frac{w^3}{6}\right)\right] \quad \textbf{(II-3)}$$

Table II.1. Bacterial dimensions and density.

Bacteria	Dimensions		Average cells density
	w (μm)	**l (**μm)	**(g cell^{-1})**
S. oneidensis MR1	0.62 ± 0.08	1.34 ± 0.64	1.73 x 10^{-13}
C. metallidurans CH34	0.55 ± 0.08	1.14 ± 0.35	1.23 x 10^{-13}

Bacterial dimensions are comparable to a previous characterization of the *S. algae*[114] and the *C. metallidurans*[115]. Likewise, average cell density is comparable with previous reports for *S. putrefaciens* (1.28 x 10^{-13} g cell^{-1})[111].

II.2 Gold recovery

II.2.1 Context

Gold is a noble metal, used as jewelry, LED backlighting in TVs, reflective glass coating for heat conservation, part of electronics, and as an active material in catalysis[116,117]. Recovery of gold from wastewater is noteworthy to suffice circular economy. But the ideal suffer some drawbacks. Even though this "gold urban mine" is significantly richer than the available primary ores (*e.g.* 300-350 g t^{-1} for mobile phone compared to 5 g t^{-1} for a typical gold mine), the composition of secondary resources is much more complex[118]. Several hydrometallurgical technologies are available to recover gold from waste. Solvent extraction and ion exchange membranes can separate selectively gold ions from leached waste streams[119–121]. Subsequently, precipitation of elementary gold by chemical reducing agents and electrochemical deposition of Au^0 plates is desirable due to its intrinsic high purity properties[121–123]. Here, the challenge lies in developing recovery processes economically worthwhile. In this sense, the approach of integrating Au recovery and valorization from secondary sources has an enormous potential to concomitantly supply materials to high-grade applications.

Gold nanoparticles (AuNPs) have attracted substantially attention as added-value products. This, based on their enhanced physicochemical properties, primarily related to their high surface area that enhance catalytic reactivity, optical properties, and chemical steadiness[124]. AuNPs are notable for application in, *e.g.*, surface enhanced Raman, medical diagnostic, drug delivery, catalytic uses, and for environment remediation[34,125,126], among others. It needs to be mentioned that the safety of AuNPs is highly controversial in terms of bio-compatibility and toxicity, but no conclusive statements have been confirmed so far[127].

Microorganisms are considered as potential 'nano-factories' for the biosynthesis of zero-valent AuNPs, with properties similar to (electro)chemically-synthesized materials[124,128]. A new bioelectrochemical configuration is proposed to recover and transform metal ions into added-value nanoparticles.

II.2.2 Microbial system assessment

a. DOE Matrix

Experimental

Microbial-mediated recovery was evaluated first using a 1/8 fractional factorial design matrix (Resolution III,2^{7-4})**, which is ideal for fast-track screening and as a basis for further optimization[129]. This design of experiments (DOE) was composed of 7 factors (*i.e.*, cells concentration, temperature, headspace, pH, gold concentration, electron donor and cell type), each of them with two levels (described in **Table II.2**), which experimental runs are organized in an orthogonal array.

Table II.2. Orthogonal experimental design matrix applied for 2^{7-4} DOE

Std. order	Experimental order	Factor						
		OD_{610}	Temperature	anoxic/oxic	pH	$[Au^{3+}]$ mM	e-donor	cell-type
1	**7 (R7)**	0.5	28 °C	*Anoxic*	5	2	Lactate[a]	MR-1
2	**2 (R2)**	1	28 °C	*Anoxic*	1	0.2	Lactate[a]	CH34
3	**1 (R1)**	0.5	37 °C	*Anoxic*	1	2	H_2[b]	CH34
4	**5 (R5)**	1	37 °C	*Anoxic*	5	0.2	H_2[b]	MR-1
5	**8 (R8)**	0.5	28 °C	*Air*	5	0.2	H_2 [b]	CH34
6	**4 (R4)**	1	28 °C	*Air*	1	2	H_2 [b]	MR-1
7	**3 (R3)**	0.5	37 °C	*Air*	1	0.2	Lactate[a]	CH34
8	**6 (R6)**	1	37 °C	*Air*	5	2	Lactate[a]	MR-1

[a]*Lactate concentration = 10 mM*

[b]*H_2 in saturation (≈0.9 mM at 25°C)*

Two response variables were chosen for this study: the metal recovery efficiency (η) and a targeted AuNPs size of 50 nm based on their catalytic applications[130,131]. To calculate the removal efficiency, gold ions concentration initially (C_0) and at the end (Ct) were measured *via* ICP (description in **Annex 1-A**). DOE experiments were conducted for 72 h in serum bottles (120 mL) filled with 50 mL of metal

** The resolution III DOE enables to estimate the main effects, starting from the null hypothesis that all the factors have none influence on the response variables. It has the advantage of minimizing the number of experiments, focusing on the main factors studied rather than the interactions between then.

solution at the specified metal concentration and pH. Firstly, metal concentration was made up from a $HAuCl_4$ stock solution (5 g L^{-1}) in a solution containing 0.15 M NaCl. pH was adjusted with either NaOH or HCl. Bottles were plugged with thick butyl rubber stoppers and sealed with an aluminum crimp. Reactors were autoclaved at 121ºC for 21 min. No metal precipitation was observed after autoclaving. Air or N_2 headspace was set according to conditions described by the matrix. Subsequently, electron donors were supplied either to the solution (sodium lactate) or at the headspace (H_2 gas). An equivalent concentration of 10 mM of lactate was added to be in excess. H_2 was purged for 10 minutes with a constant pressure of about 2 bars to achieve an equivalent of 0.9 mM H_2. This aqueous H_2 concentration was calculated using Henry's constant ($H^{cp} = 7.7 \times 10^{-6}$ mol m^3 Pa^{-1} in H_2O at 298.15 K, 1 atm)[132]. Then, cells were incoulated from the concentrated stocks to the designated concentration based on the OD_{610}. The mass of inoculated cells (*Mc*) was calculated based on equation **(II-1)**. Average values are presented in **Table II.3**.

Table II.3. Mass of inoculated cells

OD_{610}	Mc (in g)	
	MR-1	**CH34**
0.5	4.26 E-03	5.72 E-04
1	8.53 E-03	1.14 E-03

The reactors were finally placed on incubators at the corresponding temperature with a rotatory shaker (KS 400i, IKA, Germany) set at 120 rpm.

Visual results

The aim of the DOE was to maximize the $AuCl_4^-$ recovery and to transform them into valuable NPs. A first visual response before the metal content analysis is a good indicator of the microbial system performance. The color change of the reactors from the beginning of the experiments t_0 to the end t_{72h} are presented in **Figure II.3**.

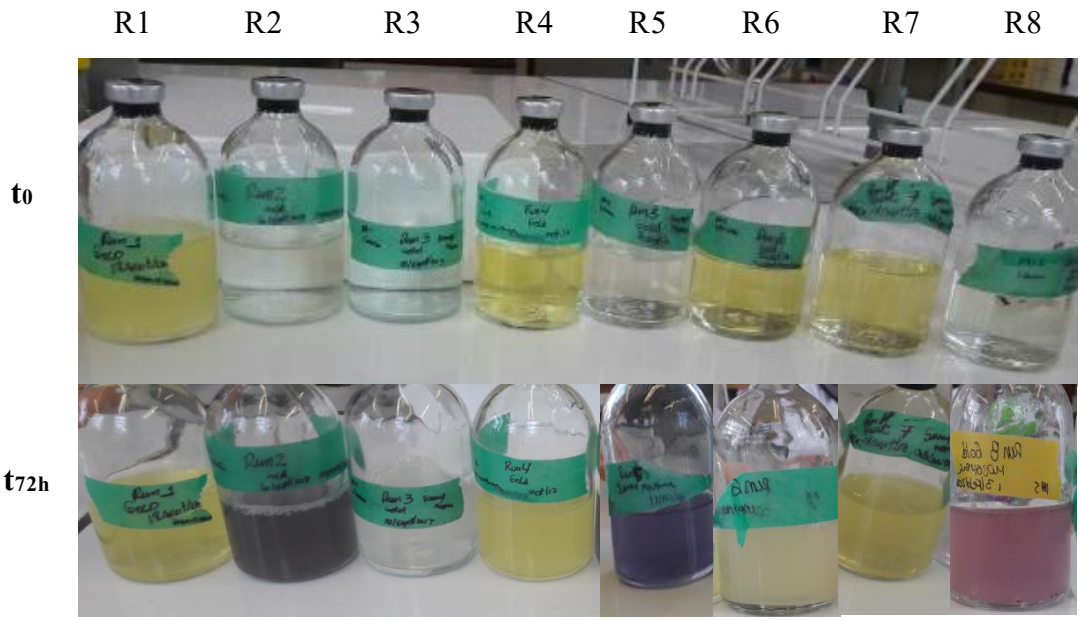

Figure II.3. Reactors at the beginning and at the end of the experiment.

At t_0, yellowish and transparent reactors represented configurations 2 mM and 0.2 mM Au, respectively. After 72 h, reactors R2, R5 and R8 turned violet, which is the characteristic color for AuNPs[133]. Reactors R1, R3, R4, R6 and R7 have a turbidity effect attributable to suspended particles originated from bacterial cells effect. This color effect gives a first overview of the reactor's evolution, but a microscopic proof is a better indicator of AuNPs. Therefore, bacterial cells were harvested from each reactor and observed at a Transmission Electron Microscope (TEM, description in **Annex 1-B)**. TEM micrographs displayed in **Figure II.4** segregate images from experiments with *C. metallidurans* CH34 and *S. oneidensis* MR1 after the DOE experiments (description in **Annex 1-B**). Strain controls (R_{0C} for *Cupriavidus* and R_{0S} for *Shewanella* species) were not exposed to gold ions and therefore couldn't produce any AuNPs.

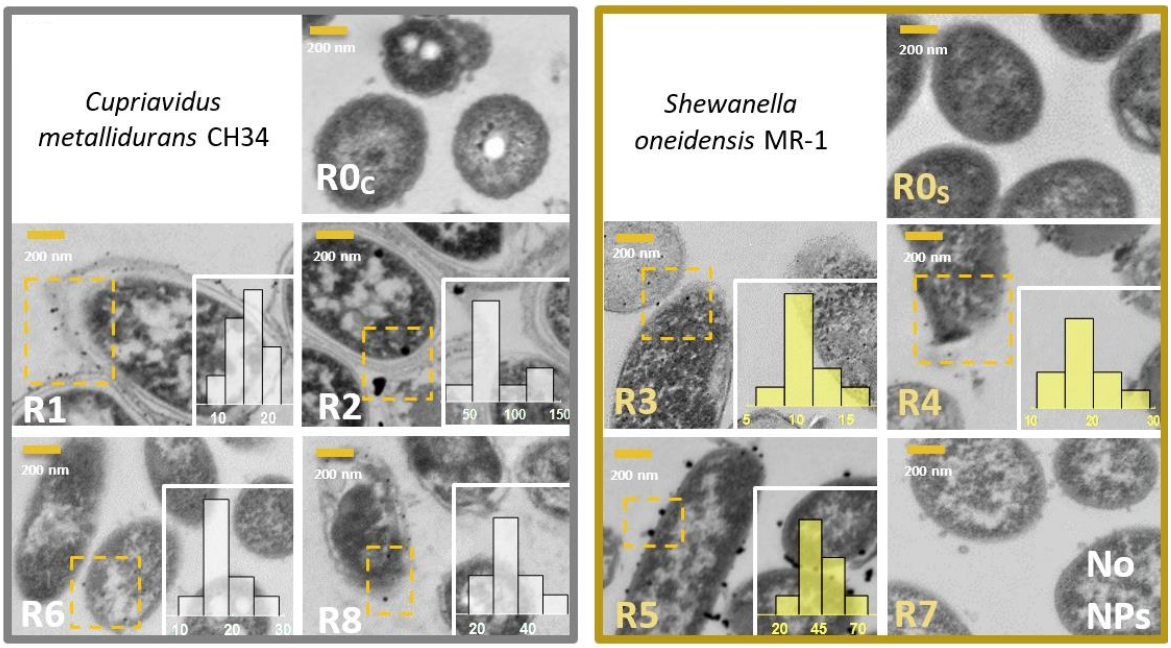

Figure II.4. TEM analysis and NP size distribution (nm) for the 8 reactors. R0c and R0s represent bacterial controls without metals for CH34 (grey) and MR-1 (yellow), respectively.

AuNP were identified as electron-dense particles either surrounding or inside the bacterial cell. This assumption is applied since gold has very dense and reactive atoms compared to bacterial molecules, appearing as a highly contrasted black color in TEM images. They were distributed at different bacteria locations and quantified by using the ImageJ software. Nanoparticles from 8 nm up to 112 nm were quantified in each configuration except R7. Intracellular AuNPs in reactor 3 were smaller (10.5 ± 2.1 nm) in comparison to those in the periplasmic space displayed in reactor 1 (15.6 ± 2.9 nm). A combination of both was displayed in reactor 4 (18.3 ±3.7 nm) and 6 (19.1 ± 3.3 nm). Larger NPs were observed extracellular or on the cell wall in the reactors 2 (103 ± 43 nm), 5 (43 ± 13 nm), and 8 (31 ± 7 nm); whose solutions exhibited a visual surface plasmon resonance (SPR) effect perceived as a purple like color (**Figure II.3**). The particle size and location are important parameters for further applications. For instance, targeted 50 nm NPs size were found in literature to be optimal for catalytic applications[130,131]. AuNPs of ≈ 60 nm are apparently more active in comparison with smaller (<10 nm) or bigger particles (>70 nm) for Raman applications as it amplifies the signal of biochemical components[134]. Finally, cells bounding to

AuNPs can act as a carrier for various applications such as catalysis in removal of pollutants or enhanced hydrogen production in microbial fuel cells[135–137].

DOE results in terms of variable responses

Following on, the microbial system performance was analyzed in terms of the metal removal efficiency (η, description in **Chapter I**, equation **I-3**) and AuNP average size. Average AuNPs size and its standard deviation were calculated based on 10 identified nanoscale precipitates from each reactor. Absolute values of the response variables are displayed in Figure II.5**.**

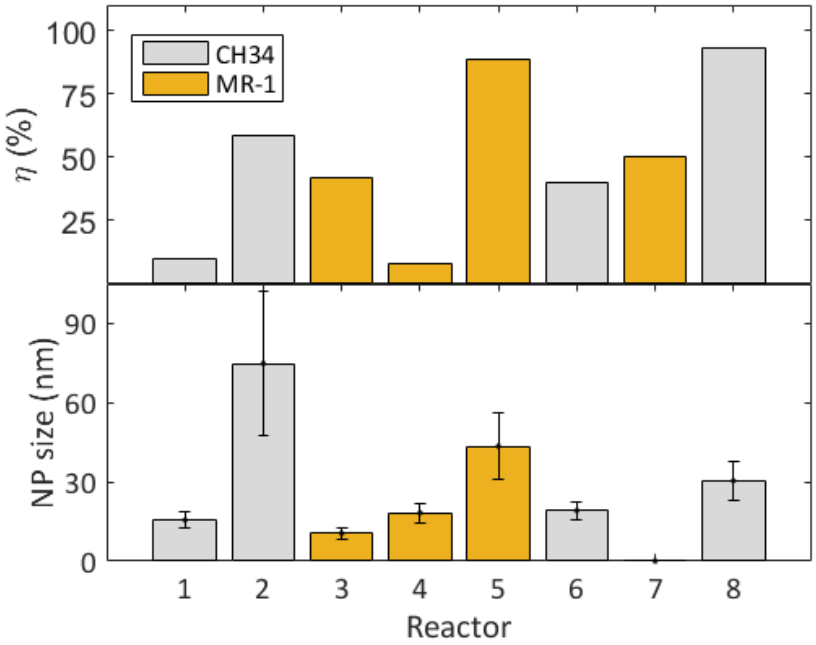

Figure II.5. DOE results in terms of gold removal efficiency (η) and average (NP).

At 72h, reactors R2, R5 and R8 gave the highest removal efficiency (58.8%, 88.5% and 92.8% respectively), having in common a low concentration of Au^{3+} (*i.e.*, 0.2 mM) and the purple coloration. The interaction of colloidal gold nanoparticles with light dictates their visible color; purple colorations are characteristic of nanoparticles of large size (typically >30 nm), which is consistent with the average AuNP sizes (**Figure II.5**). R7 had a gold removal of 50 %, which is interpreted as (bio)precipitation but not necessary attached to the bacterial cells.

Statistical analysis

To estimate which factors statistically had an active effect in the variable responses, Lenth's method was firstly employed. This is a non-parametric method applied for non-replica analysis in fractional factorial designs[138], and represented by equation (**II-4**).

$$\text{Effect magnitude} \quad F_{Effect} = \frac{2}{m} \times \sum_{i=1}^{m} (\text{algebraic sign}_{(1,-1)} \times \text{observation}_i) \quad \textbf{(II-4)}$$

Where *m* is the number of experiments, the algebraic sign represents the level of each factor (*i.e.* either -1 or 1) and $observation_i$ the experimental response. In order to express the response variables in terms of maximum or minimums, AuNP size response was rewriting as (AuNP size - 50)^2 and the minimum value was targeted. From there, a margin error (ME) was calculated based on the concept of sparse effects (Equation **(II-5)**), to identify effects that are higher than a random error[138].

$$\text{Margin error:} \quad ME = \left(4.45 \times (\bar{F}_{Effect,j})\right);\ j \in \text{Effects} \left\{ \left| F_{Effect_j} \right| < 3.75 * \bar{F}_{Effect} \right\} \quad \textbf{(II-5)}$$

Based on the Lenth's method, factors with an active effect lie outside the marginal error. Factors effect for both η and 50 nm AuNPs were calculated in displayed in **Figure II.6**.

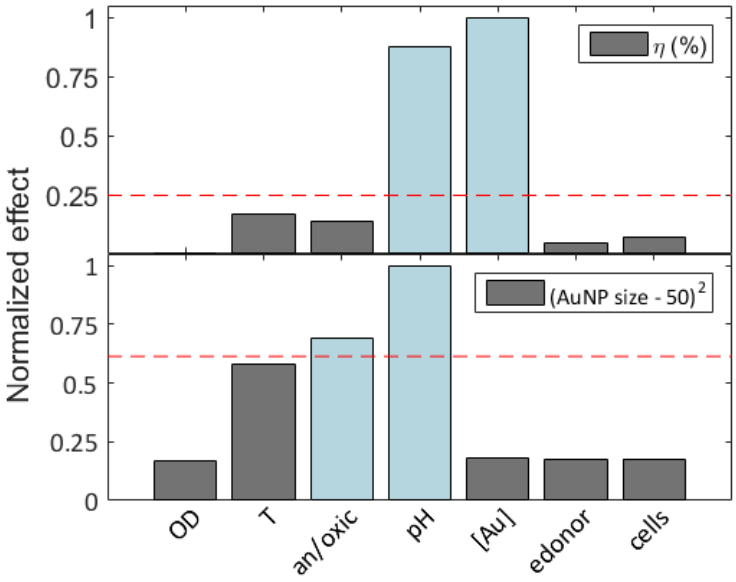

Figure II.6. Effect of each factor on η and AuNP. Values are normalized by the most significant effect. Significant effects lie out of the margin error.

To maximize gold removal efficiency, the most significant factors were the initial gold concentration ($C_{Au,0}$) and pH. Regarding the functionalized AuNPs, pH and anoxic/oxic conditions effect was above the margin error. Following which, a variance analysis (ANOVA), another technique to estimate main factors based on variations between groups (*i.e.* the seven factors)[139]. The total variation (*SS total*, described in Equation (**II-6**)) is the sum of variation between groups (*SS groups,* described in Equation (**II-7**)) and the variation within groups (*SS error groups,* described in Equation (**II-8**)). s_i represent the standard deviation of a given factor *i*. The probability of an observed result if there is no relationship between two factors, *i.e*. null hypothesis, is expressed in Equation (**II-9**). If this probability is higher than a significance level (*e.g*. 5%), the null hypothesis should be rejected.

Sum of squares for total variation: $\mathrm{SS\,total} = \mathrm{SS\,group} + \mathrm{SS\,error}$ (**II-6**)

Sum of squares for groups: $\mathrm{SS\,group} = \sum_{i=1}^{R} m_i \times \left(\bar{F}_{Effect,i} - \bar{F}_{Effect}\right)^2$ (**II-7**)

Sum of squares for error: $\mathrm{SS\,error} = \sum_{i=1}^{R} (m_i - 1) \times (s_i)^2$ (**II-8**)

Probability value: $P - value = Pr(observation \mid hypothesis)$ (**II-9**)

Main factors with their respective sum of squares for groups (*SS group*), sum of squared errors (*SS error*) and the probability value (*p-value*) are presented in **Table II.4**.

Table II.4. Main effects for maximizing η and target 50 nm AuNP with 95% confidence interval.

Variance analysis	max(η)		min(AuNP-50)^2	
	pH	$C_{Au,0}$	pH	Anoxic/oxic
SS group	19.1	-21.8	406	-289.4
SS Error	2.3	2.3	5.5	3.9
p-value	0.001	0.002	0.012	0.029

Main effects on the variable response were confirmed by the ANOVA test with p-values lower than a significance level of 5%, but some aspects must be considered. First, to maximize η, errors represent between 9% and 11% of the total variance depending on the factor. Second, main effects are confounded with the effect of interactions between factors due to the DOE resolution. SS group are normally

used to formulate an experimental model, but a second DOE focused on these main effects with a higher resolution is recommended to do so. Finally, the values sign in the SS groups express the level of preference for each factor. Therefore, the statistical analysis can led to differentiate the levels response of these significantly important factors (**Figure II.7**).

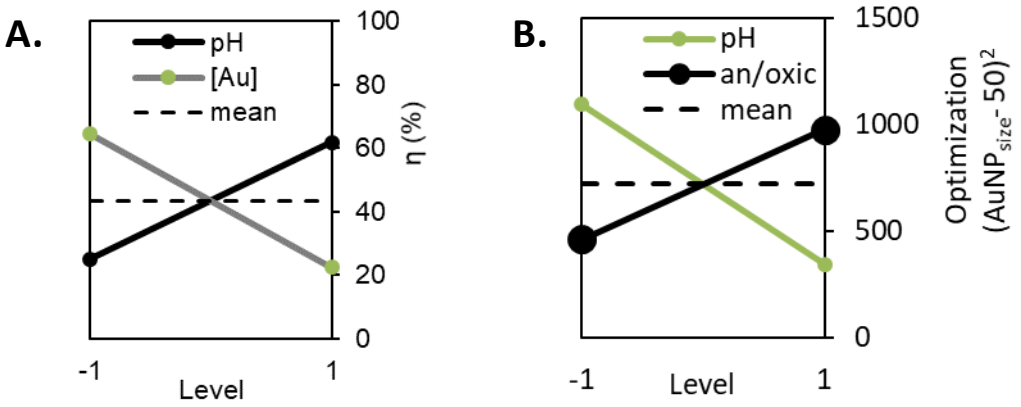

Figure II.7. Factorial plots of relevant factors A: η and B: AuNPs close to 50 nm.

A maximum η was obtained at 0.2 mM (level -1) and pH 5 (level 1). Higher $AuCl_4^-$ concentrations, *i.e.*, of 2 mM, can be considered extremely toxic for the cells. The microbial inhibitory concentration (MIC), which imposes the limits of stress responses in bacteria, is 0.2 mM Au *S. oneidensis* and 0.0008 mM Au in *C. metallidurans*[109,140]. Thus, a less toxic metal content (*e.g.* 0.2 mM Au) could favorize the metal removal from initially viable cells. Moreover, acidic conditions induces the protonation of the bacterial cell wall, leading to a passive electrostatic adsorption of the negatively charged $AuCl_4^-$ anion[141,142]. However, metal recovery was higher at pH 5 compared to pH 1. This phenomenon already observed by Ha *et al.*[143] seems to be related to the functional groups present in the cell wall. In *S. oneidensis*, phosphoryl groups (pK_a= 6.8) presumably maintain most of their positive charge at pH 5, thus, contributing to gold ions attraction. This may promote nucleation sites and colloidal stability. When the pH further moves to neutral, the studied revealed a drastic diminution of AuNP synthesis and associated it to an electrostatic repulsion on the cell surface[144].

Regarding the AuNP size, pH 5 (level 1) and anerobic headspace (level -1) resulted as desired levels to minimize $(AuNP\text{-}50)^2$. There is not a clear understanding of the

anaerobic effect on the nanoparticles size, but a few studies have shown that AuNPs may adsorb or react with O_2[145,146]. This interaction may play a role in their nucleation and further agglomeration.

b. Study case, R5 conditions

Based on the above-mentioned results, appropriate experimental conditions that lead to high gold removal and functional AuNPs (≈50 nm) synthesis were: *S. oneidensis* MR1, pH 5, anoxic conditions, and H_2 presence. Considering a specific case of reactor 5 (R5), conditions were triplicated and compared to abiotic and heat-killed cells controls. Metal removal (η_{Au}) was firstly evaluated (**Figure II.8A**). Besides, viable cells were quantified based on flow cytometry measurements **(**description in **Annex 1-D)**, and the cells viability calculated from equation (**II-10)**. Bacterial removal capacity (q), defined as the ratio between the metal mass removal and the bacterial cells mass inoculated (q in $g_{Au}\ g_{cell}^{-1}$), was also evaluated (**Figure II.8B**). It is based on equation (**II-11**); where V is the volume in litters of the solution and M_C is the mass of cells applied in grams.

Cells viability (%VC) $$\%\,VC = \frac{(VC_0 - VC_t)}{VC_0} \qquad \textbf{(II-10)}$$

Removal capacity (q) $$q = (C_0 - C_t) \times 10^{-3} \times \frac{V}{M_c} \qquad \textbf{(II-11)}$$

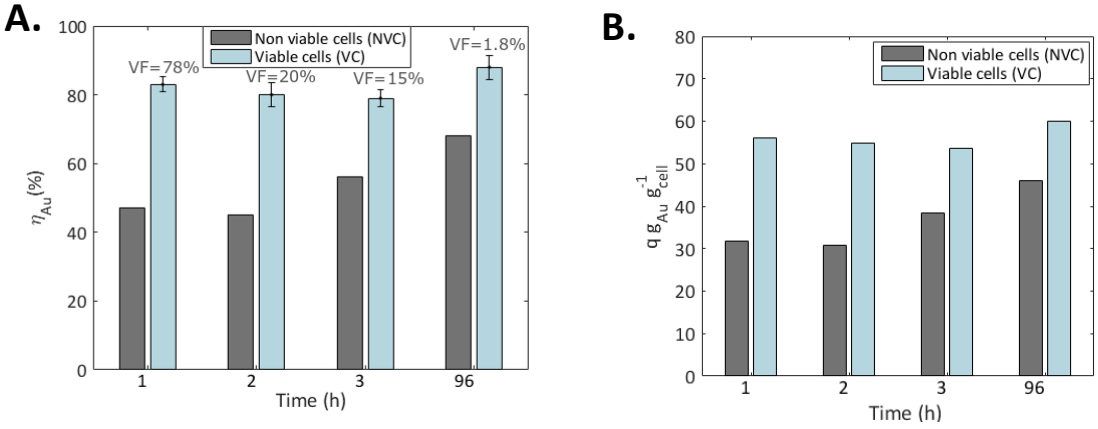

Figure II.8. Comparison between initially viable (VC) and heat-killed cells (NVC): **A**: Gold removal efficiency (η_{Au}) within time. VF values represent the percentage of remaining viable cells compared with the initial inoculated cells; **B**: removal capacity (q).

The η_{Au} of the treatment at pH 5 was 88.2 ± 3.5 %, comparable with the previous results from the DOE set-up (88.5 %). The high gold removal in the first hour followed by a slight removal during the next days has been associated with a fast biosorption followed by a slow reduction process[147]. Moreover, the control experiment with initially heat-treated cells achieved up to 67.5% removal after 4 days of incubation. The last outcome is inferred to result from the external exposure of reducing biomolecules (*e.g.*, amino acids)[148], and other sorption sites due to cell lysis occurring by the heat treatment[147]. During the first hour, initially viable cells (VC) had a removal capacity of about 55 $g_{Au}\ g^{-1}_{cell}$, considerably higher compared to the 30 $g_{Au}\ g^{-1}_{cell}$ obtained with non-viable cells (NCV). An active metabolism is therefore suspected to be involved. Within time, passive mechanisms observed in NVC have a positive effect and reach a maximum q of 47 $g_{Au}\ g^{-1}_{cell}$ after 24 h. On the other hand, active mechanisms may have considerably decreased since the quantity of viable cells decreases rapidly and could explain the possible removal capacity saturation.

Initially viable cells in presence of a soluble electron donor (*e.g.* H_2) were found to be a good substrate to catalyze the reduction of gold leading to the nanoprecipitates. Heat-killed bacteria had a reduced gold removal, and H_2 alone does not induce precipitation from abiotic $AuCl_4^-$ solutions at room temperature[135,149]. Considering this, an insoluble electron donor, *i.e.* a polarized cathode, was introduced to study the feasibility of a new bioelectrochemical system to recover gold as AuNPs.

II.2.3 Microbial electrochemical system

Set up

A two compartments reactor was set up to study the electrochemical behavior of an electrolyte solution containing gold microbial electrochemical technology (**Figure II.9**). Three reactors made of parallel Perspex frames with a with a working volume of 0.15 L per compartment were set up. A closed recirculation *via* a peristaltic pump (2.5 L h^{-1}) assured the mixing in each of the compartments.

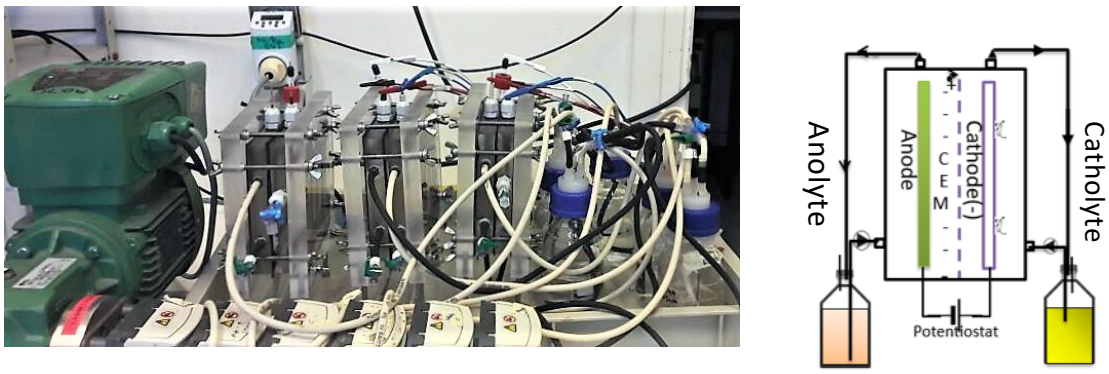

Figure II.9. Schema of the three recirculating reactors set up[150].

Reactors were placed in a temperature-controlled room at 28 °C. The catholyte aimed to replicate the microbial study case with conditions used in R5. It contained 0.2 mM Au in a 0.9 % NaCl aqueous solution, adjusted to pH 5 and purged with N_2 (Linde, Germany) for 15 minutes before the experiments. The anolyte compartment, used as sacrificial oxidizing agent, contained a 0.15 N Na_2SO_4 aqueous solution at the same anolyte pH[††]. Compartments were separated by a 64 cm^2 cation exchange membrane (CEM) from Ultrex CMI-700, Membranes International, Inc., USA.

The working electrodes were made of graphite plates (Mersem grade 1940 PT, France), with a projected surface area of 3 cm^2. These carbon based electrodes are widely used in bioelectrochemical systems for their electrochemical stability and bacterial affinity[64]. A stainless-steel mesh (AISI 316L mesh size 495 µ, Solana, Belgium) with a projected area of 10 cm^2 was used as a counter electrode. Isolated stainless-steel rods were used as current collector. An Ag/AgCl reference electrode with and electrode holder (0.205 V *vs*. SHE, 3.5 M KCl, Biologic Science Instruments, France) was placed in the cathodic compartment, where the working electrode was located. Before any experiment, reactors were washed twice with 1% v/v HNO_3. All the electrochemical experiments were controlled with a Biologic potentiostat (Model VSP, Biologic Science Instruments, France).

[††] 0.15 N Na_2SO_4 has the same normality as 0.9% NaCl. The sulphate anion in the anolyte was introduced instead of chloride present in the catholyte to avoid any chlorine production.

a. Preliminary study: Au electrochemical reduction

Cyclic voltammetry tests (CV) composed of three complete cycles were performed in a three-electrode system, with the reference electrode placed close to the cathode (working electrode). Scan rates from 5 mV s^{-1} to 20 mV s^{-1} were tested at pH 5 in abiotic conditions. The third cycle of each scan rate is displayed in **Figure II.14**.

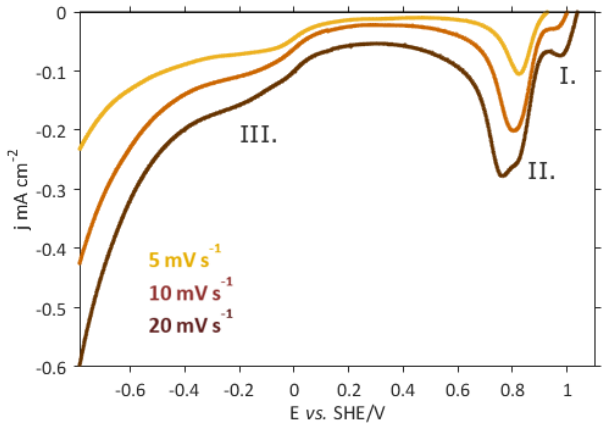

Figure II.10. One-way CV in absence of bacteria, pH=5. I, II and III represent cathodic reaction regions.

Based on Pourbaix diagram for gold in chlorine solutions (**Figure II.11**)[151], different reactions may be involved depending on the working electrode potential. A simplified list of reactions is presented in the following equations:

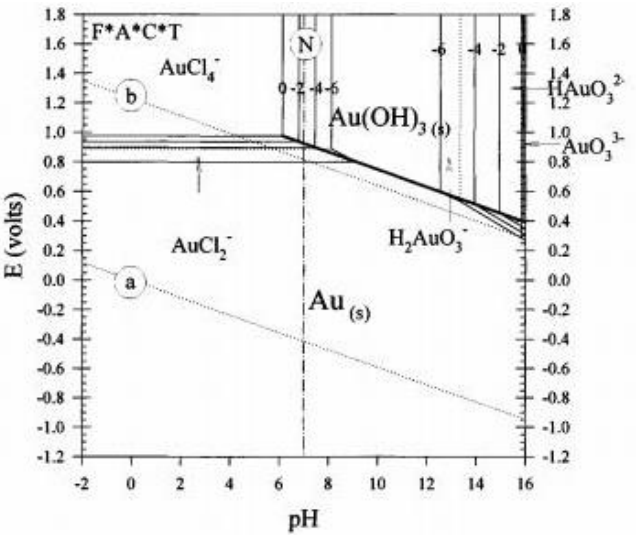

$AuCl_4^- + 2e^- \rightarrow AuCl_2^- + 4Cl^-$

$E^0 = 0.95$ V *vs.* SHE **(II-12)**

$AuCl_4^- + 3e^- \rightarrow Au^0 + 4Cl^-$

$E^0 = 0.8$ V *vs.* SHE **(II-13)**

$2H^+ + 2e^- \rightarrow H_2$

$E^0 = -0.3$ V *vs.* SHE **(II-14)**

Figure II.11. Pourbaix diagram of $AuCl_4^-$ system[152].

A first cathodic region around 1 V *vs.* SHE would fit with the partial reduction of $AuCl_4^-$ reduction to $AuCl_2^-$ (equation (**II-12**)). A second cathodic region with a considerable higher current density response predominates between 0.5 and 0.9 V. It is most likely related to zero-valent gold electrodeposition and was assumed as the main gold reduction reaction (equation(**II-13**))[151]. Both pics represent a maximum reaction rate, from which other phenomena such as gold diffusion from the bulk to the electrode vicinity become limiting. A third region at potentials below -0.3 V *vs.* SHE includes H_2 evolution (equation (**II-14**)). Once identified these regions, a polarized working electrode was explored as electron donor for gold reduction in a BES.

b. <u>BES assessment on gold recovery</u>

Experimental

Metal recovery assessment was sorted by chronoamperometry tests (CA) in abiotic and biotic conditions. A catholyte with 0.2 mM Au, pH 5 and purged with N_2 was conditioned based on the study case R5. For the biotic experiments, bacterial cells were inoculated from a fresh concentrated *S. oneidensis* MR1 stock into the catholyte at similar concentrations as in previous microbial test (OD_{610nm} =1), without provision of any additional carbon source in the system. A fixed potential of -0.3 V *vs.* SHE was applied for 72 h. Based on Nernst equation and assuming a low over potential during time, H_2 production by water electrolysis should be possible at the cathode. H_2 was therefore calculated by following Faradays law described in equation **(II-15)**. To calculate the charge related to H_2 production (Q_{H_2} in C), it was assumed that the cumulated charge (Q_{total} in C) resulted from $AuCl_4^-/Au^0$ and H^+/H_2 reactions (equation **(II-16)**). Q_{total} was defined by equation (**II-17**) and measured by the potentiostat.

$$n_{H_2} = Q_{H_2}/(z_{H^+/H_2}F) \quad \textbf{(II-15)}$$

$$Q_{H_2} = Q_{total} - n_{Au^0} z_{Au^{3+}/Au^0} F \quad \textbf{(II-16)}$$

$$Q_{total} = \int_0^{72\,h} I\,dt \quad \textbf{(II-17)}$$

Polarized cathode as electron donor for gold recovery

Gold removal efficiency (η_{Au}), the total charge (Q_{total}) and the estimated cumulated production of H_2 are presented in **Figure II.12A**. A picture of the graphite electrodes after the chrono-amperometry tests is illustrated in **Figure II.12B**.

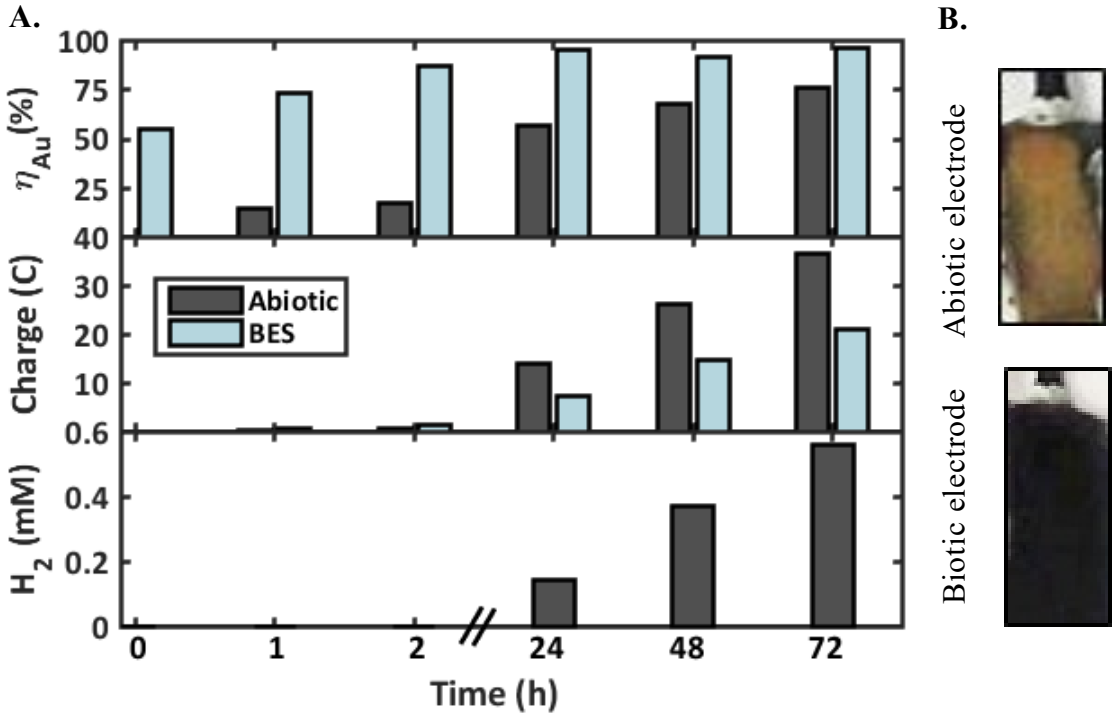

Figure II.12. Chrono-amperometry results in abiotic and biotic (BES) conditions with cathode potential fixed at -0.3 V *vs*. SHE. **A**: η_{Au}, Q_{total} and cumulated H_2 production. **B.** Graphite electrodes after the chrono-amperometry tests performed for metal recovery.

Gold removal of 55% during the first five minutes is associated to a fast biosorption as observed in the microbial system at the same conditions (**Figure II.8A**). A maximum and stable 97.1% is subsequently achieved at 24 h, which is comparable with the performance of a BES driven by a bioanode[97]. Choi *et al.* [97] recovered 98% of a 200 mg L^{-1} Au(III) solution in 12 h. The 57% electrochemically removed in the control is due to an electroreduction, considering the potential below $AuCl_4^-/Au^0$ reaction (Equation (**II-13**)). The proposed BES could combine biologic with electrochemical mechanisms to remove gold from the aqueous solution.

H_2, studied in the microbial system, has been reported as precursor of biogenic AuNPs[147,153]. Its electrochemical production *in situ* would have been interesting to investigate. However, possible H_2 buildup over time had a negligible effect over gold removal, at least during the first 2 hours. As a benchmark reference, 0.2 mM of $AuCl_4^-$ stoichiometrically requires 0.6 mM of H_2 if the redox couple ($AuCl_4^-/Au^0//H_2/H^+$) is considered (Equation (**II-13**) and Equation (**II-14**)). Gold was thus initially removed by direct interactions with bacteria combined with the cathodic environment.

Energetic balance

Q_{total} increased faster in abiotic conditions, consuming more current than biotic conditions. An energy consumption was calculated from equation (**II-18**) and presented in **Table II.5**. It consists of the product between (Q_{total}) and the cell voltage (E_{cell}):

$$E = Q_{total} \times \Delta V_{cell} \quad \textbf{(II-18)}$$

Table II.5. Bioelectrochemical configuration tests at 24 h.

Experiment	E_{cell} (V)	Q_{total} (C)	Energy (J)
Abiotic	1.7	14.2	62.3
Biotic	1.7	7.6	36.2

The energy consumption is 70% higher in the abiotic test. Considering the electrode's pictures (**Figure II.12B**), a surface change in the cathode could be responsible. The clear gold electrodeposition observed in the abiotic electrode can enhance the catalytic properties of the electrode[122,154], increasing the exchanged current. However, at 72 h 96% was BES this modified electrode didn't enhance the metal removal, thus promoting energy losses. Likewise, suspended *S. oneidensis* MR1 cells attaches relatively fast on polarized carbon surfaces (*e.g.* mediated by secreted redox species like flavines[61,155]). Gold bio-sorption could also play a role in the electrochemical reduction. Further tests varying the concentration of bacteria and gold ions are recommended to elucidate the metal-bacteria-electrode interactions. Finally, if this process was scalable to 1 kg of metal, the energy required would be of 8.8 MJ kg^{-1} for the abiotic and 3.7 MJ kg^{-1} for the biotic conditions. 208000 MJ kg^{-1} has been reported as the energy to produce 1 kg Au by

conventional techniques[10], but it takes into account extraction and separation steps that here are not considered.

Post-experiment AuNP characterization

The metal removal assessment was followed by a TEM characterization on the bacterial cells (description in **Annex 1-B**). Results are displayed in **Figure II.13**.

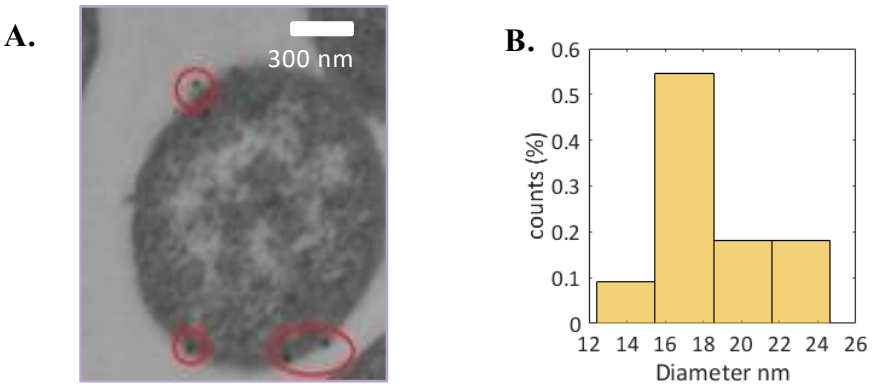

Figure II.13. A. TEM of *S. oneidensis* MR-1 after 72 h; **B**. AuNPs size distribution in counts.

AuNPs observed attached in the surrounding of the bacteria had an average size of 18 ± 2.7 nm (**Figure II.13A**). They were smaller and less dispersed, compared to non-electrochemical mediated biosynthesis (**Figure II.4**). Suggested reasons of this variations presumably include: (i) faster kinetics could induce smaller AuNPs[149], (ii) a modified electron donor transfer may influence the NPs size[135]. Nevertheless, in this BES, bacterial cells could be considered as capping agents and nucleation sites needed for NPs synthesis[34,156,157].

Complementary gold diffusion analysis

Check-up CVs from 120 mV s^{-1} to 1 mV s^{-1} were performed in abiotic conditions, before and after the chronoamperometry tests previously presented (**Figure II.12**). Results at t_0 and t_{72h} are displayed in **Figure II.14A** and **Figure II.14B** respectively. From these, a linear behavior was obtained between the cathodic current peaks (i_p) and the square root of the scan rate ($\upsilon^{1/2}$) (**Figure II.14**C and **Figure II.14**D).

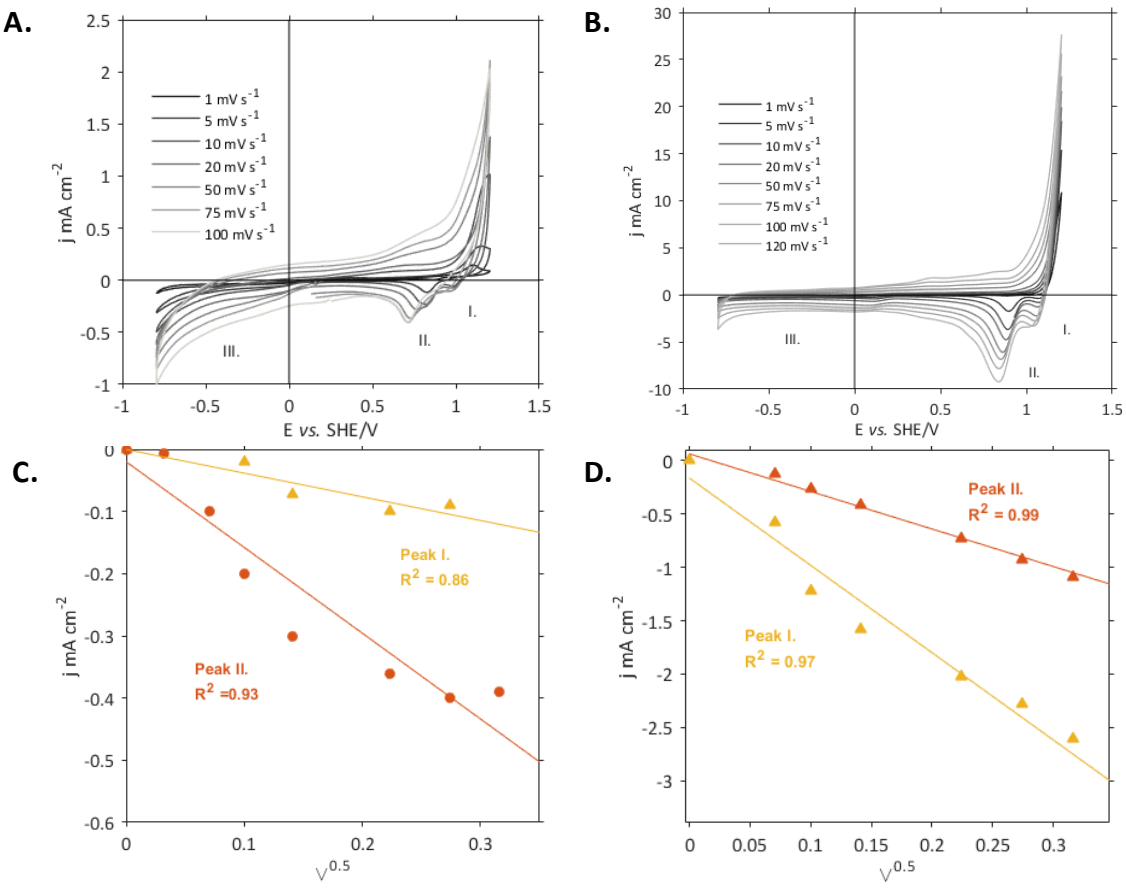

Figure II.14. Electrodynamic analysis of catholyte at initial conditions: 0.2 mM Au^{3+} in 0.9% NaCl at pH = 5, 28 °C. (**A**.) CVs before the potentiostatic test (t_0) on the graphite electrode. I, II and III represent cathodic reaction regions; (**B**.) CVs after the potentiostatic test (72 h of chronoamperometry at -0.3 V *vs.* SHE) on the resulting graphite electrode; Linearity of current peaks (j) with the square root of the scan rate ($\upsilon^{0.5}$) at t_0 (**C**) ; and at 72 h (**D**).

The cathodic current response increased at the end of the chronoamperometry experiment. For instance, the region II increased the cathodic current peak about 10 from t_0 to t_{72h}. Irreversible reactions are present (*e.g.* gold electrodeposition), since the reduction peaks shifts with the scan rate and the flatted oxidation peaks have a reduced current response[158]. Based on the linearity between i_p and $\upsilon^{1/2}$, a simplified estimation of the diffusion coefficient (D_0) for reactions $AuCl_4^-/AuCl_2^-$ and $AuCl_4^-/Au^0$ was calculated following the Randles-Sevcik equation (Equation (**II-18**)). n represents the number of electrons exchanged, A the electrode area and C_0^* the gold (III) chloride concentration in the bulk. D_0 values are presented in **Table II.6**. The R^2 represents the linearity of the I_p vs. $\upsilon^{1/2}$ relationship, and n the number of taken points.

$$i_p = 2.69x10^5\ n^{3/2}\ A\ D_0^{1/2}\ C_0^*\ \upsilon^{1/2} \quad \textbf{(II-19)}$$

Table II.6. D_0 and Randles-Sevcik linearity calculated in abiotic conditions.

Time (h)	D_0 (cm^2 s^{-1})		R^2 (%)	
	$AuCl_4^-/AuCl_2^-$	$AuCl_4^-/Au^0$	$AuCl_4^-/AuCl_2^-$	$AuCl_4^-/Au^0$
0	2.2×10^{-8}	$9.8. \times 10^{-7}$	0.86 (n=5)	0.93 (n=8)
72	1.1×10^{-7}	2.0×10^{-6}	0.99 (n=8)	0.97 (n=8)

D_0 values are subject to reversible reaction considerations but the magnitude order at t_0 are similar to other studies[154,159]. The considerably increase of D_0 (5-fold for $AuCl_4^-/AuCl_2^-$ and 2-fold for $AuCl_4^-/Au^0$) relies on the electrode surface modification since gold was clearly electrodeposited on the cathode surface. Despite this raised diffusion coefficient in the electrode, the gold removal was lower than in biotic systems. Gold mass transport is not necessarily enhanced within time, as it depends on D_0 as well as the metal concentration in the bulk, the electrostatic potential and the convective transport[160]. The diffusion coefficient is often a limitation for electrochemical metal removal from diluted solutions[161,162]. Electrodes properties, reactor designs and electrolytic baths have been studied to promote the metal removal[163,164]. Here, the use of suspended bacteria as supporting agent opens a new route for bioelectrochemical systems.

II.2.4 To sum up

A screening study confirmed the use of initially viable cells as substrate for gold removal and AuNP synthesis. pH and metal concentration were process-driven factors for high metal yield, whereas pH and oxygen degassing could be significant for the synthesis of 50 nm AuNPs. Considering a solution containing 0.2 mM Au, at pH 5, anaerobic conditions and a in presence of H_2 as electron donor, a maximum gold efficiency of 88.5% and AuNPs of 43 ± 13 nm were obtained after 72 h. *S. oneidensis* MR-1 and *C. metallidurans* CH34 mediated AuNPs formation

located either on their outer membrane, on the periplasmic space and/or intracellularly.

The introduction of a cathode as electron donor catalyzed the gold reduction up to 95% in 24h and allowed the bio-synthesis of 18 ± 2.7 nm AuNPs. Considering that the cells integrity diminished very fast, a passive mechanism was the first responsible of metal sequestration on the bacterial biomass. The use of an electron donor on initially viable bacteria enhanced the removal efficiency and contributed to the metal reduction and nanoparticle synthesis. Nevertheless, active mechanisms on viable cells would require maintaining the cells integer despite their environment. The proposed bioelectrochemical system accelerates the metal reduction without compromising the synthesis of AuNPs. The requirement of hydrogen for NPs formation in BES should be further corroborated by varying the fixed cathode potentials. Overall, BES can offer a great potential for recovering and valorizing metals from waste streams in a controlled system.

II.3 Chromium recovery

II.3.1 Context

Chromium is one of the most common ubiquitous metal pollutants in the environment. Its hardness, corrosion resistance and intense color variety are highly valorized in stainless steel alloys, leather tanning and pigments[165]. Unfortunately, the anthropogenic activities related to the usage of Cr such as mining and industrial processes are responsible for most of environmental contaminations and human exposure[165]. Chromium-laden waste streams from these processes are a real threat for the environment. In industrial wastes it is usually presented in its hexavalent form Cr(VI), which is known to be very toxic for plants and animals at high concentrations due to its high solubility, mobility and oxidizing potential. Besides, Cr(VI) is classified as human carcinogen by regulatory and non-regulatory agencies[165].

Cr recovery from aqueous solutions is therefore a real environmental and healthy challenge. Considering that Cr(VI) solubility is substantially high (*e.g.*, $Na_2Cr_2O_7$ = 2355 g L^{-1} at 20 °C), Cr(VI) removal is often focused on reducing it into its less soluble form Cr(III)[166]. In comparison of other methods (*e.g.* chemical precipitation, electrodeposition), the natural biological processes have the advantage of working in mild conditions of temperature, pH, and pressure (*i.e.* 25°C, pH 7 and 1 bar). Cr(VI) has a high mobility in water and soil, making the uptake by microorganisms (prokaryotic and eukaryotic cells) very accessible[167]. Besides, Cr(VI) bio-reduction seems to be very stable against re-oxidation[168]. Moreover, usually the biological species are indigenous species, which have access to all nutrients for their growth in their native environments. Microbial interactions with Cr(VI) may involve biosorption, intracellular accumulation, redox immobilization, among others. The (bio)synthesis of these precipitates as added-value functional materials have been rarely discussed. Chromium oxide nanoparticles Cr_2O_3 for instance have been reported as promising anode material for lithium ion batteries due to its high theoretical capacity (1058 mAh g^{-1}) and relatively low operating voltage compared to other transition metals[169]. The

synthesis of bacterially-induced metallic NPs as catalysts for electrodes materials appears as an eco-friendly and scalable method.

II.3.2 Microbial system assessment

a. DOE matrix

Experimental

Inspired on the previous DOE for gold, a Cr recovery screening was evaluated with a 1/8 fractional factorial design matrix (Resolution III, 2^{7-4}). 7 factors with two levels each were selected to evaluate the Cr removal efficiency (η_{Cr}) (**Table II.7**).

Table II.7. Orthogonal experimental design matrix applied for 2^{7-4} DOE

Experimental order	Factor						
	Medium	***[Cr] mg L^{-1}***	**Microaerophilic /aerobic[c]**	***pH***	***OD$_{610}$***	***e-donor***	***cell-type***
1	NaCl	15	Microaerophilic	2	1.3	H_2[a]	CH34
2	M9	75	Microaerophilic	2	0.65	Lactate[b]	CH34
3	NaCl	15	Aerobic	2	0.65	Lactate[b]	MR-1
4	M9	75	Aerobic	2	1.3	H_2[a]	MR-1
5	M9	15	Microaerophilic	7	0.65	H_2[a]	MR-1
6	M9	15	Aerobic	7	1.3	Lactate[b]	CH34
7	NaCl	75	Microaerophilic	7	1.3	Lactate[b]	MR-1
8	NaCl	75	Aerobic	7	0.65	H_2[a]	CH34

[a] *Lactate concentration = 10 mM*

[b] *H_2 in saturation (≈0.9 mM at 25°C)*

[c] *The specific composition of the corresponding headspace is further detailed in* **Table II.8**.

Serum bottles (120 mL) were filled with 50 mL of metal solution containing 0.15 N NaCl at the metal concentration specified in the DOE. Metal solutions were prepared from a potassium dichromate ($K_2Cr_2O_7$) stock solution of 5 g L^{-1} Cr, which allowed to maintain a systematic protocol. pH was adjusted with either NaOH or HCl and bottles were plugged with thick butyl rubber stoppers and sealed with an aluminum crimp. Reactors were then autoclaved at 121ºC for 21 min. Air or N_2 headspace was set according to conditions described by the matrix and measured by gas chromatography (description in **Annex 1-E**). Electron donors were supplied, either to the solution (sodium lactate to 10 mM) or at the headspace (H_2 gas at saturation, ≈ 0.9 mM at 25°C). Initial gas conditions are presented in **Table II.8**.

Table II.8. Average headspace conditions at the beginning of the experiments.

Condition	N_2 (%)	O_2 (%)	H_2 (%)
Aerobic	78	21	0
Microaerophilic	97.6	2.4	0
Aerobic + H_2	30.9	8.4	60.2
Microaerophilic + H_2	34.1	1.7	62.5

The total balance of the gas composition is not necessary 100%, due to an intrinsic error of the gas chromatograph detector. The electron donor consumption was calculated as initial difference between the initial and final H_2 concentration, divided by the initial H_2 concentration. Cells were finally inoculated according to **Table II.7** and reactors placed on a 28°C incubator at with a rotatory shaker (KS 400i, IKA, Germany) set at 120 rpm.

A mass balance estimation of chromium is given by Equation **II-20**. It considers the initial total Cr ions (Cr_0) measured by ICP, the $Cr(VI)_{\text{in sol.}}$ measured by UV-vis (**Annex 1-C**). Cr_t represents the filtered samples taken at different times and measured by ICP. Considering the closed system and the high solubility of Cr(VI), the total Cr removal from the solution is assumed to be retained by bacteria (Equation **II-21**). Finally, residual Cr ions that are no longer in its hexavalent form but were not removed from the solution ($Cr_{\text{reduced in sol.}}$) are deduced from the mass balance.

Mass balance $$Cr_0 = Cr(VI)_{in\ sol.} + Cr_{reduced\ in\ sol.} + Cr_{bacteria} \quad \textbf{(II-20)}$$

Where $$Cr_{bacteria} = Cr_0 - Cr_t \quad \textbf{(II-21)}$$

Chromium removal efficiency was calculated as the difference between the initial and final metal concentration, divided by the initial concentration (Equation **I-3)**. Total Cr concentration at the beginning of the experiment (t_0), at 1 h and 96 h were evaluated by ICP (description in **Annex 1-A**). Cr(VI) removal (η_{Cr}) was also evaluated over time and the Cr(VI) removal efficiency ($\eta_{Cr(VI)}$), given by equation (**II-22**)).

$$\eta_{Cr(VI)} = \frac{Cr_0 - Cr(VI)_{in\ sol.}}{C_0} \quad \textbf{(II-22)}$$

Post-DOE characterization

After the experiments, cells were characterized by TEM (description in **Annex 1-B**) and compared to cells controls that in absence of chromium (**Figure II.15**).

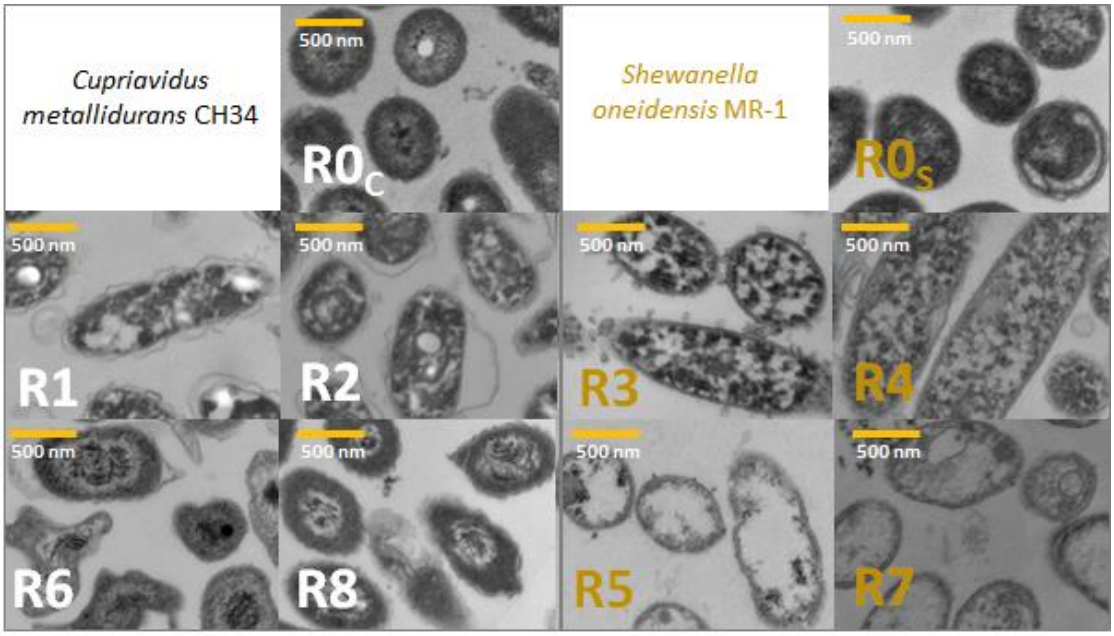

Figure II.15. TEM results for each of the reactors. R0c and R0s represent bacterial controls without metals for CH34 (white) and MR-1 (yellow), respectively.

The bacterial before exposition to Cr were set as controls (*R0C* and *R0S*), which show rounded and bacillus shapes, the last typical of the strains employed with variations that could arise due to the different stage of the cells. *C. metallidurans* CH34 at pH 2 and microaerophilic conditions (R1 and R2) exhibited a damaged external membrane and swollen inner parts. The acidic pH stress of this strain has been already sensed in its cell membrane without modifications on its size or shape[170]. Interestingly, this strain at pH 7 (R6 and R8) showed ultrastructural damage with clear variations in their morphology as an atypical stress response. Considering that both had an oxygen presence, a stress by intracellular oxidative events could explain these shape variations[170]. *S. oneidensis* MR1 in R3 and R4 kept the membrane intact despite the pH 2 and aerobic conditions in the experimental set-up. Nevertheless, the cells are not viable for active Cr(VI) removal mechanisms since the concentrations are above the Minimum Inhibitory Concentration (MIC for *S. oneidensis* MR1=0.05 mM)[171]. It is therefore important to differentiate between integer cells, *i.e.* with intact cell membranes, and viable

cells, which can normally reproduce themselves. Finally, at pH 7 and microaerophilic conditions (R5 and R7), *S. oneidensis* MR1 cells showed a higher contrasting in black electron-dense segregated particles resembling Cr precipitates, *i.e.*, presented as spheres adsorbed on the external surface or cumulated inside the nucleus. *S. oneidensis* has already been reported to form similar precipitates, identified extracellularly[172] and intracellularly[173] by means of TEM micrographs. They can be originated from by direct blockage of the uptake system, or by an active resistance mechanism involving a chromate efflux from already assimilated Cr inside the cell[171,174].

DOE results in terms of total Cr and Cr(VI) removal

Following on, the performance of the microbial system was evaluated for 96 h *via* the maximum metal recovery efficiency (η_{Cr}) and presented in **Figure II.16A**. The relative abundance of Cr in the reactors at 96 h is presented in **Figure II.16B.**

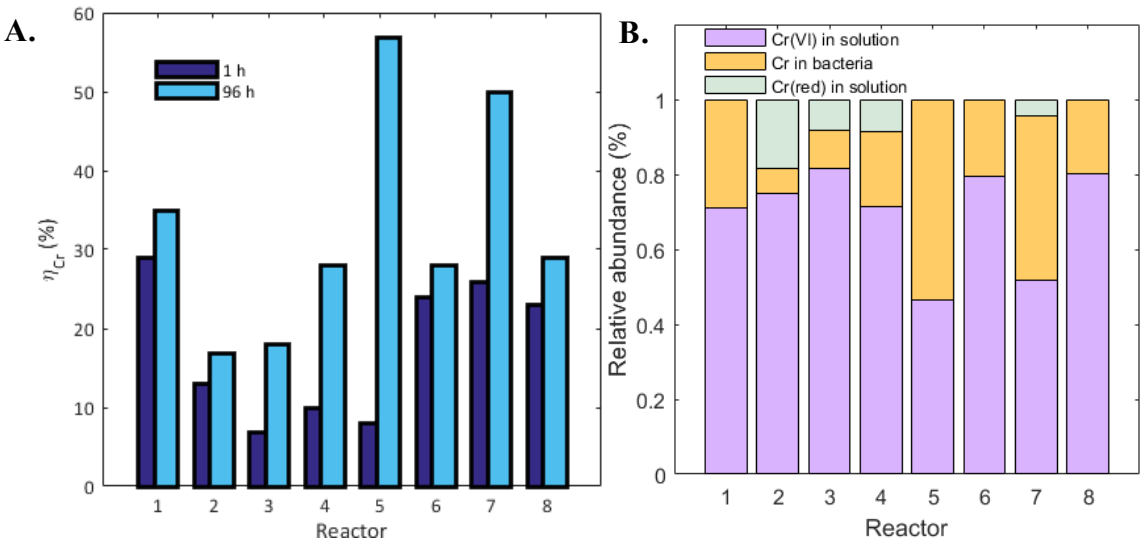

Figure II.16. A: Total Cr removed from the aqueous solution; **B**: Relative abundance of Cr elements in reactors at 96 h.

A Cr removal efficiency above 25% in 1 h was observed in most of experiments with C. *metallidurans* CH34 (*e.g.* R1, R6 and R8), which is relatively high compared to the other experiments conducted (**Figure II.16A**). After 96 h, these reactors only increased chromium removal at about 5% more from the first hour. Experiments with *S. oneidensis* MR-1 (R3, R4, R5 and R7) had a pronounced increase in chromium removal between 1 h and 96 h. A progressively accumulation of Cr inside the cell has been previously reported[168]. R5 in particular

had 53.5% of Cr removal with a low cell concentration of *S. oneidensis MR-1,* initially exposed to 15 mg L^{-1} Cr(VI), at pH 7, in microaerophilic conditions and presence of H_2. This represented the highest recovery value among all other tested conditions. As Cr ions are removed from the aqueous solutions by interactions with bacteria, it is suggested that *S. oneidensis MR-1* had a better performance against C. *metallidurans* CH34.

Based on the estimated mass balances, the conditions stablished in the DOE were not very promising as most of the reactors had more than 50% Cr(VI) remaining in the solution (**Figure II.16B**). Nevertheless, there were important differences in the Cr distribution on each reactor at the end of the experiments. R5 and R7 had the highest Cr microbial uptake, both in a microaerophilic environment, at pH 7 and with *S. Oneidensis* MR1 inoculated. The remaining Cr was found as Cr(VI), suggesting that either Cr was not necessary reduced or that the reduction involved Cr immobilization by the bacterial cellular matrix. Most of the trials with lactate as electron donor (*e.g.*, R2, R3, R7) showed a fraction of Cr reduced in solution. Lactate is a known reducing agent for Cr(VI) reduction[172], which doesn't imply Cr precipitation but at least reduces its solubility and toxicity[175].

Statistical analysis

The statistical analysis regarding the effect of each factor on the chromium removal as variable response is presented in **Figure II.17**.

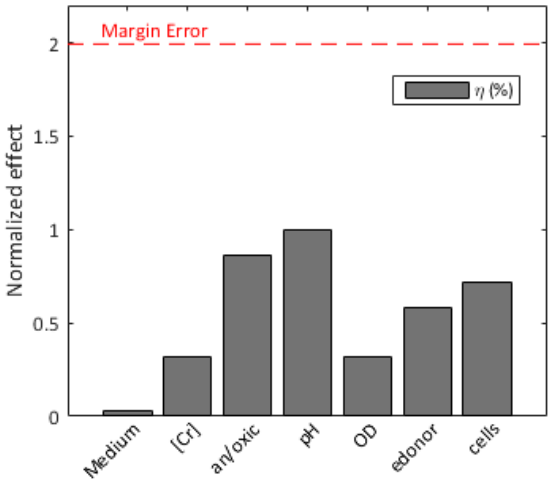

Figure II.17. Effect of each factor for response variable η_{Cr}. Values are normalized by the most significant effect, in this case is the pH.

Lenth's method for non-replica analysis showed that the margin error has a higher effect compared to the chosen effects at the studied conditions. This suggests that from the DOE matrix (**Table II.7**), there are no effects that stands out over others. Further studies in replicates for DOE or surface response methodologies should be extended for statistical analysis of the effects here illustrated. An ANOVA analysis was therefore performed to identify the main effects on the η_{Cr} (**Table II.9**).

Table II.9. Main effects for maximizing η_{Cr}. Results are given in absolute values.

Variance analysis	max(η)			
	Anoxic/oxic	pH	OD	Cells type
SS group	-4.97	6.19	5.65	-3.68
SS Error	0.05	0.05	0.05	0.05
p-value	0.006	0.005	0.005	0.008

Based on the SS group results, anoxic conditions (level -1), pH 5 (level 1), an OD_{610nm} = 1.3 (level 1) and the presence of *S. oneidensis* MR-1 (level), maximized the chromium removal. The choice between H_2 or lactate as electron donor was not relevant, neither the Cr concentration nor the medium. Besides, the sum of squares of errors represented only 1% of the total variation and p-values were lower than a significance level (5%). A second DOE with these four factors and a higher resolution could be interesting to formulate an empiric model. To complement the analysis, pH, conductivity and e- donor evolution for each of the trials were also measured (**Table II.10**).

Table II.10. pH, conductivity (σ), H_2 or lactate evolution from the DOE. NaN were not measured values.

Reactor	pH		σ mS cm^{-1}		% η_{ED}
	0 h	96 h	0 h	96 h	96 h
1	2.06	2.03	22.4	22.8	13
2	1.95	NaN	16.82	NaN	29
3	2.06	2.04	21.5	22.6	19
4	2.06	NaN	15.53	NaN	7
5	6.90	7.00	9	10.5	13
6	6.93	6.99	8	9.9	47
7	6.91	NaN	17.70	NaN	33
8	6.91	NaN	17.30	NaN	13

From these results, it is inferred that bacteria participated in the Cr(VI) removal without expressing any significant pH or conductivity change. The use of initially intact bacteria in their stationary phase pose an advantage against other techniques, as chromium was removed by this *"biological reagent"* which occupy rather smaller volumes, thus, reducing sludge post-treatment compared to a direct chemical Cr precipitation. The e^- donor consumption firstly shows that they were not completely depleted and therefore interpretated as no-limiting factors. H_2 consumption is relatively similar in R1, R4, R5 and R8, whereas lactate consumption is relatively higher in R6 (47%) compared to R2, R3 and R7.

b. Study case based on R5 conditions

Further tests were carried on based on conditions of R5, as it showed the highest Cr(VI) removal with presumable presence of nano-precipitates: *S. oneidensis MR-1* (equivalent OD_{610nm}=0.65), 15 mg L^{-1} Cr(VI), at pH 7, in microaerophilic conditions and presence of H_2. Duplicates and abiotic and heat-killed controls were analyzed. η_{Cr}, $\eta_{Cr(VI)}$, cells integrity measured by flow cytometry (description in **Annex 1-D**), and H_2 consumption were followed. Electron donor consumption (η_{ED}) was calculated based on the same principle (description in Equation **II-23**), where ED_0 and ED_t are the electron donor concentration at the initial and final sampling of the experiments. They were measured by either by the HPLC in the case of lactate (**Annex 1-G**), or by the relation between the gas composition and Henry's Law for the H_2.

Electron donor consumption $\eta_{ED} = (ED_0 - ED_t)/ED_0$ - **(II-23)**

Chromium removal efficiency (η_{Cr}), Cr(VI) removal efficiency ($\eta_{Cr(VI)}$), cells integrity and H_2 consumption are presented in **Figure II.18**.

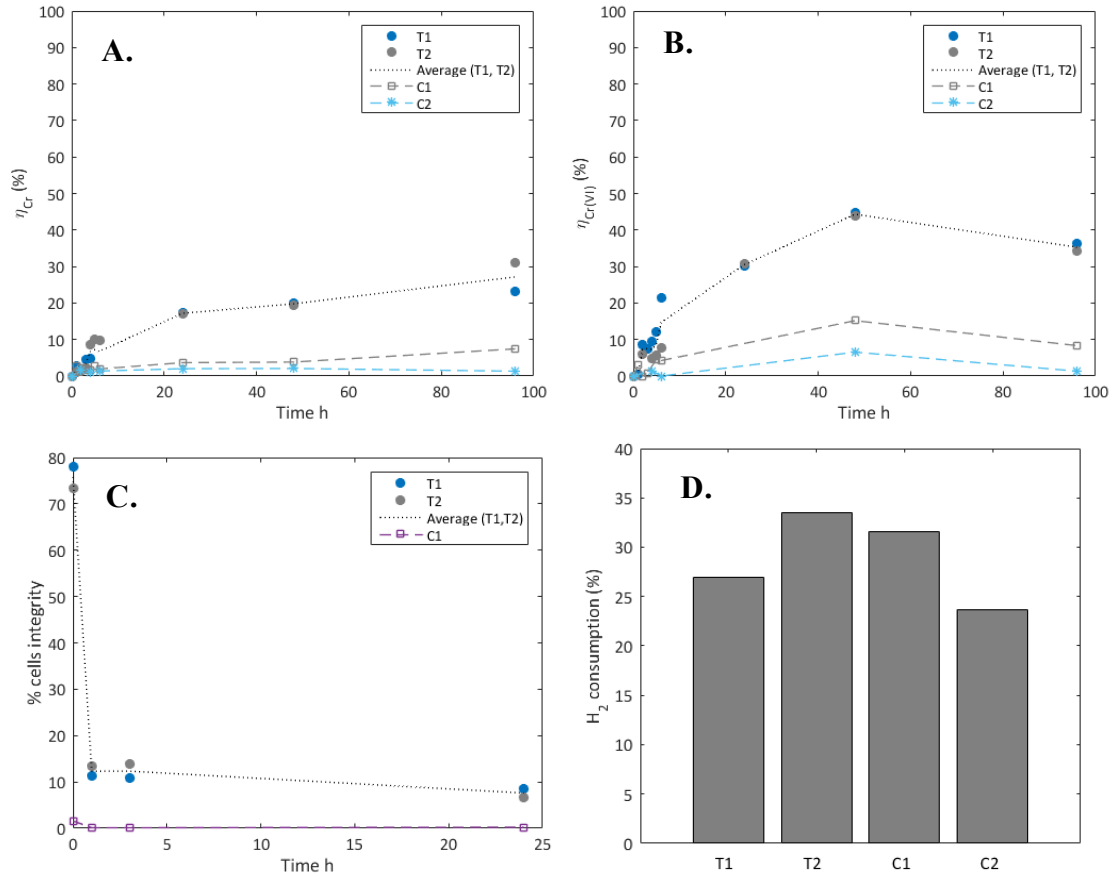

Figure II.18. A: chromium removal efficiency evolution; B: Cr(VI) removal yield; C: cells integrity; D: e- donor consumption at 96 h. Conditions: 15 mg L^{-1} Cr, microaerophilic, pH 7, H_2 presence and OD_{610}=0.65. T1 and T2 represent replicates and media the average tendency, C1 the heat-killed cells control and C2 the abiotic control.

Dynamic Cr removal in conditions of R5 in duplicates (T1, T2), compared with heat-killed cells (C1) and abiotic controls (C2), is presented in **Figure II.18A**. Duplicates with a difference of achieved a maximum removal efficiency of 31% at 96 h, lower than the expected from the DOE (53.5%). The intense samplings could be responsible of variations on the system, *e.g.* hydrogen release, pressure and volume change. In addition, the abiotic control removed only up to 2% Cr, suggesting that H_2 alone was not the main driving agent. A limited removal (<10%) was observed using heat-killed cells, confirming an active part by the initially viable cells. The transport of dichromate ions has been previously reported for *S. oneidensis* MR-1 when initially active cells were tested[174]. Cr(VI) efflux pumps have been identified in active mechanisms such as detoxifying reactive oxygen species, repairing of DNA lesions, sulfur metabolism, and iron homeostasis[176,177].

Cr(VI) removal ($\eta_{Cr(VI)}$) presented in **Figure II.18B** shows that duplicates (T1 and T2) had a relatively fast reduction within the first 24 hours, followed by a pseudo stabilization. This is a common behavior from sorption agents, where metal pollutants attach to the surface of dead, inactive or live biomass[167]. Initially viable cells would be suitable considering the low removal rate of Cr(VI) in presence of heat-killed cells (C1) and in absence of bacteria (C2). H_2 can eventually act as reducing agent at high temperatures, but heat-killed cells are probably better to avoid as the heat treatment disintegrates the binding sites of cells, limiting drastically the metal sorption.

The cells integrity behavior displayed in **Figure II.18C** reveal a drastic decrease on the percentage of integer cells during the first hours, most likely related to the toxic effect of Cr(VI). In viable cells, Cr(VI) crosses easily biologic membranes through non-specific anionic channels predominately as an chromium anion (*e.g.* CrO_4^{2-})[175]. Once inside the cells, Cr (VI) is rapidly reduced by several cellular reductants (*e.g.* glutathione, ascorbate and cysteine)[175]. Consequently, unstable Cr forms such as Cr(V) and Cr(IV) as well as the stable Cr(III) are produced at the intracellular level. These oxidation states of Cr are able to bind to proteins and DNA, causing gene mutations, chromosomal aberrations, altering the normal cell cycle and inducing genes responsible for cells auto-destruction, also called apoptosis[175]. Mostly non-integer cells would be therefore responsible for the subsequently total Cr and Cr(VI) removal. A passive mechanism is therefore suggested as main mechanism after the first hours of experiments.

Finally, H_2 calculated consumption is presented in **Figure II.18D**. Duplicated treatments consumed 27% and 33% respectively, confirming that the electron donor was not a limiting factor. However, C1 and C2 controls used 31% and 24% of H_2 respectively. Sampling effect and the H_2 volatility despite the hermetic conditions could be responsible of such variations. Even if H_2 has been speculated to play an important role for metal reduction[178], the resulting H_2 consumption is not representative to confirm its effect on the Cr reduction.

Post-experiments analysis

Raman experiments on bacterial cells were performed to characterize the CrNPs (description in **Annex 1-H**). Raman spectroscopy results from bacteria after the study case based on R5 conditions are presented in **Figure II.19**.

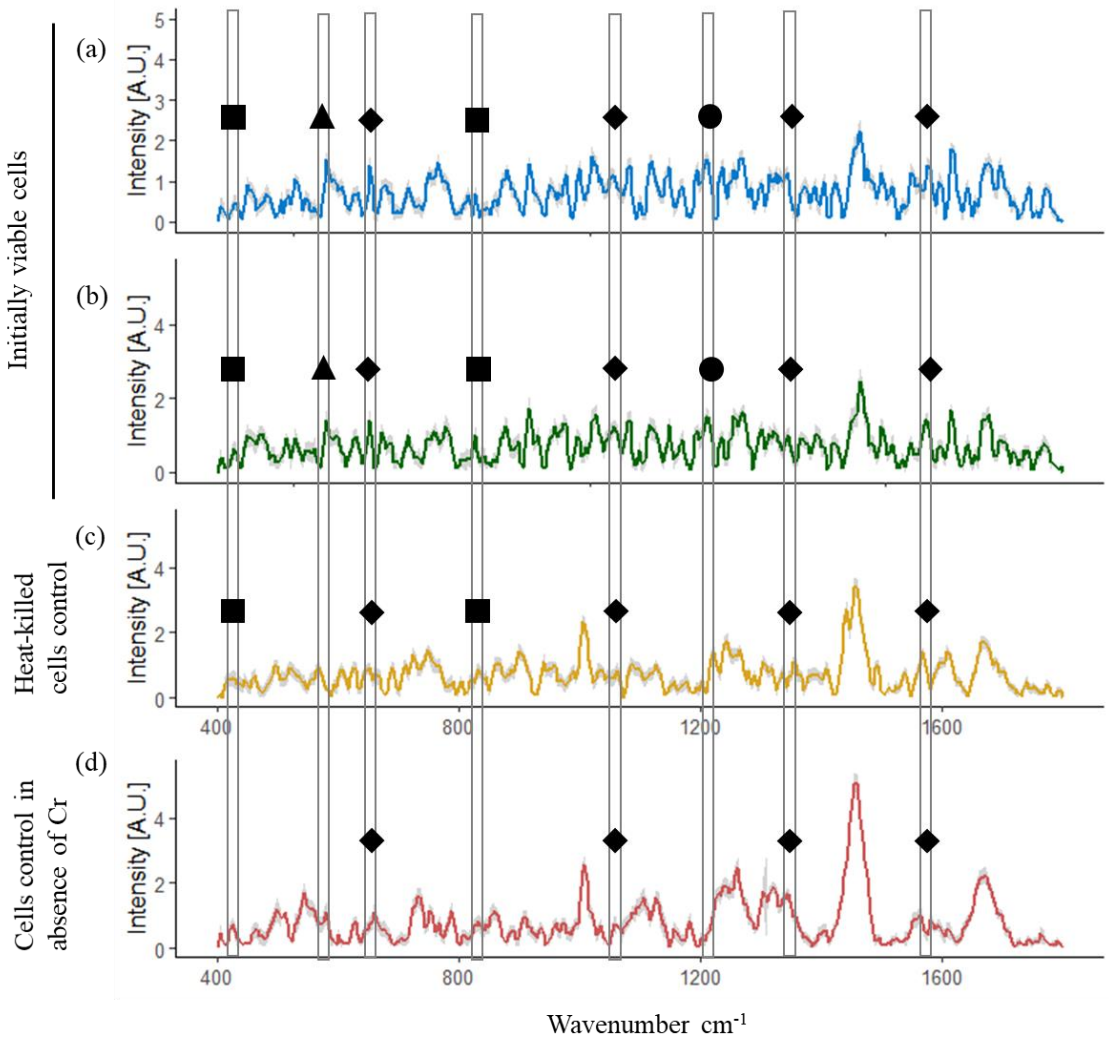

Figure II.19. Based on R5 conditions, Raman spectra for: (a) initially viable *S. oneidensis* MR1 in presence of chromium, (b) duplicate, (c) control with initially heat-killed cells in presence of chromium. (d) control with *S. oneidensis* MR1 in absence of Cr. ▲ = Cr(III), ◆ = Cytochrome – c, ■ = Cr(VI), ● = glycine.

A detailed list of fitted peaks is presented in **Annex 2-B**. Raman spectra of bacterial cells usually contain several peaks corresponding to carbon-carbon bounds (C-C), *e.g.* lipids, nucleic acids, DNA and amides[173]. Here, characteristic peaks of: Cr(VI) at 845 cm^{-1} and Cr(III) at 605 cm^{-1} were observed in the

spectra[173]. Cr(III) oxides could be interesting products as precursors for anodes in lithium ion batteries[169], but this technique is unfortunately limited by the poor signal of chromium compared to the bacterial cell. Clearer CrNPs peaks were previously observed in S. *oneidensis* by adding AuNPs on the cell surface before the Raman treatment[173]. If Cr(III) presence is confirmed in initially viable cells, a resistance mechanism would be responsible of the bio-reduction. It starts by a bacterial chromate uptake through sulfate transporters, which occurs due to the structural similarity of chromate and sulfate ions[173]. Once inside the cells, Cr (VI) is rapidly reduced by several cellular reductants as a resistance mechanism (*e.g.,* glutathione, ascorbate, cysteine and glycine)[179]. Characteristic peaks of glycine were indeed identified in initially viable cells spectra. Cytochrome-c, also identified by Raman, has been associated with Cr(VI) in *Shewanella* species[168]. Consequently, unstable Cr forms such as Cr(V), Cr(IV), and Cr(II), as well as the stable Cr(III), could be produced intracellularly[168]. These oxidation states of Cr can bind to proteins and DNA, causing gene mutations, chromosomal aberrations, altering the normal cell cycle and inducing genes responsible for the auto-destruction of cells, *aka* apoptosis[180]. The toxic effect of Cr(VI) would be definitely a problem to keep an active reduction mechanism. Therefore, the use of a cathode as electron donor for Cr abiotic reduction becomes interesting.

II.3.3 Microbial electrochemical chromium assessment

Set up

The microbial electrochemical configuration to evaluate Cr removal used the parallel Perspex frames reactors previously described (**Figure II.9**). Catholyte conditions were based on the microbial experiment R5: *S. oneidensis MR-1* (equivalent OD_{610nm}=0.65), 15 mg L^{-1} Cr(VI), at pH 7, in microaerophilic conditions and presence of H_2. The catholyte was firstly sterilized at 121°C for 21 min and purged with N_2 (Linde, Germany) for 15 minutes. Planktonic cells were inoculated into the catholyte from a concentrated bacterial stock in sterile conditions without provision of any additional carbon source in the system. The anolyte consisted of a 0.15 N Na_2SO_4 aqueous solution, at a set pH similar as in the cathodic compartment (adjusted with 1 M H_2SO_4 or 1 M NaOH). Anode and cathode were composed of a stainless-steel mesh (AISI 316L mesh size 495 µ,

Solana, Belgium), with a projected surface area of 4.8 cm^2. Electrodes were separated by a 64 cm^2 cation exchange membrane (CEM, Ultrex CMI-700, Membranes International, Inc., USA).

Recirculation of the cathodic and anodic electrolytes was set at 2.5 L h^{-1} to assure enough mixing in both compartments. It is worth mentioning that corrosion of the stainless-steel current collectors was not observed during the experiments, likely due to the low current densities achieved and circumneutral pH values. Applied potentials and electrochemical analysis were controlled with a potentiostat (Potentiostat/Galvanostat Model VSP, Biologic Science Instruments, France).

a. Abiotic electrochemical characterization of chromium

A catholyte mimicking the experimental conditions of R5, *i.e.*, 15 mg L^{-1} Cr(VI), pH 7, microaerophilic environment was firstly characterized through CV measurements. Cyclic voltammetry tests (CVs) from 120 mV s^{-1} to 1 mV s^{-1} were recorded, between the cathode and reference, to identify abiotic electrochemical reactions (**Figure II.20**).

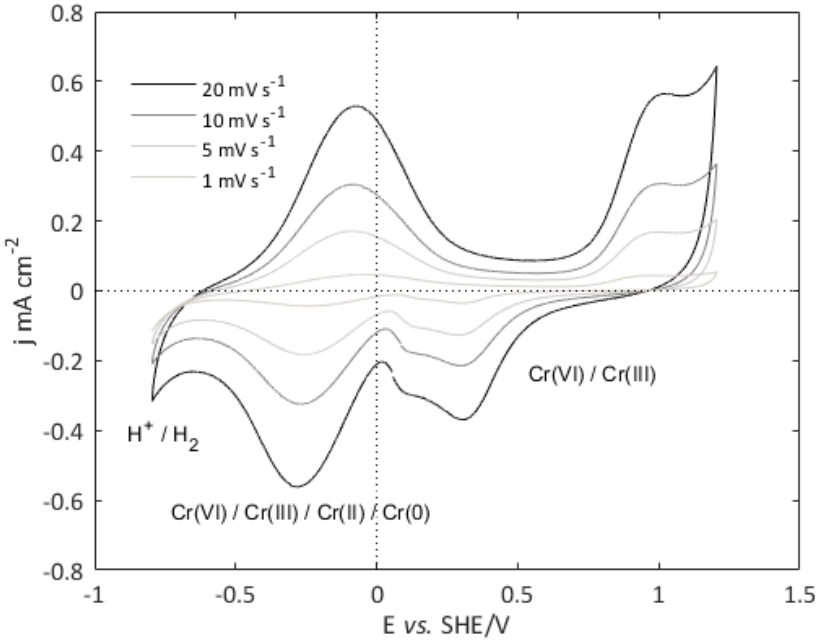

Figure II.20. CV on stainless steel cathode in absence of bacteria. Catholyte: 15 mg L Cr in M9 medium, pH 7, 28° C, recirculation 2.5 L h^{-1}. Anolyte: 0.15 N Na_2SO_4.

Three well-defined regions corresponding to electrochemical reactions are perceived from 20 mV s^{-1} to 1 mV s^{-1}. Cr reduction has however a very complex electrochemistry, with at least 55 possible reactions as defined by the Pourbaix diagram of Cr in an electrolyte containing chloride ions (**Figure II.21**)[152]. According to the Cr ionic speciation (**Annex 2-B**)[181], the soluble Cr(VI) ion from the dichromate salt has a preferential speciation of $HCrO_4^-$ and CrO_4^{2-} anions at neutral pH. $Cr_2O_7^-$ anions are mostly present in acidic conditions[181]. Based on these ions, a series of possible electrochemical reactions is summarized in **Table II.11**.

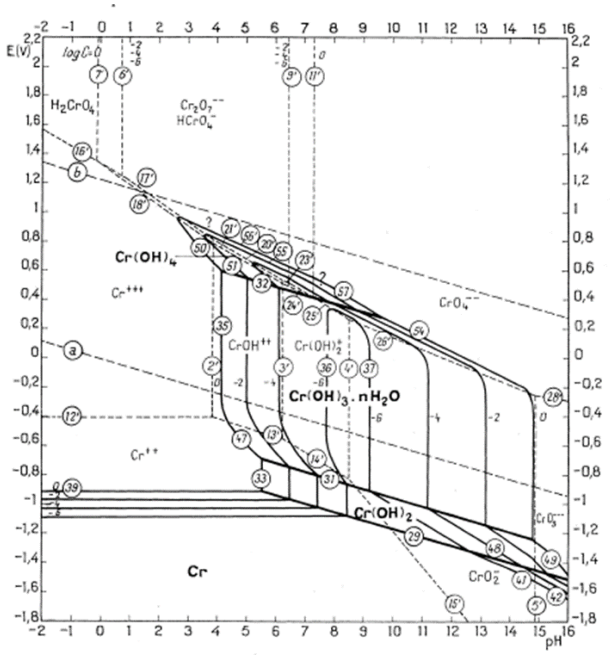

Figure II.21. Pourbaix diagram for a chromium-water system at 25°C in presence of chloride ions[152].

Table II.11. Simplified list of redox reactions linked to Cr(VI) reduction from $HCrO_4^-$ and CrO_4^{2-} anions[152].

Description	N°	Redox couple	E°*
Cr(VI) ion / Cr(III) solid	1	$HCrO_4^-$ / Cr_2O_3	0.67
	2	CrO_4^{2-} / Cr_2O_3	0.66
Cr(VI) ion / Cr(III) ion	3	$HCrO_4^-$ / Cr^{3+}	0.38
	4	CrO_4^{2-} / Cr^{3+}	0.37
	5	CrO_4^{2-} / CrO_2^-	0.39
	6	CrO_4^{2-} / CrO_3^{3-}	0.08
Cr(VI) ion / Cr(0) solid	7	$HCrO_4^-$ / Cr^0	-0.20
	8	CrO_4^{2-} / Cr^0	-0.20
Cr(III) ion / Cr(II) ion	9	Cr^{3+} / Cr^{2+}	-0.40
	10	CrO_2^- / Cr^{2+}	-0.47
Cr(II) ion / Cr(0) solid	11	Cr^{2+} / Cr^0	-0.97

* E° (V *vs*. SHE) values are corrected at pH 7 and 15 mg L^{-1} Cr.

From the CV results (**Figure II.20**), a first region from 0.4 V to 1 V *vs.* SHE/V fits with the standard potential of the reduction of Cr(VI) to Cr(III), corresponding to reactions N° 1-6 from **Table II.11**.The difference between the anodic and cathodic peak potentials (*ΔEp)* is considerably higher than 57 mV, indicating a degree of irreversibility[158]. Both solid and ionic forms of Cr(III) could appear. A second region predominates between 0 V and -0.6 V *vs.* SHE. It has a slightly higher current response and fits with the standard potential of reactions N° 7-10, where Cr(VI) is reduced to Cr(0). This is not an elementary reaction, which means that intermediate species such as Cr(IV), Cr(III) and Cr(II) can be present. The

electrochemical stability window of the electrolyte may also be compromised ($E°_{H+/H2}$ = -0.41 V *vs.* SHE at pH=7). The third region of cathodic evolution from -0.7 V *vs.* SHE includes H_2 evolution and eventually metallic Cr electrodeposition ($E°_{Cr(II)/Cr0}$ = -0.97). At these cathodic potentials, the process may become very energy intensive. Therefore, Cr(VI) removal from aqueous solutions is often based in a two steps process, where Cr(VI) is firstly reduced to Cr(III) and subsequently precipitated with a complexation agent (*e.g.*, EDTA[182]) or adjusting the pH to form for instance insoluble Cr(III) hydroxides[183].

b. Bioelectrochemical system

Total Cr and Cr(VI) removal assessment

The proposed BES technology is inspired on this principle but uses bacteria as driving agents for the Cr precipitation in a nanoscale. Chronoamperometry tests were performed on a BES at -0.8 V vs SHE and compared to an abiotic control (C1) and a biotic control with no polarization for 24 h (**Table II.12**).

Table II.12. Bioelectrochemical configuration tests.

Experiment	OD	[Cr] mg L	$E_{Cathode}$ V *vs.* SHE
C1	0 (Abiotic)	15	-0.8
C2	1.3	75	OCV
T1	1.3	15	-0.8

The choice of -0.8 V *vs.* SHE relies on the assumption that at this potential Cr(VI) will be electrochemically reduced. The chromium removal efficiency (**Figure II.22A)**, the Cr(VI) removal efficiency (**Figure II.22B**), and energy consumption (**Figure II.22C**, based on equation **(II-18)**) were evaluated over time.

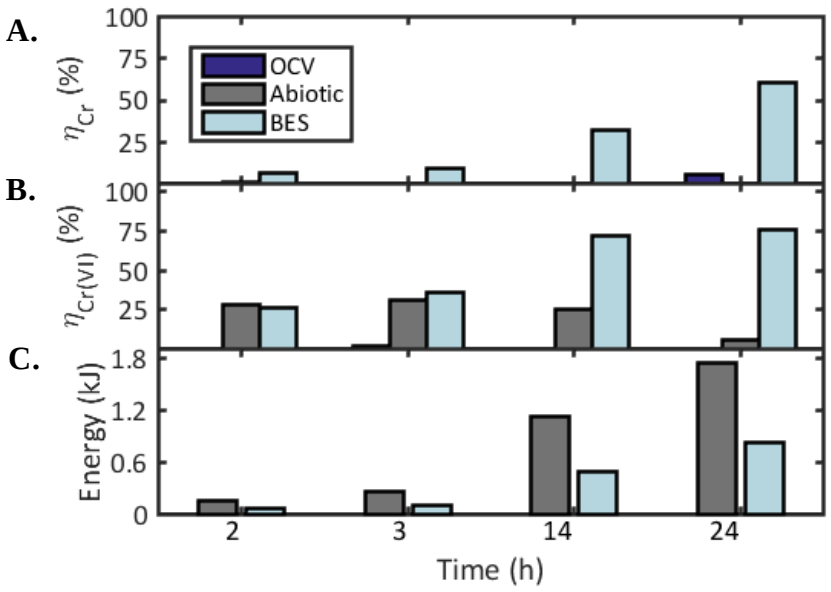

Figure II.22. Chronoamperometry results with non-polarized cathode (OCV), abiotic and BES, both with a cathode polarized at -0.8 V *vs*. SHE. **A**:Total chromium removal (η_{Cr}); **B**: Cr(VI) removal efficiency ($\eta_{Cr(VI)}$); and **C**: consumed energy over time. OCV and BES tests were inoculated with *S. Oneidensis* MR1, OD_{610nm} = 1.3.

In 24 h, the proposed BES system achieved 76% and 61% of Cr(VI) removal and total Cr removal respectively. In the same conditions (*i.e.* 15 mg L^{-1} Cr, at pH 7, in a microaerophilic environment and with *S. oneidensis* MR1 inoculated to an OD_{610nm} of 0.65), the microbial system removed only 17% Cr at 24 h (**Figure II.18**). If the reactor configuration effect is negligible, BES performance was considerably higher than the microbial system. A negligible Cr removal in biotic control (OCV) and a lower Cr(VI) removal in the abiotic control (maximum $\eta_{Cr(VI)}$= 31%) reinforce the interest of combining bacteria and the electrochemical system. Besides, Cr(VI) (bio)reduction products seem to be more stable against re-oxidation.

Microbial reduction of Cr(VI) to Cr(III) from low Cr-content streams is a promising treatment. The toxic effect of Cr(VI) on microorganisms could be limiting as it affects their metabolism and viability[87]. Interesting strategies have completely reduced Cr(VI) from catholytes in two-chamber BES, driven by bioanodes in a Cr-free chamber[89,90,184]. Others, directly reduce Cr(VI) with biocathodes inoculated

with a Cr adapted bacteria consortium[88,185]. Moreover, Cr removal is still very challenging. Li *et al.* [90] reported 66% of total Cr removal from a 204 mg L^{-1} Cr solution at pH 2.5 with a system coupling an abiotic cathode with a bioanode. The low catholyte pH seemed to affect the bioanode's performance. Huang *et al.*[88] removed 46% Cr from a 39.2 mg L^{-1} Cr solution with biocathodes at pH 7. Cr(VI) (bio)reduction pathways could have favorized the formation of soluble chromium species. Here, Cr precipitation with suspended cells and a polarized cathode aimed to add a new possible pathway for Cr(VI) reduction and further precipitation. Optimized cathodic potentials and cell mass concentration could enhance the Cr removal.

Energetic balance

Figure II.22C shows a lower energy consumption from the BES compared to the abiotic control. Their cathode polarization led to a cell voltage of about 2.4 V during the experiment in both trials. 0.8 kJ was consumed by the bioelectrochemical system during the 24 h, representing only half of the abiotic consumption. The equivalent of 1 kg Cr "produced" would have needed 129.5 MJ with the BES, which is considering high compared to 40.2 MJ kg^{-1} consumed by conventional techniques[10]. The Cr dilution factor is not considered in this comparison, but an optimized energy consumption can be achieved with a further study focused on the cathodic polarization.

Cr nanoparticles synthesis

S. oenidensis MR1 cells were characterized by TEM after the BES experiment (description in **Annex 1-B**). Results are presented in **Figure II.23**.

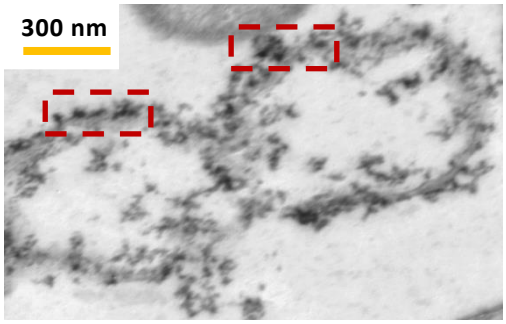

Figure II.23. TEM of *S. oneidensis* MR-1 after 24 h of operation in BES.

S. oenidensis MR1 cells with electron-dense particles of 19 nm to 36 nm surrounding the cell walls were observed. The nature of these particles needs to be confirmed by EDX or RAMAN, but they are similar to chromium nanoparticles (CrNPs) previously reported[172]. An extracellular bioreduction of Cr(VI) and subsequent extracellular precipitation of Cr(III) nanoparticles has been observed in *S. oenidensis* MR1 as a resistance mechanism against the toxic effects of Cr(VI)[172]. Here, Cr(VI) reduction induced by a polarized cathode in presence of initially viable cells could offer a new alternative for Cr removal and CrNP synthesis. The need of an active resistance mechanism to drive the process still needs to be elucidated.

II.3.4 To sum up

The screening study aimed to determine the significant factors to maximize the Cr removal from a low content solution containing Cr(VI). A microbial system achieved a maximum Cr removal of 53.5% after 96 h, with the experimental conditions of R5 (*i.e.* 15 mg L^{-1} Cr, pH 7, M9 medium, microaerophilic headspace and H_2 as electron donor). pH and oxygen statistically had the highest impact on the Cr removal, whereas the medium (either M9 or NaCl) had the lowest. Nevertheless, none of the factors resulted statistically important in the non-replica experimental conditions. This doesn't proof that the parameters do not influence the Cr removal. However, revaluations in replicates or surface response methodologies could reveal some insights. Cr(VI) and Cr(III) nanoparticles attached to bacteria are suspected to be observed by TEM and identified by its characteristic peaks in Raman spectroscopy.

A catholyte mimicking the experimental conditions of R5 was employed to evaluate the microbial electrochemical system. Despite the number of reversible reactions involved in the Cr(VI) electrochemical reduction, the BES was able to remove 76% of Cr(VI), of which 61% was removed and therefore assumed to be retained by bacteria. Finally, the presence of Cr(III) nanoparticles needs to be confirmed before assuming any added-value product.

II.4 Conclusions & perspectives

This chapter explored the feasibility of a new BES configuration where cathode plays a role of electron donor for metal removal from low metal content streams with further agglomeration as metallic nanoparticles. Two separated cases were studied: the first one with gold and the second with chromium. A screening experimental plan provided with essential insights about the suitable conditions and the understanding of bacteria-metal interactions. Then, the coupling of planktonic cells and a polarized cathode as a new bioelectrochemical approach was examined. Conclusions related to each case are summarized as follows:

Gold

(i) The first screening experimental plan conduced to a high gold removal efficiency (up to 92.8%) and the synthesis of AuNPs of sizes from 8 nm up to 112 nm in 72 h in presence of S. *oneidensis*, H_2 as electron donor and anaerobic conditions.

(ii) Initially viable *S. Oneidensis* MR1 and *C. metallidurans* CH34 were very versatile towards gold immobilization, retaining metals at a nanoscale under conditions undesired for their metabolism.

(iii) The cathodic polarization at -0.3 V *vs*. SHE accelerated the metal removal to 95% in 24 h and led to the synthesis of 18 ± 2.7 nm AuNPs.

Chromium

(i) The experimental plan conduced to a relatively low Cr removal compared to results obtained with Au (up to 53.5% in 96 h). The removal capacity of *S. Oneidensis* MR1 and *C. metallidurans* CH34 must depend on the nature of the metal and its toxicity towards microorganisms.

(ii) A first active mechanism of Cr accumulation followed by of a passive biosorption is speculated to represent the interactions between *S. Oneidensis* MR1 and chromium at pH 5, in anaerobic conditions and

presence of H_2. Potentially added-value Cr(III) nanoparticles were attached to the initially viable bacterial cells.

(iii) The cathodic polarization at -0.8 V *vs*. SHE enhanced and accelerated the Cr removal up to 61% and 76% Cr(VI) removal in 24 h. Besides, electron-dense particles resembling to chromium nanoparticles are observed surrounding the bacterial cell walls.

Synthesis of metallic nanoparticles by microbial-mediated technologies constitutes an attractive route for metal recovery from secondary sources. It opens a new spectrum of industrial applications from catalytical compounds to lithium ion batteries. Consequent research can focus on a more detailed bioelectrochemical system characterization, involving different cathodic potentials or including real waste streams. The characterization of the metallic nanoparticles would complement this by evaluating their potential for industrial applications.

CHAPTER III

Gas-Diffusion Electrode coupled with halophilic bio-anodes for metal recovery from marine environments

James Cameron's deep-sea challenge to the deepest point on Earth, National Geographic, 2012.

III.1 Introduction

As it was pointed out in **Chapter I**, our society are facing a metal supply risk due to our unsustainable metal usage and treatment. Microbial-based technologies are highlighted as potential low resources demanding alternatives for metal recovery. **Chapter II** proposes an eco-friendly technology based on metal-bacteria interactions together with an electron donor supply (*e.g.* H_2, lactate, electrode). It aimed to recover added-value products from the recovery treatment such as metallic gold and Cr(III) nanoparticles.

Several unconventional resources are appealing as alternatives to conventional mining, like secondary matrices (*e.g.* industrial and urban wastewater, e-waste) and natural extreme environments (*e.g.* marine sediments, geothermal brines). As James Cameron dived to the deepest point of the oceans in 2012, many mining companies are exploring the depth sea all over the world to find metal resources to exploit. **Chapter III** focuses on marine environments and introduces a microbial electrochemical technology based on gas diffusion electrodes (GDE) developed at VITO (Mol, Belgium). These carbon-based electrodes catalyze the formation of intermediate species (*e.g.* OH^-, H_2O_2) for metal precipitation. A special focus is made on targeting REE because of their economic importance and supply risk. The technology feasibility is evaluated with and without an energy input.

This chapter is the result of a collaboration between the GDEx team at VITO and LEPMI. It was financially supported by the French Ministry of Education and VITO.

III.2 Metals in marine deposits

III.2.1 Context

Marine resources have been exploited on small scales for thousands of years. It is only from the last century that large-scale marine mining processes have extensively grown to recover oil, gas, sand and some heavy metals beyond the beach[186]. The prospect of deep-sea mining started from the latest 1960s, when promising metal reserves were estimated all over the oceans[187]. Marine sediments stood out with a tremendous potential for future primary metal mining. The largest deposits have been found in the Pacific Ocean (**Figure III.1**), even though important sites are identified in the Atlantic, Indian and Arctic Oceans[188].

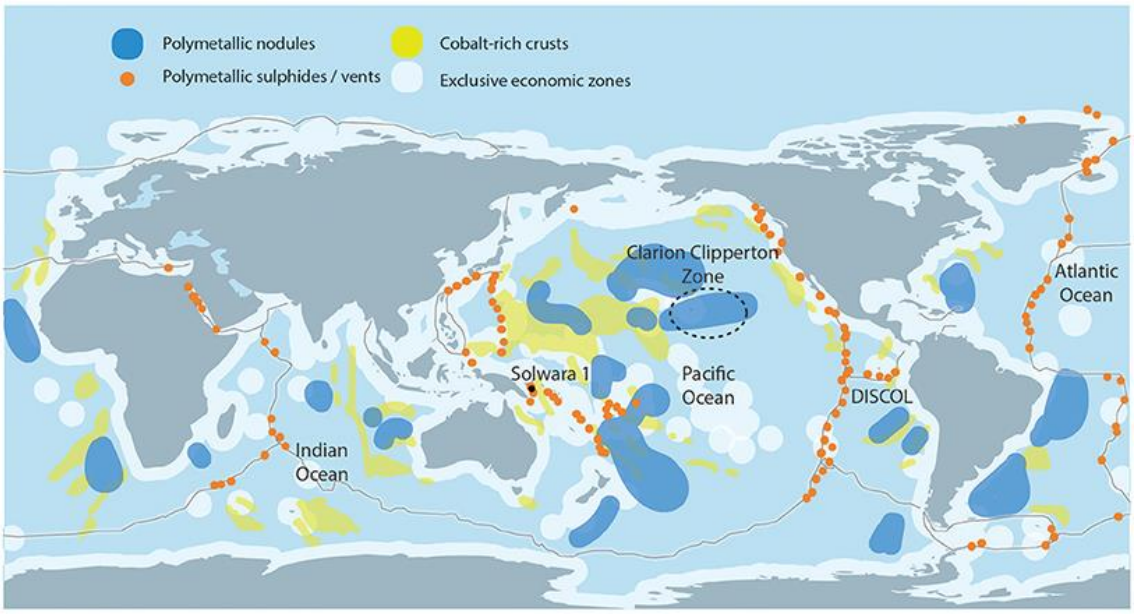

Figure III.1. Main mineral marine deposits found so far around the world[188].

Nowadays, the European Commission estimates that 5% of the world's minerals could be sourced from the sea floor by 2020[189]. Metal mining is already taking place in continental shelf areas at relatively shallow depths in New Zealand waters and is expected to start in deeper sites like Solwara 1, Papua New Guinea in 2019[188]. The interest on accelerating the marine metal mining relies on the rising demand of metals and the economic potential of explored reserves. This economic potential is clearly related to the metal diversity and abundance.

III.2.2 Metal deposits in marine environments

The importance of metal mining from marine environments relies in the fact that they can yield up to 10^4 times the desirable minerals of land deposits[190]. Besides, deposits on the seafloor contain a large variety of metals from base metals (*e.g.* Cu, Fe, Mn) to heavy metals (*e.g.* Pb, Co, Zn) and precious metals (*e.g.* Au, Ag, REE). Their geological formation and environment will determine the types of minerals and thereby the metals present. A summary of the main marine deposits and their characteristics is described in **Table III.1**.

Table III.1. Metal deposits in the ocean (values taken from Anhert *et al.*[191]).

	Main metals	Depth (m)*	Mode of occurrence	Amount/site
Sulfide-based deposits	Cu, Fe, Mn, Pb, Zn, Au, Ag	1400 – 3700	Mounds/ chimneys (10 - 100 m)	10^4 to 10^6 t
Fe-Mn crusts	Fe, Mn, Co, V, Mo, Pt	800 – 2500	Thin coated layer (0.1 – 10 cm)	$5x10^{10}$ t
Fe-Mn nodules	Fe, Mn, Ni, Cu, Co	4000 – 6000	2.5 – 25 cm spheres	$5x10^{11}$ t
REE-rich mud[192]	REE	3000	2 – 70 m beds	$>10^{14}$ t

*Economically most valuable deposits depth

a. Sulfide-based deposits

Sulfide-based deposits are the result of chemical and thermal exchanges between the ocean, the lithosphere and magmas. Deposits formed by hydrothermal vents are in particular remarkable due to their mineralogical diversity (*e.g.* iron, copper and arsenic sulfides, zinc-lead-silver ores, Mn and Fe oxides and native gold)[193]. These hydrothermal vents are enclosed rocks formed at about 2km below the sea level around volcanic arcs under the seafloor (**Figure III.2**). They expel fluids rich on nutrients and a large variety of metals at high temperatures (up to 500 °C)[193]. Besides, they host a variety of organisms (*i.e.* chemoautotrophic bacteria, tubeworms, mollusks and crustaceans)[194,195]. These organisms are acclimated to hydrostatic pressures up to 60MPa.

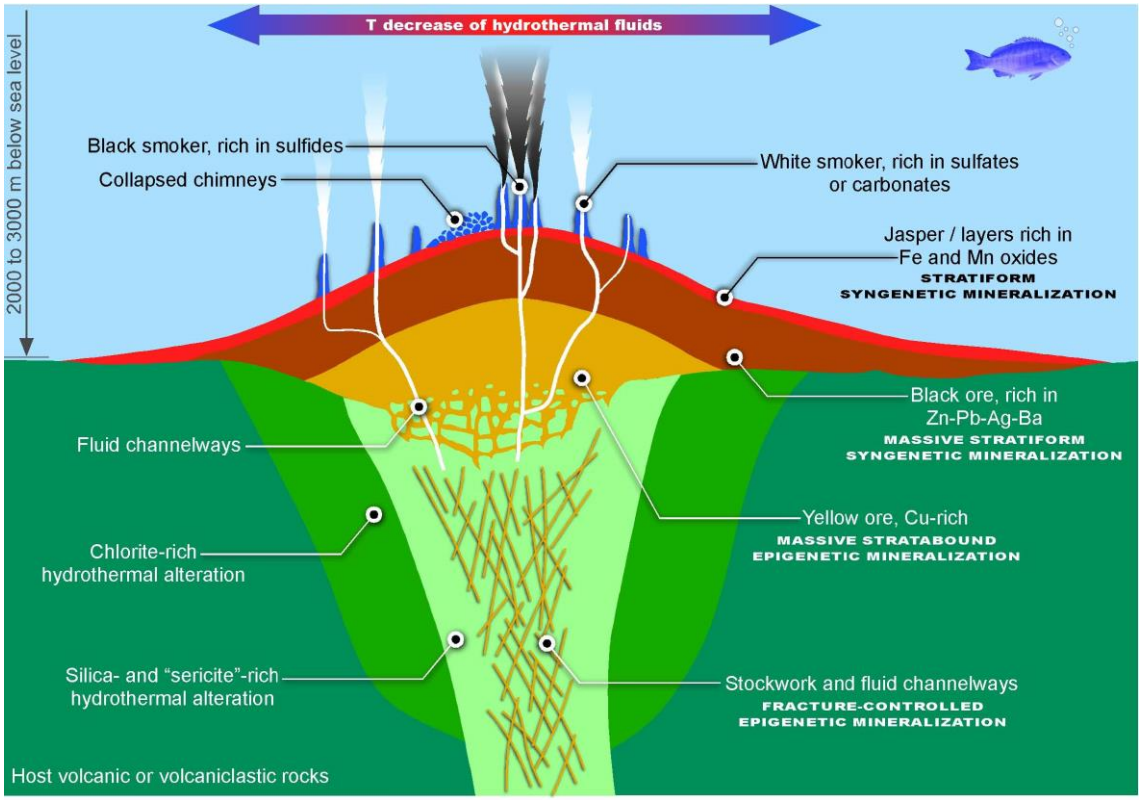

Figure III.2. Hydrothermal generation of sulfide-based deposits[193].

Some of these hydrothermal sites are known to host significant metal content. For instance, estimations on hydrothermal deposits from Solwara 1 site in Papua New Guinea are: copper (6.8 g/ 100 g_{rock}), zinc (0.4 g/100 g_{rock}), gold (4.8 ppm), and silver (23 ppm)[196]. Nautilus Minerals, one of the main companies interested in seabed mining, is planning to exploit this site and considers different treatments for metal recovery depending on the mineral. At a laboratory level, copper from chalcopyrites has been tested by conventional grinding-flotation processes[197]. Besides, gold associated with pyrite is contemplated to be recovered *via* conventional cyanidation[197], a controversial hydrometallurgical technique due to the cyanide toxicity but effective and cheap.

b. Fe-Mn crusts

Fe-Mn crusts are thin layers of cm to dm thick formed by a slow accumulation of colloidal particles on the slope of submarine mountains (hydrogenetic) and in some cases also by hydrothermal processes[190,198]. Crust deposits are predominately composed of amorphous FeOOH and poorly crystalline Fe-Mn bearing mineral called vernadite[199]. The concentration of each mineral changes depending on the location but the main metals present in these crusts are manganese (13-27% wt) and iron (6-18%)[198,199]. They are often present in the limiting oxygen zone and their mineralization is a complex process that involves the accumulation of colloidal iron (FeOOH) and manganese (MnO_2) under normal seawater conditions (Eh>0.5 V; pH≈8)[198,200]. These oxides may hydrolyze water at seawater conditions, charging their surface very negatively in the case of MnO_2 and slightly positive in the FeOOH (**Figure III.3**).

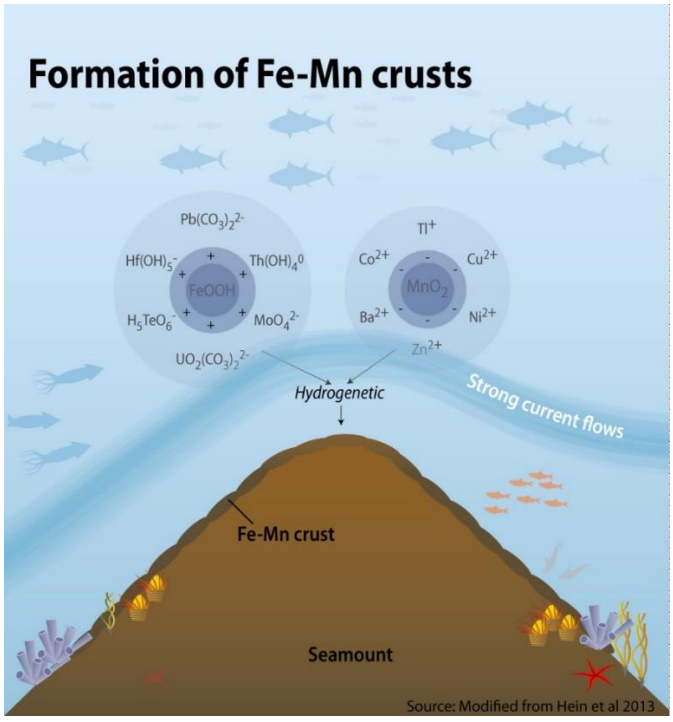

Figure III.3. Hydrogenetic formation of Fe-Mn crusts[199].

Manganese oxides will therefore most likely adsorb dissolved cations (*i.e.* Cu^{2+}, Co^{2+}, Ni^{2+}, Zn^{2+}, Ti^{+}) whereas iron oxides will adsorb anionic complexes such as carbonates (*i.e.* $REEE(CO_3)^{2-}$, $UO_2(CO_3)_2^{2-}$), hydroxides (*i.e.* $Hf(OH)_5^-$) and oxyanions (*i.e.* MoO_4^{2-}, $H_5TeO_6^-$). This phenomenon promotes the enrichment of

minor elements up to a factor 10^9, thanks to the high internal surface area of these minerals (>300 m^2/g)[198,201].

Fe-Mn crusts cover enormous seafloor areas at depths of about 400-4000 m, although the most enriched crusts are present between 800 and 2500 m[199]. Cobalt-rich crusts contain up to 2% cobalt and have been prioritized because of their economic importance[199]. Besides, they have an enormous potential for REE and yttrium (REY) recovery with deposits containing up to 100 ppm yttrium and 1000 ppm of total REE contents[202].

c. Fe-Mn nodules

Ferromanganese deposits, referred as nodules until the late 1970s and nowadays distinguished as crusts and nodules, are both potential future resources of a large variety of metals. Ferromanganese nodules are formed *via* hydrogenetic and diagenetic precipitation[191]. As Fe-Mn crusts, nodules contain non-crystalline iron hydroxides and vernadites in addition to other manganese minerals such as todorike and birnessite[199]. However, they are not necessary tightly attached to the host rock as the crusts, facilitating its recovery[198]. Large reserves of nodule deposits were recently discovered under 5000 m of Japanese waters in the Pacific Ocean (**Figure III.4**).

Figure III.4. Picture of Fe-Mn nodules and REY muds in the Pacific Ocean at 5458 m under the sea level presented.

d. REE-rich mud

Rare earth elements (REE) have been found in marine muds with concentrations up to 5000 ppm (higher than land mines) under nodule deposits (**Figure III.4**). There are enormous expectations about recovering metals from these muds as hotspots of one square kilometer were estimated to contain 1.2 Mt of REE. These reserves account for 62, 47, 32, and 56 years of annual global demand for Y, Eu, Tb, and Dy, respectively[203]. All these recent discoveries have boosted the mining industry to exploit the seabed minerals, but it still requires to overcome enormous technological challenges.

III.2.3 Technological challenges

The concept of deep sea mining is still not applied because of several technological challenges. First, the extreme conditions (*e.g.* depth, temperature, hydrostatic pressure, darkness, flow) are very difficult to work with[204,205]. The depth sea covers environments at sea level under 1000 m, where more than 100 bars of pressure is reached and where temperatures drop to 1-3°C, except for volcanic environments[206]. Mining at these conditions requires sophisticated techniques for metal extraction, concentration and transportation compared to land mining.

Second, marine deposits have to be pre-treated from the sea floor[188,199]. Nautilus Minerals, one of the main companies that want to exploit the sea bed, pretends to submerge remotely operated vehicles to mechanically remove and collect ores out of the seafloor[188]. The ores would be pumped up through a lifting system to a support vessel and transported to land for offshore processing[199] (**Figure III.5**).

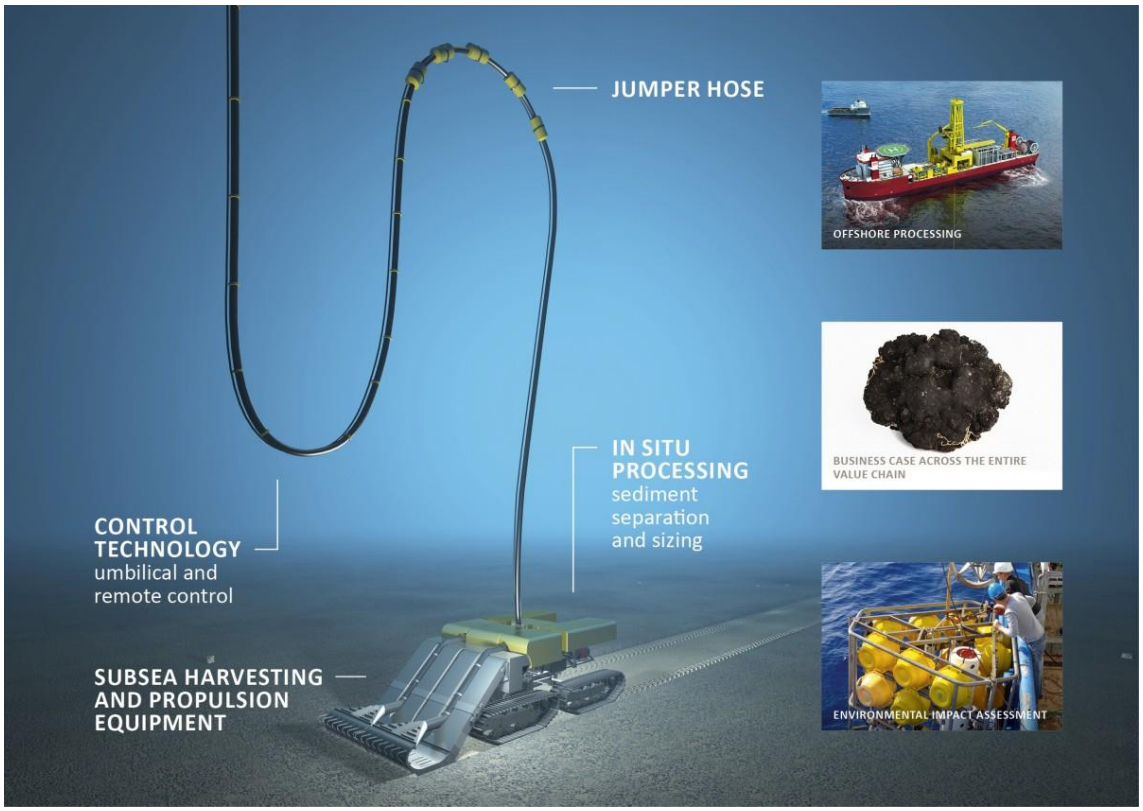

Figure III.5. Metal mining process from polymetallic nodules and REY-rich muds[207].

Third, the high risk for deep-sea ecosystems due to the noise, light, release of toxic compounds and waste[188,208]. Organisms living near the seabed, also called benthos, will be affected by their ecosystem disturbance occasioned by the dredging machines. Besides, dredged material generates sediment wastes, also called sediment plumes, that compromise the ecosystems due to pollutants presence, exposure to increased turbidity and sedimentation[209,210]. Finally, the costs associated to the metal treatment, logistics, safety measurements, among others[211,212]. These costs must be balanced with the metal resources and therefore a good knowledge of the marine deposits potential is mandatory.

Sustainable mining is a key element to focus on in order to disturb the minimum as possible the seabed and marine life, to avoid the releasing of toxic elements and to employ the less of natural resources. The aim of the study presented in this 3rd chapter is to develop a deep-sea mining process according to these principles. To do so, a Gas Diffusion Electrode (GDE) is coupled to a bioelectrochemical system (BES) and marine microorganisms are included to harvest the metals out of the

marine deposits with the less energy consumption as possible. Minerals lifting may favorize the release of sediment plumes all over the water column and *in situ* extraction of metals from the mineral deposits could mitigate this effect. This chapter covers only the first phase of the project that considers the metal precipitation proof of concept from a synthetic marine sediment already leached in acid conditions. A second phase would subsequently focus on the feasibility of bioleaching marine minerals in seawater conditions and deep-sea environments. Based on that, a third phase coupling both processes could lead to develop the first *in situ* deep sea mining technology.

III.3 BES/GDEx technology

III.3.1 General principle

BES has become a highly attractive technology for metal recovery. Even more if the aqueous medium has a high ionic conductivity such as marine environments, metal ions can be recovered by direct electrochemical reduction on the cathode or by interacting with the final electron acceptor. The BES/GDEx technology proposed focuses on the second approach, using oxygen as a final electron acceptor (**Figure III.6**). Electrons are transferred from a bioanode to a porous gas-diffusion cathode *via* an external circuit while ions migrate through an Ionic Exchange Membrane, in this case selective to cations. The oxygen reduction results in H^+ consumption and OH^- production, favorizing the precipitation of metal hydroxides and oxides. The key value of this approach relies on potentializing the array of the metals to recover regardless of the redox potential of each metal. Besides, bioanodes can provide with enough energy to do so, an enormous advantage as no energy inputs would be required.

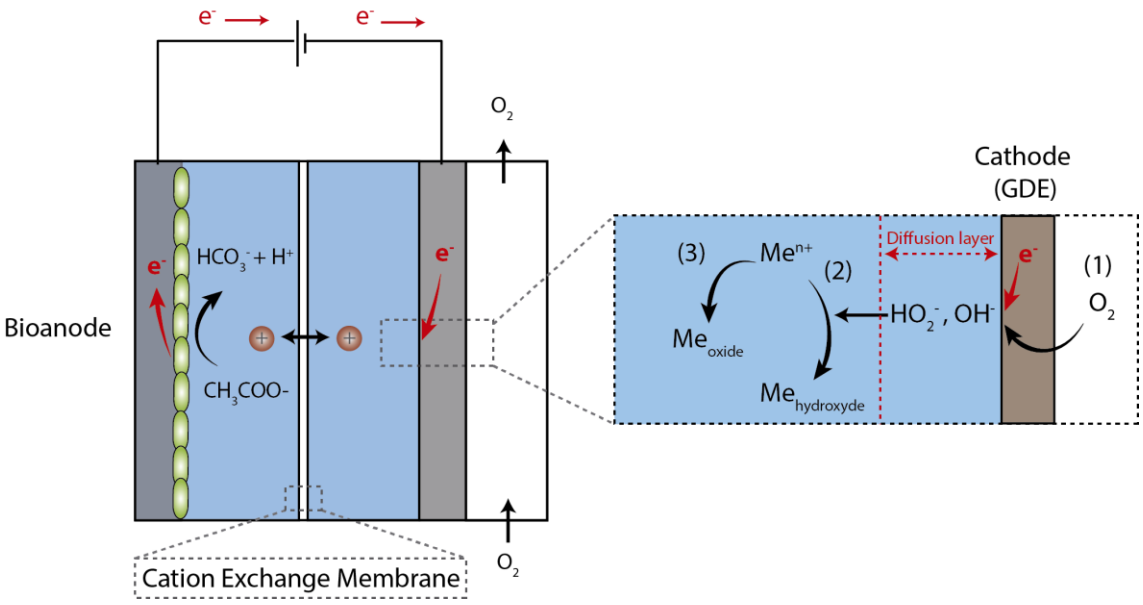

Figure III.6. BES/GDEx technology for metal recovery.

Bioanodes with the highest currents produced so far do not tolerate high salinities and operate only in solutions of low ionic conductivity (<2 S m^{-1})[213]. To give a point of comparison, conventional hydrogen production from water electrolysis uses electrolytes with much higher conductivities (between 20 S m^{-1} and 60 S m^{-1})[213]. Marine environments give the opportunity to operate the BES with relatively conductive electrolytes, thus reducing its ohmic resistance. Seawater salinity, defined as grams of dissolved inorganic matter per kilogram of water and expressed in parts per thousand (‰), is generally between 33‰ and 37‰ even at deep conditions[214,215]. Halotolerant bacteria from marine sediments have been already tested in highly conductive environments (>50 S m^{-1})[216,217].

A biofilm grown on the anode surface catalyzes the oxidation of organic matter, in this case acetate, as electron donor (Equation **III-1**) and carbon source to provide with energy to the BES while preserving the bacterial metabolism[64,218]. In marine conditions it will be essential to have electroactive but also halophilic microorganisms (tolerant to high salinity levels) attached to the anode.

$$CH_3COO^- + 4H_2O \rightarrow 2HCO_3^- + 9H^+ + 8e^- \qquad E°= 0.187 \text{ V } vs. \text{ SHE} \qquad \textbf{(III-1)}$$

The cathode developed by VITO[219] catalyzes the oxygen-reduction reaction (ORR) as intermediate reaction for further metal precipitation. This reaction can occur under different steps depending on the pH:

At pH<7

$$O_2 + 4H^+ + 4e^- \rightarrow 2H_2O \qquad E°= 1.229 \text{ V } vs. \text{ SHE} \qquad \textbf{(III-2)}$$

$$O_2 + 2H^+ + 2e^- \rightarrow H_2O_2 \qquad E°= 0.700 \text{ V } vs. \text{ SHE} \qquad \textbf{(III-3)}$$

$$H_2O_2 + 2H^+ + 2e^- \rightarrow 2H_2O \qquad E°= 1.760 \text{ V } vs. \text{ SHE} \qquad \textbf{(III-4)}$$

At pH>7

$$O_2 + H_2O + 4e^- \rightarrow 4OH^- \qquad E°= 0.401 \text{ V } vs. \text{ SHE} \qquad \textbf{(III-5)}$$

$$O_2 + H_2O + 2e^- \rightarrow HO_2^- + OH^- \qquad E°= -0.065 \text{ V } vs. \text{ SHE} \qquad \textbf{(III-6)}$$

$$H_2O + HO_2^- + 2e^- \rightarrow 3OH^- \qquad E°= 0.897 \text{ V } vs. \text{ SHE} \qquad \textbf{(III-7)}$$

Oxygen reduction consumes protons in acid conditions and produces hydroxides in alkaline medium. As far as the reduction is continued, the pH is supposed to increased. At a certain pH, metal ions (Me^n) become insoluble hydroxides and oxides start to precipitate into metal salts. Equations **III-8** and **III-9** are simplified examples of possible precipitations. Intercalation processes and other possible insoluble metal phases can also take place (*e.g.* $Me1_x(OH)_yMe2_z$)[220].

$$Me^n + n\ OH^- \rightarrow Me(OH)_n \quad \textbf{(III-8)}$$

$$Me^n + 2HO_2^- \rightarrow 2MeO_n + H_2 \quad \textbf{(III-9)}$$

A great number of microbial electrochemical technologies have been proposed to recover metals from varied metal-rich aqueous matrices[103,105,106]. They are commonly based on the electrochemical reduction of each metal, allowing a sort of selectivity as far as the cathode potential is controlled[104–106]. This poses a challenge for REE-rich aqueous systems, as they have very low redox potentials (*e.g.* $E°_{Ce3+/Ce}$ = -2.48 V *vs.* SHE; $E°_{Pr3+/Pr}$ = -2.46 V *vs.* SHE; $E°_{Nd3+/Nd}$ = -2.43 V *vs.* SHE when the REE concentration is 1 M[152]). High energy requirements are thus necessary. Besides, electrochemical reduction of REE has been conceived on non-aqueous systems such as organic solvents[221] and ionic liquids[222]. The metal precipitation by the presence of hydroxides offers a new route as it recovers metals regardless of their redox potential. As hydroxides could be also added to the system, direct precipitation with strong bases (*e.g.* NaOH, KOH) could be also conceived. The main problem of direct precipitation is generally the large amounts of chemicals to increase the pH and consequent large sludge productions. Considering that the species solubility is related to the nature of metal, its concentration and pH[223], a selective metal recovery is possible as far as metals precipitate at different pH.

Finally, a third chamber besides the GDE cathode supplies oxygen by circulating air at a slight overpressure. In that sense, air diffuses through the GDE to the catholyte to compensate the oxygen consumption and the low solubility of oxygen in water.

III.3.2 Microbial electrochemical set-up

A hermetically closed H-cell with a three electrodes configuration was implemented to study the feasibility of the BES/GDE technology (**Figure III.7**). The anode consisted of two rectangular carbon felt, each of them with a projected surface area of 20 cm^2, so a total area of 40 cm^2 was considered. The metal recovery validation employed a circular GDE of 1.3 cm^2 diameter developed at VITO[219] as cathode. It was produced by film casting and phase inversion process[219], and composed of three layers: an electrochemically active layer of activated carbon, a hydrophobic polytetrafluoroethylene gas diffusion layer, and a stainless-steel mesh as current collector. The cathode was placed at approximately 10 cm of the bioanode facing the floor.

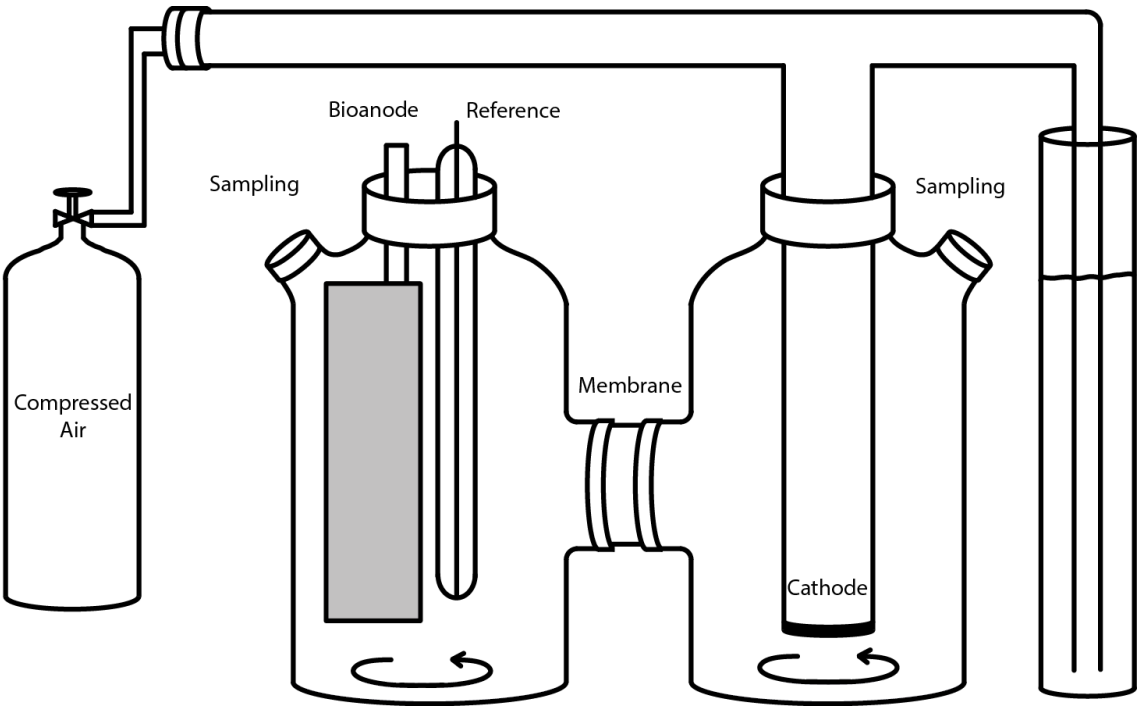

Figure III.7. BES/GDE set-up.

The active carbon layer was facing the catholyte and the diffusion layer was in contact with the air chamber. An Ag/AgCl reference electrode (0.2 V *vs*. SHE, saturated KCl, REF321, Radiometer Analytical, Hach, USA) was placed next to the anode as it was chosen as working electrode. Stainless steel current collectors connected anode and cathode to the external circuit. A 10 cm^2 membrane cation exchange membrane (CEM, Fumasep FKB PEEK reinforced M5720804) separated

both compartments. Anolyte and catholyte had a total volume of 500 mL and a constant magnetic stirring at 500 rpm assured a constant concentration in the bulk. All the experiments were performed in batch conditions and at room temperature and pressure. The third chamber was connected to a bottle of compressed air and to an air flow controller. This chamber's output had a tubing submerged into a water column of 25 cm to favorize a slight overpressure. Oxygen is expected to diffuse in the electrode diffusion layer and to react within the electrode active layer. Besides, the cation exchange membrane should retain the oxygen passage from the catholyte to the anolyte.

The initial biofilm growth step considered a 3 cm^2 long Pt wire as cathode. It is a very stable and catalytic electrode that prevented from cathodic limitations during the bioanode preparation.

III.3.3 Halophilic bioanodes start-up

a. Experimental

Halotolerant microorganisms taken from marine sediment in the Netherlands were inoculated in the anodic compartment of the microbial set-up described in Section **III.3.2.** The anolyte contained a culture medium solution based on the Starkey medium[213] (1mL per liter of trace elements; 2 $g \cdot L^{-1}$ NH_4Cl; 0.5 $g \cdot L^{-1}$ K_2HPO_4; 40 mM $NaCH_3COO$; 30 $g \cdot L^{-1}$ NaCl, ionic conductivity 48-52 S m^{-1}). The catholyte contained 30 $g \cdot L^{-1}$ NaCl and in between them, the poly-sulfonated CEM controlled cations migration between anolyte and catholyte. The carbon felt anode was polarized at 0.43 V *vs*. SHE over a period of 120 days to reach a mature biofilm.

During this period, the anolyte was fed with concentrated sodium acetate (2 M) and concentrated sodium hydroxide (2 M) at least once per week. This adjustment was equivalent to 20 mM CH_3COONa and a maximum anolyte pH of 8.5. The anolyte was initially flushed with N_2 and the reactor was kept hermetically closed, Even though the oxygen presence was not measured, the anolyte should have turned anaerobic if the oxygen was depleted over time.

b. Bioanode electroactivity

The initially marine microbial culture electroactivity behavior was studied by following the current density (*j*) and pH over time (**Figure III.8**). To do so, the anode potential was fixed at 0.43 V *vs.* SHE against the reference, an anode potential previously reported in halophilic bioanodes[213]. *j* was calculated as the absolute current measured divided by the projected surface area of the bioanode (40 cm^2), whereas the pH was constantly measured with a pH probe installed in the anolyte.

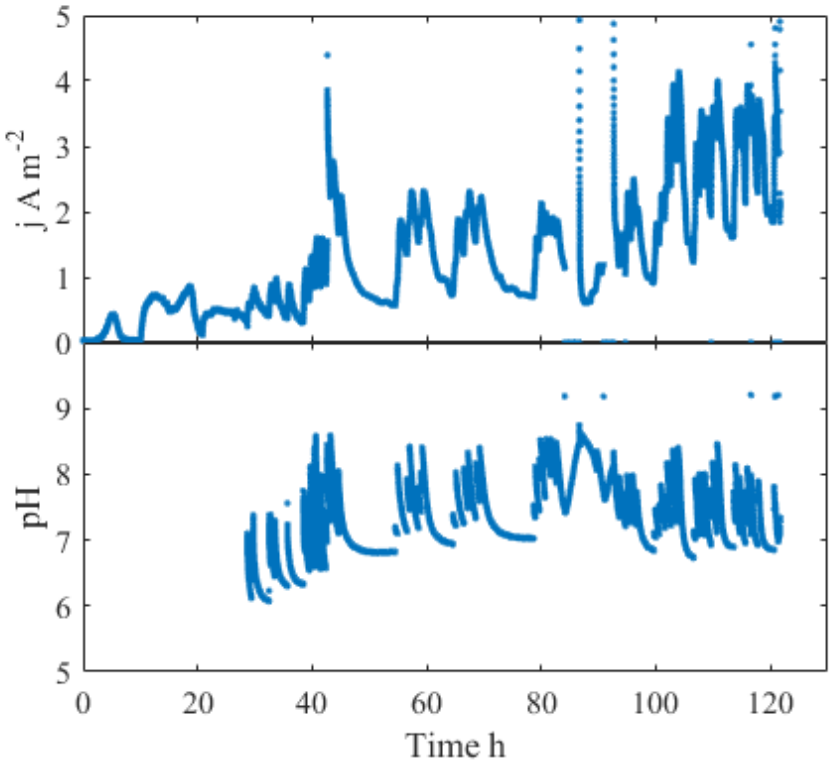

Figure III.8. Current density evolution and anolyte pH behavior during bioanode growth. Bioanode was poised at 0.43 V *vs.* SHE.

Cycles where the current increases and decreases are distinguished. A continuous feeding of substrate could maintain a constant current generation[224], but the current cycles were a good indicator of the bacterial electroactivity. Considering that the oxidation of 1 mol of acetate releases 9 H^+ (equation **III-I**), the pH decreasing tendency at every cycle was presumed to be due to the acetate microbial-electrochemical oxidation. Instead of following the acetate concentration, pH and current evolution were used as criteria to define the electroactivity of the bioanode.

For instance, from 48th to the 55th hour, pH tended to stabilize at 6.8. During this time, the current had drop to a very low values (<1 A m^{-2}). Despite the possible acetate presence in this region, the current generation was limited. Once acetate concentration and pH were (re)adjusted with 20 mM acetate and 50 mM NaOH, the current increased and non-limiting conditions had returned. In general, cycles lasted more than one week at the beginning of the biofilm growth and became faster over time. The biofilm was considered mature when it reached after several cycles where the maximum current stabilized at about 4.1 A m^{-2}. This value is relatively low compared with similar studies[213,217], where a maximum current density of 33.8 ± 17.3 A m^{-2} was obtained at the same anodic potential. The microbial community may be different, but a high effect of the cell configuration is attributed to this response. In any case, electroactive and halophilic microorganism were attached to the bioanode. Besides, high salinity media inhibits the development of methanogenic bacteria, which normally reduces the efficiency of targeted conversions[216].

When the current production is related to microbial substrate consumption, the biofilm is in turnover or non-starving conditions[225]. Non-turnover or starving conditions are therefore considered as the absence or low presence of substrate and are observed when current reaches low levels[226]. However, as the substrate consumption was not followed within time, the terms non-limiting and limiting conditions were preferred. These conditions were explored with other electrochemical techniques: cyclic voltammetry and impedance spectroscopy.

III.3.4 Bioanode electrochemical characterization

a. Experimental

Current dependency on the potential

Cyclic voltammetry (CV) measurements were carried out on the bioanode at 1 mV s^{-1} and at pH 7.5 under limiting and non-limiting conditions. The non-limiting conditions (NLC) were stablished during a cycle were current was increasing and the pH reached 7.5. The limiting conditions (LC) were stablished by completing a

cycle and then rising the pH up to 7.5. A range of scan from -0.2 V to 0.6 V *vs*. SHE was established. At this range, mechanisms of electron transfer from bacteria to the anode are often reported[218,227]. The CVs were performed after 100 days of biofilm establishment.

A five steps chronoamperometry measurement took place after the 120 days of biofilm growth. Steps went progressively from -0.2 V to 0.6 V *vs*. SHE and lasted 15 minutes each. In both chronoamperometry and CV tests, the applied potential was corrected by the bioanode ohmic resistance previously measured.

Potentiostatic Electrochemical Impedance Spectroscopy (PEIS)

PEIS estimates the electrochemical impedance (Z) by applying a sinusoidal voltage signal over a fixed potential and measuring the corresponding current response. It is a graphical method that associates the impedance behavior to an equivalent electrical circuit. The impedance is calculated as the ratio between the potential difference and the current difference. The real part (Z_R) corresponds to resistances (R) and are interpreted as power losses that are transformed into heat. The imaginary part (Zj) is a reactive impedance that accumulates the electrical energy as capacitors (C) or inductors (L). In a general simplified case, these electrical elements are associated with the impedance by the following equations:

$$Z_R = R + 0\,j \quad \textbf{(III-10)}$$

$$Z_C = 0 - j / (2\pi f\, C) \quad \textbf{(III-11)}$$

$$Z_L = 0 + j\, 2\pi f\, L \quad \textbf{(III-12)}$$

The resistive part is observed when the impedance has not imaginary component (equation **III-10**) and it is observed at frequencies of around 1 kHz and 10 mHz. The resistance at high frequencies is often related to an ohmic response (R_{ohm}) whereas at low frequencies it is the sum of the ohmic and polarization losses (R_{ohm}+ R_{pol}). In **Figure III.10**, Zr and Zj are both normalized with the resistance at low frequencies as described in the following equations:

$$\bar{Z}r = Zr / (R_{ohm} + R_{pol}) \quad \textbf{(III-13)}$$

$$\bar{Z}j = Zj / (R_{ohm} + R_{pol}) \quad \textbf{(III-14)}$$

This technique gives information about the electrochemical reactions and the transport of reactants/products in the system. PEIS was performed on the anode at the following potentials: -0.2 V, 0 V, 0.2 V, 0.4 V and 0.6 V *vs*. SHE. It scanned frequencies from 10 kHz to 0.01 Hz, an amplitude of 50 mV and a stabilization time of 15 minutes before the measurements. Resistance and mechanisms of electron transfer over the anode are intended to be elucidated. Limiting and non-limiting conditions were compared.

b. Microbial electro-catalytic activity

Results of CV and chronoamperometry at different potentials on the bioanode are presented in **Figure III.9**. Under potentials between -0.2 and 0.2 V *vs*. SHE there is not significant influence of the starvation conditions on the current produced. The biofilm electro-activity seems to appear at potentials higher than 0.2 V *vs*. SHE. At The hysteresis observed despite the slow scan rate is probably due to the large bioanode surface area.

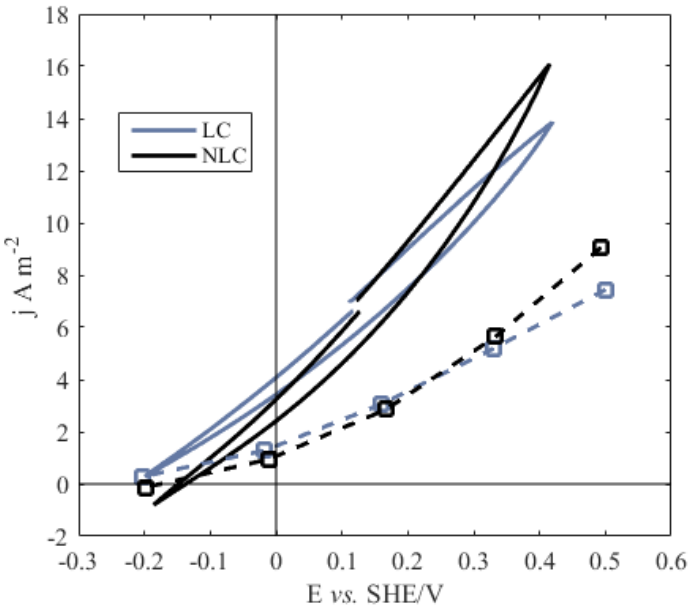

Figure III.9. Electrochemical analysis at limiting conditions (LC) and non-limiting conditions (NLC) conditions at pH $_{anolyte}$: 7.5. CV (solid lines) were performed at 1 mV.s^{-1}. Chronoamperometry values (dashed lines) are taken at 15 minutes of stabilization.

To avoid this dynamic effect, polarization by chronoamperometry of 15 minutes were also performed. As in CV measurements, the current evolution was also significantly improved under NLC conditions at potentials from 0.2 V *vs.* SHE. At 0.43 V *vs.* SHE for instance, an increase of 16% of the current produced is observed. A better microbial electro-catalytic response could be responsible of this current improvement. Now, the current response depends on the electrochemical reactions but also on minimizing the possible current losses. These losses were therefore studied by an impedance characterization.

c. Bioanode impedance behavior

The ratio between the sinusoidal potential perturbation and its corresponding current response was used to determine the impedance behavior at different frequencies (f). The obtained result is a complex number represented by a complex impedance plane in cartesian coordinates, also called Nyquist diagram (**Figure III.10**).

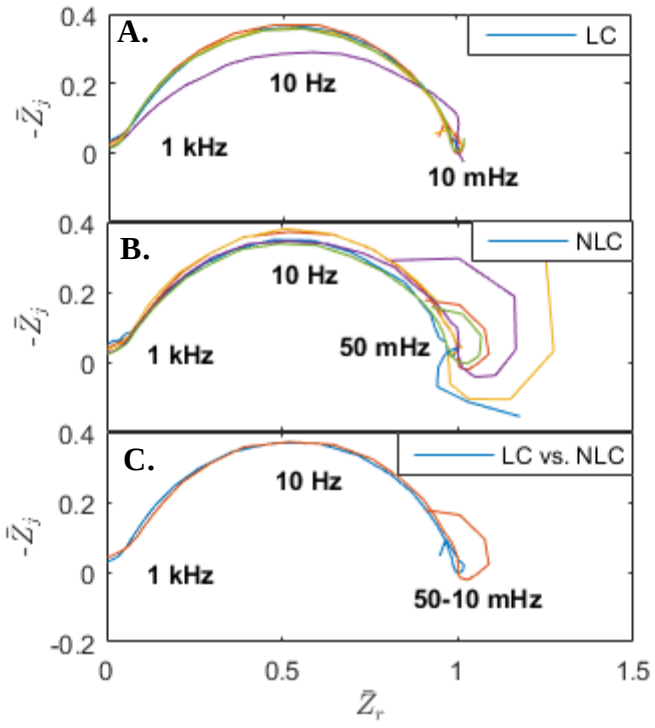

Figure III.10. PEIS results. pH $_{anolyte}$: 7.5, $pH_{catholyte}$: 3. Stabilization time: 10min. Amplitude: 10 mV. Values normalized with R_{ohm}+ R_{pol}. **A**: From -0.2 to 0.6 V *vs.* SHE in limiting conditions (LC); **B**: From -0.2 to 0.6 V *vs.* SHE in non-limiting conditions (NLC). **C**: comparison at 0.4 V *vs.* SHE.

Figure III.10A shows the impedance behavior at different potentials between -0.2 and 0.6 V *vs.* SHE. First, the imaginary impedance observed is only negative in most of the frequencies, excluding any inductive effect. The semicircle shape that goes from R_{ohm} to R_{ohm}+ R_{pol} is usually related to RC circuits and interpreted as physicochemical interphase phenomena[228]. In a perfect semicircle, the ratio from the point (R_{ohm}+ R_{pol}) / 2 would always be the same and therefore $|\bar{Z}j,_{max}|$=0.5. As $|\bar{Z}j,_{max}|$<0.5, the impedance response corresponds to several activation-energy-controlled processes. Therefore, the semicircle could be associated to different mechanisms including electron transfer processes (*e.g.* substrate/biofilm, biofilm/anode), and active species diffusion at the vicinity of the bioanode. Nonetheless, the normalized shape is very similar at almost every potential. This means that the phenomena occur at all this range of potentials and can be considered as a characteristic of our studied system.

In NLC conditions, there is also a similar effect regardless of the potential applied (**Figure III.10B**). The semicircle is overlapped at all the potentials until 50 mHz. Then, an inductive behavior followed by a capacitance is clearly observed at lower frequencies. Despite its unclear origin, a negligible effect on the power losses is assumed since the inductance impedance tends towards zero when frequencies decrease (equation **III-12**). Finally, **Figure III.10C** compares the impedance behavior in LC and NLC conditions at 0.4 V *vs.* SHE. Both graphs overlap each other, representing that no additional physicochemical phenomena are added to the system at least until 50 mHz.

The impedance spectroscopy is a powerful tool to correlate the impedance behavior to physicochemical mechanisms. To do so, some criteria must be satisfied: linearity, stability, causality and finite impedance over the frequency domain. A common mechanism to validate these criteria is the Kramers-Kronig (K-K) transform. The experimental data was compared to the K-K values in terms of the real and imaginary impedance, the impedance vector |Z| and the phase (ϕ). Results in NLC conditions are presented in **Table III.2**.

Table III.2. Comparison between experimental data and Kramers-Kronig values in NLC conditions. Frequency range: 10 kHz to 0.01 Hz.

E V *vs*. SHE	Δ Z_R (Z) (%)	Δ Z_j (Z) (%)	Δ |Z| (%)	Δ ϕ (Z) (%)
0.6	2.3	34.7	2.2	34.2
0.4	2.4	1681.0	2.4	1672.0
0.2	3.6	57.3	3.7	60.9
0	3.0	54.6	3.0	55.4
-0.2	1.9	314.6	2.0	314.3

Parameters such as the real part and the impedance vector fitted properly with the K-K relationship as the comparation analysis results showed a small difference between them. Nevertheless, the imaginary part and the phase are significantly different than the K-K transform and therefore did not satisfy the impedance criteria. Therefore, the frequency domain was reduced to a shorter range (4 kHz to 0.5 ± 0.3 Hz) and the comparison was repeated (**Table III.3**).

Table III.3. Comparison between experimental data and Kramers-Kronig values in LC and NLC conditions. Frequency range: 4 kHz to 0.5 ± 0.3 Hz.

E V *vs*. SHE	LC				NLC			
	Δ Re(Z) (%)	Δ Z_j (Z) (%)	Δ |Z| (%)	Δ ϕ (Z) (%)	Δ Re(Z) (%)	Δ Z_j (Z) (%)	Δ |Z| (%)	Δ ϕ (Z) (%)
0.6	1.3	15.7	1.3	15.4	1.0	10.1	0.9	10.3
0.4	1.2	10.1	1.2	10.1	1.2	11.3	1.1	11.4
0.2	1.2	8.0	1.2	7.9	1.1	8.1	1.0	8.7
0	1.2	12.8	1.3	12.8	1.2	18.2	1.3	17.9
-0.2	1.5	9.9	1.5	9.9	1.0	9.3	1.0	9.4

The data at this new frequency range has a better fitting with the K-K transform. It is therefore more accurate to extract parameters such as the ohmic and polarization resistance at these conditions. **Figure III.11** plots R_{ohm} and R_{pol} against the potential applied.

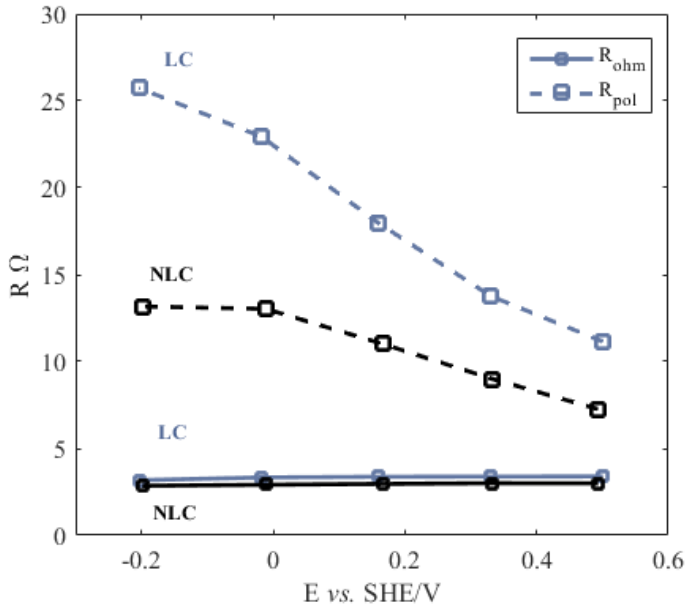

Figure III.11. Resistance from PEIS at different fixed bioanode potentials.

R_{ohm} obtained at ~ 1 kHz had an average value of 3.3 Ω (±0.09) and 2.9 Ω (±0.06) for LC and NLC respectively. This fast phenomenon was not potential-dependent and therefore fits with the ohmic resistance, which involves the bioanode, anolyte and current collector. Membrane resistance is not taking in account since the bioanode and the reference were both located in the same compartment. Regarding the resistance at low frequencies, it decreased more than twice when the bioanode potential passes from -0.2 V *vs.* to 0. 6 V *vs.* SHE, typical from a kinetic dependent phenomenon like the polarization resistance (R_{pol}). A minimum resistance of 7.3 Ω was measured at 0.6 V *vs.* SHE, which is already more than twice the ohmic resistance (2.9 Ω). Based on the Bulter-Volmer equation‡‡, the anodic current increases proportionally with the electron donor consumption and exponentially with the anode polarization. This could explain that higher polarizations could reduce the effect of an electron donor limitation. Power losses are principally affected by the limiting polarization resistance. Special attention must be taken into the electrochemical reactions, especially the oxygen reduction which is needed as intermediate for metal precipitation.

‡‡ Relationship of electrochemical reaction kinetics on electrodes.

III.3.5 GDE characterization

a. Oxygen reduction

Oxygen reduction reaction (ORR) is expected to occur in the GDE cathode. A CV measurement at 10 mV s^{-1} between 0.2 and -0.6 V *vs.* SHE was performed on the cathode to favorize the ORR reduction. The reference electrode placed this time in the catholyte side. The catholyte was composed of 30 g L^{-1} NaCl and the anolyte with the bacterial medium (section **III.3.3)**. Tests with natural air convection and with 40 mL min^{-1} of air flow were compared. For practical reasons, all the potentials are referred to SHE and current densities to the bioanode projected surface area. Results are presented in **Figure III.12**.

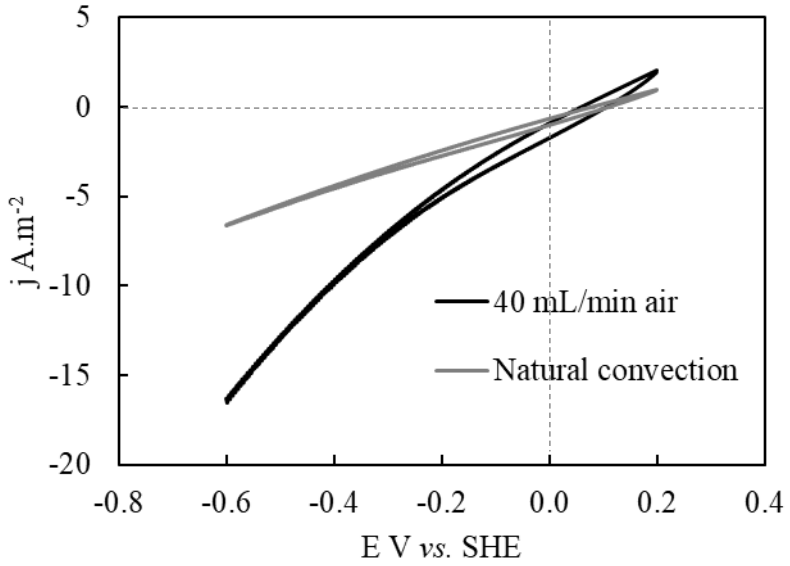

Figure III.12. CV results on the cathode at 10 mVs^{-1}. pH catholyte= 3.

Cathodic behavior under the natural air convection shows a rather linear behavior, typical from a non-faradic behavior. In presence of an additional air supply of 40 mL min^{-1}, a faradic current associated with ORR was observed from approximately -0.2 V *vs.* SHE.

b. Polarization curve in Microbial Electrolysis Cell (MEC) mode

Chronopotentiometry measurements were performed in a three-electrodes system by fixing a constant current between the bioanode and the gas diffusion cathode. Over a period of 15 minutes, currents were imposed progressively as following: 5, 10, 15, 20, 25, 30 mA. Electrodes potential, pH, charge and power were followed by the potentiostat software, ECLab. At the starting point, anolyte and catholyte pH were adjusted to 7.5 and 3 respectively. Experiments were performed after the 120 days of biofilm growth in NLC conditions.

Potentials of each electrode and the cell voltage (E_{cell}) are illustrated in **Figure III.13**. This is equivalent to execute the BES in Microbial Electrosynthesis Cell mode (MEC). The goal of this technique was to first of look at the behavior of the polarized electrodes.

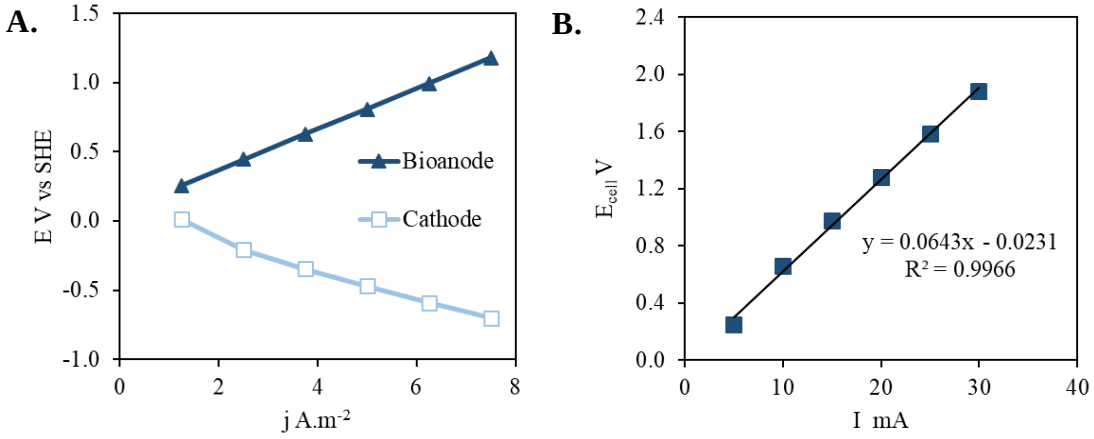

Figure III.13. MEC mode in absence of metals. **A**: Electrodes potential after 10 min applying a fixed current; **B**: Cell voltage *vs.* applied current. pH $_{anolyte}$: 7.5, pH $_{catholyte}$: 3.

The anode potential remained constant during the 10 minutes at the values presented in **Figure III.13A**. When the current was fixed at 3.8 A m^{-2}, the cathode potential was polarized at -0.35 V *vs*. SHE, which is appropriate for oxygen reduction according to the CV measurements (**Figure III.12**). At 7.5 A m^{-2}, the bioanode potential started to increase progressively until a value of 1.2 V *vs*. SHE. There is no consensus on the maximum anodic polarization electroactive

bioanodes can support, but high anodic potentials increase the risk of parasite reactions taking place over the acetate oxidation.

Moreover, a linear behavior was observed between the bioanode potential and the tested currents, which is typical from an ohmic resistance behavior. A similar linearity was observed in **Figure III.13B** between E_{cell} and the applied current. A total intern resistance of 64.3 Ω was stablished as the slope of that relation E *vs.* I. This is a typical and undesired ohmic behavior attributed to different factors: the non-optimized electrochemical geometry as electrodes were not facing each other, the distance between electrodes and consequent electrolyte resistance, and the membrane fouling. Even though the electrochemical oxygen reduction and the bioelectrochemical acetate oxidation were separately thermodynamically possible, this ohmic drop has been previously described as a major problem for the current evolution even in halophilic bioanodes[213]. Microbial bioanodes with high salinity tolerance have produced a maximum current of 85 A m^{-2} with an electrodes distance of few millimeters[229]. The system can still be substantially improved in a configuration with parallel electrodes at a minimum distance as possible between them. The MEC mode is useful tool to either control the current rate or the electrodes polarization. Higher current rates can be achieved but together with a consequent energy consumption. Therefore, an energy-added free system was also studied.

c. Polarization curves in Microbial Fuel Cell mode

External resistances were fixed over a period of 15 minutes between the bioanode and cathode, also known as Microbial Fuel Cell (MFC) mode. These external resistances influence the resulting current, power and electrodes polarization. Current and power were calculated based on the following equations:

$$E_{cell} = E_{cathode} - E_{anode} = OCV - I\,(R_{int} + R_{ext}) \quad \textbf{(III-15)}$$

$$P = I\,E_{cell} \quad \textbf{(III-16)}$$

Where R_{int} was 64.3 Ω from the previous section and R_{ext} an external measured resistance that connected anode and cathode. Electrodes potential ($E_{cathode}$ and

E_{anode}) and electrolytes pH were followed by the EClab software. As in MEC mode, pH was initially stablished at 7.5 for the anolyte, 3 for the catholyte, and experiments were performed under NLC conditions after the 120th day. The polarization curve and potential behaviors of the MFC configuration in absence of metals is presented in **Figure III.14**.

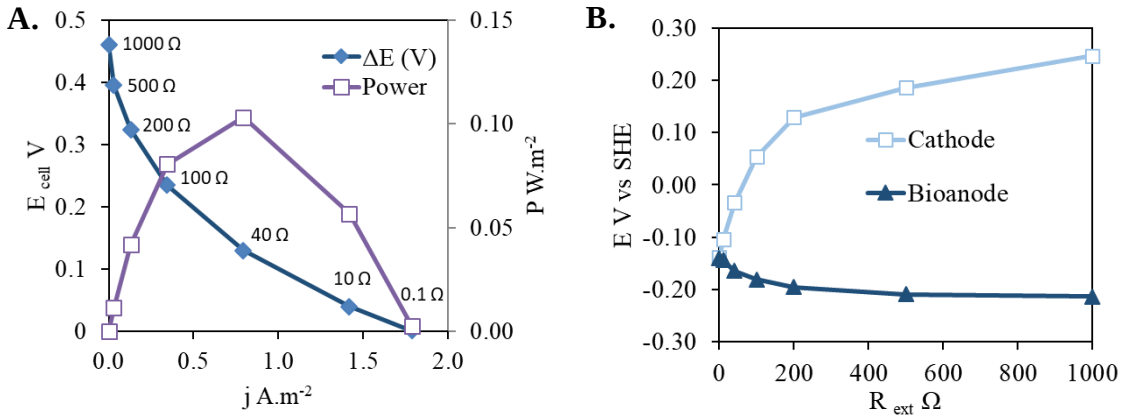

Figure III.14. Characterization in MFC mode: **A.** Polarization curve after 10 min at fixed resistances; **B.** Electrodes potential after 10 min applying a fixed resistance (MFC mode). pH $_{anolyte}$: 7.5, pH $_{catholyte}$: 3.

It is observed that a maximum current of 1.8 A m^{-2} is obtained when the cell voltage tends towards zero at the lowest external resistance (*i.e.* 0.1 Ω). This maximum current is approximately half of the maximum current obtained in MEC mode by polarizing the anode at 0.43 V *vs.* SHE. Likewise, the current density tends towards zero as the resistance tends to 1000 Ω. The power, which depends on both current and cell voltage, has a maximum value of 0.1 W m^{-2} at 0.8 A m^{-2}. This value was obtained when a load of 10 Ω was connected on the system. Metal recovery aims to prioritize maximum current over the maximum power, so 0.1 Ω was the best resistance. In **Figure III.14B**, the polarization behavior is observed at fixed resistances. When the load corresponds to 1000 Ω, the cathode is for instance at 0.25 V *vs.* SHE. Based on the CV results (**Figure III.12**), this potential is not enough to favorize the cathodic current related to the oxygen reduction. On the other hand, negative potentials are obtained at external resistances lower than 40 Ω. Therefore, low resistances are also suitable in terms of cathodic polarization.

III.4 Coupling bioanode and GDE for metal recovery

III.4.1 Experimental

a. Catholyte medium preparation

Inspired from REE-rich sediments found close to the Namibian coasts[230], a solution containing metals salts ($CuCl_2$, $MnCl_2 \cdot 2H_2O$, $ZnCl_2$, $NiCl_2$, $La(NO_3) \cdot 6H_2O$, $Nd(NO_3) \cdot 6H_2O$, $Sm(NO_3) \cdot 6H_2O$, $Ce(NO_3) \cdot 6H_2O$) was used to simulate leached metals from marine environments. The solution was prepared from x10 concentrated stocks, contained 30 $g.L^{-1}$ NaCl (0.5 M) and was adjusted to pH 3 with 30% HCl. Metals present in the were then analyzed by a High Resolution Inductively Coupled Plasma Mass Spectrometer (HR-ICP-MS, VITO). The concentration of metal ions and the ICP limit of measure are presented in Table III.4. The ICP limits are given by the ICP equipment and the calibration curve for each metal.

Table III.4. Synthetic leached metal aqueous matrix composition from marine environments.

Metal	mg L^{-1}	ICP limit µg L^{-1}
Cu	220	<100
Mn	100	<100
Ni	50	<100
Zn	100	<100
La	75	<10
Nd	75	<10
Sm	75	<10
Ce	50	<10

The technology was tested in both MEC and MFC mode. The MEC configuration applied a chronoamperometry over the bioanode of 0.43 V *vs.* SHE as in the

biofilm growth. The MFC test used an external resistance of 0.1 Ω between the bioanode and cathode. To do so, the electrodes current collectors were connected in series through a resistance box and the corresponding resistance measured with a multimeter. In both MFC and MEC, the system had an Ag/AgCl reference electrode in the anolyte side. Electrodes potential, anolyte and catholyte pH were followed with the potentiostat in MFC mode. Current and charge were also recorded in MEC mode. The tests had blank controls with a catholyte containing 30 $g.L^{-1}$ NaCl at an initial pH 3. The OCV was measured by leaving the system disconnected for several hours until a stable value was achieved.

III.4.2 MEC mode

b. Blank control

As mentioned before, the BES/GDE technology aims to increase the pH of the catholyte to favorize the metal precipitation and subsequent recovery. A control experiment in absence of metals was firstly tested polarizing the bioanode at 0.43 V *vs.* SHE. Results presented in **Figure III.15** reveal the current, potential and pH evolution over time.

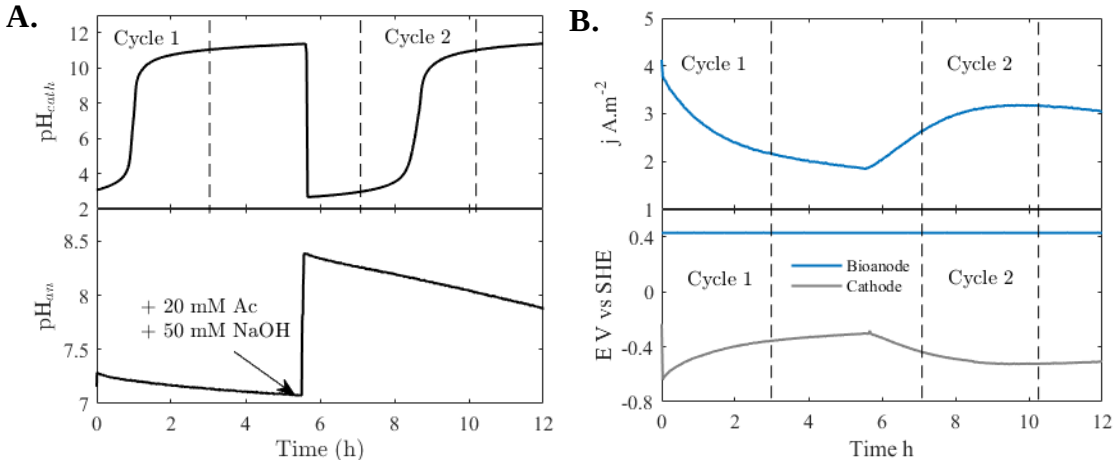

Figure III.15. BES technology control in absence of metals and MEC mode: **A.** pH evolution of catholyte (pH_{cath}) and anolyte (pH_{an}) within time; **B**. Current density and electrode potential behavior.

Since metals should be precipitated at pH 11, cathodic cycles were defined as the lapse of passage from the initial catholyte pH of 3 to 11 (**Figure III.15A**). Two

cycles were therefore differentiated during the experiment. Once the pH exceeded 11, the pH adjustment to 3 defined the beginning of the 2nd cycle. At the same time, 20 mM of acetate were added to the anolyte and its pH adjusted to 8-8.3.

The measured current density presented in **Figure III.15B** is related to an electron transfer between the electrodes driven by an external energy input. The first cycle had a maximum current density of 4 A m^{-2} corresponding to the electrode starting polarization. The cathode polarization is linked to the current evolution, decreasing in the 1st cycle with the current and then increasing and stabilizing as the current in the 2nd cycle. Nevertheless, the cathode potential was always lower than the bioanode, a common behavior in non-thermodynamically favorable processes as the MEC mode.

The catholyte's pH increases as far as the transferred electrons are used to reduce oxygen in the cathode. This reaction consumes protons at pH<7, produces hydroxide ions at pH>7 and may have several intermediate steps[152]. Based on the cumulated charge at these conditions (Q_{total} in C), a cathodic faradic efficiency (η_F) was calculated with equation (**III-17**). To do so, the measured charge in acid conditions ($Q_{meas}^{pH<7}$ in C) was calculated as proton molar consumption (Δn_{H+} in mol L^{-1}) multiplied by the catholyte volume (V_{Cath} in L) and the faraday constant (F in C mol^{-1}) (equation **III-18**). The charge in basic conditions ($Q_{meas}^{pH>7}$ in C) used the OH^- molar consumption (Δn_{OH-} in mol L^{-1}) instead of the protons (equation **III-19**). To simplify the calculations, reactions were assumed to consume one electron per proton consumed and one per hydroxide produced (equations **III-2** and **III-5**).

$$\eta_F = (Q_{meas}^{pH<7} + Q_{meas}^{pH>7}) / Q_{total} \quad \textbf{(III-17)}$$

$$Q_{meas}^{pH<7} = \Delta n_{H+} \times V_{Cath} \times F \quad \textbf{(III-18)}$$

$$Q_{meas}^{pH>7} = \Delta n_{OH-} \times V_{Cath} \times F \quad \textbf{(III-19)}$$

The performance results on MEC mode are presented in **Table III.5**. Q_{meas} are related to the calculated charge for passing from pH≈3 to pH≈11 and therefore are very similar for both cycles.

Table III.5. Parameters related to MEC performance in absence of metals.

Cycle	pH	Q_{meas} (C)	Q_{total} (C)	η_F (%)	J (A m^{-2})	t_{total} (h)
1	3 to 7	44.69	45.96	83	2.38	5.56
	7 to 11	49.88	67.44			
2	3 to 7	47.43	58.67	75	3.05	2.97
	7 to 11	49.82	70.74			

The consumed charge (Q_{total}) was relatively higher from pH 7 to 11 compared to the acidic conditions. A Q_{total} increase of 46.5% and 20% from acid to basic conditions during the first and second cycle respectively could be related to the ORR reaction. ORR consists of multiple adsorption/desorption and reaction steps involving species such as O, OH, O_2^-, HO_2^-, and H_2O_2[231]. Under alkaline media and with the GDE electrode, one of these steps could be limited. Besides, a potential lost is possible since there is an abrupt difference between the ORR redox potential in acidic media (equation **III-2,** equation **III-3** and equation **III-4**), and in alkaline media (equation **III-5,** equation **III-6** and equation **III-7**).

An overall high cathodic faradic efficiency was obtained in both cycles. The average current (**J**) was 28% higher in the second cycle and the time reduced about 46 %. The initial anolyte pH is probably linked, since it was not the same for each cycle (7.3 and 8.3 for the first and second one respectively). The pH influence on the electroactivity and current response could be interesting to analyze.

c. MEC with a metal rich catholyte

MEC results with a simulated metal-rich marine solution as catholyte are observed in **Figure III.16**. First, three distinguished precipitation plateaus at different catholyte's pH were observed (**Figure III.16A**). To do so, two anolyte cycles were required (**Figure III.16B**).

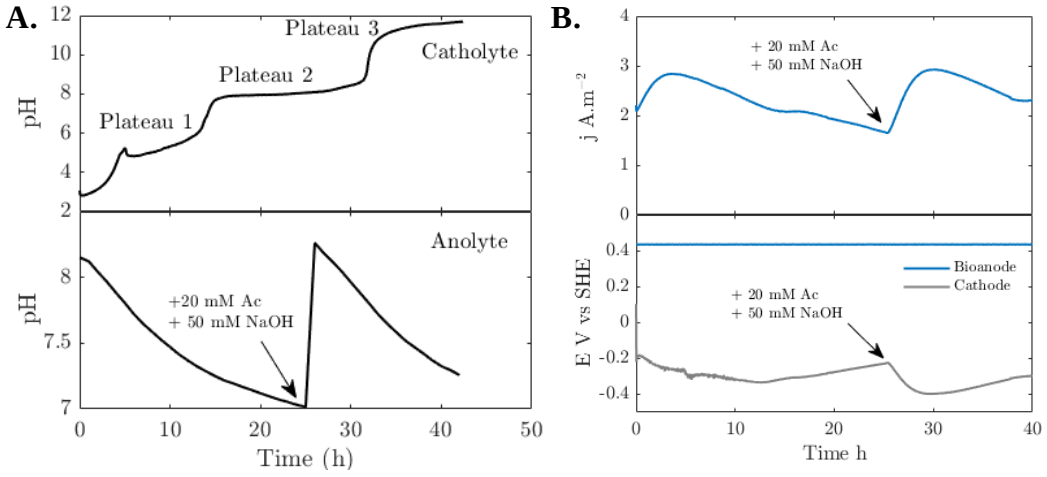

Figure III.16. Metal recovery in MEC mode: **A.** pH evolution within time; **B.** Current density and electrode potential behavior.

The precipitation plateaus observed at pH of 6.4, 8 and 11 result from a hydroxide generation followed by a metal precipitation (equation (**III-8**)). Indeed, in these regions hydroxides generation rate is proportional to the metal complexation rate and therefore OH^- produced do not affect the overall pH. A single cathodic cycle evaluated took 33.7 h to reach a pH 11, at least six times longer than the metals-free catholyte. At this point, liquid samples analyzed by ICP revaled no traces of metals remained. A more detailed study on metal removal is presented in Section **III.4.4**. Metal ions passage trough the membrane to the anolyte was not quantified but assumed insignifcant compared to the Na^+ passage, due to its high initial concentration (0.5 M) and its transport facility in cation exchange membranes[232].

The anolyte pH decreased from 8.2 to 7 in 24h as acetate consumption acidified the system. Then, the pH was adjusted to 8.4 and 20 mM of acetate added to prevent the bioanode from LC conditions. The current density consumed and electrodes potential behavior, observed in **Figure III.16B**, shows the effect of this anolyte adjustment. A similar behavior as in absence of metals is perceived (**Figure III.15B)**, since the current and cathode polarization increase till a maximum point and then return to lower values (<2 A m^{-2}). Besides, the average current of 2.35 A m^{-2} is comparable with 2.38 A m^{-2} and 3.05 A m^{-2} of the control test (**Table III.5**). The presence of metals does not seem to affect the levels of current consumed.

An energy consumption was calculated as the product between total cumulated charge (Q_{total}) and the cell voltage (E_{cell}). This BES configuration removed all the metals from the catholyte spending 0.84 kJ. Considering a total metal mass of 374 mg initially diluted in the catholyte according to the ICP analysis, it represents 2.24 MJ per 1 kg of metal removed from the solution. This is equivalent to the embodied energy to produce a brick[2]. However, the energetic balance in separation and purification steps would be necessary to compare it with conventional metal production technologies. The advantage of bioanodes is still the thermodinamically faisability to avoid an electrical energy input in the system. The microbial electrochemical system in MFC mode was therefore analyzed.

III.4.3 MFC mode

a. Blank control

The microbial fuel cell control in absence of metals with an external resistance of 0.1 Ω is presented in **Figure III.17**. Four catholyte cycles from pH 3 to 11 were performed and synchronized with four anolyte adjustments (**Figure III.17A**). The current response observed in **Figure III.17B** is calculated from equation **III-15** and normalized with the projected surface area of the bioanode. The measured OCV was 0.3 V and the total resistance (R_{int} + R_{ext}) taken was 64.1 Ω.

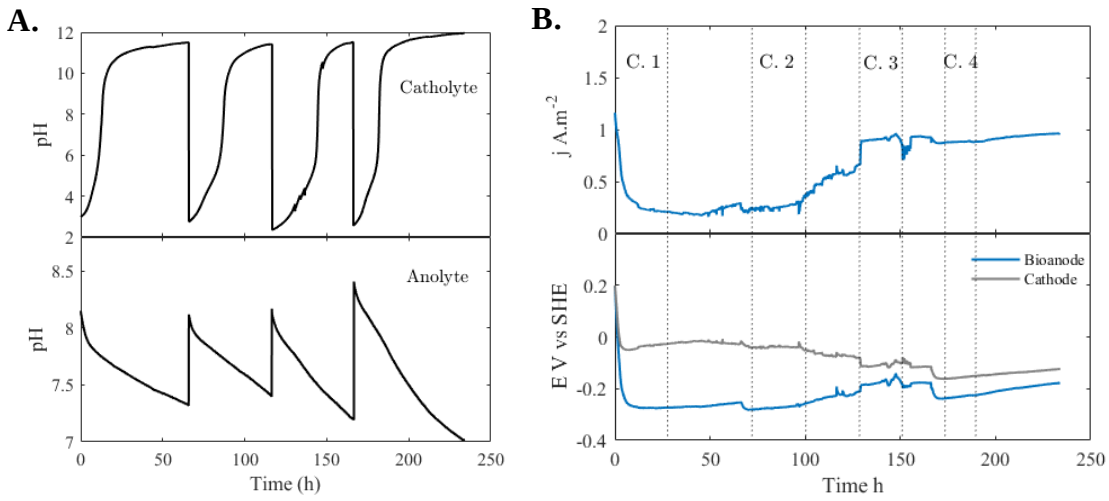

Figure III.17. BES control in absence of metals and in MFC mode: **A.** pH evolution within time; **B.** Current density and electrode potential behavior. C.1, C.2, C.3 and C.4 represent the catholyte cycles from pH 3 to 11.

The exchanged current is intended to decrease the anolyte pH and to increase the catholyte's one. Slower anolyte and catholyte cycles compared to the MEC more are thus a sign of lower electrochemical reactions. As electrons are being transferred spontaneously, it is normal to except a lower electrochemical activity compared to a system with a supplementary energy input to polarize the electrodes.

Regarding the current response, a first low current response during the first cycles is observed (**Figure III.17B**). It was attributed to a connection problem between the bioanode and the cathode. The bioanode potential remained constant at around -0.25 V *vs.* SHE whereas the cathode had an initial potential near 0 *vs.* SHE and then tended to reach a similar bioanode potential. High electrodes differences were already observed in polarization curves when external resistances were increased (**Figure III.14**). After the second cycle, the current increased as the potential difference was reduced. There is not a common law for the optimum electrode potential regardless the microbial community. However, the low potentials present in the MFC mode are most likely related to redox mediators of microbial processes[53,233]. What matter the most is that it is relatively stable and at low external resistances, it keeps the cathode potential at negative values, favorizing the oxygen reduction.

Regarding the energetic performance of the MFC mode, a panel of parameters was calculated for each cycle and displayed in **Table III.6**.

Table III.6. Parameters related to MFC performance in absence of metals.

Cycle	Condition	Q_{meas} (C)	Q_{total} (C)	η_F (%)	J (A m^{-2})	t_{total} (h)
1	3 to 7	49.88	88.70	71	0.35	27.8
	7 to 11	48.74	50.92			
2	3 to 7	48.22	59.99	84	0.26	30.8
	7 to 11	48.26	55.23			
3	3 to 7	48.23	217.42	30	0.88	25.0
	7 to 11	48.90	101.06			
4	3 to 7	48.15	144.01	47	0.88	16.1
	7 to 11	48.32	59.76			

The measured charge is very similar to the calculated in MEC conditions. The cumulated charge is however more significant in acidic conditions. Considering that the electrodes are less polarized in the MFC system, it is possible that at these conditions the resistance losses are higher in acidic media. At least for the bioanode, the polarization resistance increased from 12 to 25 Ω when the potential passed from 0.4 V to -0.2 V (**Figure III.11**). Moreover, both the current and the efficiency are important to accelerate the cycle. The fourth cycle had the best compromise between the electrons transfer and the resistance loses as it lasted 16 h. Both parameters are important in presence of metals, as more reaction can also take place and influence the performance of the system.

b. MFC with a metal rich catholyte

A cathodic cycle was performed in presence of the same synthetic leached marine deposits employed in the MEC mode (**Table III.4**). Anolyte's and catholyte's pH as well as the current generation and the electrodes potential behavior are presented in **Figure III.18**. The three precipitation plateaus previously observed in MEC mode are relatively defined.

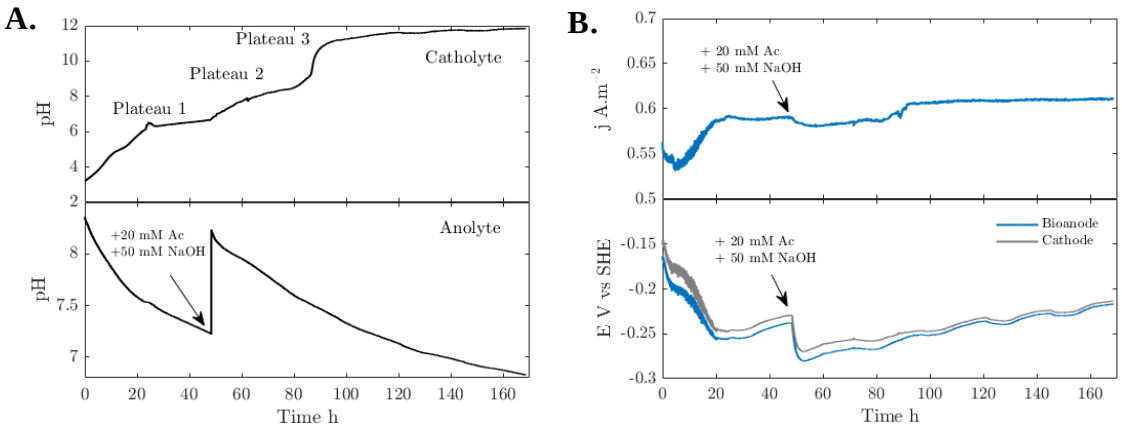

Figure III.18. Metal recovery in MFC mode: **A.** pH evolution within time; **B.** Current density and electrode potential.

The cathodic cycle took 92.8 h to reach a pH 11, at least three times more than the blank control. The longer time is certainly due to the presence of metals, as OH- complexes with metals and retain the pH from increasing as in the MEC mode. It is

also 2.8 times longer than the MEC test, since the MFC mode does not polarize the electrodes as much as the MEC and redox reactions are therefore less favorized.

The calculated current density showed in **Figure III.18B** is an indicator of the electron transfer and not a supplementary energy generation. It passes from 0.55 A m^{-2} to 0.6 A m^{-2} as electrodes are being polarized during the first 20 h. A stable current exchange is subsequently achieved for the following 150 h, despite the anolyte cycles (pH and concentration adjustments). As observed in the bioanode CV (**Figure III.9**), the current response was not sensitive to the limiting conditions when the bioanode potential was fixed at values lower than 0.2 V *vs*. SHE. Other factors such as the overall high resistance and an acetate excess in the electrolyte cannot be discarded. Once the pH reached 11, all the metals had disappeared from the catholyte solution without any electrical energy input. Energy requirements were still necessary for the air flow and electrolytes mixing, but this is a first step towards an eco-friendlier metal recovery technology.

III.4.4 BES/GDE comparison between MFC and MEC

a. Energy efficiency and removal time

From previous results in MFC and MEC configurations, the BES/GDE system was evaluated in terms of efficiency and metal removal time. The pH change charge ($Q_{\Delta pH}$) is the cumulated charge in acid and basic conditions ($Q_{meas}^{pH<7} + Q_{meas}^{pH>7}$). The metal charge ($Q_{metal}$) was calculated based on the metal concentration measured by ICP and consequent stoichiometric OH^- required (equation **III-8**). The number of OH^- moles required to precipitate these metals were then associated to a coulombic charge by the Faraday's Law. The efficiency in presence of metals is therefore defined as:

$$\eta_F = (Q_{meas}^{pH<7} + Q_{meas}^{pH>7} + Q_{metal}) / Q_{total} \quad \textbf{(III-20)}$$

Parameters evaluating the energy efficiency and removal time in MFC and MEC mode are presented in **Table III.7**.

Table III.7. Performance of BES/GDE technology for metal recovery.

System	Q ΔpH (C)	Q $_{metal}$ (C)	Q $_{total}$ (C)	η $_F$	Time (h)
MFC	78.6	1021.6	1505.7	73%	92.8
MEC	89.2	1022.7	1140.4	98%	33.7

Results reveal that the MEC configuration is both more efficient and faster for metal precipitation. This is an interesting result since the MEC is significantly improving the performance of the system with a relatively low energy consumption (0.84 kJ).

b. Metal removal assessment

As mentioned before, the exchanged current in both MFC and MEC systems was intended to increase the catholyte's pH in order to precipitate the metals. Three catholytes precipitation plateaus were identified and could be a sign of selectivity. Catholyte samples were analyzed at the end of these plateaus by ICP and metal removal was estimated (equation **I-3)** and presented in **Table III.8**.

Table III.8. Metal removal assessment of the BES/GDE technology

System	pH	Metal removal percentage (%)							
		Ce	La	Nd	Sm	Mn	Ni	Cu	Zn
MFC	6.4	13.1	10.0	10.9	13.9	4.2	4.6	96.5	10.5
	8.2	85.5	68.1	82.5	89.4	51.7	78.5	99.8	77.6
	11.08	100.0	100.0	100.0	100.0	100.0	100.0	100.0	100.0
	11.8	100.0	100.0	100.0	100.0	100.0	100.0	100.0	99.5
MEC	6.4	26.2	21.2	29.5	39.1	10.9	19.4	100.0	25.4
	8.2	76.5	52.0	73.7	91.6	45.1	61.9	99.9	83.7
	11	100.0	100.0	100.0	100.0	99.9	99.8	100.0	99.6

During the first plateau at pH 6.4, more than 96% of copper was removed from the catholyte. As Cu^{2+} has the lowest solubility among the metals studied, it is normal to recover it at the lowest pH. It is however remarkable that in MFC mode, most of the other metals remained in solution. In MEC mode, some metals like Sm and Nd were partially eliminated due to a possible metal intercalation in the copper

precipitation. This could be enhanced by a faster precipitation as it is the case in the MEC mode. Then, at the second plateau at 8.2, most of the metals precipitate in a high proportion. Samarium is the one that precipitated the most, but it is highly mixed with other metals and therefore a low selectivity was achieved. At pH 11, no metals were longer measured in solution. This is indeed a good pH to assure the total metal precipitation.

These precipitation plateaus are not only linked to the metals but also to their oxidation state and complementary ions. The oxidation state can for instance affect the metal solubility and carbonates and sulfates present in some deposits could favorize or not the metal complexation and precipitation selectivity. These results give an overview of possible ideal recovery pH but experiments with real leached deposits are necessary to validate it. Considering an overall *in situ* process coupling electrobioleaching and metal recovery, the geochemical environment of the deposits site will also determine the type and variety of microorganisms. Sulfide deposits seem to host a larger community and to be more dynamic in terms of pH, temperature and metal composition. It is difficult to measure the impact of microbial electrochemical systems on these environments as well as challenging regarding the dynamic conditions to deal with. Fe-Mn crusts occupy larger sites and are commonly present in the limiting oxygen zone, so mostly anaerobic microorganisms will be present. Not clear consequences about the oxygenation of this environment have been examined, but the air flow required to favorize the cathodic reduction could have a negative impact on the ecosystem. Nodules may be easier to manage as they are not attached to the seabed as the crusts and their reserves seem to be larger than crusts and sulfide deposits. The challenge will be related to the deeper conditions (4000 – 6000 m), where the carbon sources and conditions for life in general may be more limited. The REE rich mud also seems to have a tremendous potential in terms of metals. Not much information about the environment has been found so far. However as for nodules, the deep will be the most challenging part.

III.4.5 Sum-up

The potential of microbial electrochemical cells in marine environments has already been studied[234,235]. Halophilic microorganisms have demonstrated an electroactive behavior and offer an opportunity to use microbial electrochemical systems in marine conditions. A bioanode poised at 0.43 V *vs*. SHE exchanged a maximum current density of 4.1 A m^{-2}. The electroactivity was nevertheless hidden by the overall ohmic resistance (64 Ω), from which the bioanode influence is considerably low (3 Ω). Moreover, the GDE cathode proved a pronounced ORR reaction under cathodic potentials lower to -0.2 V *vs*. SHE. The coupling of the bioanode and the GDE achieved a 100% of metal precipitation in both MEC and MFC mode. This precipitation obtained at pH 11 took 33.7 h and 92.8 h for the MEC and MFC respectively. The most important finding was to proof that metal recovery was possible by coupling an ORR reaction from a GDE cathode with an oxidation catalyzed by halophilic bioanode with no energy input for the electrodes polarization.

III.5 Conclusions & perspectives

The BES/GDE technology opens a new route for metal recovery from leachates of marine metallic deposits. The three compartments system (anolyte/catholyte/air chamber) was studied at a laboratory scale with a classical H-cell geometry. Metals from base to REE precipitated from simulated leached marine deposits in the cathodic compartment. The main mechanism is the oxygen reduction on the GDE cathode and consequent pH increase of the catholyte. This reaction was enhanced by an external oxygen supply from the air chamber and driven by the anolyte oxidation catalyzed by the halophilic bioanode. Both bioanode and cathode were firstly analyzed separately. Then, the system was studied in MEC and MFC mode. For each case, some conclusions were found:

Bioanode

(i) The halophilic bioanode polarized at 0.43 V *vs.* SHE was able to catalyze an oxidation process with characteristic phases of bioanodes. The pH and current were used as indicators of limiting and non-limiting conditions.

(ii) The electroactivity at 0.43 V *vs.* SHE and under non-limiting conditions is convenient as the polarization resistance is decreased.

BES/GDE coupling

(i) The oxygen reduction is enhanced in presence of the air flow and when the cathode potential is negative.

(ii) The bioanode ohmic is considerably low (3 Ω) compared to the overall ohmic resistance (64 Ω) as observed in the MEC mode. This phenomenon is characteristic of an unoptimized geometry and membrane (bio)fouling.

(iii) By lowering the external resistance, the exchanged current was maximized up to 1.8 A m^{-2}. It also reduced the cell voltage and thus the output power. However, the cathode potential is more polarized at the lowest resistance and therefore it is more convenient for the oxygen reduction.

Metal recovery assessment

(i) The BES/GDE system had the robustness to work either by an external energy (MEC) or resistance (MFC) input. Independly of the nature of the metal, they all precipitated at pH 11 and was particulary selective on Cu at pH 6.4.

(ii) Despite the high ohmic behavior, the polarized system in MEC mode was able to increase the catholyte's pH from 3 to 11 in 3 hours and an energy consumption on the electrodes of 0.28 mA h^{-1}. It was 10 times longer in presence of metals but this time depends on the initial metallic charge.

(iii) The MFC took from 16 to 30 hours to pass from pH 3 to 11 due to a lower electron transfer compared to the MEC. The metal precipitation was completed after 5 days with a 73% efficiency due to a more visible bioanode polarization resistance.

Regarding the perspectives, a set up with closer electrodes could be useful to avoid the high ohmic behavior. Current variations observed in MEC mode can be diminished in a continous flow configuration. Furthermore, the MFC system does not produce and transfer as much electrons as the MEC mode and it has repercussions on the system efficiency and metal recovery time. However, it is still possible to have 100 % of metal precipitation with no energy input on the electrodes. Besides, the system is less sensible to the starvation conditions, giving more flexibility in terms of electron donor supply. The system is more sensible to the resistance variations, so proper connections must be checked within time. In any case, this technology has proven its potential for metal recovery in high saline conditions with a low energy input.

A second plan of the global project will consider the feasibility of metals electro-bioleaching from marine deposits. *In situ* metal electrobioleaching would couple microbial, chemical and electrochemical mechanisms to dissolve metals at the marine conditions. This process has already been proven for recovery of copper, nickel and cobalt from land concentrates (*ie.* sphalerite, chalcopyrite) and marine ferromanganese minerals under acidic conditions[236]. Bacteria could indeed pre-solubilize the metals and then precipitate them in situ, preventing from environmental impacts of mineral drilling, digging and transport trough the water

column. Before that, the metal precipitation with the BES/GDE technology must be evaluated under deep sea conditions. So far, the halophilic bacteria in highly saline environment and metals concentration were simulated. Some of other criteria that must be evaluated are:

(i) Electroactivity of halophilic bioanodes with organic matter other than the acetate.
(ii) The electroactivity of bioanodes and oxygen reduction at deep sea temperature and pressure, depending on the geological conditions of the mineral sites.
(iii) The process must be remotely monitored.

Despite the well-known temperature sensitivity of bioreactors, a recent study from Heidrich *et al*[237]. shows that MFC at 7.5 °C had similar power densities and coulombic efficiencies compared to MFC at 26.5 °C. Besides, the dominant microorganisms kept electroactive properties regardless the temperature, especially from *Geobacter* species. Nevertheless, the choice of the substrate, acetate or wastewater in this case, seems to have a more significant effect on both reactor performance and microbial diversity[237]. The high pressures could also play an important role in the BES performance. Unfortunately, no relevant studies on microorganisms electroactivity at deep sea level pressures have been found so far.

CHAPTER IV

Ionic Liquid catholyte for neodymium recovery

Representation of the resources supporting green energy technologies. Taken from M. Gras PhD presentation defence.

IV.1 Introduction

The previous chapter revealed the potential of BES to generate OH^- as intermediate species leading to metal precipitation. **Chapter IV** aims to use directly the metal ion as final electron acceptor, a common arrangement for metal electrodeposition. The examined metal is neodymium (Nd), a Rare Earth Element (REE) known for its high value on renewable technologies and energy devices (*e.g.* permanent magnets, batteries, electric vehicles). Nd electrodeposition is paradoxically far from being a green process due to the use of organic solvents at high temperatures, releasing toxic compounds and consuming pointless energy. Ionic liquids seek to replace the organic solvents for this purpose and are currently at a research level.

Chapter IV goes beyond the classic BES by combining an aqueous/ionic liquid system for Nd electrodeposition. An electroactive bioanode is firstly grown in an aqueous system. Once the biofilm is firmly established, the catholyte is replaced by an ionic liquid with dissolved Nd and the Nd electrodeposition feasibility is tested. A critical questioning regarding our configuration is highlighted but also opens to interesting perspectives of ionic liquids in BES.

This chapter is the result of a collaboration between members of the Interfacial Electrochemistry and Processes team at LEPMI. It was financially supported by the French Ministry of Education.

IV.2 Secondary mining of neodymium

IV.2.1 Context

Rare earth elements (REE) are nowadays crucial in modern technologies. The apogee of electronic devices and low carbon technologies have benefited from the unique properties of REE. A broad range of REE are currently used in renewable energy generation and storage, energy efficient lights, electric cars, and auto catalysts, among others[238] (**Figure IV.1**). These "rare" elements are actually more abundant than common industrial metals such as copper, zinc, nickel and lead[239,240]. The word "rare" arises from the historical technological barriers in separating and extracting them from the mineral deposits[239]. Despite their abundance, they stand out as critical raw materials due to their exponentially increasing demand in these modern technologies, the lack of comparable substitute and the monopolization of supply sources[240]. As observed in **Chapter III**, marine sediments extraction intends to reduce their criticality, but REE recycling from end of life products is required to relieve to some extent the supply risk. Besides, secondary mining is the cornerstone for a sustainable development[240].

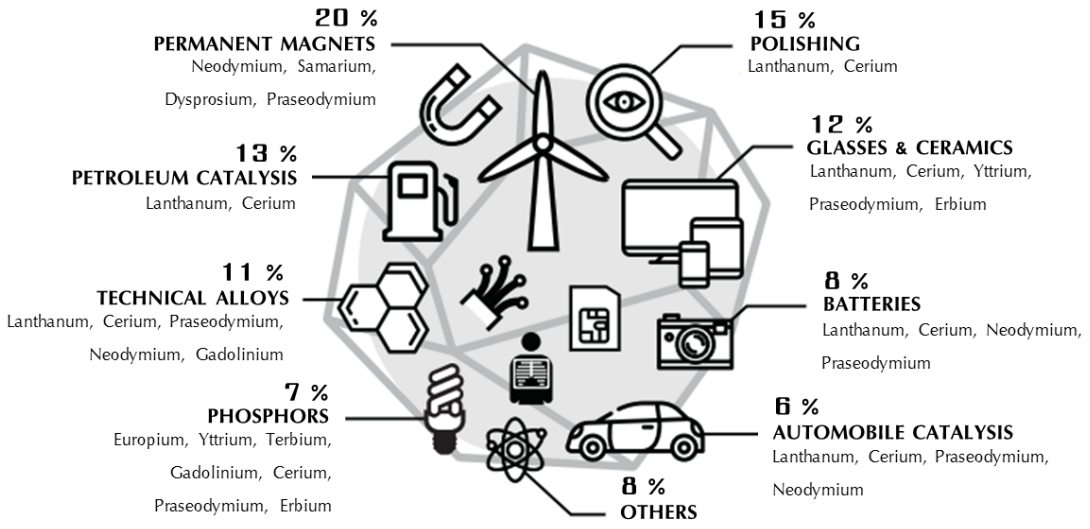

Figure IV.1. Panorama in 2014 of REE applications[238].

Special policies have been adopted to encourage REE recycling in the European Union, Japan and China[241,242]. Some of the bottlenecks are the minor REE content in the final applications, the technical difficulties and energy cost to extract them with an economic profit, and the abundance of primary supply[240].

Here, a new microbial electrochemical configuration based on metal electrodeposition is proposed to address the energetic cost. The technique consists of reducing electrochemically soluble metal cations from an electrolyte, which leads to the precipitation of reduced metals as layers deposited on the cathode surface (**Figure IV.2**).

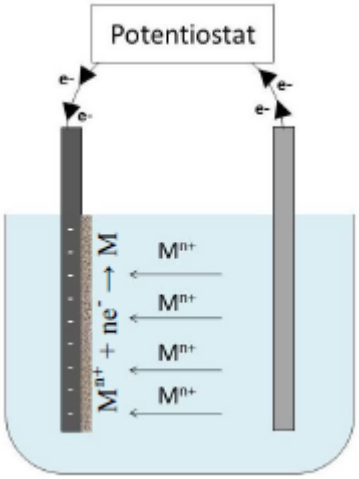

Figure IV.2. Simplified schema of metal electrodeposition[222].

This reduction is thermodynamically possible when the cathode is polarized at a potential below the standard potential of the metal (E_0). REE electrodeposition is complicated since their standard potentials are particularly very low (*e.g.* $E°_{Ce3+/Ce}$ = -2.48 V *vs.* SHE; $E°_{Pr3+/Pr}$ = -2.46 V *vs.* SHE; $E°_{Nd3+/Nd}$ = -2.43 V *vs.* SHE when the REE concentration is 1 M[152]). This implies a high cathodic polarization which costs energy and requires a special environment, including electrochemically stable electrodes and electrolytes.

Rare earths are inherently difficult to separate because of their similar chemical properties and the processing of pure REE is complex[240]. In a first approach, it was decided to work with a single and pure element. The work presented is this chapter

investigates the electrodeposition of Nd. Nd is the third most abundant REE and is a key component of new generation permanent magnets, which are widely used by the electronic and automotive industry[239], and more recently for wind turbines[238].

Nd electrodeposition is a challenging reaction. Its equilibrium potential is defined by Equation (**IV-1**), where C_{Nd3+} represents the concentration of Nd^{3+} in mg L^{-1}.

$$Nd^{3+} + 3e^{-} \rightarrow Nd \qquad E_0 \text{ (V } vs. \text{ SHE)} = -2.431 + \log(C_{Nd3+}) \qquad \textbf{(IV-1)}$$

According to the Pourbaix diagram (**Figure IV.3**), the solid Nd region is situated significantly below the water cathodic electrochemical stability (a dotted line). Nd electrodeposition is not suitable in aqueous solvents, since water electrolysis leads to supplementary energy losses and restricting the deposit quality. Moreover, pure Nd cannot be deposited from aqueous systems as hydrogen and metal hydroxides or oxides are produced[243].

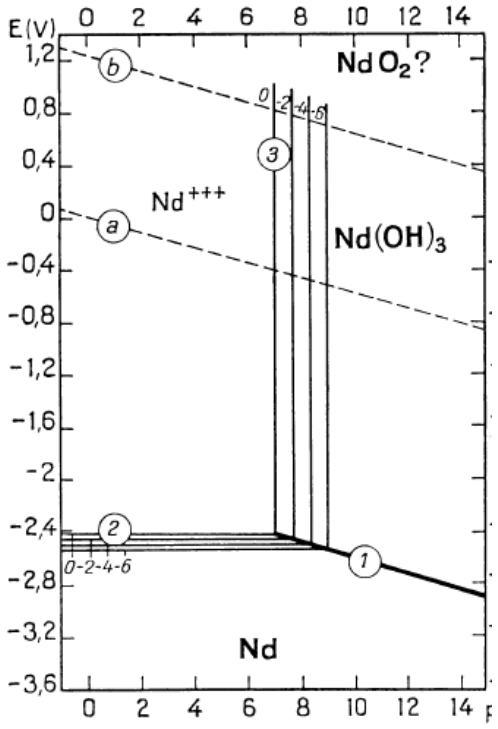

Figure IV.3. Pourbaix diagram of Nd ions in an aqueous system, where a and b dotted lines represent the electrochemical window of water[152].

The electrochemical stability is commonly referred to the solvent electrochemical window (*e.g.* 1.23 V for water), defined as the voltage difference between the cathodic and anodic limit. Conventional volatile organic compounds (VOC) have a larger electrochemical window (*e.g.* 5.0 V for acetonitrile, 3.5 V for dichloromethane and 4.4 V for dimethylsulfoxide)[244]. Unfortunately, VOCs are toxic, flammable and volatile[245]. Molten salts such as $AlCl_3$–NaCl–KCl have an electrochemical window comparable with VOC but operate at temperatures from 150 to 1050°C depending on its composition[246]. In this Chapter, ionic liquids are considered as solvents for Nd electrodeposition. They offer energy costs savings compared to the high-temperature molten salts and they are much safer to work with than VOC[222,245]. Besides, ionic liquids electrochemical windows can exceed 6 V, resulting wider than conventional VOC[247].

IV.2.2 Ionic liquids: solvents of the future?

a. Definition

Ionic Liquids (ILs) are polar solvents often defined as salts that melt below 100 °C, forming liquid phases composed of basically cations and anions[245]. Room temperature ionic liquids (RTILs) are even liquid at 25°C. ILs could operate at temperatures over 100 °C due to their low vapor pressure and high thermal stability, but RTILs interest relies on reducing the energy cost. Cations are usually organic compounds with either a nitrogen based cyclic skeleton (*e.g.* imidazolium, pyrrolidinium, pyridinium), or a non-cyclic one with ammonium, phosphonium or sulfonium molecules. Anions such as chloride $[Cl]^-$ and bromide $[Br]^-$ can yield to hydrophilic ionic liquids whereas fluorinated (*e.g.* $[PF_6]^-$, $[BF_4]^-$) lead a level hydrophobicity depending on the associated cation. The ability to synthesize RTILs with different cations or anions makes them "designer solvents" with remarkable physicochemical properties in terms of miscibility, metal dissolution, polarity, viscosity, density and conductivity, among others. Their main bottleneck is commonly mentioned to be their high price, which can be 5 to 20 times more expensive than organic solvents[248].

From primary to secondary REE-rich matrixes, separation and extraction processes with ILs have recently emerged as sustainable and efficient alternatives to acid leaching and solvent extraction. They have been designed with functional groups able to coordinate to metal ions, facilitating the dissolution of metal oxides and salts[249]. These metal ions can be subsequently stripped from the IL phase to an acidic solution[250] or precipitated in the same IL by electrodeposition[222].

b. Nd electrodeposition from $[C_1C_4Pyr]^+[Tf_2N]^-$: advantages and limitations

1-Methyl 2-Butyl Pyrrolidinium bis(trifluoro-methyl-sulfonyl) imide (**Figure IV.4**), also known as $[C_1C_4Pyr]^+[Tf_2N]^-$, is a common RTIL studied for metal electrodeposition[251–253].

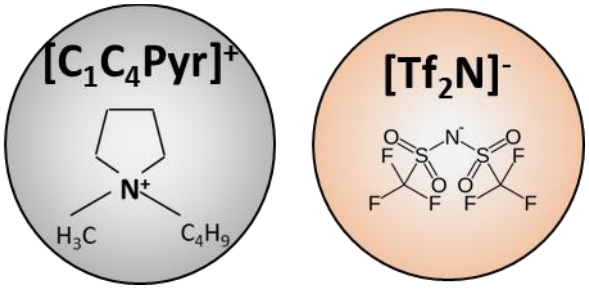

Figure IV.4. Chemical structure of $[C_1C_4Pyr]^+[Tf_2N]^-$.

At 25°C, it has a good compromise between a wide electrochemical stability (5.2 V), a reasonable ionic conductivity (2.2 mS cm^{-1}) and viscosity (89 cP) compared to other ILs (**Table IV.1**). It also has non-volatile and non-flammable properties.

Table IV.1. Viscosity (η), density (ρ), conductivity (κ), and electrochemical windows (EW) at about 293 K for some aprotic IL solvents. Values taken from Barrosse-Antle *et al*., 2010[244].

Ionic Liquid	η [cP]	ρ [g cm^{-3}]	κ [mS cm^{-1}]	EW [V]
$[C_2mim][Tf_2N]$	34	1.53	8.8	4.3
$[C_4mim][Tf_2N]$	52	1.44	3.9	4.8
$[C_8mim][Tf_2N]$	74	1.33	–	5
$[C_4dmim][Tf_2N]$	105	1.42	2.0	5.2
$[C_6mim][FAP]$	74	1.56	1.3	5.3
$[C_1C_4pyrr][Tf_2N]$	**89**	**1.40**	**2.2**	**5.2**
$[C_4mim][PF_6]$	371	1.37	1.5	4.7

$[C_1C_4Pyr]^+$ is a large organic cation composed of a cyclic quaternary ammonium with a low symmetry due to the presence of two different alkyl chains, methyl from one side and butyl from the other. The quaternary ammonium ion is among the most electrochemically stable compounds[254], and the carbon chains give this cation a hydrophobicity character[§§]. $[Tf_2N]^-$ is commonly used as anion for synthesizing hydrophobic ILs, with relatively low viscosities and high electrical conductivities[245]. As $[Tf_2N]^-$ has a poor solvating power to cations[255], the metal cations dissolution is slow but once dissolved, its reactivity becomes easier to study[256,257].

IL electrochemical properties are nevertheless very sensitive to parameters such as water content, oxygen presence and electrodes nature. **Figure IV.5** shows some examples of the electrochemical reduction behavior of the $[C_1C_4Pyr]^+[Tf_2N]^-$ solvent and the effect of different water contents and oxygen bubbling.

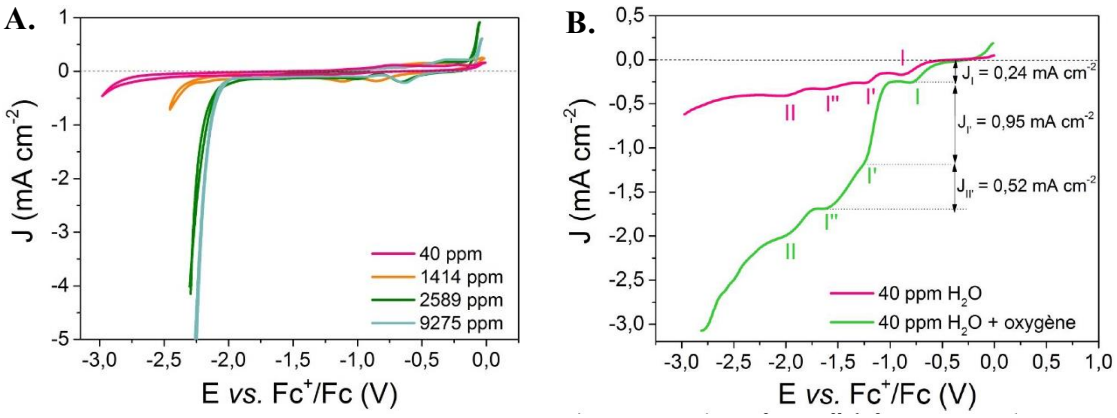

Figure IV.5. CV at 50 mV s^{-1} and 25°C on $[C_1C_4Pyr]^+[Tf_2N]^-$ with a gold working electrode. **A**: Water content influence (in ppm) in an argon headspace; **B**: O_2 bubbling influence, I: oxygen reduction, II: electrolyte reduction. Results extracted from Bonnaud et *al,* 2017.[222].

In **Figure IV.5A**, the cathodic polarization of a gold electrode resulted in a visible electrochemical reduction of the solvent at about -3 V *vs.* Fc^+/Fc with 40 ppm

[§§] There are discrepancies in the literature about the influence of the alkyl chains on the electrochemical stability of the quaternary ammonium ion[254].

water, represented by the exponential current evolution. This reduction stability was clearly induced by the water-content increase. The solvent stability starts to be disturbed at -2.2 V *vs.* Fc^+/Fc in presence of 2589 ppm water[222]. O_2 also influences the current response under a cathodic polarization (**Figure IV.5B**). The current evolution is certainly increased by the presence of bubbled oxygen and associated to different steps of oxygen reduction. Although the $[Tf_2N]^-$ degradation consequences are uncertain, the reduction of fluoride anions could for instance lead to the formation of toxic and corrosive products such as hydrogen fluoride[245,258].

The nature of the working electrode also contributes to the electrolyte stability. For instance, crystalline gold (Au) and platinum (Pt) electrodes can provoke secondary reactions such as the $[Tf_2N]^-$ anion reduction[259]. CF_3^- is a by-product of this reaction, an undesired anion for the Nd electrodeposition as it can complex Nd as a insoluble fluoride metal salt[222]. Carbon-based electrodes seem to avoid this reaction[222] and were therefore considered here as working electrodes.

The metal reduction on the working electrode must be followed by an oxidation reaction on the counter electrode, which is so far unclear in ILs solvents. Despite the high electrochemical stability of ILs and the nature of the working electrode, the upper end of the electrochemical window is usually limited by the anion oxidation[254]. Besides, the oxidation of $[Tf_2N]^-$ at low cathodic potentials has been previously evoked in the litterature[222,260]. A "sacrificial" oxidizing agent is therefore recommended to be included, either as dissolved ion (*e.g.*, ferrocene[222]) or the anode itself (*e.g.*, copper[261]). Nevertheless, traces of IL have been observed on metal deposits in presence of a supplementary oxidizing agent and could be attributed to an electrochemical oxidation of the IL[222]. IL degradations affect the deposit quality but also the solvent functionality in industrial processes, as its recyclability could be drastically affected by impurities and solvent degradation[262]. This chapter covers an exploratory experimental study of Nd electrodeposition in a two-compartments bioelectrochemical system, isolating the metal reduction from the anodic (bio)oxidation.

IV.3 Nd recovery with BES/RTIL system

IV.3.1 General principle

a. Overall system

Metal recovery by electroplating with bioelectrochemical systems has been extensively studied[95,98,105,263–265]. Bioelectrodes can reduce the energetic cost required to drive a cathodic polarization that leads to a metal reduction at the cathode surface. High purity metal deposits are subsequently expected to be recovered from the cathode. REE electrodeposition is a challenge due to the high cathodic polarization required, which implies a consequent energy cost, electrodes that catalyze the desired reaction and electrochemically stable electrolytes. For the last 20 years ILs have gain significant interest as electrolytes but stability issues are still to be solved. A new BES configuration (illustrated in **Figure IV.6**) displaces the oxidation to an aqueous second compartment, where the IL oxidation is prevented. Besides, a bioanode is intended to reduce the energetic cost by catalyzing the anodic reaction.

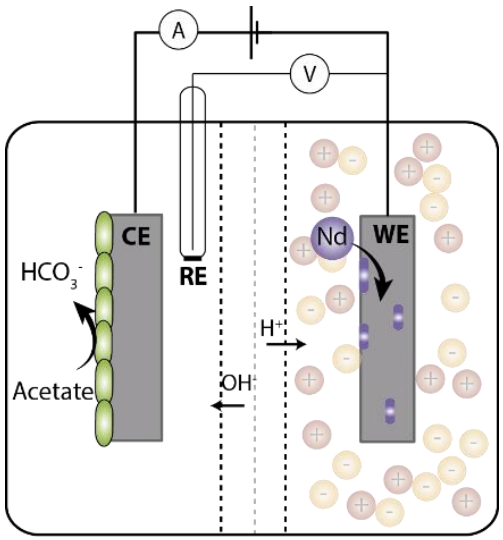

Figure IV.6. Microbial Electrochemical System for Nd electrodeposition with an IL catholyte.

b. Membrane choice

The proposed configuration separates the IL and the biological system by a membrane. The choice of a suitable membrane is extremely important, since there are several incompatibilities between the two compartments:

- Water crossover from the aqueous phase to the IL catholyte, which narrows the IL electrochemical window
- the probably low biofilm viability in an IL solvent,
- the biofilm stability under high cathodic polarization
- Metal crossover or complexation

For this first approach, the BES configuration included a bipolar membrane (**Figure IV.7**), which is an hydrophobic separator that provides a proton transfer to the catholyte to compensate the cations reduction and hydroxides to the anolyte to balance the anions oxidation[266]. It is composed of two polymer layers carrying fixed charges: an anion exchange membrane (AEM) and a cation exchange membrane (CEM).

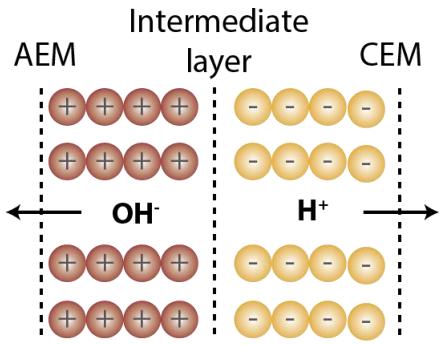

Figure IV.7. Bipolar membrane schema.

The desired function of bipolar membranes is to dissociate water into H^+ and OH^- ions at the bipolar junction between the two polymer layers without any side reactions (*e.g.*, H_2 and O_2 formation) or co-ions flux[267]. This reaction is generally driven by an applied electric field on the system. Produced protons and hydroxide ions then migrate out of the membrane through the respective permeable layers.

Even though in practice these desired assumptions are not fully respected, a few reports[95,268] have shown the compatibility of bipolar membranes with bioelectrochemical systems for metal reduction.

c. Sacrificial oxidizing agent

The cathodic Nd electrodeposition requires a non-limiting oxidizing agent in the anodic compartment. The first oxidizing agent investigated is acetate. It is a common biodegradable compound widely used by electroactive bioanodes as substrate for current production[218] and energy storage[269]. These electroactive bacteria use a limited number of substrates, acetate being the most common among different strains[270]. Acetate oxidation (described in Chapter III, **equation III-1**), promotes an electron transfer towards the cathode, where the metal reduction takes place. This electron transfer is thermodynamically not spontaneous due to the low redox potential of Nd compared to the acetate (E°=0.187 V *vs.* SHE at pH 7). A microbial electrolysis cell is therefore required, which implies the addition of a supplementary energy source.

The second studied oxidizing agent is ferrocyanide. Ferricyanide/ferrocyanide is a very chemically stable couple commonly used as redox shuttle for different applications including bioelectrochemical systems[269]. It can be used in its ferrocyanide form as oxidizing agent to reduce the Nd, but also as reducing agent to couple with (bio)oxidation processes involved in the bioanode growth. This reaction is given by equation **IV-2**.

$$Fe[CN]_6^{4-} \leftrightarrow Fe[CN]_6^{3-} + e^- \qquad \textbf{(IV-2)}$$

In this study, electroactive bacteria are not intended to catalyze this reaction. This chemical agent is a used as point of comparison. Considering that in this configuration the Nd reduction is thermodynamically not spontaneous, the addition of an energy source is required. The standard redox potential of this reaction reported in the literature is 0.43 V *vs*. SHE at 30°C[271]. This redox potential is advantageous as oxidizing agent since it is considerably lower than water oxidation

(H_2O/O_2, E°=0.75 V *vs.* SHE at pH 8), and at the same time higher as reducing agent compared to the H_2O/H_2 reduction (E°=-0.47 V *vs.* SHE at pH 8).

In a first preliminary study, an electroactive biofilm is characterized in a single chamber in presence of acetate. Then, it is proposed to explore the electrochemical behavior of Nd reduction in a two compartments system with two different oxidizing agents: acetate and ferrocyanide. A bipolar membrane is used as separator between the IL catholyte containing the Nd ions and the anolyte with the oxidizing agent.

IV.3.2 Preliminary experiments

a. Biofilm start-up in a single chamber reactor

Before any experiments with ILs, a preliminary study focused on a bioanode growth from a pure culture of *Geobacter sulfurreducens* strain in a single chamber reactor. The study aimed to have a first approach of a biofilm growth from one of the most known electroactive bacteria[272]. The reactor was filled with 0.12 L of modified *Geobacter* culture medium[273] containing: 2.5 g L^{-1} $NaHCO_3$, 1.5 g L^{-1} NH_4Cl, 1.64 g L^{-1} CH_3COONa, 0.6 g L^{-1} NaH_2PO_4, 0.1 g L^{-1} KCl, 10 mL L^{-1} of modified Wolfe's mineral solution and 1 mL of Wolfe's vitamin solution concentrated 10 times. The reactor was autoclaved at 120°C for 15 min and bubbled with 100% argon. Finally, a 10%v/v *Geobacter sulfurreducens* solution (strain reference DSMZ 12127, Germany) was inoculated into the solution in sterile conditions.

A three electrodes system was introduced in the electrolyte, with two carbon felts (University of Reading, England) as anode and cathode (projected surface area: 13.75 cm^2) and a saturated Ag/AgCl as reference electrode (**Figure IV.8**). The anode was initially polarized at different potentials where *Geobacter* species use the electrode as electron acceptor[274]. All the electrochemical measurements were performed with a VersaSTAT 3 potensiostat (AMETEK® scientific instruments).

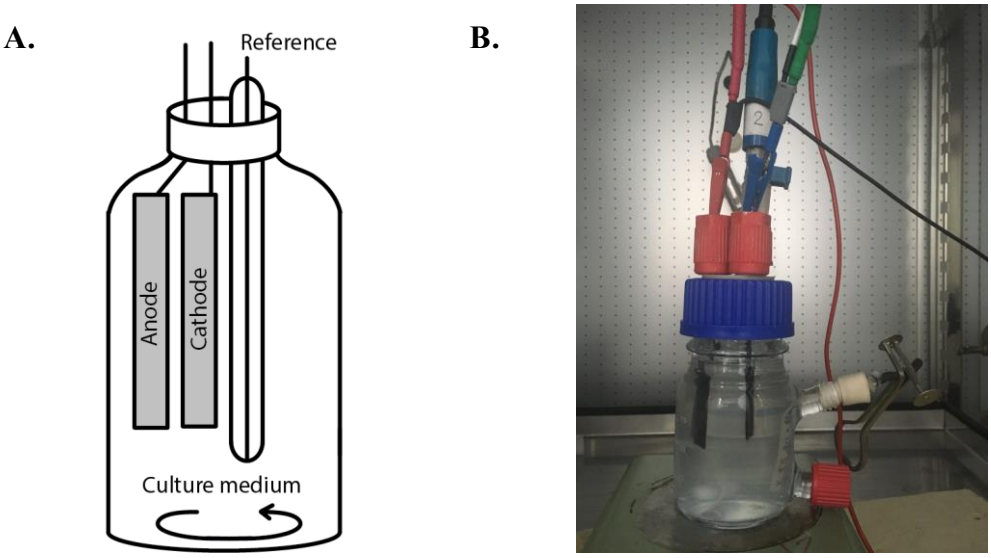

Figure IV.8. Single chamber configuration for *Geobacter sulfurreducens* growth: **A** schema; **B:** picture of set up.

b. Electrochemical characterization

A single chamber system with low internal resistance due to the absence of a membrane aimed to confirm the electroactivity of bacteria in a simplified configuration. The biofilm growth on the anode surface was studied by applying a potential difference between the anode and the reference, in an initially sterilized culture medium (CM) inoculated with *Geobacter sulfurreducens* cells. This configuration corresponds to a Microbial Electrolysis Cell (MEC), where an exchanged current is consumed to promote the electrochemical reactions. Parameters such as optical density (OD), pH, current density (against bioanode surface) and potential evolution were followed during time (**Figure IV.9**). Setting the anode potential at a value slightly above the acetate redox potential (-0.28 V *vs.* SHE at pH 7[270]), provides with a control over the electron transfer from the electroactive bacteria to the anode[218].

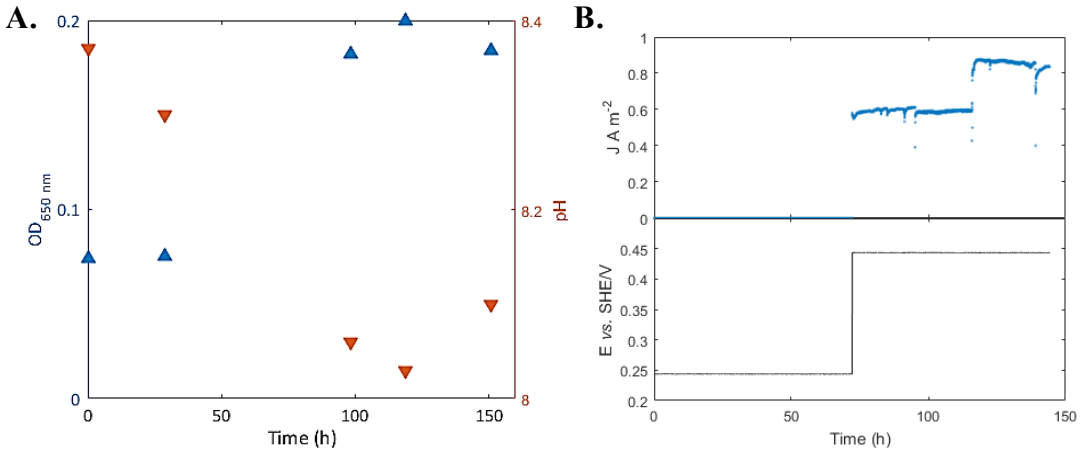

Figure IV.9. *Geobacter sulfurreducens* growth in the electrolyte: **A**. Anolyte OD (▲) and pH measurements (▼). **B**: Current density and cathode potential behavior. Chronoamperometry at 0.2 V *vs*. SHE started at 80 h from the inoculation.

The OD measurements presented in **Figure IV.9A** were associated with the evolution of bacteria concentration in suspension. It is not easy to correlate the suspended cells growth with the biofilm growth, but it is at least a point of reference. The initial stable OD represents a lag phase of about 30 h, where inoculated cells are adapted to their new environment. A pseudo-stationary phase is reached 60 h later, where the OD has increased up to 0.18 and seems stable. The slow OD evolution is indeed typical from a *Geobacter* cells culture in suspension, and the growth stage should be linked with the biofilm electroactivity[275]. The pH passed from 8.4 to 8.1 in 150 h, assuring a relatively stable pH at which *Geobacter* can grow[270].

Electrochemical measurements displayed in **Figure IV.9B** did not evidence any current evolution during the first anodic polarization at 0.25 V *vs.* SHE. The next polarization at 0.45 V *vs.* SHE increased the current density up to stable value around 0.6 A m^{-2}. A current increase to 0.9 A m^{-2} was subsequently observed at 130 h. It is probably linked to a modification of the electrochemical connections, since no other parameters were modified. Although higher exchanged current densities have been obtained in similar studies[270], a stable response was obtained over a period of 150 h. This was attributed to stable electrochemical reactions, where both reducing and oxidizing agents were not limiting. The total exchanged charge Q measured by the potentiostat was 247 C. Based on Faraday's law and the

total reactor volume, this charge theoretically corresponds to a maximum acetate consumption of 2.7 mM. Considering that the initial acetate concentration in the electrolyte was 10 mM, the acetate was in excess during the experiment. Nevertheless, following chronoamperometries didn't show any current response at the same potential. The system could be susceptible to aerobic conditions and/or bacterial contamination.

Cyclic voltammetry measurements were also performed to compare the resulted bioanode with an abiotic anode in a reactor containing a sterile culture medium (**Figure IV.10**).

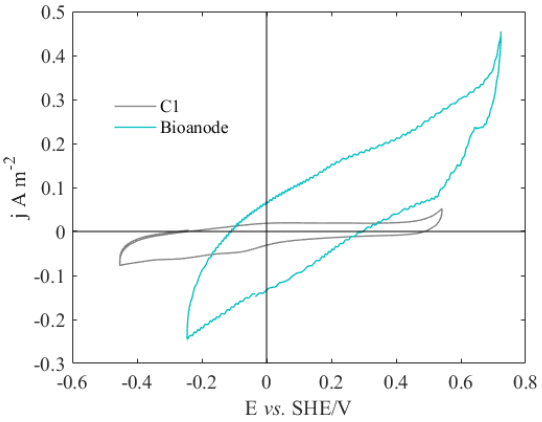

Figure IV.10. CV in a single chamber on a graphite electrode: Abiotic anode (C1) and developed bioanode in initially abiotic culture medium. CE: Platinum wire. Scan rate: 1 mV s^{-1}, T: 30°C.

The bioanode had an enhanced electrochemical response compared to the abiotic anode (C1), specially for the oxidation reaction. This suggests a catalytic effect of the biofilm towards an electrochemical oxidation reaction in the *Geobacter* culture medium.

These preliminary experiments show common techniques to study the electroactivity of exoelectrogen bacteria such as *Geobacter sulfurreducens*. It is commonly accepted that this is one of the most electroactive bacteria, which is highly expected in bioelectrochemical systems. BES with mixed cultures

dominated by *Geobacter sulfurreducens* perform similarly to pure cultures of *Geobacter sulfurreducens* with acetic acid as electron donor[276]. Besides, mixed cultures are more robust regarding the environmental conditions and have a better resistance to contamination of non-electroactive species.

IV.4 Technology validation

IV.4.1 Biofilm growth in a two-compartments system

a. Biofilm start-up

The two-compartments set up used a mixed culture from a *Geobacter*-rich medium initially fed with wastewater from a brewery in a fluid-bed BES reactor[63]. The set up displayed in **Figure IV.11A** consisted of two symmetrically parallel anodic and cathodic compartments, built from a polypropylene plate using a digital milling machine (ShopBot 3D) at Grenoble's FabLab[***]. Three identical reactors were connected in series in a closed system to favorize the growth of supporting bioanodes (**Figure IV.11B**).

A.

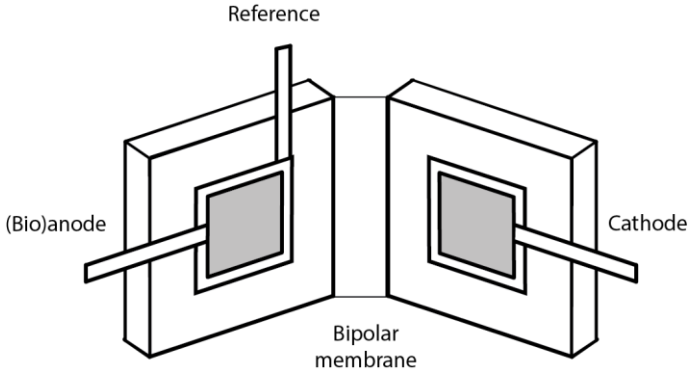

B.

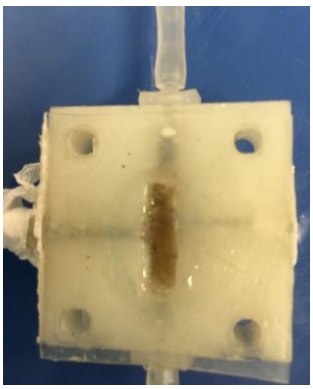

Figure IV.11. Two compartments set up. **A:** cell set-up; **B:** Picture of closed circuit for biofilm growth and internal section of bioelectrochemical reactor, bioanode side.

[***] FabLab: fabrication laboratory based on the *Do it yourself* and the free and open-source movement.

The choice of this mixed culture was to have a preselected electroactive bacterial community more robust in the long term towards environmental conditions (*e.g.* potential contaminations, N_2:CO_2 supply, O_2 concentration). The anolyte was composed of the culture medium previously described, sterilized (120°C, 15 min), degassed (Ar bubbling, 15 min), and inoculated with a 10%v/v sample of the mixed culture. The catholyte contained 100 mM potassium ferricyanide solution, $K_4Fe(CN)_6$. A constant external resistance of 50 Ω was connected between anode and cathode to assure current passage and cells were kept in this configuration at 30°C over a month. Once the bioanodes were established, chronoamperometry tests were performed to study the bioanode electroactivity.

Small volume reactors were chosen to maximize the electrode surface per compartment volume and to compensate the current high cost of ILs[222]. The total liquid volume per compartment was 2 mL. Both anode and cathode were composed of 0.2 cm^2 extruded graphite plate with low porosity (Mersen, France), polished with sand paper and connected to isolated stainless-steel wires. They were distanced of approximately 1 cm and separated by a bipolar membrane[†††] (FUMA-Tech, Germany). An Ag/AgCl reference (0.205 V *vs*. SHE, 3.5 M KCl, Biologic Science Instruments, France) was placed in the anolyte, avoiding any contamination in the ionic liquid. Anolytes and catholytes were continuously recirculated in a closed system at 50mL.h^{-1} with a peristaltic pump (Masterflex's Consol Drive). Their respective 100 mL reservoirs were maintained at 30°C in an incubator chamber and were renewed at least once per week.

b. Bioanode electroactivity

Bioanodes "growth" from the reactors connected in series were punctually followed by connecting a multimeter between anode and cathode. The cells voltage was used as first indicator of the targeted bioanodes electroactivity. This is a

[†††] The bipolar membrane was composed of three compact layers: a cation exchange membrane of 40 µm thickness, composed of sulfonic acid groups in polyether ketone; a 20 µm thick anion exchange membrane with polysulfoned bicyclic amines; and a 10 nm thick intermediate bipolar junction of tertiary ammonium groups to catalyze water splitting.

simple and economic technique that considers the ferrocyanide redox potential as reference, allowing to follow the bioanode potential evolution. Besides, it suppresses the constant use of a reference electrode for a long period, which is less practical in terms of maintenance and represents a supplementary cost. At the starting point, this cell voltage was about 0.1 V. After several weeks, the cell voltage of reactors reached values up to 0.5 V. Chronoamperometry tests were performed on one of the reactors by fixing a cell voltage of 0.5 V with the potentiostat and previously renewed anolyte and catholyte. Current and power responses are observed in **Figure IV.12**. Considering that both anode and cathode had the same projected surface area, current and power densities were calculated based on 0.2 cm^2 electrodes.

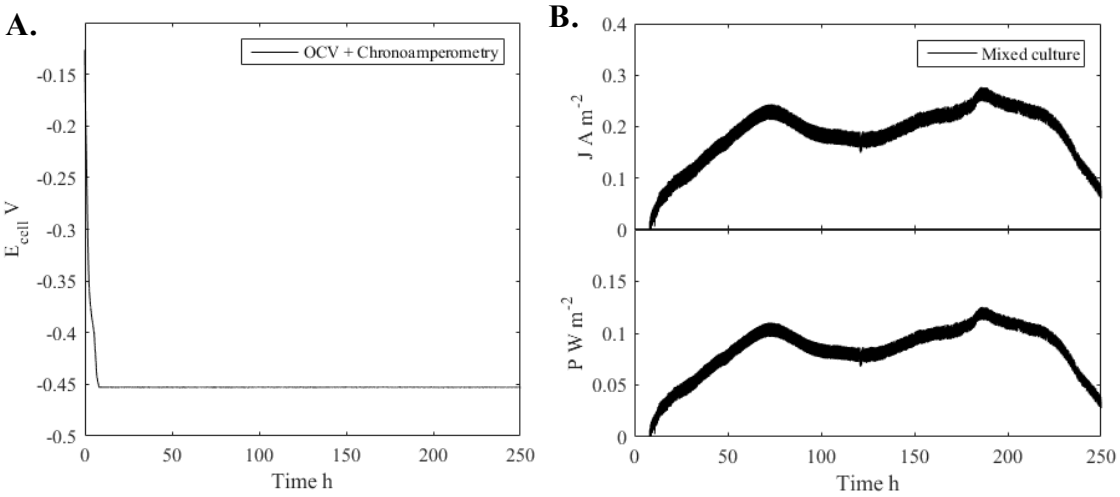

Figure IV.12. A: cell potential evolution. **B:** Current and power evolution of a two compartments BES with a U_{cell} = 0.5 V at 30°C.

The cell voltage was firstly followed in an open circuit and once it reached a cell value of -0.45 V, the cell voltage was maintained fixed (**Figure IV.12A**). Since the chronoamperometry started, current increased progressively until a maximum of 0.28 A m^{-2} (**Figure IV.12B**). The low current density response of this mixed culture cannot be compared to the pure culture electroactivity unless the BES architecture is the same[218]. Nevertheless, the bipolar membrane is responsible to an extend of increasing the energy losses. The activation resistance of this membrane has been considered as a major limitation for BES performance[277]. Although the fact of maximizing the current density is essential, the bipolar membrane had an

important role of selectivity towards the aqueous system and IL interactions. This configuration was therefore kept for the IL characterization.

IV.4.2 Electrochemical behavior of the IL in a two-compartments system

a. Experimental

The electrochemical characterization of the two-compartments configuration is based on the experimental set-ups presented in **Figure IV.13**. Two different oxidizing agents in the aqueous phase were separately tested in the anolyte: ferrocyanide (**Figure IV.13A**) and acetate (**Figure IV.13B**). To prepare the catholyte, an equivalent of 50 mM Nd from a $[Nd][Tf_2N]_3$ salt was dissolved in a $[C_1C_4Pyr]^+[Tf_2N]^-$ solution and dried at 40°C under vacuum for at least 24 h. Argon bubbling for 15 minutes was preconditioned before any electrochemical measurement to expel the oxygen from the solvent.

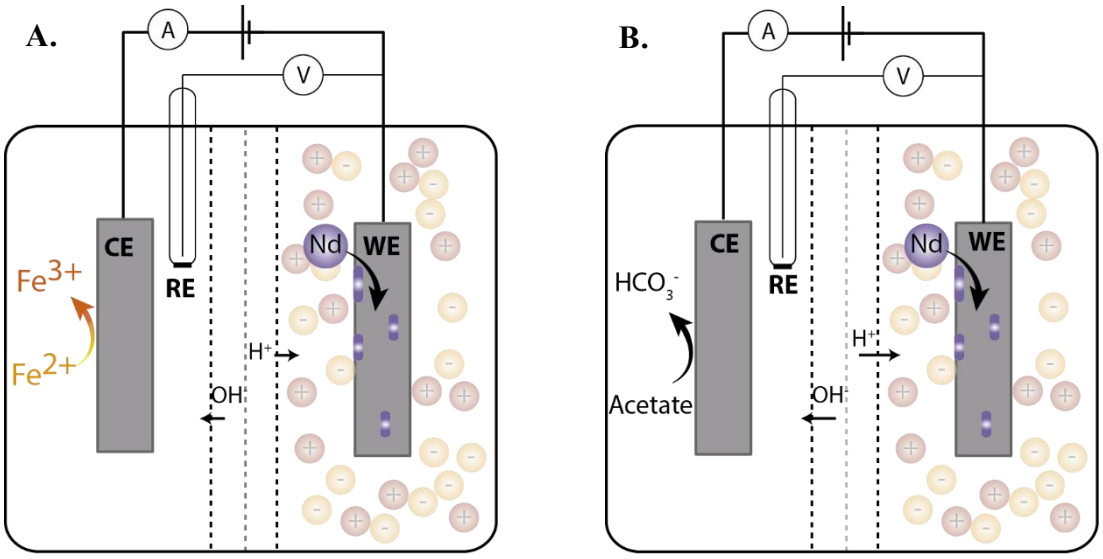

Figure IV.13. Nd electrodeposition set up with two sacrificial oxidizing agents in the anolyte: **A**. Potassium ferrocyanide. **B**: acetate in bacterial culture medium.

Cyclic and linear sweep voltammetry measurements were performed from the open current voltage (OCV) to potentials below the IL electrochemical window. Both anode and cathode's potential were followed against an Ag/AgCl reference electrode placed at the anolyte compartment. The advantage of this configuration

is the use a common reference electrode without any contact with the IL phase, where the IL is normally incompatible[278]. Nevertheless, due to the ohmic resistance between the working electrode and the reference electrode, a corrected cathode's potential (E^* in V) was calculated *via* equation **IV-3**.

$$E^* = E - (R_{ohm} * I_{meas}) \quad \textbf{(IV-3)}$$

Where E is the measured potential difference in V between cathode and reference electrode, R_{ohm} is the ohmic resistance in Ω, measured before the electrodeposition by a galvanostatic impedance spectroscopy (GEIS), and I_{meas} the current measured in A. Impedance spectroscopic experiments were run before the chronoamperometry tests from 200 kHz to 0.1 Hz between cathode and reference electrode. Impedance signal oscillated with an amplitude of 50mV around the OCV. The ohmic resistance obtained at high frequencies contains the ohmic contribution of electrodes, electrolyte, bipolar membrane and interphases.

b. Abiotic system

The electrochemical reduction and oxidation on the working (WE) and counter electrode (CE) were respectively followed by CV measurements (**Figure IV.14**).

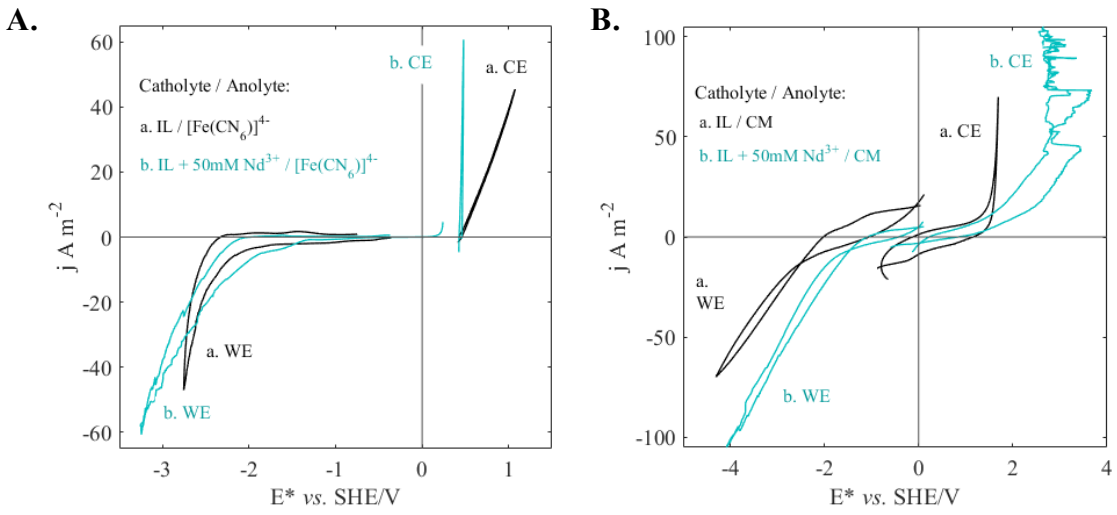

Figure IV.14. CVs on the abiotic system in batch at 30 °C and catholyte: $[C1C4Pyr]^+[Tf_2N]^-$. **A**: Anolyte: 100 mM potassium ferrocyanide, at 1 mV s^{-1}. **B**: Anolyte: culture medium (CM), at 10 mV s^{-1}. WE: graphite working electrode, CE: graphite counter electrode. E* corrected with ohmic resistances.

The catholyte stability in presence of a Nd^{3+} salt dissolved in the IL was compared by following the WE behavior. The electrochemical stability of the culture medium and the ferrocyanide anolytes was determined *via* the CE evolution. Cathode electrode potential was corrected by the ohmic resistance with equation **IV-2**, whereas the anode accuracy was assured by the low distance between the reference and the anode.

Regardless of the anolyte, the cathodic current evolution when the solvent contained Nd (b. WE) showed a faradic behavior starting from approximately -2 V *vs.* SHE. This reaction involves Nd^{3+} reduction, but parasite reactions such as water reduction and IL degradation may also take place. For instance, the IL solvent reduction started at around – 2.4 V *vs.* SHE (a. WE), compromising the solvent stability. Besides, water transported from the anolyte to the catholyte can react at these polarization levels. The electrochemical window of the IL was nevertheless wider in absence of Nd, which is important to reduce Nd without reducing the solvent.

The anodic current followed on the counter electrode (CE) was certainly affected by the anolyte. In presence of ferrocyanide (**Figure IV.14A**), the anode potential required to assure the reduction of Nd was remarkably stable. The cathode was polarized from 0.2 V *vs.* SHE to -3.2 V *vs*. SHE, whereas the anode polarization shifted from 0.43 V *vs.* SHE to 0.46 V *vs.* SHE. On the contrary, the anode in the synthetic bacteria medium was highly polarized (**Figure IV.14B**). It exceeded the anolyte electrochemical window, indicating water oxidation as main responsible of the faradic current.

c. Biotic system

The same previous configuration with a culture medium and in presence of a bioanode was used to characterize the Nd electrochemical behavior. Working and counter electrode's potential were measured during a cathodic LSV to follow the catholyte reduction and anolyte oxidation respectively (**Figure IV.15**). During this measurement, the cathodic behavior of the IL in presence of Nd^{3+} starts at about -1 *vs.* SHE. Considering that Nd reduction occurs at lower cathodic potentials, this faradic behavior is associated with other reactions. This could be related to a water crossover, since the water presence could reduce the IL electrochemical window. However, a bacterial effect cannot be discarded.

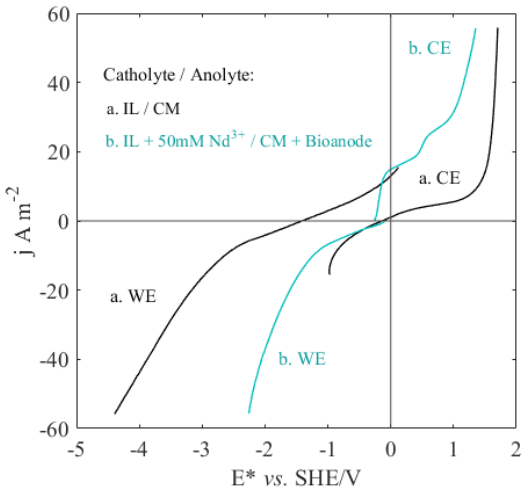

Figure IV.15. LSV on the two IL/BES system at 10 mV s^{-1}. Catholyte: $[C1C4Pyr]^+[Tf_2N]^-$, anolyte: culture medium (CM). WE: graphite working electrode, CE: graphite counter bioelectrode previously established. E* corrected with ohmic resistances.

The bioanode performed different oxidization steps before reaching the water oxidation in the synthetic medium. The first step could be related to acetate oxidation since it occurs between -0.25 V *vs*. SHE and -0.1 V *vs*. SHE, just above its standard redox potential. At these pseudo stationary conditions, the limiting current density for acetate oxidation in the bioanode (j_{max}) would be of 14 $A.m^{-2}$. At higher currents, the anode potential increased as other reactions became more influent, including water oxidation.

The low oxidation potential acetate compared to ferrocyanide (ΔE) represents a cell voltage diminution up to 0.67V since the anode potential is closer to the cathode potential for neodymium reduction. Acetate oxidation catalyzed by bacteria is limited to a low current range but has a thermodynamic voltage gain. Therefore, a power save in the system is possible as far these conditions are maintained.

IV.4.3 Neodymium electrodeposition assessment

a. Experimental

The Nd electrodeposition assessment was performed in the two-compartments configuration with acetate as oxidizing agent (**Figure IV.13B**). An equivalent of 50 mM Nd^{3+} in a $[Nd][Tf_2N]_3$ solvent was used as catholyte, whereas the anolyte was the culture medium previously described with 20 mM acetate. As mentioned before, an energy supply is required to have a cathodic polarization that favorizes the Nd reduction. A progressive cathodic polarization was preconditioned by a galvanodynamic technique based on Bonnaud's protocol[222]. From 0 to 1 mA, an applied current between cathode and anode was increased stepwise, with a step height of 0.025 mA and steps that lasted 45 s each. At 1 mA, the current was maintained constant for a period of 6 h *via* a galvanostatic technique. This protocol intends to avoid a sudden high cathodic polarization, which seems to induce a capacitive response on the system[222]. This capacitive behavior would rather store the input electric charge instead of favorizing the Nd electrochemical reduction. Besides, a maximum fixed current density of 5 A m^{-2} in the bioanode should allow an adequate polarization for acetate oxidation according to the CV measurements displayed in **Figure IV.15**.

At the end of the electrodeposition tests, the cell was dismantled, and the cathode's surface washed twice with Ethanol 99% to clean possible traces of the IL solvent. To avoid any oxidation, electrodes were stored in a glove box filled with N_2 99%

until they were characterized. Cathode was observed with a Field Emission Gun Scanning Electron Microscope (FEG SEM) and elements present on the surface were semi-quantified by energy dispersive X-ray spectroscopy (EDS), described in **Annex 1-F**.

b. IL/culture medium with abiotic anode

A first Nd electrodeposition test using an abiotic anode was assessed. A current density of 5 A m^{-2} was fixed between the cathode and anode. The fixed current and cathode potential evolution are presented in **Figure IV.16**.

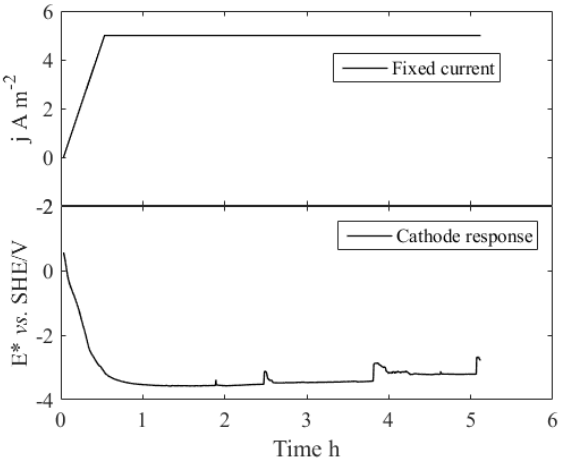

Figure IV.16. Electrodeposition electrochemical assessment on a two compartments system. Catholyte: $[C1C4Pyr]^+[Tf_2N]^-$ +50 mM Nd^{3+}, anolyte: culture medium with 20 mM acetate, with an abiotic anode. E* corrected with R_{ohm}: 52.9 Ω.

The dynamic current evolution during the first 30 minutes allowed the cathode to reach progressively a cathodic potential low enough to reduce Nd. A brusque cathodic polarization could indeed favorize an accumulation of an electrochemical double layer composed of charged species at the vicinity of the cathode surface[222]. This accumulation represents an energetic barrier for the electrons transfer. It is very important to avoid supplementary energetic losses since the IL already has an inherent low conductivity at room temperature[279], and Nd^{3+} diffusion coefficient is estimated to be in the order of 10^{-8} cm^2 s^{-1} approximately[280].

Once the system reached 5 A m^{-2}, the cathode potential stabilized towards a range between – 3.5 V *vs.* SHE and – 3.3 V *vs.* SHE. Thus, the electrochemical reduction occurring in the IL should be relatively constant. Despite the hydrophobicity of the bipolar membrane, water could pass from the anolyte to the catholyte, inducing supplementary reactions and compromising the faradic efficiency of Nd reduction. Based on the Faraday's law, the total coulombic charge consumed (16.5 C) was theoretically sufficient to reduce the Nd^{3+} mass present in the 50 mM Nd^{3+} solution. The final Nd concentration in the IL was unfortunately not measured.

Obtained deposits were subsequently analyzed by SEM-EDS. The microstructure of a specific region on the cathode surface was amplified x500 (Figure IV.17**a**). The fractionated microstructure is probably linked with the non-homogenous deposit substrate, in this case the graphite electrode. A, B and C dots point at zones with differentiated gray contrasts, analyzed by EDS and displayed in Figure IV.17**b**.

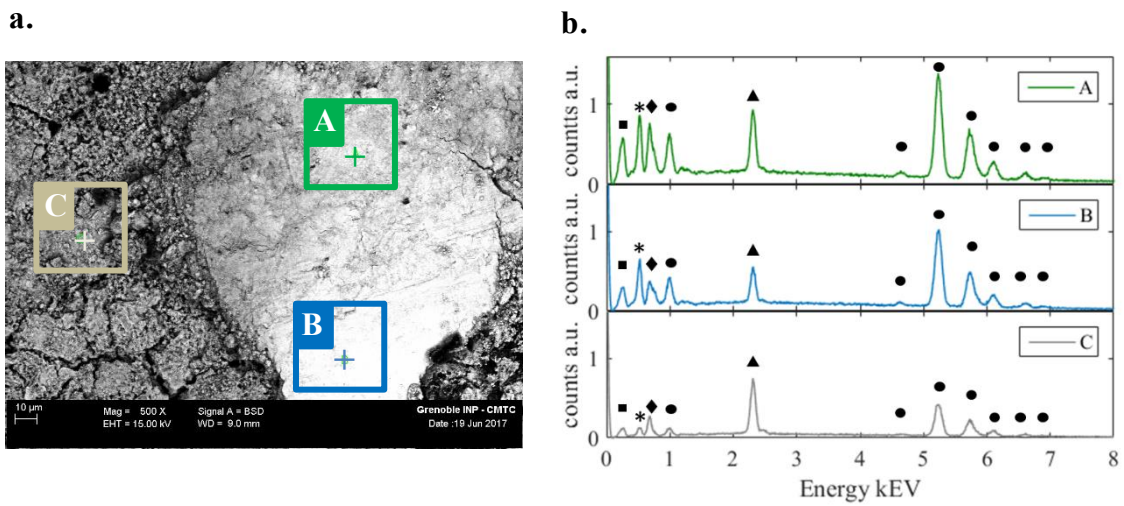

Figure IV.17. Graphite cathode characterization post electrodeposition tests, anolyte: culture medium, anode: abiotic graphite. a. SEM images magnification x500; b. EDX spectra on two deposit points. Symbols correspond to characteristic peaks of elements (● : Nd, ▲: S, ◆ : F, * : O, ■ : C).

The contrasted gray color zones observed in the SEM image had EDS spectra with several peaks that fitted with the Nd characteristic response. Characteristic peaks of sulfur and fluor, oxygen and carbon also fitted with the samples. All these

elements are present in the solvent anion, representing IL traces on the deposit. The relative atomic percentage of each identified element and its relative measurement error were hence quantified based on the obtained signal from the EDS spectra and displayed in **Table III.1**. This semi-quantitative technique doesn't quantify the Nd total deposited mass, but it is used as indicator of relative atomic purity compared to other elements.

Table IV.2. Elemental analysis of the electrodeposited deposits from a IL/abiotic culture medium system, obtained at different points previously identified.

Points	Elemental analysis (atomic %)				
	Nd	O	S	F	N
A	31.3 ± 2.9	32.4 ± 14.3	6.2 ± 4.1	5.6 ± 15.1	1.9 ± 23.8
B	35.4 ± 2.9	36.2 ± 14.9	9.8 ± 4.4	11.6 ± 17.6	6.9 ± 27.8
C	31.3 ± 3.0	16.5 ± 20.9	28.0 ± 3.9	20.6 ± 17.6	3.7 ± 48.3

EDS results show that at least 31% of the deposit contained Nd. However, it is important to take into account that some identified elements such as oxygen, fluor and nitrogen, had a high measurement error. It is recommended to consider that EDS is reliable to identify these light elements, but not necessary to quantify them[222]. Besides, the non-planar morphology alters the photons excitation and their corresponding response. Compared to sulfur element that has a more reliable value, Nd was up to 5 times more concentrated. The Nd:S ratio was therefore used as indicator of Nd deposits purity. Points A, B and C had a Nd:S ratio of 5.0, 3.6 and 0.1, respectively. Considering that 3 $[TF_2N]^-$ anions containing two S elements each are required to combine with one Nd^{3+} atom, Nd was definitely concentrated at these punctual points.

c. Nd electrodeposition coupling IL/BES with a bioanode

A second study used a previously developed bioanode to evaluate the Nd electrodeposition in an IL/BES system. A current density of 5 A m^{-2} was fixed between the cathode and the bioanode. The fixed current and the cathode potential response are presented in **Figure IV.18**.

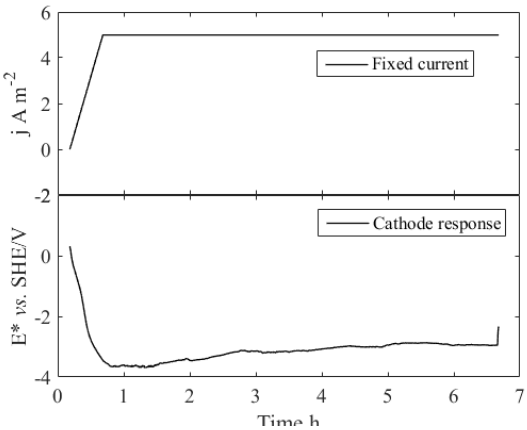

Figure IV.18. Electrodeposition assessment on a two compartments system. Catholyte: $[C1C4Pyr]^+[Tf_2N]^-$ +50 mM Nd^{3+}, anolyte: culture medium with 20 mM acetate, with a bioanode. E* corrected with R_{ohm} = 60 Ω.

The cathode polarization went up to -3.5 V *vs*. SHE during the first dynamic current phase, and then slowly shifted to -3 V *vs*. SHE. This behavior is very similar to the previous cathodic polarization in presence of an abiotic anode. Thus, the anolyte was not a limiting factor. Subsequently, the resulting deposit was characterized by SEM -EDS (**Figure IV.19**).

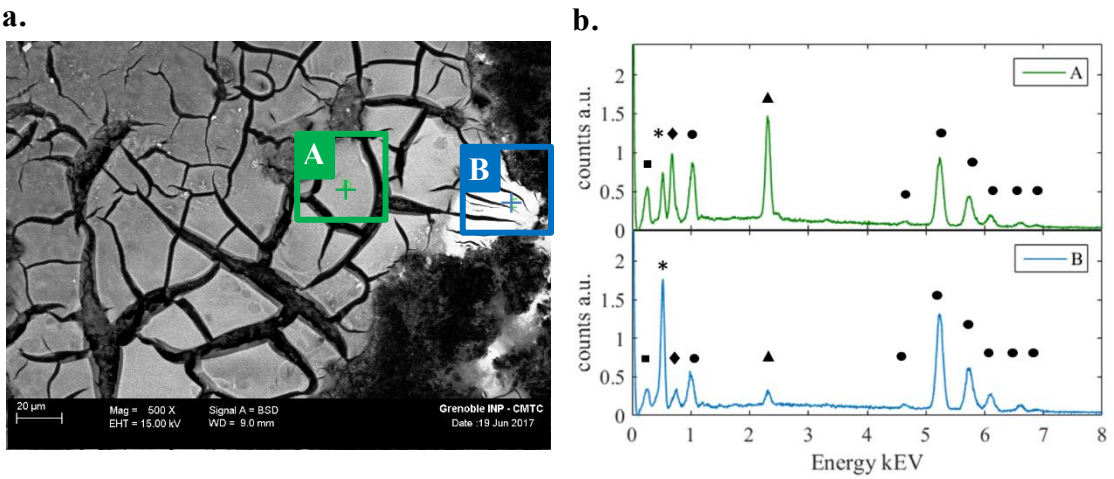

Figure IV.19. Graphite cathode characterization post electrodeposition tests, anolyte: culture medium, bioanode on graphite. **a**. SEM images magnification x500; **b**. EDX spectra on two deposit points. Symbols correspond to characteristic peaks of elements (● : Nd, ▲: S, ◆ : F, * : O, ■ : C).

The fractionated microstructure obtained (**Figure IV.19**a) is influenced by the graphite support as for the abiotic deposit. Two areas distinguished by their

contrasted gray color were characterized by EDS. Points A and B from the micrograph represent each of these areas. Their EDS spectra are presented in **Figure IV.19b**.

Characteristic peaks of Nd, S, F, O and C were identified again. **Table IV.3** shows the elemental analysis of points A and B. The Nd:S ratio of the atomic percentage was very different from point A to B. While point A had a Nd:S ratio of 1.4, point B had 10.8 times more atoms of Nd than S. Traces of other elements symbolize that the IL was still present in the deposit. In both abiotic and biotic systems, the Nd:S ratio was punctually higher than in a single chamber Nd electrodeposition containing $[C1C4Pyr]^+[Tf_2N]^-$ [222]. The biofilm doesn't affect negatively the Nd deposit, but its relevance is questioned.

Table IV.3. Elemental analysis of the electrodeposited deposits from an IL/BES system, obtained at different points previously identified.

Points	Elemental analysis (atomic %)				
	Nd	O	S	F	N
A	23.2 ± 3.0	27.0 ± 15.0	17.0 ± 3.9	25.5 ± 14.2	7.2 ± 25.4
B	26.0 ± 2.9	58.8 ± 12.8	2.4 ± 6.0	0.2 ± 50.9	12.3 ± 19.1

A simplified energetical balance comparing the abiotic and biotic systems is presented in **Table IV.4**.

Table IV.4. Energetic balance of biotic and biotic systems at 5h of the chronoamperometry test.

System	$E_{average}$ (V *vs.* SHE)	Q (C)	E (J)
Abiotic	3.6	16	57.8
Biotic	3.4	15.5	53.4

The cathode polarization and the total consumed charge were slightly superior in the abiotic system. The consumed energy related to the cathodic polarization calculated as the charge times the cathodic potential was 7.5% higher. This energetic gain in the biotic system could be linked to a catalytical effect of bacteria, but many other parameters must be considered: this energy doesn't

consider the anodic polarization, which may be similar considering they have both the same anolyte; the water crossover overpassed the miscibility of water in this IL, decreasing the energy performance regardless of the bacteria presence; the Nd quantification would allow to calculate the recovery efficiency and the pertinence of both abiotic and biotic systems.

From the obtained results, the stability of the IL is still not solved. This possesses many challenges:

- The solvent recyclability is compromised as far as the IL solvent is degraded during the electrodeposition.
- Water content in the catholyte must be prevented or highly reduced to lower the risk of parasite reactions such as water electrolysis.
- The choice of a membrane with lower water permeability or a biphasic system without membrane must be considered. Membrane-less biphasic systems containing bacteria-rich aqueous phase and an IL phase have been already explored[281]. It is nevertheless highly recommended to avoid the water electroactivity in the IL phase.

IV.4.4 To sum up

Preliminary results in a single chamber cell let to study the biofilm electroactivity in a simplified system. Under the studied experimental conditions, a maximum current density of 0.9 A m^{-2} (against bioanode surface) was exchanged in the bioanode composed of *Geobacter sulfurreducens*. In a two compartments system, electroactive biofilms were grown with a low current density. An optimized architecture could ensure a better performance, but the bipolar membrane was kept for its selectiveness towards the possible exchanged ions between the aqueous and IL solvents.

Nd deposits were punctually and heterogeneously identified on the graphite surface. They put in evidence other components such as sulfur and fluorine,

normally present in the ionic liquid. A possible IL degradation is suspected. These punctual measurements show a tendency of higher Nd:S ratio when the bioanode was employed, suggesting that the deposits contained a higher purity of Nd. The use of a bioanode to catalyze the sacrificial oxidation was not counterproductive for the Nd deposition, but its relevance remains questionable. It is recommended to analyze the bioanode stability during and after the electrodeposition. Parameters such as the anode potential and the acetate concentration would be good indicators to follow the oxidation reaction evolution. Finally, the Nd mass balance after the experiment would lever to quantify the Nd deposits and therefore to complement the technology performance evaluation.

IV.5 Conclusions & perspectives

The acceptance of ionic liquids as solvent of the future for REE electrodeposition requires to assure the stability during the process. In this exploratory study, two compartments system intended to decorrelate the cathodic reduction of Nd from a "sacrificial" oxidation reaction, with the intention of avoiding any IL oxidation. An electrochemical characterization to identify the viability of the Nd electrodeposition on acetate and ferrocyanide as electron donors was performed. Besides, a bioanode aimed to reduce the energetic barrier of the process. Conclusions can be highlighted as follows:

Bioanode growth

(iv) A single chamber reactor is a useful reference point to characterize a complex system that combines two different environments.

(v) A simple technique using ferricyanide as electron acceptor in a two compartments system enabled the development of an electroactive bioanode.

Ionic liquid compatibility with BES

(i) Nd was successfully deposited on a cathode surface using ferrocyanide and water as sacrificial oxidizing agents in a two compartments system.

(ii) The bioanode contribution to the Nd recovery by lowering the energy consumption during the electrodeposition is possible but needs to be confirmed in another configuration.

Many questions arose as perspectives from this study:

- Is it worth to increase the bioanode surface to improve the stability towards the acetate oxidation instead of favorizing the water electrolysis?
- Is it possible to design an IL more compatible with aqueous solutions at very low cathodic polarizations?

- Can functionalized membranes avoid the water crossover without significant supplementary resistances that compromise the energy performance?

Conclusion and Perspectives

"From the established goals…"

Metals are in the core of a sustainable development. To tackle the economic and environmental requirements for the metal provisioning, sustainable processes are targeted as priority for both primary and secondary mining. This work is thus focusing on the recovery of metals from synthetic solutions, prospecting its application in matrices such as minerals, marine sediments and end of life products.

While conventional hydrometallurgical treatments use large amounts of chemicals, energy and resources, this project aimed to develop greener processes by using bioelectrochemical systems. These systems present numerous potential applications on metal recovery processes from low-metal content aqueous matrices. Combining the expertise of LEPMI, Ghent University and VITO, three bioelectrochemical strategies were investigated during this work and can be summarized as follows:

(i) Metal-bacteria interactions

Shewanella oneidensis and *Cupriavidus metallidurans* are sustainable driven agents for metal recovery and metal nanoparticle synthesis. The facility to growth these bacterial cultures of these strains under sterile conditions and their versatility towards interactions with metal ions was exploited to recover separately gold and chromium. Initially viable pure cultures of these strains were an excellent support for gold recovery, retaining up to 92.8% gold in presence of H_2 as electron donor, pH 5 and anoxic conditions over a period of 72 h. Besides, these suspended cells successfully synthetized 50 nm Au nanoparticles at the external bacteria cell wall. These are potentially functional products as catalysts for applications from medical

diagnostic to environment remediation. A combination of active and passive mechanisms are suspected to be involved. The Chromium removal on the other hand was not as effective as gold. A maximum chromium uptake of 53.5% was obtained in 96 h from *Shewanella oneidensis*, at pH 5, anoxic conditions and H_2 as electron donor. Cr(III) nanoparticles are suspected to be formed on the bacterial surface and inside the cell. Even though both metals are not necessarily essential for bacterial metabolism, interactions between the metal and bacteria are indeed not the same. Cr(VI) for instance leaded to lower accumulation capacities by bacteria compared to Au(III). The toxic effect of Cr(IV) may be a limiting factor.

The introduction of a cathode as electron donor for metal bio-recovery at a nanoscale was explored for the first time. A cathodic polarization at -0.3 V *vs.* SHE accelerated the metal uptake to 95 % in 24 h. The synthesis of 18 nm AuNPs on bacterial external walls were also achieved. For Cr(VI), a cathode potential fixed at -0.8 V *vs.* SHE enhanced the Cr removal up to 61 % in 24 h. Cr(III) nanoparticles were speculated, but a size distribution analysis was not possible as for gold. Microorganisms had a role of nano-particles substrate, whereas the cathode polarization assured the metal ions reduction.

(ii) Advanced electrodes for metal precipitation in saline environments

Gas diffusion electrodes hold a great advantage regarding the oxygen reduction reaction as intermediate for metal precipitation. Here, ORR in a GDE was coupled to a bioelectrochemical oxidation to increase the solution pH and indirectly precipitate metal ions from an acidic (pH 3) and conductive (30 g L^{-1} NaCl) solution. The oxygen diffusion, known as a limiting factor for ORR, was enhanced by a supplementary air supply that crossed a gas diffusion cathode developed at VITO. Driven by a halophilic electroactive bioanode poised at 0.4 V *vs.* SHE, a panel of elements from transition metals to REE were successfully 100% recovered in 33.7 h. The formation of distinguished precipitation plateaus allowed a selective separation of metals. To give an example, copper was 100% recovered in the first plateau at a pH of 6.4 and 91.6 % of samarium recovered at the second plateau at pH 8.2. In a microbial fuel cell configuration, where no external energy inputs

stimulate the electrodes polarization, the same panel of metals was 100 % recovered, this time in 92.8 h. Similar precipitation plateaus were observed, with 96.5 % copper and 89.4 % samarium recovered in first and second plateau respectively. Precipitation of other metals on these plateaus is nevertheless unavoidable and a further step to separate these metals is therefore required.

(iii) BES/IL coupling system for Nd electrodeposition

Hydrophobic room temperature ionic liquids are potential solvent candidates to replace commercial VOC and molten salts used for REE electrodeposition processes. Low oxidation electrochemical stability during time is a key bottleneck addressed by the addition of a sacrificial oxidizing agent in a second compartment and separated by a bipolar membrane. Nd electrodeposition in a $[C_1C_4Pyr]^+[Tf_2N]^-$ solvent was successfully achieved with a bioanode assuring the oxidation reaction. Considering the quantity of Nd atoms per sulfur atoms as indicator of the deposit purity, a maximum Nd:S ratio of 10.8 achieved symbolize a highly pure Nd deposit. Besides, an abiotic anode also achieved a Nd deposit with a maximum Nd:S ratio of 5. Energy savings of 7.5 % are suggested by the use of a bioanode compared to the abiotic, but analysis on the anode energetic consumption would be interesting to complement the energetic balance. From CV measurements, current densities lower than 14 A m^{-2} (against bioanode surface) are recommended to maintain an adequate bioanode potential for acetate oxidation. Finally, ferrocyanide could also be contemplated as oxidizing agent, considering its stable redox potential and the voltage gain compared to the water oxidation.

"...to the research prospects."

(i) Metal-bacteria interactions

Microorganisms as potential 'nano-factories' powered by electrochemical systems opens a new route of bioelectrochemical configurations. The establishment of optimal conditions for both metal recovery and nanoparticles synthesis needs to take into account a deeper study on the fixed cathode potential, the electrode-bacteria-metal interactions and its potentials applications to other metal-containing streams. Metallic nanoparticles tests on specific applications could also help to evaluate the applicability of these expected added-value products.

(ii) Advanced electrodes for metal precipitation in saline environments

An optimized geometry minimizing the distance between electrodes is mandatory to maximize the halophilic bioanodes capacity to drive the oxygen reduction reaction. The stability of the cathode is also important to evaluate, since oxygen and saline conditions increase the risk of corrosion. The electrode performance evolution within metal recovery cycles could be interesting to study. Leached marine mineral are also pertinent to test, since they contain other elements that complex differently the metals present.

(iii) BES/IL coupling system for Nd electrodeposition

A better understanding of the Nd electrodeposition kinetics in ILs could contribute to the establishment of an optimum set up. The effect of a sacrificial oxidizing agent in an aqueous phase could diminish the oxidative degradation of the IL, but the IL could still be degraded by the water crossover. The choice of a compatible membrane for both IL and aqueous compartments is therefore mandatory (*i.e.* limiting the water passage whilst keeping a low resistance). Besides, the water effect in reducing the energy efficiency of the process is known, but its effect on the recyclability of the IL would be interesting to check.

References

(1) Hagelüken, C.; Meskers, C. E. M. *Complex Life Cycles of Precious and Special Metals*; The MIT Press, 2009.

(2) Gutowski, T. G.; Sahni, S.; Allwood, J. M.; Ashby, M. F.; Worrell, E. The Energy Required to Produce Materials: Constraints on Energy-Intensity Improvements, Parameters of Demand. *Phil Trans R Soc A* **2013**, *371* (1986), 20120003. https://doi.org/10.1098/rsta.2012.0003.

(3) Simmons, J.; Zepf, V. *Materials Critical to the Energy Industry: An Introduction*; University of Augsburg: Augsburg, 2014.

(4) Rifkin, J. *The Third Industrial Revolution: How Lateral Power Is Transforming Energy, the Economy and the World*; Palgrave MacMillan, 2011.

(5) Mudd, G. M. The Environmental Sustainability of Mining in Australia: Key Mega-Trends and Looming Constraints. *Resour. Policy* **2010**, *35* (2), 98–115.

(6) Öhrlund, I. Future Metal Demand from Photovoltaic Cells and Wind Turbines - Investigating the Potential Risk of Disabling a Shift to Renewable Energy Systems. https://doi.org/http://dx.doi.org/10.13140/RG.2.1.4524.9049.

(7) Pitron, G. *La Guerre Des Métaux Rares, La Face Cachée de La Transition Énergétique et Numérique*; Les Liens qui Libèrent, 2018.

(8) Henckens, M. L. C. M.; van Ierland, E. C.; Driessen, P. P. J.; Worrell, E. Mineral Resources: Geological Scarcity, Market Price Trends, and Future Generations. *Resour. Policy* **2016**, *49*, 102–111. https://doi.org/10.1016/j.resourpol.2016.04.012.

(9) Graedel, T. E.; Harper, E. M.; Nassar, N. T.; Nuss, P.; Reck, B. K. Criticality of Metals and Metalloids. *Proc. Natl. Acad. Sci.* **2015**, *112* (14), 4257–4262. https://doi.org/10.1073/pnas.1500415112.

(10) Nuss, P.; Eckelman, M. J. Life Cycle Assessment of Metals: A Scientific Synthesis. *PLOS ONE* **2014**, *9* (7), e101298. https://doi.org/10.1371/journal.pone.0101298.

(11) MONIER, Véronique; PLANCHON, Mariane; LEMEILLET, Alexis; SAÏDI, Nada; SCAPIM-YAMAGUCHI, Taylla. *ADEME, Deloitte Développement Durable*; 2017; p 210.

(12) Hagelüken, C. *The EU Circular Economy Package - an Opportunity to Improve Metals Recycling*; 2017.

(13) Vorobiova, K. Innovation Themes. *EIT RawMaterials*.

(14) Løvik, A.; Hagelüken, C.; Wäger, P. Improving Supply Security of Critical Metals: Current Developments and Research in the EU. *Sustain. Mater. Technol.* **2018**, *15*. https://doi.org/10.1016/j.susmat.2018.01.003.

(15) Hagelüken, C. High-Tech Recycling of Critical Metals: Opportunities and Challenges; 2014.

(16) Wang, H.; Ren, Z. J. Bioelectrochemical Metal Recovery from Wastewater: A Review. *Water Res.* **2014**, *66*, 219–232. https://doi.org/10.1016/j.watres.2014.08.013.

(17) Hegazi, H. A. Removal of Heavy Metals from Wastewater Using Agricultural and Industrial Wastes as Adsorbents. *HBRC J.* **2013**, *9* (3), 276–282. https://doi.org/10.1016/j.hbrcj.2013.08.004.

(18) Gras, M.; Papaiconomou, N.; Schaeffer, N.; Chainet, E.; Tedjar, F.; Coutinho, J. A. P.; Billard, I. Ionic-Liquid-Based Acidic Aqueous Biphasic

Systems for Simultaneous Leaching and Extraction of Metallic Ions. *Angew. Chem. Int. Ed.* **2018**, *57* (6), 1563–1566. https://doi.org/10.1002/anie.201711068.

(19) Gaur, N.; Flora, G.; Yadav, M.; Tiwari, A. A Review with Recent Advancements on Bioremediation-Based Abolition of Heavy Metals. *Environ. Sci. Process. Impacts* **2014**, *16* (2), 180–193. https://doi.org/10.1039/C3EM00491K.

(20) Nancharaiah, Y. V.; Mohan, S. V.; Lens, P. N. L. Biological and Bioelectrochemical Recovery of Critical and Scarce Metals. *Trends Biotechnol.* **2016**, *34* (2), 137–155. https://doi.org/10.1016/j.tibtech.2015.11.003.

(21) Konhauser, K. O.; Lalonde, S. V.; Phoenix, V. R. Bacterial Biomineralization: Where to from Here? *Geobiology* **2008**, *6* (3), 298–302. https://doi.org/10.1111/j.1472-4669.2008.00151.x.

(22) Beveridge, T. J.; Murray, R. G. Uptake and Retention of Metals by Cell Walls of Bacillus Subtilis. *J. Bacteriol.* **1976**, *127* (3), 1502–1518.

(23) Johnson, D. B.; Hallberg, K. B. The Microbiology of Acidic Mine Waters. *Res. Microbiol.* **2003**, *154* (7), 466–473. https://doi.org/10.1016/S0923-2508(03)00114-1.

(24) Zinder, B.; Furrer, G.; Stumm, W. The Coordination Chemistry of Weathering: II. Dissolution of Fe(III) Oxides. *Geochim. Cosmochim. Acta* **1986**, *50* (9), 1861–1869. https://doi.org/10.1016/0016-7037(86)90244-9.

(25) Dehner, C. A.; Awaya, J. D.; Maurice, P. A.; DuBois, J. L. Roles of Siderophores, Oxalate, and Ascorbate in Mobilization of Iron from Hematite by the Aerobic Bacterium Pseudomonas Mendocina. *Appl. Environ. Microbiol.* **2010**, *76* (7), 2041–2048. https://doi.org/10.1128/AEM.02349-09.

(26) Bosecker, K. Bioleaching: Metal Solubilization by Microorganisms. *FEMS Microbiol. Rev.* **1997**, *20* (3), 591–604. https://doi.org/10.1016/S0168-6445(97)00036-3.

(27) Lovley, D. R. Dissimilatory Metal Reduction. *Annu. Rev. Microbiol.* **1993**, *47* (1), 263–290. https://doi.org/10.1146/annurev.mi.47.100193.001403.

(28) Brandl, H. Microbial Leaching of Metals. In *Biotechnology Set*; Wiley-Blackwell, 2008; pp 191–224. https://doi.org/10.1002/9783527620999.ch8k.

(29) Gadd, G. M. Metals, Minerals and Microbes: Geomicrobiology and Bioremediation. *Microbiology* **2010**, *156* (3), 609–643. https://doi.org/10.1099/mic.0.037143-0.

(30) Haferburg, G.; Kothe, E. Microbes and Metals: Interactions in the Environment. *J. Basic Microbiol.* **2007**, *47* (6), 453–467. https://doi.org/10.1002/jobm.200700275.

(31) Volesky, B. Detoxification of Metal-Bearing Effluents: Biosorption for the next Century. *Hydrometallurgy* **2001**, *59* (2), 203–216. https://doi.org/10.1016/S0304-386X(00)00160-2.

(32) Dominguez-Benetton, X.; Varia, J. C.; Pozo, G.; Modin, O.; Ter Heijne, A.; Fransaer, J.; Rabaey, K. Metal Recovery by Microbial Electro-Metallurgy. *Prog. Mater. Sci.* **2018**, *94*, 435–461. https://doi.org/10.1016/j.pmatsci.2018.01.007.

(33) Klaus-Joerger, T.; Joerger, R.; Olsson, E.; Granqvist, C.-G. Bacteria as Workers in the Living Factory: Metal-Accumulating Bacteria and Their Potential for Materials Science. *Trends Biotechnol.* **2001**, *19* (1), 15–20. https://doi.org/10.1016/S0167-7799(00)01514-6.

(34) Castro, L.; Blázquez, M. L.; Muñoz, J. Á.; González, F. G.; Ballester, A. Mechanism and Applications of Metal Nanoparticles Prepared by Bio-Mediated Process. *Rev. Adv. Sci. Eng.* **2014**, *3* (3), 199–216. https://doi.org/10.1166/rase.2014.1064.

(35) Suresh, A. K.; Pelletier, D. A.; Wang, W.; Broich, M. L.; Moon, J.-W.; Gu, B.; Allison, D. P.; Joy, D. C.; Phelps, T. J.; Doktycz, M. J. Biofabrication of Discrete Spherical Gold Nanoparticles Using the Metal-Reducing Bacterium Shewanella Oneidensis. *Acta Biomater.* **2011**, *7* (5), 2148–2152. https://doi.org/10.1016/j.actbio.2011.01.023.

(36) Kim, D.-H.; Park, S.; Kim, M.-G.; Hur, H.-G. Accumulation of Amorphous Cr(III)–Te(IV) Nanoparticles on the Surface of Shewanella Oneidensis MR-1 through Reduction of Cr(VI). *Environ. Sci. Technol.* **2014**, *48* (24), 14599–14606. https://doi.org/10.1021/es504587s.

(37) Zhou, N.-Q.; Tian, L.-J.; Wang, Y.-C.; Li, D.-B.; Li, P.-P.; Zhang, X.; Yu, H.-Q. Extracellular Biosynthesis of Copper Sulfide Nanoparticles by Shewanella Oneidensis MR-1 as a Photothermal Agent. *Enzyme Microb. Technol.* **2016**, *95*, 230–235. https://doi.org/10.1016/j.enzmictec.2016.04.002.

(38) Ng, C. K.; Tan, T. K. C.; Song, H.; Cao, B. Reductive Formation of Palladium Nanoparticles by Shewanella Oneidensis: Role of Outer Membrane Cytochromes and Hydrogenases. *RSC Adv.* **2013**, *3* (44), 22498–22503. https://doi.org/10.1039/C3RA44143A.

(39) Montero-Silva, F. Synthesis Of Extracellular Stable Gold Nanoparticles By Cupriavidus Metallidurans CH34 Cells. *bioRxiv* **2018**, 139949. https://doi.org/10.1101/139949.

(40) Campbell, G.; MacLean, L.; Reith, F.; Brewe, D.; Gordon, R.; Southam, G.; Campbell, G.; MacLean, L.; Reith, F.; Brewe, D.; et al. Immobilisation of Platinum by Cupriavidus Metallidurans. *Minerals* **2018**, *8* (1), 10. https://doi.org/10.3390/min8010010.

(41) Ascencio, J. A.; Canizal, G.; Medina-Flores, A.; Bejar, L.; Tavera, L.; Matamoros, H.; Liu, H. B. Neodymium Nanoparticles: Biosynthesis and Structural Analysis. *J. Nanosci. Nanotechnol.* **2006**, *6* (4), 1044–1049.

(42) Ascencio, J. A.; Rincon, A. C.; Canizal, G. Synthesis and Theoretical Analysis of Samarium Nanoparticles: Perspectives in Nuclear Medicine. *J. Phys. Chem. B* **2005**, *109* (18), 8806–8812. https://doi.org/10.1021/jp0460083.

(43) Dozie-Nwachukwu, S. O.; Obayemi, J. D.; Danyuo, Y. T.; Etuk-Udo, G.; Chi, Y.; Hu, J.; Anuku, N.; Odusanya, O. S.; Malatesta, K.; Soboyejo, W. O. Biosynthesis of Gold Nanoparticles and Gold/Prodigiosin Nanoparticles with Serratia Marcescens Bacteria. *Waste Biomass Valorization* **2017**, *8* (6), 2045–2059. https://doi.org/10.1007/s12649-016-9734-7.

(44) Hasan, S. S.; Singh, S.; Parikh, R. Y.; Dharne, M. S.; Patole, M. S.; Prasad, B. L. V.; Shouche, Y. S. Bacterial Synthesis of Copper/Copper Oxide Nanoparticles. *J. Nanosci. Nanotechnol.* **2008**, *8* (6), 3191–3196.

(45) Nazari, P.; Faramarzi, M. A.; Sepehrizadeh, Z.; Mofid, M. R.; Bazaz, R. D.; Shahverdi, A. R. Biosynthesis of Bismuth Nanoparticles Using Serratia Marcescens Isolated from the Caspian Sea and Their Characterisation. *IET Nanobiotechnol.* **2012**, *6* (2), 58–62. https://doi.org/10.1049/iet-nbt.2010.0043.

(46) Avendaño, R.; Chaves, N.; Fuentes, P.; Sánchez, E.; Jiménez, J. I.; Chavarría, M. Production of Selenium Nanoparticles in Pseudomonas Putida KT2440. *Sci. Rep.* **2016**, *6*. https://doi.org/10.1038/srep37155.

(47) Gopinath, V.; Priyadarshini, S.; Loke, M. F.; Arunkumar, J.; Marsili, E.; MubarakAli, D.; Velusamy, P.; Vadivelu, J. Biogenic Synthesis, Characterization of Antibacterial Silver Nanoparticles and Its Cell Cytotoxicity. *Arab. J. Chem.* **2017**, *10* (8), 1107–1117. https://doi.org/10.1016/j.arabjc.2015.11.011.

(48) De Corte, S.; Hennebel, T.; De Gusseme, B.; Verstraete, W.; Boon, N. Bio-Palladium: From Metal Recovery to Catalytic Applications. *Microb. Biotechnol.* **2012**, *5* (1), 5–17. https://doi.org/10.1111/j.1751-7915.2011.00265.x.

(49) Das, D. *Microbial Fuel Cell: A Bioelectrochemical System That Converts Waste to Watts*; Springer, 2017.

(50) Mohan, S. V.; Pandey, A.; Varjani, S. *Biomass, Biofuels, Biochemicals: Microbial Electrochemical Technology: Sustainable Platform for Fuels, Chemicals and Remediation*; Elsevier, 2018.

(51) Carrara, S.; Iniewski, K. *Handbook of Bioelectronics: Directly Interfacing Electronics and Biological Systems*; Cambridge University Press, 2015.

(52) Logan, B. E. Scaling up Microbial Fuel Cells and Other Bioelectrochemical Systems. *Appl. Microbiol. Biotechnol.* **2010**, *85* (6), 1665–1671. https://doi.org/10.1007/s00253-009-2378-9.

(53) Sydow, A.; Krieg, T.; Mayer, F.; Schrader, J.; Holtmann, D. Electroactive Bacteria—Molecular Mechanisms and Genetic Tools. *Appl. Microbiol. Biotechnol.* **2014**, *98* (20), 8481–8495. https://doi.org/10.1007/s00253-014-6005-z.

(54) Reimers, C. E.; Li, C.; Graw, M. F.; Schrader, P. S.; Wolf, M. The Identification of Cable Bacteria Attached to the Anode of a Benthic Microbial

Fuel Cell: Evidence of Long Distance Extracellular Electron Transport to Electrodes. *Front. Microbiol.* **2017**, *8*. https://doi.org/10.3389/fmicb.2017.02055.

(55) Wrighton, K. C.; Agbo, P.; Warnecke, F.; Weber, K. A.; Brodie, E. L.; DeSantis, T. Z.; Hugenholtz, P.; Andersen, G. L.; Coates, J. D. A Novel Ecological Role of the Firmicutes Identified in Thermophilic Microbial Fuel Cells. *ISME J.* **2008**, *2* (11), 1146–1156. https://doi.org/10.1038/ismej.2008.48.

(56) Kalia, V. C. *Microbial Factories: Biofuels, Waste Treatment:*; Springer, 2016.

(57) Call, D. F.; Wagner, R. C.; Logan, B. E. Hydrogen Production by Geobacter Species and a Mixed Consortium in a Microbial Electrolysis Cell. *Appl. Environ. Microbiol.* **2009**, *75* (24), 7579–7587. https://doi.org/10.1128/AEM.01760-09.

(58) Logan, B. E.; Hamelers, B.; Rozendal, R.; Schröder, U.; Keller, J.; Freguia, S.; Aelterman, P.; Verstraete, W.; Rabaey, K. Microbial Fuel Cells: Methodology and Technology. *Environ. Sci. Technol.* **2006**, *40* (17), 5181–5192. https://doi.org/10.1021/es0605016.

(59) Methé, B. A.; Nelson, K. E.; Eisen, J. A.; Paulsen, I. T.; Nelson, W.; Heidelberg, J. F.; Wu, D.; Wu, M.; Ward, N.; Beanan, M. J.; et al. Genome of Geobacter Sulfurreducens: Metal Reduction in Subsurface Environments. *Science* **2003**, *302* (5652), 1967–1969. https://doi.org/10.1126/science.1088727.

(60) Saffarini, D.; Brockman, K.; Beliaev, A.; Bouhenni, R.; Shirodkar, S. Shewanella Oneidensis and Extracellular Electron Transfer to Metal Oxides. In *Bacteria-Metal Interactions*; 2015; pp 21–40.

(61) Marsili, E.; Baron, D. B.; Shikhare, I. D.; Coursolle, D.; Gralnick, J. A.; Bond, D. R. Shewanella Secretes Flavins That Mediate Extracellular Electron Transfer. *Proc. Natl. Acad. Sci. U. S. A.* **2008**, *105* (10), 3968–3973. https://doi.org/10.1073/pnas.0710525105.

(62) Richter, K.; Schicklberger, M.; Gescher, J. Dissimilatory Reduction of Extracellular Electron Acceptors in Anaerobic Respiration. *Appl. Environ. Microbiol.* **2012**, *78* (4), 913–921. https://doi.org/10.1128/AEM.06803-11.

(63) Belleville, Pierre. De La Modélisation Multiphysique Des Biofilms Anodiques Pour Le Développement Des Systèmes Bioélectrochimiques., Grenoble-Alpes University, 2018.

(64) Xie, X.; Criddle, C.; Cui, Y. Design and Fabrication of Bioelectrodes for Microbial Bioelectrochemical Systems. *Energy Env. Sci* **2015**, *8* (12), 3418–3441. https://doi.org/10.1039/C5EE01862E.

(65) Lepage, G.; Albernaz, F. O.; Perrier, G.; Merlin, G. Characterization of a Microbial Fuel Cell with Reticulated Carbon Foam Electrodes. *Bioresour. Technol.* **2012**, *124*, 199–207. https://doi.org/10.1016/j.biortech.2012.07.067.

(66) Feng, Y.; Yang, Q.; Wang, X.; Logan, B. E. Treatment of Carbon Fiber Brush Anodes for Improving Power Generation in Air-Cathode Microbial Fuel Cells. *J. Power Sources* **2010**, *195* (7), 1841–1844. https://doi.org/10.1016/j.jpowsour.2009.10.030.

(67) Shen, Y.; Zhou, Y.; Chen, S.; Yang, F.; Zheng, S.; Hou, H. Carbon Nanofibers Modified Graphite Felt for High Performance Anode in High Substrate Concentration Microbial Fuel Cells. *ScientificWorldJournal* **2014**, *2014*, 130185. https://doi.org/10.1155/2014/130185.

(68) Champavert, J.; Ben Rejeb, S.; Innocent, C.; Pontié, M. Microbial Fuel Cell Based on Ni-Tetra Sulfonated Phthalocyanine Cathode and Graphene Modified Bioanode. *J. Electroanal. Chem.* **2015**, *757*, 270–276. https://doi.org/10.1016/j.jelechem.2015.09.012.

(69) Manickam, S. S.; Karra, U.; Huang, L.; Bui, N.-N.; Li, B.; McCutcheon, J. R. Activated Carbon Nanofiber Anodes for Microbial Fuel Cells. *Carbon* **2013**, *53*, 19–28. https://doi.org/10.1016/j.carbon.2012.10.009.

(70) Liu, Y.; Kim, H.; Franklin, R.; Bond, D. R. Gold Line Array Electrodes Increase Substrate Affinity and Current Density of Electricity-Producing G. Sulfurreducens Biofilms. *Energy Environ. Sci.* **2010**, *3* (11), 1782–1788. https://doi.org/10.1039/C0EE00242A.

(71) Baudler, A.; Schmidt, I.; Langner, M.; Greiner, A.; Schröder, U. Does It Have to Be Carbon? Metal Anodes in Microbial Fuel Cells and Related Bioelectrochemical Systems. *Energy Environ. Sci.* **2015**, *8* (7), 2048–2055. https://doi.org/10.1039/C5EE00866B.

(72) Oliot, M.; Galier, S.; Roux de Balmann, H.; Bergel, A. Ion Transport in Microbial Fuel Cells: Key Roles, Theory and Critical Review. *Appl. Energy* **2016**, *183*, 1682–1704. https://doi.org/10.1016/j.apenergy.2016.09.043.

(73) Lepage, G.; Perrier, G.; Merlin, G.; Aryal, N.; Dominguez-Benetton, X. Multifactorial Evaluation of the Electrochemical Response of a Microbial Fuel Cell. *RSC Adv.* **2014**, *4* (45), 23815–23825. https://doi.org/10.1039/C4RA03879G.

(74) Dharmalingam, S.; Kugarajah, V.; Sugumar, M. Chapter 1.7 - Membranes for Microbial Fuel Cells. In *Microbial Electrochemical Technology*; Mohan, S. V., Varjani, S., Pandey, A., Eds.; Biomass, Biofuels and Biochemicals;

Elsevier, 2019; pp 143–194. https://doi.org/10.1016/B978-0-444-64052-9.00007-8.

(75) Pontié, M.; Ben Rejeb, S.; Legrand, J. Anti-Microbial Approach onto Cationic-Exchange Membranes. *Sep. Purif. Technol.* **2012**, *101*, 91–97. https://doi.org/10.1016/j.seppur.2012.09.022.

(76) Luo, Y.; Zhang, F.; Wei, B.; Liu, G.; Zhang, R.; Logan, B. E. The Use of Cloth Fabric Diffusion Layers for Scalable Microbial Fuel Cells. *Biochem. Eng. J.* **2013**, *73*, 49–52. https://doi.org/10.1016/j.bej.2013.01.011.

(77) Tang, X.; Guo, K.; Li, H.; Du, Z.; Tian, J. Microfiltration Membrane Performance in Two-Chamber Microbial Fuel Cells. *Biochem. Eng. J.* **2010**, *52* (2), 194–198. https://doi.org/10.1016/j.bej.2010.08.007.

(78) Zuo, Y.; Cheng, S.; Call, D.; Logan, B. E. Tubular Membrane Cathodes for Scalable Power Generation in Microbial Fuel Cells. *Environ. Sci. Technol.* **2007**, *41* (9), 3347–3353.

(79) Winfield, J.; Chambers, L. D.; Rossiter, J.; Greenman, J.; Ieropoulos, I. Urine-Activated Origami Microbial Fuel Cells to Signal Proof of Life. *J. Mater. Chem. A* **2015**, *3* (13), 7058–7065. https://doi.org/10.1039/C5TA00687B.

(80) Hernández-Fernández, F. J.; Pérez de los Ríos, A.; Mateo-Ramírez, F.; Godínez, C.; Lozano-Blanco, L. J.; Moreno, J. I.; Tomás-Alonso, F. New Application of Supported Ionic Liquids Membranes as Proton Exchange Membranes in Microbial Fuel Cell for Waste Water Treatment. *Chem. Eng. J.* **2015**, *279*, 115–119. https://doi.org/10.1016/j.cej.2015.04.036.

(81) ter Heijne, A.; Hamelers, H. V. M.; de Wilde, V.; Rozendal, R. A.; Buisman, C. J. N. A Bipolar Membrane Combined with Ferric Iron Reduction

as an Efficient Cathode System in Microbial Fuel Cells. *Environ. Sci. Technol.* **2006**, *40* (17), 5200–5205. https://doi.org/10.1021/es0608545.

(82) Kracke, F.; Vassilev, I.; KrÃ¶mer, J. O. Microbial Electron Transport and Energy Conservation Â€“ the Foundation for Optimizing Bioelectrochemical Systems. *Front. Microbiol.* **2015**, *6*. https://doi.org/10.3389/fmicb.2015.00575.

(83) Cheng, S.; Logan, B. E. Sustainable and Efficient Biohydrogen Production via Electrohydrogenesis. *Proc. Natl. Acad. Sci.* **2007**, *104* (47), 18871–18873. https://doi.org/10.1073/pnas.0706379104.

(84) Jeremiasse, A. W.; Hamelers, H. V. M.; Buisman, C. J. N. Microbial Electrolysis Cell with a Microbial Biocathode. *Bioelectrochemistry* **2010**, *78* (1), 39–43. https://doi.org/10.1016/j.bioelechem.2009.05.005.

(85) Ganigué, R.; Puig, S.; Batlle-Vilanova, P.; Balaguer, M. D.; Colprim, J. Microbial Electrosynthesis of Butyrate from Carbon Dioxide. *Chem. Commun.* **2015**, *51* (15), 3235–3238. https://doi.org/10.1039/C4CC10121A.

(86) Spirito, C. M.; Richter, H.; Rabaey, K.; Stams, A. J.; Angenent, L. T. Chain Elongation in Anaerobic Reactor Microbiomes to Recover Resources from Waste. *Curr. Opin. Biotechnol.* **2014**, *27*, 115–122. https://doi.org/10.1016/j.copbio.2014.01.003.

(87) Nancharaiah, Y. V.; Venkata Mohan, S.; Lens, P. N. L. Metals Removal and Recovery in Bioelectrochemical Systems: A Review. *Bioresour. Technol.* **2015**, *195*, 102–114. https://doi.org/10.1016/j.biortech.2015.06.058.

(88) Huang, L.; Chen, J.; Quan, X.; Yang, F. Enhancement of Hexavalent Chromium Reduction and Electricity Production from a Biocathode Microbial Fuel Cell. *Bioprocess Biosyst. Eng.* **2010**, *33* (8), 937–945. https://doi.org/10.1007/s00449-010-0417-7.

(89) Gangadharan, P.; Nambi, I. M. Hexavalent Chromium Reduction and Energy Recovery by Using Dual-Chambered Microbial Fuel Cell. *Water Sci. Technol.* **2015**, *71* (3), 353–358. https://doi.org/10.2166/wst.2014.524.

(90) Li, Z.; Zhang, X.; Lei, L. Electricity Production during the Treatment of Real Electroplating Wastewater Containing Cr6+ Using Microbial Fuel Cell. *Process Biochem.* **2008**, *43* (12), 1352–1358. https://doi.org/10.1016/j.procbio.2008.08.005.

(91) Jiang, L.; Huang, L.; Sun, Y. Recovery of Flakey Cobalt from Aqueous Co(II) with Simultaneous Hydrogen Production in Microbial Electrolysis Cells. *Int. J. Hydrog. Energy* **2014**, *39* (2), 654–663. https://doi.org/10.1016/j.ijhydene.2013.10.112.

(92) Huang, L.; Li, T.; Liu, C.; Quan, X.; Chen, L.; Wang, A.; Chen, G. Synergetic Interactions Improve Cobalt Leaching from Lithium Cobalt Oxide in Microbial Fuel Cells. *Bioresour. Technol.* **2013**, *128*, 539–546. https://doi.org/10.1016/j.biortech.2012.11.011.

(93) Tao, H.-C.; Liang, M.; Li, W.; Zhang, L.-J.; Ni, J.-R.; Wu, W.-M. Removal of Copper from Aqueous Solution by Electrodeposition in Cathode Chamber of Microbial Fuel Cell. *J. Hazard. Mater.* **2011**, *189* (1–2), 186–192. https://doi.org/10.1016/j.jhazmat.2011.02.018.

(94) Tao, H.-C.; Zhang, L.-J.; Gao, Z.-Y.; Wu, W.-M. Copper Reduction in a Pilot-Scale Membrane-Free Bioelectrochemical Reactor. *Bioresour. Technol.* **2011**, *102* (22), 10334–10339. https://doi.org/10.1016/j.biortech.2011.08.116.

(95) Heijne, A. T.; Liu, F.; Weijden, R. van der; Weijma, J.; Buisman, C. J. N.; Hamelers, H. V. M. Copper Recovery Combined with Electricity Production in

a Microbial Fuel Cell. *Environ. Sci. Technol.* **2010**, *44* (11), 4376–4381. https://doi.org/10.1021/es100526g.

(96) Choi, C.; Hu, N.; Lim, B. Cadmium Recovery by Coupling Double Microbial Fuel Cells. *Bioresour. Technol.* **2014**, *170*, 361–369. https://doi.org/10.1016/j.biortech.2014.07.087.

(97) Choi, C.; Hu, N. The Modeling of Gold Recovery from Tetrachloroaurate Wastewater Using a Microbial Fuel Cell. *Bioresour. Technol.* **2013**, *133*, 589–598. https://doi.org/10.1016/j.biortech.2013.01.143.

(98) Wang, Z.; Lim, B.; Choi, C. Removal of Hg2+ as an Electron Acceptor Coupled with Power Generation Using a Microbial Fuel Cell. *Bioresour. Technol.* **2011**, *102* (10), 6304–6307. https://doi.org/10.1016/j.biortech.2011.02.027.

(99) Catal, T.; Bermek, H.; Liu, H. Removal of Selenite from Wastewater Using Microbial Fuel Cells. *Biotechnol. Lett.* **2009**, *31* (8), 1211–1216. https://doi.org/10.1007/s10529-009-9990-8.

(100) Choi, C.; Cui, Y. Recovery of Silver from Wastewater Coupled with Power Generation Using a Microbial Fuel Cell. *Bioresour. Technol.* **2012**, *107*, 522–525. https://doi.org/10.1016/j.biortech.2011.12.058.

(101) Wang, Y.-H.; Wang, B.-S.; Pan, B.; Chen, Q.-Y.; Yan, W. Electricity Production from a Bio-Electrochemical Cell for Silver Recovery in Alkaline Media. *Appl. Energy* **2013**, *112*, 1337–1341. https://doi.org/10.1016/j.apenergy.2013.01.012.

(102) Qin, B.; Luo, H.; Liu, G.; Zhang, R.; Chen, S.; Hou, Y.; Luo, Y. Nickel Ion Removal from Wastewater Using the Microbial Electrolysis Cell. *Bioresour. Technol.* **2012**, *121*, 458–461. https://doi.org/10.1016/j.biortech.2012.06.068.

(103) Zhang, B.; Zhao, H.; Shi, C.; Zhou, S.; Ni, J. Simultaneous Removal of Sulfide and Organics with Vanadium(V) Reduction in Microbial Fuel Cells. *J. Chem. Technol. Biotechnol.* **2009**, *84* (12), 1780–1786. https://doi.org/10.1002/jctb.2244.

(104) Zhang, B.; Feng, C.; Ni, J.; Zhang, J.; Huang, W. Simultaneous Reduction of Vanadium (V) and Chromium (VI) with Enhanced Energy Recovery Based on Microbial Fuel Cell Technology. *J. Power Sources* **2012**, *204*, 34–39. https://doi.org/10.1016/j.jpowsour.2012.01.013.

(105) Modin, O.; Wang, X.; Wu, X.; Rauch, S.; Fedje, K. K. Bioelectrochemical Recovery of Cu, Pb, Cd, and Zn from Dilute Solutions. *J. Hazard. Mater.* **2012**, *235–236*, 291–297. https://doi.org/10.1016/j.jhazmat.2012.07.058.

(106) Luo, H.; Liu, G.; Zhang, R.; Bai, Y.; Fu, S.; Hou, Y. Heavy Metal Recovery Combined with H2 Production from Artificial Acid Mine Drainage Using the Microbial Electrolysis Cell. *J. Hazard. Mater.* **2014**, *270*, 153–159. https://doi.org/10.1016/j.jhazmat.2014.01.050.

(107) Tao, H.-C.; Gao, Z.-Y.; Ding, H.; Xu, N.; Wu, W.-M. Recovery of Silver from Silver(I)-Containing Solutions in Bioelectrochemical Reactors. *Bioresour. Technol.* **2012**, *111*, 92–97. https://doi.org/10.1016/j.biortech.2012.02.029.

(108) Tandukar, M.; Huber, S. J.; Onodera, T.; Pavlostathis, S. G. Biological Chromium(VI) Reduction in the Cathode of a Microbial Fuel Cell. *Environ. Sci. Technol.* **2009**, *43* (21), 8159–8165. https://doi.org/10.1021/es9014184.

(109) Monsieurs, P.; Moors, H.; Houdt, R. Van; Janssen, P. J.; Janssen, A.; Coninx, I.; Mergeay, M.; Leys, N. Heavy Metal Resistance in Cupriavidus

Metallidurans CH34 Is Governed by an Intricate Transcriptional Network. **2011**, 1133–1151. https://doi.org/10.1007/s10534-011-9473-y.

(110) Nancharaiah, Y. V.; Venkata Mohan, S.; Lens, P. N. L. Metals Removal and Recovery in Bioelectrochemical Systems: A Review. *Bioresour. Technol.* **2015**, *195*, 102–114. https://doi.org/10.1016/j.biortech.2015.06.058.

(111) Varia, J.; Martínez, S. S.; Orta, S. V.; Bull, S.; Roy, S. Bioelectrochemical Metal Remediation and Recovery of Au3+, Co2+ and Fe3+ Metal Ions. *Electrochimica Acta* **2013**, *95*, 125–131. https://doi.org/10.1016/j.electacta.2013.02.051.

(112) Norland, S.; Heldal, M.; Tumyr, O. On the Relation between Dry Matter and Volume of Bacteria. *Microb. Ecol.* **1987**, *13*, 95–101. https://doi.org/10.1007/BF02011246.

(113) Loferer-Krößbacher, M.; Klima, J.; Psenner, R. Determination of Bacterial Cell Dry Mass by Transmission Electron Microscopy and Densitometric Image Analysis. *Appl. Environ. Microbiol.* **1998**, *64*, 688–694.

(114) Konishi, Y.; Tsukiyama, T.; Ohno, K.; Saitoh, N.; Nomura, T.; Nagamine, S. Intracellular Recovery of Gold by Microbial Reduction of AuCl 4 - Ions Using the Anaerobic Bacterium Shewanella Algae. *Hydrometallurgy* **2006**, *81* (1), 24–29. https://doi.org/10.1016/j.hydromet.2005.09.006.

(115) Goris, J.; Vos, P. De; Coenye, T.; Hoste, B.; Janssens, D.; Brim, H.; Diels, L.; Mergeay, M.; Kersters, K.; Vandamme, P. Classification of Metal-Resistant Bacteria from Industrial Biotopes as Ralstonia Campinensis Sp. Nov., Ralstonia Metallidurans Sp. Nov. and Ralstonia Basilensis Steinle 1998 Emend. *Int. J. Syst. Evol. Microbiol.* **2001**, No. 2001, 1773–1782. https://doi.org/10.1099/00207713-51-5-1773.

(116) Grzelczak, M.; Pérez-Juste, J.; Mulvaney, P.; Liz-Marzán, L. M. Shape Control in Gold Nanoparticle Synthesis. *Chem. Soc. Rev.* **2008**, *37* (9), 1783–1791. https://doi.org/10.1039/B711490G.

(117) Haruta, M. Gold as a Novel Catalyst in the 21st Century: Preparation, Working Mechanism and Applications. *Gold Bull.* **2004**, *37* (1), 27–36. https://doi.org/10.1007/BF03215514.

(118) Hagelüken, C.; Corti, C. W. Recycling of Gold from Electronics: Cost-Effective Use through 'Design for Recycling.' *Gold Bull.* **2010**, *43* (3), 209–220. https://doi.org/10.1007/BF03214988.

(119) Doidge, E. D.; Carson, I.; Tasker, P. A.; Ellis, R. J.; Morrison, C. A.; Love, J. B. A Simple Primary Amide for the Selective Recovery of Gold from Secondary Resources. *Angew. Chem. Int. Ed.* **2016**, *55* (40), 12436–12439. https://doi.org/10.1002/anie.201606113.

(120) Cyganowski, P.; Garbera, K.; Leśniewicz, A.; Wolska, J.; Pohl, P.; Jermakowicz-Bartkowiak, D. The Recovery of Gold from the Aqua Regia Leachate of Electronic Parts Using a Core–Shell Type Anion Exchange Resin. *J. Saudi Chem. Soc.* **2017**, *21* (6), 741–750. https://doi.org/10.1016/j.jscs.2017.03.007.

(121) Murakami, H.; Nishihama, S.; Yoshizuka, K. Separation and Recovery of Gold from Waste LED Using Ion Exchange Method. *Hydrometallurgy* **2015**, *157*, 194–198. https://doi.org/10.1016/j.hydromet.2015.08.014.

(122) Green, T. A. Gold Electrodeposition for Microelectronic, Optoelectronic and Microsystem Applications. *Gold Bull.* **2007**, *40* (2), 105–114. https://doi.org/10.1007/BF03215566.

(123) Lekka, M.; Masavetas, I.; Benedetti, A. V.; Moutsatsou, A.; Fedrizzi, L. Gold Recovery from Waste Electrical and Electronic Equipment by Electrodeposition: A Feasibility Study. *Hydrometallurgy* **2015**, *157*, 97–106. https://doi.org/10.1016/j.hydromet.2015.07.017.

(124) Gericke, M.; Pinches, A. Microbial Production of Gold Nanoparticles. *Gold Bull.* **2006**, *39* (1), 22–28. https://doi.org/10.1007/BF03215529.

(125) Song, C. Y.; Yang, B. Y.; Chen, W. Q.; Dou, Y. X.; Yang, Y. J.; Zhou, N.; Wang, L. H. Gold Nanoflowers with Tunable Sheet-like Petals: Facile Synthesis, SERS Performances and Cell Imaging. *J Mater Chem B* **2016**, *4* (44), 7112–7118. https://doi.org/10.1039/C6TB01046F.

(126) Hutchings, G. J.; Brust, M.; Schmidbaur, H. Gold—an Introductory Perspective. *Chem. Soc. Rev.* **2008**. https://doi.org/10.1039/b810747p.

(127) Fratoddi, I.; Venditti, I.; Cametti, C.; Russo, M. V. How Toxic Are Gold Nanoparticles? The State-of-the-Art. *Nano Res.* **2015**, *8* (6), 1771–1799. https://doi.org/10.1007/s12274-014-0697-3.

(128) Husseiny, M. I.; El-Aziz, M. A.; Badr, Y.; Mahmoud, M. A. Biosynthesis of Gold Nanoparticles Using Pseudomonas Aeruginosa. *Spectrochim. Acta. A. Mol. Biomol. Spectrosc.* **2007**, *67* (3), 1003–1006. https://doi.org/10.1016/j.saa.2006.09.028.

(129) Box, G. E.; Hunter, J. S.; Hunter, W. G. *Statistics for Experimenters : An Introduction to Design, Data Analysis, and Model Building*; New York (N.Y.) : Wiley: New York, 1978.

(130) Macaskie, L. E.; Deplanche, K. Catalytic Activity of Biomanufactured Au Nanocatalysts in the Selective Oxidation of Glycerol. *J. Biotechnol.* **2008**, *136*. https://doi.org/10.1016/j.jbiotec.2008.07.863.

(131) Carrettin, S.; McMorn, P.; Johnston, P.; Griffin, K.; Kielyc, C.; Attarda, G. A.; Hutchings, G. J. Oxidation of Glycerol Using Supported Gold Catalysts. *Top. Catal.* **2004**, *27* (1–4). https://doi.org/1022-5528/04/0200–0131/0.

(132) Sander, R. Compilation of Henry's Law Constants (Version 4.0) for Water as Solvent. *Atmospheric Chem. Phys.* **2015**, *15* (8), 4399–4981. https://doi.org/10.5194/acp-15-4399-2015.

(133) Menon, S.; S, R.; S, V. K. A Review on Biogenic Synthesis of Gold Nanoparticles, Characterization, and Its Applications. *Resour.-Effic. Technol.* **2017**, *3* (4), 516–527. https://doi.org/10.1016/j.reffit.2017.08.002.

(134) Krug, J. T.; Wang, G. D.; Emory, S. R.; Nie, S. Efficient Raman Enhancement and Intermittent Light Emission Observed in Single Gold Nanocrystals. *J. Am. Chem. Soc.* **1999**, *121* (39), 9208–9214. https://doi.org/10.1021/ja992058n.

(135) Deplanche, K.; Macaskie, L. E. Biorecovery of Gold by Escherichia Coli and Desulfovibrio Desulfuricans. *Biotechnol. Bioeng.* **2008**, *99* (5), 1055–1064. https://doi.org/10.1002/bit.21688.

(136) De Windt, W.; Aelterman, P.; Verstraete, W. Bioreductive Deposition of Palladium (0) Nanoparticles on Shewanella Oneidensis with Catalytic Activity towards Reductive Dechlorination of Polychlorinated Biphenyls. *Environ. Microbiol.* **2005**, *7* (3), 314–325. https://doi.org/10.1111/j.1462-2920.2005.00696.x.

(137) Hennebel, T.; De Gusseme, B.; Boon, N.; Verstraete, W. Biogenic Metals in Advanced Water Treatment. *Trends Biotechnol.* **2009**, *27* (2), 90–98. https://doi.org/10.1016/j.tibtech.2008.11.002.

(138) Lenth, R. V. Quick and Easy Analysis of Unreplicated Fractional Factorials. *Technometrics* **1989**, *31*, 469–473.

(139) Lazic, Z. I. R. Design of Experiments in Chemical Engineering A Practical Guide. **2004**, 610. https://doi.org/10.1002/3527604162.

(140) Suresh, A. K.; Pelletier, D. A.; Wang, W.; Broich, M. L.; Moon, J. W.; Gu, B.; Allison, D. P.; Joy, D. C.; Phelps, T. J.; Doktycz, M. J. Biofabrication of Discrete Spherical Gold Nanoparticles Using the Metal-Reducing Bacterium Shewanella Oneidensis. *Acta Biomater.* **2011**, *7* (5), 2148–2152. https://doi.org/10.1016/j.actbio.2011.01.023.

(141) Varia, J.; Martínez, S. S.; Orta, S. V.; Bull, S.; Roy, S. Bioelectrochemical Metal Remediation and Recovery of Au3+, Co2+ and Fe3+ Metal Ions. *Electrochimica Acta* **2013**, *95* (July), 125–131. https://doi.org/10.1016/j.electacta.2013.02.051.

(142) Nakajima, A. Accumulation of Gold by Microorganisms. *World J. Microbiol. Biotechnol.* **2003**, *19* (4), 369–374. https://doi.org/10.1023/A:1023944905364.

(143) Ha, J.; Gélabert, A.; Spormann, A. M.; Brown, G. E. Role of Extracellular Polymeric Substances in Metal Ion Complexation on Shewanella Oneidensis: Batch Uptake, Thermodynamic Modeling, ATR-FTIR, and EXAFS Study. *Geochim. Cosmochim. Acta* **2010**, *74* (1), 1–15. https://doi.org/10.1016/j.gca.2009.06.031.

(144) Wu, J.-W.; Ng, I.-S. Biofabrication of Gold Nanoparticles by Shewanella Species. *Bioresour. Bioprocess.* **2017**, *4* (1), 50. https://doi.org/10.1186/s40643-017-0181-5.

(145) Miller, J. T.; Kropf, A. J.; Zha, Y.; Regalbuto, J. R.; Delannoy, L.; Louis, C.; Bus, E.; van Bokhoven, J. A. The Effect of Gold Particle Size on AuAu Bond Length and Reactivity toward Oxygen in Supported Catalysts. *J. Catal.* **2006**, *240* (2), 222–234. https://doi.org/10.1016/j.jcat.2006.04.004.

(146) Fu, L.; Wu, N. Q.; Yang, J. H.; Qu, F.; Johnson, D. L.; Kung, M. C.; Kung, H. H.; Dravid, V. P. Direct Evidence of Oxidized Gold on Supported Gold Catalysts. *J. Phys. Chem. B* **2005**, *109* (9), 3704–3706. https://doi.org/10.1021/jp045117e.

(147) De Corte, S.; Hennebel, T.; Verschuere, S.; Cuvelier, C.; Verstraete, W.; Boon, N. Gold Nanoparticle Formation Using Shewanella Oneidensis: A Fast Biosorption and Slow Reduction Process. *J. Chem. Technol. Biotechnol.* **2011**, *86* (4), 547–553. https://doi.org/10.1002/jctb.2549.

(148) Nies, D. H. Microbial Heavy-Metal Resistance. *Appl. Microbiol. Biotechnol.* **1999**, *51* (6), 730–750.

(149) Konishi, Y.; Tsukiyama, T.; Tachimi, T.; Saitoh, N.; Nomura, T.; Nagamine, S. Microbial Deposition of Gold Nanoparticles by the Metal-Reducing Bacterium Shewanella Algae. *Electrochimica Acta* **2007**, *53* (1), 186–192. https://doi.org/10.1016/j.electacta.2007.02.073.

(150) Mosquera, Suanny. Microbial-Electrochemical Systems for Metal Recovery, Ghent University, 2018.

(151) Thompson, W. T.; Kaye, M. H.; Bale, C. W.; Pelton, A. D. Pourbaix Diagrams for Multielement Systems. In *Uhlig's Corrosion Handbook*; Wiley-Blackwell, 2011; pp 103–109. https://doi.org/10.1002/9780470872864.ch8.

(152) Pourbaix, M. J. N. *Atlas d'équilibres électrochimiques*; Centre belge d'étude de la corrosion, Ed.; Gauthier-Villars & Cie: Paris, France, 1963.

(153) Varia, J.; Zegeye, A.; Roy, S.; Yahaya, S.; Bull, S. Shewanella Putrefaciens for the Remediation of Au3+, Co2+ and Fe3+ Metal Ions from Aqueous Systems. *Biochem. Eng. J.* **2014**, *85*, 101–109. https://doi.org/10.1016/j.bej.2014.02.002.

(154) Sullivan, A. M.; Kohl, P. A. Electrochemical Study of the Gold Thiosulfate Reduction. *J. Electrochem. Soc.* **1997**, *144* (5), 1686–1690. https://doi.org/10.1149/1.1837660.

(155) Baron, D.; LaBelle, E.; Coursolle, D.; Gralnick, J. A.; Bond, D. R. Electrochemical Measurement of Electron Transfer Kinetics by Shewanella Oneidensis MR-1. *J. Biol. Chem.* **2009**, *284* (42), 28865–28873. https://doi.org/10.1074/jbc.M109.043455.

(156) Pasula, R. R.; Lim, S. Engineering Nanoparticle Synthesis Using Microbial Factories. *Eng. Biol.* **2017**, *1* (1), 12–17. https://doi.org/10.1049/enb.2017.0009.

(157) Dahl, J. A. ; M. Toward Greener Nanosynthesis. *Chem. Rev.* **2007**, *107* (6), 2228–2269. https://doi.org/10.1021/cr050943k.

(158) Elgrishi, N.; Rountree, K. J.; McCarthy, B. D.; Rountree, E. S.; Eisenhart, T. T.; Dempsey, J. L. A Practical Beginner's Guide to Cyclic Voltammetry. *J. Chem. Educ.* **2018**, *95* (2), 197–206. https://doi.org/10.1021/acs.jchemed.7b00361.

(159) Varia, J.; Martinez, S. S.; Velasquez-Orta, S.; Bull, S. Microbiological Influence of Metal Ion Electrodeposition: Studies Using Graphite Electrodes, [AuCl4]- and Shewanella Putrefaciens. *Electrochimica Acta* **2014**, *115*, 344–351. https://doi.org/10.1016/j.electacta.2013.10.166.

(160) Vieil, E. The Mass-Transfer Rate in Electrochemistry. *J. Electroanal. Chem. Interfacial Electrochem.* **1991**, *297* (1), 61–92. https://doi.org/10.1016/0022-0728(91)85359-W.

(161) Cheh, H. Y. Electrodeposition of Gold by Pulsed Current. *J. Electrochem. Soc.* **1971**, *118* (4), 551–557. https://doi.org/10.1149/1.2408110.

(162) Surfleet, B.; Crowle, V. A. Quantitative Recovery of Metals from Dilute Solutions. *Trans. IMF* **1972**, *50* (1), 227–232. https://doi.org/10.1080/00202967.1972.11870253.

(163) Walsh, F. C.; Reade, G. W. Electrochemical Techniques for the Treatment of Dilute Metal-Ion Solutions. In *Studies in Environmental Science*; Sequeira, C. A. C., Ed.; Environmental Oriented Electrochemistry; Elsevier, 1994; Vol. 59, pp 3–44. https://doi.org/10.1016/S0166-1116(08)70546-6.

(164) Khattab, I. A.; Shaffei, M. F.; Shaaban, N. A.; Hussein, H. S.; Abd El-Rehim, S. S. Electrochemical Removal of Copper Ions from Dilute Solutions Using Packed Bed Electrode. Part I. *Egypt. J. Pet.* **2013**, *22* (1), 199–203. https://doi.org/10.1016/j.ejpe.2012.09.011.

(165) Tchounwou, P. B.; Yedjou, C. G.; Patlolla, A. K.; Sutton, D. J. Heavy Metals Toxicity and the Environment. *EXS* **2012**, *101*, 133–164. https://doi.org/10.1007/978-3-7643-8340-4_6.

(166) Pradhan, D.; Sukla, L. B.; Sawyer, M.; Rahman, P. K. S. M. (Pattanathu). Recent Bioreduction of Hexavalent Chromium in Wastewater Treatment: A Review. *J. Ind. Eng. Chem.* **2017**. https://doi.org/10.1016/j.jiec.2017.06.040.

(167) Jobby, R.; Jha, P.; Yadav, A. K.; Desai, N. Biosorption and Biotransformation of Hexavalent Chromium [Cr(VI)]: A Comprehensive

Review. *Chemosphere* **2018**, *207*, 255–266. https://doi.org/10.1016/j.chemosphere.2018.05.050.

(168) Gong, Y.; Werth, C. J.; He, Y.; Su, Y.; Zhang, Y.; Zhou, X. Intracellular versus Extracellular Accumulation of Hexavalent Chromium Reduction Products by Geobacter Sulfurreducens PCA. *Environ. Pollut. Barking Essex 1987* **2018**, *240*, 485–492. https://doi.org/10.1016/j.envpol.2018.04.046.

(169) Zhao, Y.; Wang, J.; Ma, C.; Li, Y. Cr2O3 Ultrasmall Nanoparticles Filled Carbon Nanocapsules Deriving from Cr(VI) for Enhanced Lithium Storage. *Chem. Phys. Lett.* **2018**, *704*, 31–36. https://doi.org/10.1016/j.cplett.2018.05.036.

(170) Baatout, S.; Leys, N.; Hendrickx, L.; Dams, A.; Mergeay, M. Physiological Changes Induced in Bacteria Following PH Stress as a Model for Space Research. *Acta Astronaut.* **2007**, *60* (4), 451–459. https://doi.org/10.1016/j.actaastro.2006.09.012.

(171) Viamajala, S.; Peyton, B. M.; Sani, R. K.; Apel, W. A.; Petersen, J. N. Toxic Effects of Chromium(VI) on Anaerobic and Aerobic Growth of Shewanella Oneidensis MR-1. *Biotechnol. Prog.* **2004**, *20* (1), 87–95. https://doi.org/10.1021/bp034131q.

(172) Belchik, S. M.; Kennedy, D. W.; Dohnalkova, A. C.; Wang, Y.; Sevinc, P. C.; Wu, H.; Lin, Y.; Lu, H. P.; Fredrickson, J. K.; Shi, L. Extracellular Reduction of Hexavalent Chromium by Cytochromes MtrC and OmcA of Shewanella Oneidensis MR-1. *Appl. Environ. Microbiol.* **2011**, *77* (12), 4035–4041. https://doi.org/10.1128/AEM.02463-10.

(173) Ravindranath, S. P.; Henne, K. L.; Thompson, D. K.; Irudayaraj, J. Surface-Enhanced Raman Imaging of Intracellular Bioreduction of Chromate in

Shewanella Oneidensis. *PLOS ONE* **2011**, *6* (2), e16634. https://doi.org/10.1371/journal.pone.0016634.

(174) Baaziz, H.; Gambari, C.; Boyeldieu, A.; Ali Chaouche, A.; Alatou, R.; Méjean, V.; Jourlin-Castelli, C.; Fons, M. ChrASO, the Chromate Efflux Pump of Shewanella Oneidensis, Improves Chromate Survival and Reduction. *PLoS ONE* **2017**, *12* (11). https://doi.org/10.1371/journal.pone.0188516.

(175) Cromo Esavalente: VLP e il Monitoraggio Biologico Tradizionale. *Frareg*.

(176) Viti, C.; Marchi, E.; Decorosi, F.; Giovannetti, L. Molecular Mechanisms of Cr(VI) Resistance in Bacteria and Fungi. *FEMS Microbiol. Rev.* **2014**, *38* (4), 633–659. https://doi.org/10.1111/1574-6976.12051.

(177) Monsieurs, P.; Moors, H.; Van Houdt, R.; Janssen, P. J.; Janssen, A.; Coninx, I.; Mergeay, M.; Leys, N. Heavy Metal Resistance in Cupriavidus Metallidurans CH34 Is Governed by an Intricate Transcriptional Network. *Biometals Int. J. Role Met. Ions Biol. Biochem. Med.* **2011**, *24* (6), 1133–1151. https://doi.org/10.1007/s10534-011-9473-y.

(178) Liu, C.; Gorby, Y. A.; Zachara, J. M.; Fredrickson, J. K.; Brown, C. F. Reduction Kinetics of Fe(III), Co(III), U(VI), Cr(VI), and Tc(VII) in Cultures of Dissimilatory Metal-Reducing Bacteria. *Biotechnol. Bioeng.* **2002**, *80* (6), 637–649. https://doi.org/10.1002/bit.10430.

(179) Codd, R.; Dillon, C. T.; Levina, A.; Lay, P. A. Studies on the Genotoxicity of Chromium: From the Test Tube to the Cell. *Coord. Chem. Rev.* **2001**, *216–217*, 537–582. https://doi.org/10.1016/S0010-8545(00)00408-2.

(180) Chiu, A.; Shi, J.; Lee, W.; Hill, R.; Wakeman, T.; Katz, A.; Xu, B.; Dalal, N.; Robertson, J.; Chen, C.; et al. Review of Chromium (VI) Apoptosis, Cell-Cycle-Arrest, and Carcinogenesis. *J. Environ. Sci. Health Part C Environ.*

Carcinog. Ecotoxicol. Rev. **2010**, *28* (3), 188–230. https://doi.org/10.1080/10590501.2010.504980.

(181) Ni, C.; Liu, S.; Cui, L.; Han, Z.; Wang, L.; Chen, R.; Liu, H. Adsorption Performance of Cr(VI) onto Al-Free and Al-Substituted Ferrihydrites. *RSC Adv.* **2016**, *6* (71), 66412–66419. https://doi.org/10.1039/C6RA09465A.

(182) Balaska, F.; Bencheikh-Lehocine, M.; Chikhi, M.; Meniai, A.-H.; Bouledjouidja, A. Experimental Study and Simulation of Complexation Reaction of Chromium by EDTA for Its Recovery by Ultrafiltration. *Energy Procedia* **2012**, *19*, 249–258. https://doi.org/10.1016/j.egypro.2012.05.204.

(183) Golub, D.; Oren, Y. Removal of Chromium from Aqueous Solutions by Treatment with Porous Carbon Electrodes: Electrochemical Principles. *J. Appl. Electrochem.* **1989**, *19* (3), 311–316. https://doi.org/10.1007/BF01015228.

(184) Li, Y.; Lu, A.; Ding, H.; Jin, S.; Yan, Y.; Wang, C.; Zen, C.; Wang, X. Cr(VI) Reduction at Rutile-Catalyzed Cathode in Microbial Fuel Cells. *Electrochem. Commun.* **2009**, *11* (7), 1496–1499. https://doi.org/10.1016/j.elecom.2009.05.039.

(185) Huang, L.; Chai, X.; Chen, G.; Logan, B. E. Effect of Set Potential on Hexavalent Chromium Reduction and Electricity Generation from Biocathode Microbial Fuel Cells. *Environ. Sci. Technol.* **2011**, *45* (11), 5025–5031. https://doi.org/10.1021/es103875d.

(186) Emery, K.O.; Broadus, J.M. Overview: Marine Mineral Reserves and Resources, 1988.

(187) Mero, J. L. *The Mineral Resources of the Sea, By John L. Mero*; Elsevier Publishing Company, 1969.

(188) Miller, K. A.; Thompson, K. F.; Johnston, P.; Santillo, D. An Overview of Seabed Mining Including the Current State of Development, Environmental Impacts, and Knowledge Gaps. *Front. Mar. Sci.* **2018**, *4*. https://doi.org/10.3389/fmars.2017.00418.

(189) Ehlers, P. Blue Growth and Ocean Governance—How to Balance the Use and the Protection of the Seas. *WMU J. Marit. Aff.* **2016**, *15* (2), 187–203. https://doi.org/10.1007/s13437-016-0104-x.

(190) Hein, J.; Koschinsky, A. Deep-Ocean Ferromanganese Crusts and Nodules. *Geochem. Miner. Depos. Treatise Geochem. 2nd Ed.* **2014**, *13*, 273–291.

(191) Ahnert, A.; Borowski, C. Environmental Risk Assessment of Anthropogenic Activity in the Deep-Sea. *J. Aquat. Ecosyst. Stress Recovery* **2000**, *7* (4), 299–315. https://doi.org/10.1023/A:1009963912171.

(192) Kato, Y.; Fujinaga, K.; Nakamura, K.; Takaya, Y.; Kitamura, K.; Ohta, J.; Toda, R.; Nakashima, T.; Iwamori, H. Deep-Sea Mud in the Pacific Ocean as a Potential Resource for Rare-Earth Elements. *Nat. Geosci.* **2011**, *4* (8), 535–539. https://doi.org/10.1038/ngeo1185.

(193) Colín-García, M.; Ortega-Gutiérrez, F.; Heredia, A.; Negrón-Mendoza, A.; Ramos-Bernal, S.; Cordero, G.; Camprubí, A.; Beraldi, H. Hydrothermal Vents and Prebiotic Chemistry: A Review. *Bol. Soc. Geológica Mex.* **2016**, *68* (3), 599–620.

(194) Ramirez-Llodra, E.; Brandt, A.; Danovaro, R.; De Mol, B.; Escobar, E.; German, C. R.; Levin, L. A.; Martinez Arbizu, P.; Menot, L.; Buhl-Mortensen, P.; et al. Deep, Diverse and Definitely Different: Unique Attributes of the World's Largest Ecosystem. *Biogeosciences* **2010**, *7* (9), 2851–2899. https://doi.org/10.5194/bg-7-2851-2010.

(195) Dover, C. L. V.; German, C. R.; Speer, K. G.; Parson, L. M.; Vrijenhoek, R. C. Evolution and Biogeography of Deep-Sea Vent and Seep Invertebrates. *Science* **2002**, *295* (5558), 1253–1257. https://doi.org/10.1126/science.1067361.

(196) Hoagland, P.; Beaulieu, S.; Tivey, M. A.; Eggert, R. G.; German, C.; Glowka, L.; Lin, J. Deep-Sea Mining of Seafloor Massive Sulfides. *Mar. Policy* **2010**, *34* (3), 728–732. https://doi.org/10.1016/j.marpol.2009.12.001.

(197) Lipton, I.; Gleeson, E.; Munro, P. *Preliminary Economic Assesment of the Solwara Project, Bismarck Sea.*; Nautilus Minerals Niugini Ltd, 2018; p 274.

(198) Sharma, R. *Deep-Sea Mining: Resource Potential, Technical and Environmental Considerations*; Springer, 2017.

(199) Baker, E.; Beaudoin, Y. Cobalt-Rich Ferromanganese Crusts. A Physical, Biological, Environmental, and Technical Review. *GRID-Arendal* **2014**, *1C*, 52.

(200) Rickard, D. Chapter 3 - Sedimentary Iron Biogeochemistry. In *Developments in Sedimentology*; Rickard, D., Ed.; Sulfidic Sediments and Sedimentary Rocks; Elsevier, 2012; Vol. 65, pp 85–119. https://doi.org/10.1016/B978-0-444-52989-3.00003-9.

(201) Koschinsky, A.; Halbach, P. Sequential Leaching of Marine Ferromanganese Precipitates: Genetic Implications. *Geochim. Cosmochim. Acta* **1995**, *59* (24), 5113–5132. https://doi.org/10.1016/0016-7037(95)00358-4.

(202) Hein, J. Cobalt-Rich Ferromanganese Crusts: Global Distribution, Composition, Origin and Research Activities. In *Study*; 2004; Vol. 2, pp 188–256.

(203) Takaya, Y.; Yasukawa, K.; Kawasaki, T.; Fujinaga, K.; Ohta, J.; Usui, Y.; Nakamura, K.; Kimura, J. I.; Chang, Q.; Hamada, M.; et al. The Tremendous Potential of Deep-Sea Mud as a Source of Rare-Earth Elements. *Sci. Rep.* **2018**, *8* (1), 5763. https://doi.org/10.1038/s41598-018-23948-5.

(204) Thorpe, S. A. *An Introduction to Ocean Turbulence*; Cambridge University Press, 2007.

(205) Germanovich, L. N.; Hurt, R. S.; Smith, J. E.; Genc, G.; Lowell, R. P. Measuring Fluid Flow and Heat Output in Seafloor Hydrothermal Environments. *J. Geophys. Res. Solid Earth* **2015**, *120* (12), 8031–8055. https://doi.org/10.1002/2015JB012245.

(206) Zhang, Z.; Wu, Y.; Zhang, X.-H. Cultivation of Microbes from the Deep-Sea Environments. *Deep Sea Res. Part II Top. Stud. Oceanogr.* **2018**, *155*, 34–43. https://doi.org/10.1016/j.dsr2.2017.07.008.

(207) Blue Nodules project http://www.blue-nodules.eu/ (accessed Feb 12, 2019).

(208) Hauton, C.; Brown, A.; Thatje, S.; Mestre, N. C.; Bebianno, M. J.; Martins, I.; Bettencourt, R.; Canals, M.; Sanchez-Vidal, A.; Shillito, B.; et al. Identifying Toxic Impacts of Metals Potentially Released during Deep-Sea Mining—A Synthesis of the Challenges to Quantifying Risk. *Front. Mar. Sci.* **2017**, *4*. https://doi.org/10.3389/fmars.2017.00368.

(209) Erftemeijer, P. L. A.; Riegl, B.; Hoeksema, B. W.; Todd, P. A. Environmental Impacts of Dredging and Other Sediment Disturbances on Corals: A Review. *Mar. Pollut. Bull.* **2012**, *64* (9), 1737–1765. https://doi.org/10.1016/j.marpolbul.2012.05.008.

(210) Barnes, B. B.; Hu, C.; Kovach, C.; Silverstein, R. N. Sediment Plumes Induced by the Port of Miami Dredging: Analysis and Interpretation Using

Landsat and MODIS Data. *Remote Sens. Environ.* **2015**, *170*, 328–339. https://doi.org/10.1016/j.rse.2015.09.023.

(211) Boschen, R. E.; Rowden, A. A.; Clark, M. R.; Gardner, J. P. A. Mining of Deep-Sea Seafloor Massive Sulfides: A Review of the Deposits, Their Benthic Communities, Impacts from Mining, Regulatory Frameworks and Management Strategies. *Ocean Coast. Manag.* **2013**, *84*, 54–67. https://doi.org/10.1016/j.ocecoaman.2013.07.005.

(212) Ecorys. *Study to Investigate the State of Knowledge of Deep-Sea Mining*; Text; 2014.

(213) Rousseau, R.; Santaella, C.; Bonnafous, A.; Achouak, W.; Godon, J.-J.; Delia, M.-L.; Bergel, A. Halotolerant Bioanodes: The Applied Potential Modulates the Electrochemical Characteristics, the Biofilm Structure and the Ratio of the Two Dominant Genera. *Bioelectrochemistry* **2016**, *112*, 24–32. https://doi.org/10.1016/j.bioelechem.2016.06.006.

(214) Harris, G. Salinity. In *Encyclopedia of Inland Waters*; Likens, G. E., Ed.; Academic Press: Oxford, 2009; pp 79–84. https://doi.org/10.1016/B978-012370626-3.00103-4.

(215) Dore, J. E.; Lukas, R.; Sadler, D. W.; Church, M. J.; Karl, D. M. Physical and Biogeochemical Modulation of Ocean Acidification in the Central North Pacific. *Proc. Natl. Acad. Sci.* **2009**, *106* (30), 12235–12240. https://doi.org/10.1073/pnas.0906044106.

(216) González-Muñoz, M.; Dominguez-Benetton, X.; Domínguez-Maldonado, J.; Valdés-Lozano, D.; Pacheco-Catalán, D.; Ortega-Morales, O.; Alzate-Gaviria, L. Polarization Potential Has No Effect on Maximum Current Density

Produced by Halotolerant Bioanodes. *Energies* **2018**, *11* (3), 529. https://doi.org/10.3390/en11030529.

(217) Dominguez-Benetton, X.; Godon, J. J.; Rousseau, R.; Erable, B.; Bergel, A.; Délia, M. L. Exploring Natural vs. Synthetic Minimal Media to Boost Current Generation with Electrochemically-Active Marine Bioanodes. *J. Environ. Chem. Eng.* **2016**, *4* (2), 2362–2369. https://doi.org/10.1016/j.jece.2016.04.021.

(218) Logan, B. E. Exoelectrogenic Bacteria That Power Microbial Fuel Cells. *Nat. Rev. Microbiol.* **2009**, *7* (5), 375–381. https://doi.org/10.1038/nrmicro2113.

(219) Srikanth, S.; Pant, D.; Dominguez-Benetton, X.; Genné, I.; Vanbroekhoven, K.; Vermeiren, P.; Alvarez-Gallego, Y. Gas Diffusion Electrodes Manufactured by Casting Evaluation as Air Cathodes for Microbial Fuel Cells (MFC). *Materials* **2016**, *9* (7), 601. https://doi.org/10.3390/ma9070601.

(220) Chang, Z.; Evans, D.; Duan, X.; Boutinaud, P.; de Roy, M.; Forano, C. Preparation and Characterization of Rare Earth-Containing Layered Double Hydroxides. *J. Phys. Chem. Solids* **2006**, *67* (5), 1054–1057. https://doi.org/10.1016/j.jpcs.2006.01.025.

(221) Simka, W.; Puszczyk, D.; Nawrat, G. Electrodeposition of Metals from Non-Aqueous Solutions. *Electrochimica Acta* **2009**, *54* (23), 5307–5319. https://doi.org/10.1016/j.electacta.2009.04.028.

(222) Bonnaud, C. Vers une méthode de recyclage et de valorisation des aimants permanents à base de terres rares par électrochimie en milieux liquides ioniques. phdthesis, Université Grenoble Alpes, 2017.

(223) Provazi, K.; Campos, B. A.; Espinosa, D. C. R.; Tenório, J. A. S. Metal Separation from Mixed Types of Batteries Using Selective Precipitation and Liquid–Liquid Extraction Techniques. *Waste Manag.* **2011**, *31* (1), 59–64. https://doi.org/10.1016/j.wasman.2010.08.021.

(224) Min, B.; Logan, B. E. Continuous Electricity Generation from Domestic Wastewater and Organic Substrates in a Flat Plate Microbial Fuel Cell. *Environ. Sci. Technol.* **2004**, *38* (21), 5809–5814. https://doi.org/10.1021/es0491026.

(225) Carmona-Martínez, A. A.; Lacroix, R.; Trably, E.; Da Silva, S.; Bernet, N. On the Actual Anode Area That Contributes to the Current Density Produced by Electroactive Biofilms. *Electrochimica Acta* **2018**, *259*, 395–401. https://doi.org/10.1016/j.electacta.2017.10.200.

(226) Vicari, F.; Asensio, Y.; Fernandez-Marchante, C. M.; Lobato, J.; Cañizares, P.; Scialdone, O.; Rodrigo, M. A. Influence of the Initial Sludge Characteristics and Acclimation on the Long-Term Performance of Double-Compartment Acetate-Fed Microbial Fuel Cells. *J. Electroanal. Chem.* **2018**, *825*, 1–7. https://doi.org/10.1016/j.jelechem.2018.08.003.

(227) Katuri, K. P.; Kavanagh, P.; Rengaraj, S.; Leech, D. Geobacter Sulfurreducens Biofilms Developed under Different Growth Conditions on Glassy Carbon Electrodes: Insights Using Cyclic Voltammetry. *Chem. Commun. Camb. Engl.* **2010**, *46* (26), 4758–4760. https://doi.org/10.1039/c003342a.

(228) Orazem, M. E.; Tribollet, B. *Electrochemical Impedance Spectroscopy*; John Wiley & Sons, 2017.

(229) Rousseau, R.; Dominguez-Benetton, X.; Délia, M.-L.; Bergel, A. Microbial Bioanodes with High Salinity Tolerance for Microbial Fuel Cells and Microbial Electrolysis Cells. *Electrochem. Commun.* **2013**, *33*, 1–4. https://doi.org/10.1016/j.elecom.2013.04.002.

(230) Orani, A. M.; Vassileva, E.; Wysocka, I.; Angelidis, M.; Rozmaric, M.; Louw, D. Baseline Study on Trace and Rare Earth Elements in Marine Sediments Collected along the Namibian Coast. *Mar. Pollut. Bull.* **2018**, *131*, 386–395. https://doi.org/10.1016/j.marpolbul.2018.04.021.

(231) Ge, X.; Sumboja, A.; Wuu, D.; An, T.; Li, B.; Goh, F. W. T.; Hor, T. S. A.; Zong, Y.; Liu, Z. Oxygen Reduction in Alkaline Media: From Mechanisms to Recent Advances of Catalysts. *ACS Catal.* **2015**, *5* (8), 4643–4667. https://doi.org/10.1021/acscatal.5b00524.

(232) Okada, T.; Møller-Holst, S.; Gorseth, O.; Kjelstrup, S. Transport and Equilibrium Properties of Nafion® Membranes with H+ and Na+ Ions. *J. Electroanal. Chem.* **1998**, *442* (1), 137–145. https://doi.org/10.1016/S0022-0728(97)00499-3.

(233) Harnisch, F.; Freguia, S. A Basic Tutorial on Cyclic Voltammetry for the Investigation of Electroactive Microbial Biofilms. *Chem. Asian J.* **2012**, *7* (3), 466–475. https://doi.org/10.1002/asia.201100740.

(234) Bond, D. R.; Holmes, D. E.; Tender, L. M.; Lovley, D. R. Electrode-Reducing Microorganisms That Harvest Energy from Marine Sediments. *Science* **2002**, *295* (5554), 483–485. https://doi.org/10.1126/science.1066771.

(235) Massaglia, G.; Margaria, V.; Sacco, A.; Tommasi, T.; Pentassuglia, S.; Ahmed, D.; Mo, R.; Pirri, C. F.; Quaglio, M. In Situ Continuous Current

Production from Marine Floating Microbial Fuel Cells. *Appl. Energy* **2018**, *230*, 78–85. https://doi.org/10.1016/j.apenergy.2018.08.061.

(236) Natarajan, K. A. *Biotechnology of Metals: Principles, Recovery Methods and Environmental Concerns*; Elsevier, 2018.

(237) Heidrich, E. S.; Dolfing, J.; Wade, M. J.; Sloan, W. T.; Quince, C.; Curtis, T. P. Temperature, Inocula and Substrate: Contrasting Electroactive Consortia, Diversity and Performance in Microbial Fuel Cells. *Bioelectrochemistry Amst. Neth.* **2018**, *119*, 43–50. https://doi.org/10.1016/j.bioelechem.2017.07.006.

(238) de Pas, A. Les terres rares. *brgm*. 2017, p 7.

(239) Gupta, C. K.; Krishnamurthy, N. *Extractive Metallurgy of Rare Earths*; CRC Press: Boca Raton, Fla, 2005.

(240) Golev, A.; Scott, M.; Erskine, P. D.; Ali, S. H.; Ballantyne, G. R. Rare Earths Supply Chains: Current Status, Constraints and Opportunities. *Resour. Policy* **2014**, *41*, 52–59. https://doi.org/10.1016/j.resourpol.2014.03.004.

(241) Aizawa, H.; Yoshida, H.; Sakai, S. Current Results and Future Perspectives for Japanese Recycling of Home Electrical Appliances. *Resour. Conserv. Recycl.* **2008**, *52* (12), 1399–1410. https://doi.org/10.1016/j.resconrec.2008.07.013.

(242) Hicks, C.; Dietmar, R.; Eugster, M. The Recycling and Disposal of Electrical and Electronic Waste in China—Legislative and Market Responses. *Environ. Impact Assess. Rev.* **2005**, *25* (5), 459–471. https://doi.org/10.1016/j.eiar.2005.04.007.

(243) Powell, J. E. The Chemistry of the Lanthanides. *Inorg. Chem.* **1964**, *3* (7), 1070–1070. https://doi.org/10.1021/ic50017a055.

(244) Barrosse-Antle, L. E.; Bond, A. M.; Compton, R. G.; O'Mahony, A. M.; Rogers, E. I.; Silvester, D. S. Voltammetry in Room Temperature Ionic Liquids: Comparisons and Contrasts with Conventional Electrochemical Solvents. *Chem. – Asian J.* **2010**, *5* (2), 202–230. https://doi.org/10.1002/asia.200900191.

(245) Binnemans, K. Lanthanides and Actinides in Ionic Liquids. *Chem. Rev.* **2007**, *107* (6), 2592–2614. https://doi.org/10.1021/cr050979c.

(246) Gu, Y.; Liu, J.; Qu, S.; Deng, Y.; Han, X.; Hu, W.; Zhong, C. Electrodeposition of Alloys and Compounds from High-Temperature Molten Salts. *J. Alloys Compd.* **2017**, *690*, 228–238. https://doi.org/10.1016/j.jallcom.2016.08.104.

(247) Li, Q.; Jiang, J.; Li, G.; Zhao, W.; Zhao, X.; Mu, T. The Electrochemical Stability of Ionic Liquids and Deep Eutectic Solvents. *Sci. CHINA Chem.* **2016**, *59* (5), 571–577. https://doi.org/10.1007/s11426-016-5566-3.

(248) Plechkova, N. V.; Seddon, K. R. Applications of Ionic Liquids in the Chemical Industry. *Chem Soc Rev* **2008**, *37* (1), 123–150. https://doi.org/10.1039/B006677J.

(249) Nockemann, P.; Thijs, B.; Hecke, K. V.; Meervelt, L. V.; Binnemans, K. Polynuclear Metal Complexes Obtained from the Task-Specific Ionic Liquid Betainium Bistriflimide. *Cryst. Growth Des.* **2008**, *8* (4), 1353–1363. https://doi.org/10.1021/cg701187t.

(250) Dupont, D.; Binnemans, K. Recycling of Rare Earths from NdFeB Magnets Using a Combined Leaching/Extraction System Based on the Acidity and Thermomorphism of the Ionic Liquid [Hbet][Tf2N]. *Green Chem.* **2015**, *17* (4), 2150–2163. https://doi.org/10.1039/C5GC00155B.

(251) Gasparotto, L. H. S.; Borisenko, N.; Bocchi, N.; Abedin, S. Z. E.; Endres, F. In Situ STM Investigation of the Lithium Underpotential Deposition on Au(111) in the Air- and Water-Stable Ionic Liquid 1-Butyl-1-Methylpyrrolidinium Bis(Trifluoromethylsulfonyl)Amide. *Phys. Chem. Chem. Phys.* **2009**, *11* (47), 11140–11145. https://doi.org/10.1039/B916809E.

(252) Liu, F.; Deng, Y.; Han, X.; Hu, W.; Zhong, C. Electrodeposition of Metals and Alloys from Ionic Liquids. *J. Alloys Compd.* **2016**, *654* (Supplement C), 163–170. https://doi.org/10.1016/j.jallcom.2015.09.137.

(253) Rousse, C.; Beaufils, S.; Fricoteaux, P. Electrodeposition of Cu–Zn Thin Films from Room Temperature Ionic Liquid. *Electrochimica Acta* **2013**, *107* (Supplement C), 624–631. https://doi.org/10.1016/j.electacta.2013.06.053.

(254) Mousavi, M. P. S.; Kashefolgheta, S.; Stein, A.; Bühlmann, P. Electrochemical Stability of Quaternary Ammonium Cations: An Experimental and Computational Study. *J. Electrochem. Soc.* **2016**, *163* (2), H74–H80. https://doi.org/10.1149/2.0671602jes.

(255) Mehdi, H.; Binnemans, K.; Hecke, K. V.; Meervelt, L. V.; Nockemann, P. Hydrophobic Ionic Liquids with Strongly Coordinating Anions. *Chem. Commun.* **2009**, *46* (2), 234–236. https://doi.org/10.1039/B914977E.

(256) Domańska, U. Physico-Chemical Properties and Phase Behaviour of Pyrrolidinium-Based Ionic Liquids. *Int. J. Mol. Sci.* **2010**, *11* (4), 1825–1841. https://doi.org/10.3390/ijms11041825.

(257) Bortolini, O.; Chiappe, C.; Ghilardi, T.; Massi, A.; Pomelli, C. S. Dissolution of Metal Salts in Bis(Trifluoromethylsulfonyl)Imide-Based Ionic Liquids: Studying the Affinity of Metal Cations Toward a “Weakly

Coordinating" Anion. *J. Phys. Chem. A* **2015**, *119* (21), 5078–5087. https://doi.org/10.1021/jp507437g.

(258) De Vos, N.; Maton, C.; Stevens, C. V. Electrochemical Stability of Ionic Liquids: General Influences and Degradation Mechanisms. *ChemElectroChem* **2014**, *1* (8), 1258–1270. https://doi.org/10.1002/celc.201402086.

(259) Markevich, E.; Sharabi, R.; Borgel, V.; Gottlieb, H.; Salitra, G.; Aurbach, D.; Semrau, G.; Schmidt, M. A. In Situ FTIR Study of the Decomposition of N-Butyl-N-Methylpyrrolidinium Bis(Trifluoromethanesulfonyl)Amide Ionic Liquid during Cathodic Polarization of Lithium and Graphite Electrodes. *Electrochimica Acta* **2010**, *55* (8), 2687–2696. https://doi.org/10.1016/j.electacta.2009.12.030.

(260) Howlett, P. C.; Izgorodina, E. I.; Forsyth, M.; MacFarlane, D. R. Electrochemistry at Negative Potentials in Bis(Trifluoromethanesulfonyl)Amide Ionic Liquids. **2006**.

(261) Murase, K.; Nitta, K.; Hirato, T.; Awakura, Y. Electrochemical Behaviour of Copper in Trimethyl-n-Hexylammonium Bis((Trifluoromethyl)Sulfonyl)Amide, an Ammonium Imide-Type Room Temperature Molten Salt. *J. Appl. Electrochem.* **2001**, *31* (10), 1089–1094. https://doi.org/10.1023/A:1012255601793.

(262) Abu-Eishah, S. I. Ionic Liquids Recycling for Reuse. *Ion. Liq. - Cl. Prop.* **2011**. https://doi.org/10.5772/23267.

(263) Fedje, K.; Modin, O.; Strömvall, A.-M. Copper Recovery from Polluted Soils Using Acidic Washing and Bioelectrochemical Systems. *Metals* **2015**, *5* (3), 1328–1348. https://doi.org/10.3390/met5031328.

(264) Wang, Q.; Huang, L.; Pan, Y.; Zhou, P.; Quan, X.; Logan, B. E.; Chen, H. Cooperative Cathode Electrode and in Situ Deposited Copper for Subsequent Enhanced Cd(II) Removal and Hydrogen Evolution in Bioelectrochemical Systems. *Bioresour. Technol.* **2016**, *200*, 565–571. https://doi.org/10.1016/j.biortech.2015.10.084.

(265) Zhang, L.-J.; Tao, H.-C.; Wei, X.-Y.; Lei, T.; Li, J.-B.; Wang, A.-J.; Wu, W.-M. Bioelectrochemical Recovery of Ammonia–Copper(II) Complexes from Wastewater Using a Dual Chamber Microbial Fuel Cell. *Chemosphere* **2012**, *89* (10), 1177–1182. https://doi.org/10.1016/j.chemosphere.2012.08.011.

(266) Aritomi, T.; van den Boomgaard, T.; Strathmann, H. Current-Voltage Curve of a Bipolar Membrane at High Current Density. *Desalination* **1996**, *104* (1), 13–18. https://doi.org/10.1016/0011-9164(96)00021-5.

(267) Wilhelm, F. . *Bipolar Membrane Electrodialysis: Membrane Development and Transport Characteristics*; Twente University Press: Enschede, 2001.

(268) ter Heijne, A.; Hamelers, H. V. M.; de Wilde, V.; Rozendal, R. A.; Buisman, C. J. N. A Bipolar Membrane Combined with Ferric Iron Reduction as an Efficient Cathode System in Microbial Fuel Cells †. *Environ. Sci. Technol.* **2006**, *40* (17), 5200–5205. https://doi.org/10.1021/es0608545.

(269) Belleville, P.; Guillet, F.; Pons, A.; Deseure, J.; Merlin, G.; Druart, F.; Ramousse, J.; Grindler, E. Low Voltage Water Electrolysis: Decoupling Hydrogen Production Using Bioelectrochemical System. *Int. J. Hydrog. Energy* **2018**, *43* (32), 14867–14875. https://doi.org/10.1016/j.ijhydene.2018.06.080.

(270) Logan, B. E.; Rabaey, K. Conversion of Wastes into Bioelectricity and Chemicals by Using Microbial Electrochemical Technologies. *Science* **2012**, *337* (6095), 686–690. https://doi.org/10.1126/science.1217412.

(271) O'Reilly, J. E. Oxidation-Reduction Potential of the Ferro-Ferricyanide System in Buffer Solutions. *Biochim. Biophys. Acta BBA - Bioenerg.* **1973**, *292* (3), 509–515. https://doi.org/10.1016/0005-2728(73)90001-7.

(272) Speers, A. M.; Reguera, G. Theoretical and Practical Considerations for Culturing Geobacter Biofilms in Microbial Fuel Cells and Other Bioelectrochemical Systems. In *Biofilms in Bioelectrochemical Systems*; John Wiley & Sons, Ltd, 2015; pp 37–60. https://doi.org/10.1002/9781119097426.ch2.

(273) DSMZ GmbH. Geobacter Sulfurreducens Medium. 2016.

(274) Bond, D. R.; Lovley, D. R. Electricity Production by Geobacter Sulfurreducens Attached to Electrodes. *Appl. Environ. Microbiol.* **2003**, *69* (3), 1548–1555. https://doi.org/10.1128/AEM.69.3.1548-1555.2003.

(275) Marsili, E.; Sun, J.; Bond, D. R. Voltammetry and Growth Physiology of Geobacter Sulfurreducens Biofilms as a Function of Growth Stage and Imposed Electrode Potential. *Electroanalysis* **2010**, *22* (7–8), 865–874. https://doi.org/10.1002/elan.200800007.

(276) Kiely, P. D.; Regan, J. M.; Logan, B. E. The Electric Picnic: Synergistic Requirements for Exoelectrogenic Microbial Communities. *Curr. Opin. Biotechnol.* **2011**, *22* (3), 378–385. https://doi.org/10.1016/j.copbio.2011.03.003.

(277) Harnisch, F.; Schröder, U. Selectivity versus Mobility: Separation of Anode and Cathode in Microbial Bioelectrochemical Systems. *ChemSusChem* **2009**, *2* (10), 921–926. https://doi.org/10.1002/cssc.200900111.

(278) Bonnaud, C.; Billard, I.; Papaiconomou, N.; Chainet, E.; Leprêtre, J. C. Rationale for the Implementation of Reference Electrodes in Ionic Liquids. *Phys. Chem. Chem. Phys.* **2016**, *18* (11), 8148–8157. https://doi.org/10.1039/C5CP07652H.

(279) Bazito, F. F. C.; Kawano, Y.; Torresi, R. M. Synthesis and Characterization of Two Ionic Liquids with Emphasis on Their Chemical Stability towards Metallic Lithium. *Electrochimica Acta* **2007**, *52* (23), 6427–6437. https://doi.org/10.1016/j.electacta.2007.04.064.

(280) Tsuda, N.; Matsumiya, M.; Tsunashima, K.; Kodama, S. Electrochemical Behavior and Solvation Analysis of Rare Earth Complexes in Ionic Liquids Media Investigated by SECM and Raman Spectroscopy. *ECS Trans.* **2013**, *50* (11), 539–548. https://doi.org/10.1149/05011.0539ecst.

(281) Pfruender, H.; Amidjojo, M.; Kragl, U.; Weuster-Botz, D. Efficient Whole-Cell Biotransformation in a Biphasic Ionic Liquid/Water System. *Angew. Chem. Int. Ed Engl.* **2004**, *43* (34), 4529–4531. https://doi.org/10.1002/anie.200460241.

(282) Van Nevel, S.; Koetzsch, S.; Weilenmann, H. U.; Boon, N.; Hammes, F. Routine Bacterial Analysis with Automated Flow Cytometry. *J. Microbiol. Methods* **2013**, *94* (2), 73–76. https://doi.org/10.1016/j.mimet.2013.05.007.

(283) Buysschaert, B.; Kerckhof, F. M.; Vandamme, P.; De Baets, B.; Boon, N. Flow Cytometric Fingerprinting for Microbial Strain Discrimination and

Physiological Characterization. *Cytometry A* **2018**, *93* (2), 201–212. https://doi.org/10.1002/cyto.a.23302.

Annexes

Annex 1: Analytical techniques

1-A: Inductively coupled plasma, optical emission spectroscopy (ICP-OES)

The metal concentrations from experimental assays were measured by inductively coupled plasma optical emission spectrometry (ICP-OES) (Varian Vista-MPX CCD simultaneous, Australia). Samples were firstly filtered (0.2 µm disposable syringe filters, Macherey-Nagel, Germany) and diluted with 1% v/v HNO_3. They are injected in a plasma at approximatively 8000 K through a capillary, where species are ionized and emit photons. The wavelength of the emitted photons is characteristic of the element and can be analyzed by an optical detector. The intensity of photons is directly linked to the concentration of the element and can be determined by the preparation of calibration curves.

1-B: Transmission Electron Microscopy (TEM)

1.5 mL samples were centrifuged (Eppendorf, 5430) for 5 minutes at room temperature and 5000 rcf. The supernatant was discarded, and the pellet was fixed with 1 mL of fixing solution (4% paraformaldehyde, 5% glutaraldehyde in 0.1 M cacodylate buffer from VWR, Merck, USA). The samples were centrifuged once again, and stained with OsO_4 (VWR, Merck, USA). Following this, the sample was dehydrated stepwise with alcohol (30,50,70, 100%, supplier, country). The pellets were then embedded at room temperature in Epon medium. Semithin sections of 1 µm were first stained with toluidine blue, for initial visual observation of the cells. Subsequently, ultrathin sections (≈ 60 nm) were cut with a diamond knife and contrasted with uranyl acetate and lead citrate. With the help of a Zeiss TEM 900 (Carl Zeiss, Oberkochen, Germany) at 50kv, a beam of electrons is transmitted on the sample and based on their interactions an image is given. The dimensions (width and length) of the bacteria cells and particles were determined using ImageJ software (National Institutes of Health, NHS).

1-C: UV-visible spectrophotometer

This is a method used to identify concentration and chemical nature of species based on the absorbance intensity and wavelength respectively. Samples of 1 to 2 mL are hit by a light beam at a precise wavelength, and the ratio between the incident and transmitted beam intensities allows us to measure absorbance.

Characteristic peaks of gold nanoparticles were identified by scanning the UV-vis spectra from 300 nm to 800 nm on a light wave spectrophotometer (Biochrom WPA1100nm II, UK). The Cr(VI) concentration was estimated from the absorbance when fixing the wavelength at 540 nm. To do so, samples were firstly centrifugated and diluted with distillated water and 1,5-diphenylcarbazide as an indicator reagent for the complexation reaction with Cr(VI), as described in the standard colorimetric method EPA 7196 A (ref: Epa. METHOD 7196A - Colorimetric Method. 1992. p. 1-6).

1-D: Flow cytometry (FC)

Concentrated bacterial solutions and reactor samples were analysed by flow cytometry (FC) to obtain information about the number of cells and their viability based on membrane integrity[282]. Samples were diluted using freshly filtered NaCl 0.9% w/v. To determine the total cell count, cells were stained with SYBR® Green I (SG, 100x concentrate in 0.22 μm-filtered dimethyl sulfoxide, Invitrogen). For viability analysis, SYBR® Green I was combined with propidium iodide (SGPI, 100x concentrate SYBR® Green I, Invitrogen, and 50x 20 mM propidium iodide, Invitrogen, in 0.22 μm-filtered dimethyl sulfoxide). PI only enters cells with a damaged or permeabilized membrane, thus, differentiating intact versus putative dead or damaged cells which displayed an increasing red fluorescence emission when membrane damaged-cells increases[283]. Bacteria viability ratio is provided by quantification of cell densities in the different fluorescent channels. Stained samples were incubated for 13 min at 37 °C. Measurements were obtained by the Accuri C6 flow cytometer equipped with a 20 mW 488 nm blue laser with autosampler. The performance of the instrument was monitored daily and calibrated with the CS&T calibration beads (BD Biosciences, Belgium). The occurrence of cells was determined by analysing the number of events per volume

on green *vs.* red fluorescence plot in the BD CSampler Plus software (version 1.0.264.21, BD Biosciences, Belgium) on gating defined by the FC density plots.

1-E: Gas chromatograph (GC)

Headspace gas composition of reactors was analysed with a compact gas chromatograph (GC) (Global Analyser Solutions, Breda, The Netherlands). It contained a Molsieve 5A precolumn and Porabond column (O_2, N_2, CH_4, H_2) and an Rt-Q-bond precolumn and column (CO_2, N_2O). 1 mL samples were taken with a syringe equipped with a valve and immediately injected and analysed in the Porabond column at the beginning and at the end of the experiments.

1-F: SEM - EDS

A Scanning Electron Microscope (SEM, ZEISS® Ultra-55 FEG) was used to characterize the cathodes after the electrodeposition tests. An electron beam scanned the surface of a conductive material leading to the emission of various particles (*e.g.*, secondary electrons (SE), backscattered electrons (BSE) or even X-rays). SE and BSE give topographic and chemical information respectively. Sample were placed at a working distance (WD) of 9 mm. Besides, an energy dispersive X-ray spectroscopy detector (EDS, XFlash 5030) was used to identify and semi-quantify chemical elements present at the surface of the material. The signal for both imaging and elements semi-quantification used an acceleration voltage of 15 kV.

1-G: HPLC

Lactate concentration was measured with a High Performance Liquid Chromatography (HPLC) technique. 1 mL samples were firstly filtered (0.2 µm disposable syringe filters, Macherey-Nagel, Germany) and diluted with 10% v/v distillated water. They were subsequently analyzed in an ion chromatography 930 dual channel compact IC flex with 944 professional UV/Vis detector Vario (Metrohm, Switzerland).

1-H: Raman spectroscopy

After being treated, bacterial cells were harvested and fixed in paraformaldehyde 4%. First, 1mL of the sample was centrifuged at 1,957 x g for 5 minutes at room

temperature. After discarding the supernatant, the pellet was resuspended in 0.2 µm filtered Phosphate-buffered saline (PBS, Thermo-Fisher) at 4°C. Samples were centrifuged at 1,957 x g for 5 minutes at room temperature. After discarding the supernatant, the pellet was resuspended in 0.2 µm filtered (RC Minisart filter, Sigma-Aldrich) 4% paraformaldehyde, and allowed to fix for an hour. To wash the cells, they were centrifuged (5 minutes at 1,957 x g and room temperature) and resuspended in 1mL of cold (4°C) PBS twice. Then, samples were centrifuged and resuspended in fresh Milli-Q water (Merck-Millipore) and four 5µL drops were put on the CaF2 slide (grade 13 mm diameter by 0.5 mm polished disc, Crystran Ltd.) and allowed to dry until evaporation at room temperature. Finally, the slides were immediately analyzed using Raman spectroscopy with a WITec Alpha300R+ spectroscope with a 785 nm laser (Toptica, Germany). To analyze the Raman spectra, the program R was used (R Core Team, 2018). Spectra were pre-processed with the Micro-Raman package. First, they were cut in the region 370-1800 cm^{-1}. Then, baseline correction was done using the SNIP algorithm with 10 iterations. Data normalization was done with the MALDIquant package (v1.16.2, Gibb & Korbinian, 2012),using the area under the curve (AUC).

Annex 2: Supplementary materials

2-A: Ionic distribution

Gold(III) in a chloride solution and chromium (VI).

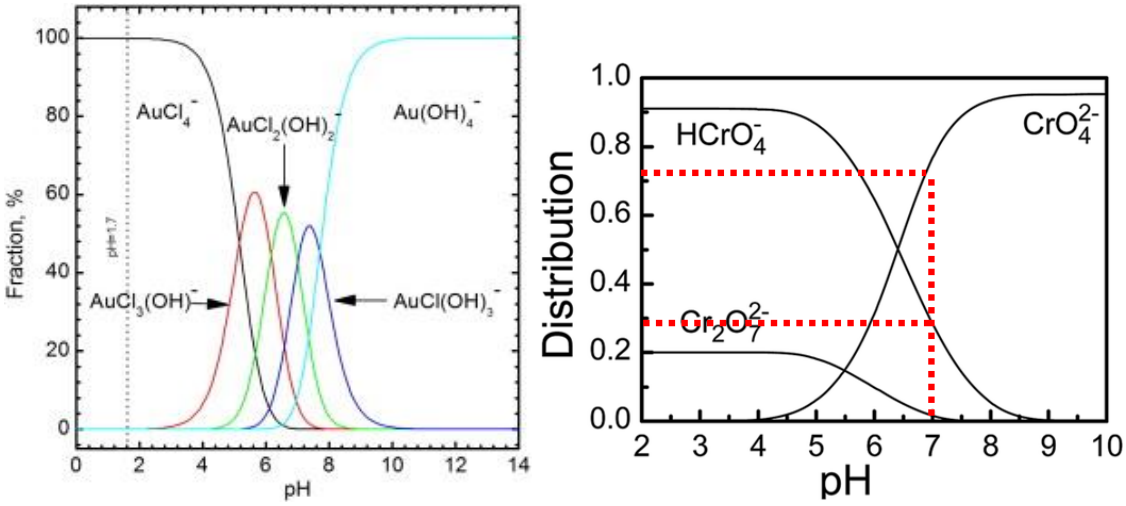

2- B: Raman peaks analysis for initially-viable bacteria with chromium

Wavelength (cm^{-1})	Intensity (A.U.)	Closest identified region (cm^{-1})	Tentative peak assignment
544	0.209	545	Cr (III)
605	0.798	606	Cr(III)
752	1.028	750	Cytochrome - c
845	0.439	846	Cr (VI)
1005	1.636	1030-1130	Carbohydrates, mainly –C-C- (skeletal), C-O, deformation (C-O-H)
1009	1.634	1030-1130	Carbohydrates, mainly –C-C- (skeletal), C-O, deformation (C-O-H)
1013	1.620	1030-1130	Carbohydrates, mainly –C-C- (skeletal), C-O, deformation (C-O-H)
1128	0.770	1128	Cytochrome - c
1204	1.050	1204	Glycine
1244	1.552	1248	Amide III
1255	1.634	1245	Adenine, amide III
1258	1.749	1258	Amide III, adenine, cytosine
1262	1.545	1260	CH2 in-plane deformation of lipids
1312	1.089	1311	Cytochrome - c
1441	1.706	1440	CH_2 and CH_3 deformation vibrations (lipid)
1445	1.758	1446	CH_2 bending mode of proteins and lipids
1448	1.848	1450	CH_2 bending
1452	2.105	1451-1453	CH_2/CH_3 deformation, PHB
1455	2.549	1451-1453	CH_2/CH_3 deformation, PHB
1459	2.652	1454	Overlapping asymmetric CH_3 bending and CH_2 scissoring (elastin, collagen, and phospholipids)
1462	2.138	1458	Nucleic acid modes
1466	1.574	1463	Fermi interaction $\delta(CH_2)$ and γ (CH_2)
1582	0.486	1582	Cytochrome - c
1612	1.560	1608	Cytosine (NH_2)
1669	1.514	1667	Protein band , C=C stretching band
1675	1.543	1676	Amide I (β-sheet)